RSC Applied Polymers

Accepted Manuscript

This article can be cited before page numbers have been issued, to do this please use: S. K. Srivastava, *RSC Appl. Polym.*, 2025, DOI: 10.1039/D5LP00230C.

ROYAL SOCIETY OF CHEMISTRY

rsc.li/RSCApplPolym

Recent Advances on Hollow and Core-Shell Intrinsically Conducting Polymers for Their Applications in Electromagnetic Interference Shielding/Microwave Absorption, Removal of Metal Ions/Dyes and Supercapacitors

View Article Online
DOI: 10.1039/D5LP00230C

Suneel Kumar Srivastava*+

Department of Chemistry
Indian Institute of Technology, Kharagpur-721302, India

Abstract

In recent years, considerable attention has been paid to the hollow micro-nano structured intrinsically conducting polymers, like polyaniline, polypyrrole, polythiophene and poly(3,4-ethylenedioxythiophene. These structures combine the hollow shape of the conducting properties. The availability of the shells and inner voids accounts for the tunable physical/chemical properties offer low density, high surface area, and reduced length for both mass and charge transport, they offer their promising applications in the remediation of environments and energy, In view of this, present article is focused on the synthesis methods of intrinsically conducting polymers and the effect of different parameters on their properties followed by the hard and soft template approaches including template free methods reported in the fabrication of hollow intrinsically conducting polymers, their encapsulation and nanocomposites. In addition, formation of core-shell composites based on ICPs have also been reviewed, Subsequently, review highlights the application of hollow microspheres, 1 D hollow nanostructures, encapsulated hollow ICPs s well as hollow and core-shell nanocomposites in electromagnetic interference shielding, removal of heavy metal ions and different dye from waste water and as efficient electrode materials in supercapacitors. Finally, review ends with the summary and future perceptive on the on hollow structured and core-shell conducting polymers and their applications in the above field of applications.

---

*E mail: suneel@chem.iitkgp.ac.in

+https://orcid.org/0000-0002-9297-2282

1. Introduction

Intrinsically conducting polymers (ICPs) comprising polyaniline (PANI), polypyrrole (PPy), polythiophene (PT), and poly(3,4-ethylenedioxythiophene) (PEDOT) are considered as special class of polymers due to their light weight, ease of fabrication, good environmental stability low cost, high mechanical flexibility, and good biocompatibility.[1] **Figure 1 (inset)** shows the schematic chemical structures of different monomer of all these ICPs.[2] They exhibit tunable surface area, electrical conductivity, optical properties, unique redox tenability. high electrochemical response.[3] As a result, ICPs find their applications in various advanced fields, such as sensing,[4] solar cell,[5] battery,[6] supercapacitor.[7] removal water pollutants,[8] electromagnetic interference shielding and microwave absorption,[9] healthcare monitoring,[10] photocatalysis and opportunities for artificial intelligence,[11] biomedical applications,[12] drug delivery,[13] removal of water pollutants,[14,15] and electrocatalysis.[16]

The physical properties of PANI, PPy, PTH and PEDOT are influenced by their morphology.[16] In this regard, PANI compared to other ICPs has been studied extensively for various reasons till date considering the different morphologies, such as granules,[17] nanoparticles,[17] spongy,[18] dendrite,[19] nano-neddles,[20] nanocables,[21] nanotubes,[21,22] nanofiber,[23] nanowire,[24] nanobelts,[25] nanorods,[26] nanostick,[27] nanoflakes,[28] microspheres,[29] nanocapsules,[30] flower like nanosheet clusters,[31] coral like,[32] honeycomb,[33] worm-like interlinked structures,[34] tetragonal star like,[35] nanospheres[36] etc. Polypyrrole, polythiophene and PEDOT also exist in many of these morphologies. It is well established that manipulation of the morphology could lead the enhancement in the physicochemical properties and the performance of conducting polymers. [37,38] In this regard, 'hollow structure' ICPs with void space inside a distinct shell and its dimensions in the micrometer-/nanometer range have been receiving the considerable amount of attention in recent years.[39-50] The synthesis of such

View Article Online
DOI: 10.1039/D5LP00230C

hollow materials with a single or double shells of various compositions and morphologies has been reported following the hard-templating, soft-templating and template free methods.[49]

Hollow structures can be of different shapes as schematically illustrated in **Figure 2.**[41] From this perceptive, the hollow spheres are considered to be more advantageous than the corresponding solid counterparts due to the presence of the large fraction of empty spaces inside and intact shell(s).[50] The interior geometry, surface functionality, high specific surface area, high conductivity, as well as the controllable chemical and physical properties of the hollow ICPs nanostructures make them the most promising candidates in several application stated earlier.[6,51] In addition, much attention has also been received by nanotubes characterized by their unique hollow tubular structure.[52] Further, the introduction of nanomaterial(s) in these conducting polymers could introduce unique properties, such as high surface area, high electrical conductivity and other features that could enhance their performances in the multifaceted applications.[49-53]

The microwave (MW) radiation emitted from various electrical and electronic devices adversely degrades their performance [9,54] and very harmful to human health.[55] Therefore, electromagnetic interference (EMI) shielding and microwave absorption materials are essentially needed in mitigating such electromagnetic pollution.[56-59] In this context, hollow conducting polymers on combining with fillers (such as magnetic nanoparticles) can also facilitate enhanced electromagnetic interference shielding and microwave absorption due to the dielectric loss owing to the intrinsic conductivity and magnetic loss arising from the polymer and filler respectively. The unique hollow morphology of conducting polymers with increased surface area prevents secondary electromagnetic pollution due to reflection. Furthermore, the presence of multiple internal reflections and the trapping of EM waves contribute to their excellent performance in electromagnetic interference shielding and microwave absorption. It may be noted that hollow ICPs can interact with EM waves and

View Article Online
DOI: 10.1039/D5LP00230C

convert the energy of the microwaves into heat and its dissipation.[9] In addition, hollow PANI and PPy have been extensively studied as adsorbents in the removal of heavy metals and dyes in the water.[60-64] The excellent adsorption performance of hollow conducting polymers in the removal of metals and dyes is ascribed to their large specific surface area and its tunable surface properties. The available functional binding sites in the conducting polymers readily interact with pollutants through various mechanisms and account their effectiveness as adsorbents. Recently, hollow ICPs have also been used in supercapacitor applications due to their low cost and properties.[7] It may be noted that the unique hollow spherical morphology of the ICPs accounts for its larger surface area, significantly lower density, high loading capacity, and shorter ions diffusion paths facilitate achieving the high-power density, fast charge and discharge rates, and long cycle life. [65] In addition, hollow conducting polymers also improve cycling stability by allowing for controlled volume changes during redox reactions.[53]

In recent years, core-shell structured materials formed by the judicious tuning of the core as well as the shell (s) are receiving considerable attention due to their applications in a variety of fields.[66-68] In this regard, the core-shell materials exhibiting enhanced magnetic and dielectric loss has the ability to outperform in electromagnetic interference shielding and microwave absorption.[69] In addition, impedance matching in the core-shell materials creates numerous interfaces for multiple reflections and facilitates attenuation of microwaves due to multiple reflections.[9] Core-shell materials formed by combining a functional conducting polymer shell with a stable core are also receiving more attention as adsorbents in the removal of pollutants in water.[68] The choice is mainly guided by the unique properties of both the core and the shell in achieving high adsorption capacity, separation efficiency, and reusability compared to the conductive polymers exhibiting the low solubility, limited active sites, poor mechanical strength, and separation difficulties. Most importantly, magnetic core can

View Article Online
DOI: 10.1039/D5LP00230C

facilitate the complete separation of the core-shell adsorbents from water by applying an additional magnetic field.[70,71] Core-shell approach has also been used in fabricating ICP based the electrode materials with excellent electrochemical performance in supercapacitor applications.[7] The attractive choice is motivated by the synergistic combination of the core and shell materials leading to the high specific surface area for abundant reaction sites, mechanical stability, good electrical conductivity for fast charge transfer, faster diffusion kinetics, high specific capacitance, and longer cyclability.[72,73]

In view of this, several review articles have appeared in recent years on intrinsically conducting polymers focused on the electromagnetic interference shielding and microwave absorption, [2,9,54,74-80] removal of heavy metal ions [60-64,81-85] organic dyes [60-64,86-91] in wastewater and supercapacitors.[7,65,72,73,92-98] and several others also referred in subsequent sections. However, considering the rapid developments, there exist a lack of a comprehensive review on highlighting the novel contribution of hollow and core-shell intrinsically conducting polymers with their applications in mitigating the electronic/environmental pollutions and their applications in energy storage.

Motivated by this, present review is aimed in highlighting the novel contribution made by intrinsically conducting polymers in this regard by focusing exclusively on hollow and core-shell morphologies across the three distinct application fields (EMI shielding, adsorption, supercapacitors). Accordingly, the present article is focused on preparation of hollow intrinsically conducting polymers (PANI, PPy, PTP, PEDOT) and core-shell materials comprising ICP through different approaches. This is followed by their applications as in electromagnetic interference shielding/microwave absorption, removal of heavy metals ions/dyes in water and supercapacitors **(Figure 1).** Finally, the review article ends with the future perceptive and summary. Overall, the fabrication of unique hollow and core-shell

View Article Online
DOI: 10.1039/D5LP00230C

morphology of important intrinsically conducting polymers and their role in the multifaceted applications reviewed in this article clearly compliments the existing literature

2. Intrinsically Conducting Polymers

Recently, considerable interest has aroused in the inherently conducting polymers (ICPs) during the past decades due to their several advantages, such as easy modification, chemical diversity, corrosion resistance, morphology, and tunable conductivity and applications.[99,100] The different properties of these polymers are related to the conjugated chains with alternating single and double bonds and the delocalized π-electrons.[96] The conducting polymers have been doped by different methods in order to achieve high conductivities.[101-104] In general, conductivity increases with the increasing doping level and becomes saturated at high doping levels for most of the conducting polymers.[105] The doping is introduced in ICPs through the backbone of polymer chain by neutral dopants (I_2, Br_2, AsF_2, H_2SO_4, $FeCl_3$ etc), ionic dopants ($LiClO_4$, $FeClO_4$, CF_3SO_3Na, $BuNClO_4$ etc), organic dopants (CF_3COOH, CF_3SO_3Na etc) and polymeric dopants such as poly(styrene sulphonic acid), poly(vinyl sulphonic acid), and poly(acrylic acid. [106,107]

The electrical properties of conducting polymers are modified by *p*- and *n*-type doping.[105] The delocalization of the charge carriers over the polymer chain accounts for their electronic conductivity.[102] Generally, the negatively charged carriers in *n*-doping are not as stable as positively charged ones. This makes *p*-type doping more attractive in academic research as well as for it's all practical application purposes.[102,108,109]. **Figure 3(A)** describes the electronic and chemical structures of polythiophene as representative conducting polymer subjected to the p-type doping and n-type doping.[102] The electronic bands and chemical structures illustrating undoped, polaron, bipolaron and fully doped states of polypyrrole are also described in **Figure 3(B).**[102.]

View Article Online
DOI: 10.1039/D5LP00230C

3. Synthesis of Hollow and Core-Shell Nanocomposites of Intrinsically Conducting Polymers

3.1 Chemical Methods

3.1.1 Polyaniline

Polyaniline is one of the most common intrinsically conducting polymer and prepared typically by chemical oxidation method using aniline monomer in an acidic medium (HCl or H_2SO_4) in presence of oxidants, such as $FeCl_3$, $(NH_4)_2S_2O_8$, H_2O_2 KIO_3. [110-112] The formation of polyaniline is indicated by the observed change in the colour of the reaction medium. The acidic condition has a vital influence on yield and conductivity of the PANI and appropriate for subsequent doping.[113] According to Armes and Miller,[114] yield and conductivity of the polyaniline in the chemical synthesis depend on the initial oxidant/monomer mole ratio. The investigations are also reported on the influence of polymerization temperature on molecular weight, crystallinity, and electrical conductivity of polyaniline.[115] **Figure 4** describes the chemical polymerization mechanism of polyaniline in the acidic medium.[99] Generally, chemical polymerization of aniline is carried out at 0 to 5 irrespective of the solvent, oxidant and surfactant used.[116-118] The detailed on the synthesis of polyanilines and its properties have also been recently reviewed.[119]

3.1.2 Polypyrrole

Polypyrrole was initially created as a black powdery material by the chemical oxidation of a pyrrole monomer in the presence of hydrogen peroxide.[120] However, processability, morphology, conductivity and environmental stability are some key issues that need to be addressed for wide range application of chemically prepared PPy.[121-123] Polypyrrole has been prepared by combining the anionic surfactants (sodium dodecyl benzene sulfonate, sodium alkyl naphthalenesulfonate, sodium alkylsulfonate) and $Fe_2(SO_4)_3$ (oxidant) exhibiting high conductivity and superior environmental stability [124]

View Article Online
DOI: 10.1039/D5LP00230C

Further studies have also shown the enhanced conductivity and environmental stability of chemically prepared polypyrrole in presence of aqueous solution containing $Fe_2(SO_4)_3$ (oxidant) sulfonic surfactant and a phenol derivative.[125] The chemical oxidative polymerization of pyrrole monomer is usually reported at room temperature in aqueous solution.[126]

The mechanism of pyrrole monomer polymerization has also received considerable amount of attention.[127-131] The most widely accepted polymerization mechanism of PPy is displayed in **Figure 5 (A)**.[128] The oxidation of a pyrrole monomer yields a radical cation in the initiation step. Subsequently, the coupling of the two generated radical cations deprotonation take place to produces a bipyrrole.[130] This bipyrrole in the propagation step is oxidized again and couples with another oxidized segment in the propagation step **(Figure 5 (B)**.[128] Further continuation of the re-oxidation, coupling, and deprotonation ultimately leads to the formation of polypyrrole.

Another chemical oxidative polymerization mechanism of has also been proposed**.** According to this, the radical cation in the propagation step of this mechanism reacts with a neutral monomer.[131] The dimer formed in this manner is oxidized to a dimeric radical cation that subsequently attacks another neutral monomer to form a trimer **(Figure 6 A)**[128] and polymer chains grow by the repeated process to ultimately form polypyrrole**.** Recently, Tan and Ghandi [127] observed that commonly used mechanism **(Scheme 5B)** for polymerization of pyrrole is not well suitable for the formation of in PPy in aqueous medium. Instead, polymerization of polypyrrole mechanism follows a different mechanism as schematically shown in **Figure 6.**[128]

3.1.3 Polythiophene

Polythiophene and its derivatives have been receiving much attention due to their wide range of applications in in electronic devices.[132] The formation of polythiophene can be

View Article Online
DOI: 10.1039/D5LP00230C

accompanied via the chemical oxidative polymerization of thiophene involves by oxidizing thiophene monomers using an oxidizing agent.[133,134] The most commonly accepted mechanism involves the formation of radical cations as a result of the oxidative polymerization of thiophene monomer. The synthesis of different water soluble polythiophenes has been reviewed for their multifunctional applications.[135]

3.1.4 Poly(3,4-ethylenedioxythiophene)

Poly(3,4-ethylenedioxythiophene) (PEDOT) exhibit high conductivity, good physical and chemical stability and facilitates its easy doping and solution processing making it most appropriate in several advanced applications.[136-138] It can be prepared by the oxidative chemical polymerization of EDOT monomers in presence of oxidants, such as $FeCl_3$, $Ce(SO_4)_2$ and $(NH_4)_2Ce(NO_3)_6$,[139,140] oxidative chemical vapour deposition,[141,142] Ha et al [143] studied effect of the processing parameters influencing the oxidative polymerization of 3,4-ethylenedioxythiophene (EDOT) and a methanol-substituted derivative in maximizing the conductivity of the polymer. Ali et al [144] studied the effects of iron(III) p-toluenesulfonate hexahydrate oxidant on the growth of conductive PEDOT nanofilms prepared by vapor phase polymerization.

3.2 Electrodeposition Methods

The electrodeposition method has been proved to be a versatile route for growing the conducting polymers on the substrate for the small-scale synthesis within a short reaction time under mild reaction conditions.[145] This technique is simple, rapid, cost effective and ensures a good control of the micro/nanostructured polymer morphology achieved with accurate process control compared to other technique. [146-153] The process is carried out under usually performed using constant current or voltage approach typically in a three-electrode (reference, working, and counter) cell containing the electrolyte and the monomer solution).The monomer of the conducting polymer undergoes electrochemical

View Article Online
DOI: 10.1039/D5LP00230C

polymerization and subsequently deposited on the surface of the substrate (Ti,[147] Mg,[149] Pt,[150] stainless steel,[150] carbon cloth,[151] glassy C,[152] indium tin oxide,[153] graphite sheet[154] etc. The effect of counter ions on the physical properties of polypyrrole electrochemically deposited on a Pt electrode is reported.[155] The codeposition method has also been reported similar to the electrode coating. by dissolving the insulating polymer (host) in the electrolyte solution that also contains the monomer of the conductive polymer.[156]

Figure 7 describes the electrochemical polymerization mechanisms of polyaniline carried out in the electrolyte solution of aniline and acid through application of a potential difference between the working and counter electrodes.[99]

3.3 Other Methods

In addition, several other preparative methods of conducting polymers have been used, such as photopolymerization,[157] radio-frequency plasma polymerization,[158] organometallic cross coupling reaction[159] and vacuum vapour phase polymerization.[160,161]

The properties of the conducting polymers are influenced by oxidant, monomer molar ratio, type of oxidizing agents, pH, polymerization temperature, time, concentration. electrolyte concentration, and degree of doping.[162-165] The electrical conductivity of most of the conducting polymer increases with dopant concentration and becomes saturated at high doping level.[104] Temperature is another parameter playing a significant role in the synthesis of ICPs. The selection of solvent is also an important factor in the Generally, polymerization of PANI and PPy is reported using solvents like. water, MeOH, THF, DMF, DMSO acetonitrile, propylene carbonate and sea waters.[41,166-168] However, aqueous medium as a solvent is most desirable due to its relatively low cost, ease of handling and nontoxic.

4. Synthesis of Hollow and Core-Shell ICPs

The synthesis of hollow polymeric micro/nanospheres and micro/nanotubes of ICPs have been receiving much attention in recent years due to the promising applications in the

View Article Online
DOI: 10.1039/D5LP00230C

electromagnetic interference shielding and microwave absorption, environmental remediation and energy storage devices. In view of this, ICPs exhibiting multifaceted types of hollow morphology, such as, hollow micros-.nanosphere, micro-, nanotubes, have been achieved through different approaches, This include the direct and template-directed synthesis, core-shell approach, self-assembly and electrospinning and described below.

4.1 Hard Template Method for Single Shelled Hollow ICP s

Recently, template-assisted synthesis has attracted much attention in the fabricating the materials of well-defined morphology with in terms of the shape and the size ranging in nanometer to micrometer range.[169-172] In this regard, template assisted methods are considered as one of most accepted approach in the synthesis of the hollow structured intrinsically conducting polymer materials. These templates can be classified into two types, namely, hard and soft templates, based on the difference in their structure. **(Figure 8 a).**[173] Hard templates are rigid structures in contrast to the soft templates characterized by the flexible structures with each approach guided by its own advantages and disadvantages.[174] The synthesis of materials using different types of templates are schematically shown in **Figure 8 (b)**.[175]

However, the main challenge in the preparation of hollow morphology such as spheres using template methods lies in the availability of the suitable templates of definite size/shape, surface property, production availability and their subsequent removal through chemical or thermal means as an additional step to produce a void space.[176] In this regard, hard template has a very vast advantages, such as adjustable pore structure and morphology, nevertheless, the hard template method also has disadvantages.[171] It usually requires a core surface modification to ensure successful coating of shell substances.[173] Hollow structures can also be prepared by soft template method as the viable option .[175,176] Though, the hard template has high reproducibility and stability, its separation may be troublesome and damage the

View Article Online
DOI: 10.1039/D5LP00230C

structure of the desired materials with hollow morphology.[171] On the other hand, soft template is easier to prepare the nanomaterials of various size, sharp structure due to the simplicity of the process involved and also its easy to removal than the hard template.[171] In addition, the soft template are sensitive to solution environments (pH, solvents, ionic strength etc.) thereby limiting the application of the soft-core template processes.[177] The hollow morphology achieved by the hard template procedure. is guided by its adjustable pore structure and morphology. As a result, several hollow nanostructures can be fabricated considering the availability of the wide range of such hard templates. [178]

4.1.1 Aluminium Oxide

Anodized aluminium oxide (AAO) exhibits regular porous channels and can be prepared by subjecting aluminium to electrochemical oxidation in acidic solutions.[179] The pore diameter of the AAO could be adjusted by controlling the parameters of the anodization process, such as temperature, concentration, current density etc. [180] AAO is used as a template to synthesize 1-D nanostructure due to its several advantages, such as commercially availability, high chemically stability, uniform pore size, and their removal following established methods. Xiong et al. [181] used AAO for the synthesis of highly ordered polyaniline nanotube arrays by in situ polymerization. The electrochemical polymerization method has been used in the preparation of doped and de-doped nanotubes and nanowires of polypyrrole, polyaniline, and poly(3,4-ethylenedioxythiophene) using Al_2O_3 nanoporous templates.[182] In another work, polypyrrole nano-tubule arrays has been prepared by the electrochemical alternating current (ac)-polymerization method using AAO membranes as the template.[183]

Cheng et al.[184] prepared highly uniform and ordered polypyrrole nanotube arrays with the help of the porous anodic aluminium oxide following chemical oxidation polymerization for 2 hours. The functional polypyrrole nanotubes have been fabricated using the anodized aluminium oxide membrane as template in liquid phase polymerization conditions.[185] In

View Article Online
DOI: 10.1039/D5LP00230C

another method, Jang et al [186] adopted one-step vapour deposition polymerization in synthesizing highly uniform surface and tuneable wall thickness polypyrrole nanotubes using anodic aluminium oxide template membranes soaked in ferric chloride aqueous solution.

The quasi- polyaniline hollow nanotubes (outer dia: 230 nm) were prepared by dipping method based on the highly ordered porous anodic alumina membrane.[187] Poly (3, 4-ethylenedioxythiophene) tosylate film was grown in confined anodized aluminium oxide (nanopores) transferred onto cleaned ITO glass substrates following the chemical polymerization of the mixture comprising the solution of EDOT, iron (III)-tosylate in butanol and pyridine.[188] Liu et al [189] electrochemically synthesized PEDOT nanotube arrays in the cylindrical pores of an alumina template membrane using acetonitrile solution of 20 mM EDOT.

4.1.2 Mesoporous Silica

Mesoporous silica has attracted attention in various applications due to its high specific area, good hydrophobicity, low cytotoxicity, large pore volume and tunable pore size.[171,190.] Mesoporous silica has also been used as a template in the preparation of intrinsically conducting polymers, like PANI and PPy with hollow structures. The process involves coating silica particles with PANI (PPy) followed by the expulsion of the silica template (core) by etching it in NaOH or HF to leave behind a hollow PANI (PPy) shell, respectively.

Fu et al [191] prepared initially silica nanoparticles with surface grafted polymer of 4-vinylaniline (SiO_2-g-PVAn) according to the scheme as displayed in **Figure 9 (a).** Subsequent surface oxidative graft copolymerization of aniline using the aniline moieties of PVAn and deprotonation followed by exposure to HF produced hollow nanosphere of P(VAn-graft-PANI) (Thickness of shell: ~ 15-40 nm, Core void dia: ~ 25 nm). Mesoporous polyaniline hollow nanosphere with its average diameter and thickness of 330 nm shell 78 nm,

View Article Online
DOI: 10.1039/D5LP00230C

respectively has been prepared using SiO_2@resorcinol-formaldehyde/SiO_2 as substrate followed by in situ polymerization of aniline on its surface and subsequent expulsion of the silica shell by dispersing it in HF at room temperature.[192] Li et al [193] prepared Pt/PPy hollow hybrid microspheres by using NH_2-functionized SiO_2 as template decorated by the H_2PtCl_6. **(Figure 9 (b)).** In another work, SiO_2/Polymethacrylic acid (PMAA) microspheres were used as templates to synthesize hollow polypyrrole microspheres **(Figure 9 (c)).**[194]

4.1.3 Organic Polymers and Other Inorganic Materials

4.1.3.1 Hollow Polyaniline

Among several hard templates, polystyrene microspheres attracted more attention in synthesizing the spherical-shaped particles, spherical core-shell and the hollow structure.[195-199] Bai et al [200] prepared colloidal hollow spheres of conducting polymers (PANI and PPy) by using sulfonated polystyrene beads as templating agent. In another work, hollow PANI and PPy microspheres were prepared by oxidative chemical oxidation of the respective monomers using sulfonated polystyrene microspheres as template (size: 2.2–3.4 μm).[201] Niu et al [202] prepared PANI capsules and hollow PANI spheres with controlled shell thickness and cavity size using sulfonated polystyrene as a template. Sulfonated polystyrene particles have been used as template to synthesize hollow polyaniline [203] and polypyrrole [204] by emulsion polymerization of the individual monomers in acid solution and ammonium persulphate (oxidant). Saraf et al [205] prepared hollow microsphere of PANI doped with styrene sulfonic acid (size: 0.5-1 μm) through chemical route by maintaining dopant: monomer: oxidant ratio as 1:1:1.

Mangeney et al [206] used polystyrene latex particles (dia:1.33 μm) to prepare PPy-coated PS latex polystyrene bearing surface protonated N-propyl amino functional groups in aqueous solution by copolymerization of pyrrole and *N*-aminated pyrrole (pyrrole-NH_2) using $FeCl_3$. Further, fabricated PS-PPyNH_2) particles were subsequently decorated with citrate

View Article Online
DOI: 10.1039/D5LP00230C

stabilized gold nanoparticles, as shown in **Figure 9(d)**. The uniform polyaniline thin shells and hollow capsules were fabricated using polyelectrolyte-coated microspheres as templates.[207] Monodisperse hollow polyaniline nanospheres with controlled surface smoothness were synthesized by in situ polymerization of aniline monomers adsorbed on a carboxyl functionalized polystyrene surface.[208] In another work, Sung et al [209] synthesized submicron size hollow PANI dicarboxylate salt to study the influences of alkyl chain length, functional group and stable dispersion on its electrorheological performance.

Polyaniline/Au composite hollow spheres were successfully synthesized using polystyrene/sulfonated polystyrene using as the templates.[210] The thickness of PANI shell can be well controlled by adjusting the amount of aniline monomer. **Figure 10 (A-D)** shows morphology of PANI (A: SEM; C: TEM) and PANI/Au (B: SEM; D: TEM) composite hollow spheres under specified preparative conditions. The possible formation of hollow PANI spheres and its Au composites are presented in **Figure 11.** Gao et al [211] fabricated hollow polyaniline microspheres in presence of Cu rings as template using $H_4SiW_{12}O_{40}$ and ammonium persulfate as dopant and oxidant, respectively. Zhang and Liu [212] synthesized hollow polyaniline nanoparticles via the chemical oxidative polymerization of aniline using the γ-Fe_2O_3 nanoparticles as the reactive templates in the presence of hydrochloric acid. Their studies have shown reacting temperature playing a vital role in the formation of the hollow nanoparticles. The halloysite was used as hard-template to prepare polyaniline–polypyrrole binary composite nanotube.[213] Gao and coworkers [214] demonstrated fabrication of polyaniline nanotubes using the inner eggshell membrane as a template. Their investigations revealed the key role the pore size of the template in the formation of polyaniline nanotubes.

Zhu et al. [215] reported double surfactant-layer of polyvinylpyrroldine (PVP) and sodium dodecyl sulfate (SDS) assisted oxidative polymerization using monodispersed metal oxides (CuO, Fe_2O_3, In_2O_3) as templates **(Figure 12 (a).** Following this, hollow PANI

View Article Online
DOI: 10.1039/D5LP00230C

nanocapsules were prepared by dissolving metal oxides it in acid solution. The method has also been used to prepare nanocomposites of CuO/PANI, Fe_2O_3/PANI, In_2O_3/PANI and Fe_2O_3/Si O_2/PANI. Further investigations revealed the formation of well-controlled core/shell metal oxides/PANI nanocomposites and PANI capsules. Hollow octahedral PANI nanocapsules are fabricated using Cu_2O (octahedral) as template in presence of H_3PO_4.[216,217] It may be noted that the removal of Cu_2O template is not required compared to other conventional methods due to its reaction ammonium persulfate (oxidant) to form a soluble Cu^{2+} salt during the process of the polymerization. The synthesis of nanoring's and flat hollow capsules of polyaniline were also reported via the chemical oxidative polymerization of aniline using $VOPO_4$ $2H_2O$ nanoplates acting as oxidant and sacrificial template.[218]

4.1.3.2 Hollow Polypyrrole

More common synthetic approach in the fabrication of the hollow polypyrrole microsphere were followed by core (polystyrene, PS)/shell (polypyrrole) approach. This involved the in-situ chemical oxidative copolymerization of pyrrole monomer on the surface of sulfonated PS microsphere followed by the extraction of the PS cores in suitable solvent like tetrahydrofuran. [219-224] Zhang et al [225] prepared polypyrrole-polystyrene (PPy-PS) hybrid hollow spheres by oxidative polymerization of pyrrole $FeCl_3$ $6H_2O$ in an emulsion of PS latex as shown in **Figure 12 (b).** It is suggested that the formation of PPy-PS. hybrid hollow spheres could be induced by capillary force that exist among the PPy nanoparticles (granular) deposited on the surfaces of PS latex at the initial of reaction. Hollow polypyrrole microcapsules (dia: 527 nm, shell thickness: 20 nm) are reported by the cosolvent approach using polystyrene core as a template.[226] Marinakos et al [227] used Au nanoparticles as templates in synthesizing nanometer-sized hollow PPy nanocapsules. Mesoporous hollow polypyrrole spheres has been fabricated by chemical polymerization method using silica spheres as hard templates.[228] Su et al [229] reported synthesis of polypyrrole hollow nanospheres using

View Article Online
DOI: 10.1039/D5LP00230C

poly(methyl methacrylate) nanospheres as templates. Chang et al [230] carried out in situ polymerization of pyrrole in the presence of polystyrene (PS) latex particles. Subsequent removal of core (PS) resulted in the formation of hollow spherical polypyrrole balls.

According to Qu and Shi,[231] the direct electrochemical oxidation of pyrrole in an aqueous solution of poly(styrene sulfonic acid) resulted in the microstructures with hollow interiors comprising of microspheres, microcrocks, microbowls, micropumpkins. A stepwise electropolymerization process has been adopted in producing the nanostructured arrays of hollow polypyrrole with a conical shape.[232] The pores of nanoporous polycarbonate membrane were used as templates to chemically synthesize polypyrrole nanotubules.[233] Kros et al [234] carried out the polymerization of monomers (e.g., pyrrole, thiophenes) inside the pores of track-etched polymeric membranes. The hollow tubules formed in this manner exhibited relatively enhanced electrical properties compared to their respective bulk analogues.d In another work, ZSM-5 molecular sieve used as template to synthesize hollow pyrrole–platinum complex spheres following the chemical polymerization of pyrrole with potassium hexachloroplatinate (IV) as oxidant.[235] Dubai et al [236] synthesized polypyrrole nanotubes using MnO_2 as sacrificial template in presence of pyrrole 1 M HCl and $K_2Cr_2O_7$. Hollow nanotubes of polypyrrole has been prepared rapidly by chemical oxidative polymerization of pyrrole in the presence of V_2O_5 nanofibers (sacrificial template) and FeCl3 as oxidant. This is followed by the removal of template by dissolving it in aq. 1.0 M HCl.[237] In another work, MnO_2 powder has been selected for simultaneously dual role as oxidizing agent as well as sacrificial template in the chemical synthesis of hollow sea urchin shaped polypyrrole.[238] In another work, polystyrene beads were used as the sacrifice template to prepare hollow polypyrrole nanoparticles.[239] Capsular PPy hollow nanofibers were fabricated by polymerizing pyrrole monomer on hollow V_2O_5 fibers (template) and subjecterd to acid

View Article Online
DOI: 10.1039/D5LP00230C

etching to remove the V_2O_5 template.[240] In addition, Fe_3O_4@polypyrrole hollow capsules [241] and Fe_3O_4@PPy yolk/shell composites [242] were also prepared by hard-template method.

4.1.3.3 Hollow Poly(3,4 ethylenedioxythiophene) (PEDOT)

Rehmen et al [243] carried out vapor deposition of tosylate-doped PEDOT in fabricating the hollow nanosphere coatings using polystyrene as template on carbon paper electrodes. In another work, PEDOT hollow nanospheres were successfully synthesized from SiO_2/PEDOT core/shell nanospheres by subjecting SiO_2 to chemical oxidative polymerization followed by etching of SiO_2 by hydrofluoric acid.[244] Luo et al [245] coated functionalized PEDOT on polystyrene core in aqueous solutions. The subsequent removal of this core by dissolving it in the appropriate organic solvent produced hollow PEDOT particles with single holes and PEDOT capsules. According to Zhang et al,[246] PEDOT hollow spheres were fabricated using sulfonated polystyrene spheres template-assisted interfacial polymerization and introduced in the MXene film as attractive flexible electrode for energy storage. ZnO microflower arrays has been used as template to synthesize hollow microflower arrays of PEDOT with several two-dimensional hollow nanopetals on each microflower.[247] Cheng et al [248] electrodeposited poly(3,4-ethylenedioxythiophene) hollow microflowers film on fluorine-doped tin oxide glass substrate using a film of ZnO microflowers as the template.

4.2 Soft Template Method and Template Free Approach for Single Shelled ICPs

The choice of soft template is guided by its multifaceted advantages such as the simplicity of the process, good repeatability and with no requirement on its removal. This method is invariably used in the synthesis of conducting polymers nanotubes, hollow spheres and yolk-shell sphere type materials [173,176,249-253] In this regard, several structural directing agents such as surfactants, block copolymers, amino acids, urea, methyl orange etc. The presence of these molecule aligns the monomers of the conducting polymers in solution and

View Article Online
DOI: 10.1039/D5LP00230C

account for facilitating the overall polymerization process into the desired nanostructures like tubes or spheres by forming micelles or self-assembled structures around the monomers.

4.2.1 Hollow Polyaniline

Zhang et al, [254] used a self-assembly method. to synthesize PANI nanotubes (dia: 150-340 nm) in the presence of inorganic acids (e.g., HCl, H_2SO_4, HBF_4, and H_3PO_4) as dopants with and without a surfactant. In presence of a surfactant (sodium dodecylbenzenesulfonate and hexadecyltrimethylammonium bromide), formation of the nanostructures takes place die to the formation of micelles by anilinium cations and surfactant anions acted as templates, whereas micelles anilinium cations formed in the absence of a surfactant. were considered as templates Further investigations indicated morphology, size, and electrical properties of the resulting nanostructuresare to be guided by experimental conditions and dopant structure. The role of acidity profile in the nanotubular growth of polyaniline has been analysed to study its preparatory conditions by oxidizing aniline with ammonium peroxydisulfate in 0.4 M acetic acid.[255.] These findings indicated that the neutral aniline molecules are oxidized to non-conducting aniline oligomers` at pH > 3 and act templates for the subsequent growth of PANI nanotubes.

Han et al[256] synthesized polyaniline nanotubes by the oxidative polymerization of aniline in dilute solution in the presence of cetyltrimethylammonium bromide. The self-assembled PANI nanotubes comprising the rectangular cross sectional shape have been synthesized by in-situ chemical oxidation polymerization in presence of citric acid as the dopant.[257] In another study, Zhang et al [258] prepared polyaniline nanotubes (outer dia: 165–240 nm, inner dia: 10–70 nm) by a self-assembly process using carboxylic acids (propionic acid, lactic acid, succinic acid, malonic acid, tartaric acid, and citric acid) as dopants. They also investigated the effect of hydrogen bond on the formation of nanotubes and aggregated dendrites of polyaniline. The highly crystalline polyaniline nanotubes and nanofibers have

View Article Online
DOI: 10.1039/D5LP00230C

been synthesized in the presence of dicarboxylic acids (oxalic acid, malonic acid, succinic acid, glutaric acid, and adipic acid) acting as-dopants).[259] Zhang et al [260] fabricated nanotubular polyaniline (self-assembled) following the chemically synthesized by ammonium persulfate oxidation of aniline in presence of amino acid. The role of the amino acids in this work is guided by their effect on the initial soft-template for the growth of nanotube based on the formation of micelles or oligomeric species during the initial stage of aniline oxidation. Rana et al [261] used soft template method to prepare PANI nanotubes of almost uniform diameter by selecting benzene 1,2,4,5-tetracarboxylic acid acting simultaneously as dopant acid as well as structure-directing agent. Huang and Wan [262] investigated the influence of molecular structure of sulfonic acids on tubular morphology of the doped PANI. According. to this, β-NSA doped PANI exhibited tubular morphology by preparing it by in situ doping polymerization method. Hollow PEDOT spheres (dia: 1.7–4.6 μm) was synthesized by aqueous chemical polymerization using self-assembled membrane of poly(3,4-ethylenedioxythiophene) doped with acetic acid at room temperature and ammonium persulfate as oxidant.[263]

Alternatively, synthesis of self-assembly polyaniline nanostructure has also been reported using itaconic acid,[264] camphor sulfonic acid,[265] polymeric acids: poly(4-styrenesulfonic acid), poly(acrylic acid), poly(methyl vinyl ether-alt-maleic acid),[266] malic acid, succinic acid, citric acid, tartaric acid [267] as dopants. Mu et al [268] reported the fabrication of self-assembled polyaniline nanotubes doped with D-tartaric acid for high-performance supercapacitor applications. Zhang and Wan [269] synthesized chiral polyaniline nanotubes following the self-assembly process using the (1R)-(−)-10-camphorsulfonic acid (L-CSA) and (1S)-(+)-10-camphorsulfonic acid (D-CSA). It is noted that the formation yields and the size of the doped polyaniline nanotubes is guided by the molar ratio of CSA to aniline. Panigrahi and Srivastava [270] reported synthesis of polyaniline hollow microspheres by the ultrasound assisted emulsion polymerization technique using polystyrene microspheres as a template,

View Article Online
DOI: 10.1039/D5LP00230C

Zhang et al [271] reported a self-assembly process for the syntheses of polyaniline nanotubes (dia:130–250 nm) doped with α-naphthalene sulfonic acid, β-naphthalene sulfonic acid, 1,5-naphthalene disulfonic acid. According to Sun and Deng,[272] DL-tartaric acid played an important role as a dopant in determining the morphology of polyaniline prepared by interfacial oxidation polymerization of aniline using APS as the initiator. These findings led to the formation of spherical mushroom-like morphology and nanotubes of polyaniline corresponding to the DL-tartaric acid concentration of ~ 0.02 M and ~0.04 M respectively

Qiu et al [273] synthesized polyaniline nanotubes (dia:100-300 nm, length: up to 2 μm) through a template-free polymerization using $(NH_4)_2S_2O_8$ as an oxidant and a protonic acid dopant (C_{60}-$(OSO_3H)_6$ or $PAMAM_{4.0}$ [naphthyl $(SO_3H)_2]_{24}$). The formation of oriented arrays of polyaniline nanotubes (60 to 150 nm in diameter) are also reported by hydrogen-bonding directionality in the presence of a crown ether derivative and ammonium persulfate in HCl solution.[274] Poly (2-acrylamido -2-methylpropane sulfonic acid) has been used as a dopant as well as soft template for the synthesis of uniform hollow microsphere of PANI (dia: 410 nm, shell thickness: 72 nm) in aqueous solution following in situ polymerization of aniline in presence of ammonium persulfate.[275] Huang et al [276] reported a template-free method following inversed microemulsion polymerization in fabricating polyaniline hollow microspheres (outer dia: 4-6 mm, shell thickness: 150-250 nm) using β-naphthlene sulfoinic acid as dopant. Zhu et al [277] prepared superhydrophobic rambutan-like hollow spheres of polyaniline by a self-assembly method in the presence of perfluorooctane sulfonic acid (dopant and soft template).

Zhang and Wan [278] reported transformation of self-assembled polyaniline from 1 D nanotubes (dia: ~109-150 nm) to hollow microspheres by changing the molar ratio of the dopant (salicylic acid) to monomer (aniline). The freeze electron microscopy studies revealed

View Article Online
DOI: 10.1039/D5LP00230C

the role of hollow spherical micelles comprising of salicylic acid/aniline as templates in the formation of nanotubes/hollow spheres. The driving force in the self-assembly of hollow microspheres might be due to be the hydrogen bond of -OH group (salicylic acid) and amine group (polyaniline). Liang et al [279] synthesized polypyrrole nanotube aerogels by using the weakly interconnected network of self-assembled nanotubes of lithocholic acid as a soft template.

Hollow nanospheres of methyl substituted polyaniline [280] and poly(*m*-methylaniline) [281] microspheres were prepared through the self-assembly processes in presence of ammonium persulfate. Tavandashti et al [282] studied transition of polyaniline from nanotubes to nanospheres following a soft template route as schematically displayed in **Figure 13 (a,b)**. According to this, the fabrication of polyaniline nanospheres was carried out via the oxidative polymerization of aniline in the presence of β-naphthalenesulfonic acid (β-NSA) as both surfactant and dopant, and am monium persulfate as oxidant at 2–5 ^{0}C. Further, the morphology control of polyaniline was achieved by changing the reaction conditions. Ding et al [283] prepared PANI nanotubes with diameters of 100–150 nm of single nanotubes by carrying out by the direct oxidation with APS in the absence of hard templates and acidic dopants. During this, the formation of the hollow spheres at the initial stage is accompanied by the micelles (soft template) formed by the aniline monomer in aqueous solution. Further, investigations revealed decrease in pH with increasing polymerization time resulted the change on the morphology from the hollow spheres to short and long tubes. Triton X-100 has been selected as soft template to fabricate poly(aniline-copyrrole) hollow nanospheres via oxidative polymerization of aniline.[284] In micelles-mediated phase transfer method, perfluorooctanoic acid/aniline acted as soft templates to form hollow nano/microspheres of polyaniline with mesoporous brain-like convex-fold shell structures.[285]

View Article Online
DOI: 10.1039/D5LP00230C

Vitamin C upon the addition of aniline monomer ([Vitamin C]/[Aniline] = 0.25) produced polyaniline nanotubes (dia.: 80–120 nm, length extending to several micrometers) *via* the oxidative polymerization method.[22] Ren and others [286] adopted a soft template method in the fabrication of polyaniline microtubes acidic solution using methyl orange as dopant in the presence of aniline monomer and ammonium peroxydisulfate. According to this, methyl orange is self-assembled into supramolecular aggregates and acts as templates in the formation of PANI microtubes. Urea has also been used as a soft template in the synthesis of polyaniline nanotubes by in situ chemical oxidative polymerization of aniline monomer.[287] Orellana and Roberts [288] used a simple approach to preparing polypyrrole microtubes without the need for a solution or substrate-based template. Wang et al [289] synthesized polypyrrole nanotubes of ~50 nm diameter and a length extending to several micrometers using pyrrole, $FeCl_3 \cdot 6H_2O$, and methyl orange as monomer, initiator, and soft template respectively.

A self-assembly method has been used to synthesize polyaniline nanotubes in the excess of $(NH_4)_2S_2O_8$ oxidant.[290] This could be ascribed due to the formation of aniline dimer cation-radicals acting as effective surfactants. Zhang et al [291] fabricated polyaniline hollow spheres with controllable size and shell thickness through the oxidation-reduction reaction driven approach under hydrothermal conditions in the absence of any sacrificial templates and organic surfactants and using H_2O_2 and Fe^{3+} as oxidant and catalyst, respectively. Hollow polyaniline microsphere were also been prepared by polymerization of aniline in aqueous medium using $K_3[Fe(CN)_6]$ as oxidant.[292] Wei and Wan [293] synthesized hollow microspheres of PANI (dia: 450-1370 nm) using aniline emulsion template doped with ß-naphthalene sulfonic acid at –10 °C in presence of ammonium persulfate acting as the oxidant. The investigations are also reported on the synthesis formation of PANI nanotubes, nanotubes with

View Article Online
DOI: 10.1039/D5LP00230C

rectangular and circular cross section hollow microsphere [294] and 3D hollow microspheres assembled from 1D PANI nanowires.[295]

Liu et al [296] reported a template-free method to synthesize polyaniline film (Thickness: 100 nm) embedded with PANI nanotubes without any surfactant or organic acid. Their studies revealed that oligomers with certain structures are responsible for the growth of the nanotubes. A micelle soft-template method was used in fabricating PANI nanotubes (External dia: 110 internal dia:, 10 nm, length: several μm) in the presence of oxalic acid as a dopant.[297] Tajima et al [298] used nanobubble soft templates formed by ultrasonic irradiation in the synthesis of hollow polypyrrole spheres.

4.2.2 Hollow Polypyrrole, Polythiophene and PEDOT

In comparison to polyaniline, fabrication of other hollow ICPs, especially polythiophene and polythiophene and PEDOT received lesser attention. Bhetattara al [299] employed a sacrificial template-based synthetic approach in fabricating polypyrrole hollow fiber by using sacrificial removal of electrospun polycaprolactone acting as a soft template. In another method, one step in-situ polymerization has been employed to synthesize azo functionalized polypyrrole nanotubes in presence of $FeCl_3$ and methyl orange.[300] In this, the formation of fibrillar complex of $FeCl_3$ and methyl orange acts as reactive self-degraded template to facilitate hollow nanotubular structure of PPy. Wang et al.[301] prepared micro/nanoscale highly electroactive PPy galvanostatically with hollow 'horn' like structure in a p-toluenesulfonate alkaline solution without any templates.

Xia et al [302] used poly(vinylpyrr1olidone) (PVP) as a soft template on order to fabricate PEDOT exhibiting hollow spheres (size:130-820 nm) via self-assembly method**.** Bian et al [303] used star like unimolecular micelles as templated for the controlled syntheses of hollow nanostructure of polythiophene nanoparticles, A reverse emulsion polymerization is described using sodium bis(2-ethylhexyl) sulfosuccinate cylindrical micelles as the template at room

View Article Online
DOI: 10.1039/D5LP00230C

temperature for synthesis of PEDOT nanotubes (dia: 50-100 nm, length: 10-20 mm).[304] The synthesis of self-assembled 3D hierarchical PEDOT micro/nanostructures including hollow spheres and double-layer bowls from 1D-nanofi were carried by a template-free method in the presence of the perfluorosebacic acid as the dopant and $FeCl_3$ $6H_2O$ as the oxidant.[305] Ali et al [306] synthesized PEDOT/Au hollow nanospheres by in-situ polymerization method comprising the ratio of EDOT and $HAuCl_4$ from 2:1 to 1:2. In another study, surfactant free Ouzo emulsion method was used to synthesize hollow or partially collapsed bowls of PEDOT using $FeCl_3 \cdot 6H_2O$, acetone, and toluene as oxidant, solvent, and anti-solvent, respectively (**Figure 14 a)**.[307] This method has also been extended in successfully synthesizing PANI, PPy and PTh. **Figure 14 (b-d)** describe the SEM images of PEDOT under different experimental conditions. Ni et al [308] used chemical polymerization of EDOT to synthesize hollow PEDOT microsphere in presence of ammonium persulfate (oxidant) and PVP (micelles). Sui et al [309] synthesized hollow microspheres of PEDOT (size: 0.5 to 10 μm) by chemically oxidative polymerization of EDOT using ammonium persulfate in a catanionic surfactant solution comprising mixture of cetyltrimethylammonium bromide and sodium dodecylbenzenesulfonate. Recently, Ge et al [195] prepared honeycomb-shaped photothermal polypyrrole by electropolymerization.

4.3 Electrospinning Method

Electrospinning is relatively inexpensive, simple and versatile method used in fabricating hollow (and core-shell polymer fibers) for their variety of applications.[310,311] The electrospun poly(amic acid) fiber membrane has been used as a template to fabricate hollow polyaniline nanofibers by in-situ polymerization of aniline.[312] The formation of highly aligned PEDOT nano- and microscale fibers and tubes are reported based on this technique and oxidative chemical polymerization,.[313] The electrospinning preparation methods of several other hollow conducting polymers are described in subsequent sections under applications.

4.4 Synthesis of Double Shelled Hollow Spheres of ICPs

In comparison to single shell hollow spheres, hollow-spheres with multi-shell structures receive extra advantages from inner structures.[314] The permeable shell and void space between each shell in the unique hollow structure accounts for interesting properties, such as, sequential absorbing/scattering peculiarity, shorten the diffusion distance for mass and charge transport for their multifaced applications. In this regard, very limited work has been reported on the preparation of intrinsically conducting polymers exhibiting double shell type of morphology. Bei and Xia [315] reported synthesis of double-shelled polypyrrole hollow particles with a structure similar to that of a thermal bottle using polystyrene hollow spheres (templates) containing a hole on the surface were used as templates. The choice of such template facilitated the diffusion of monomer and act as a initiator to form uniform PPy coatings on its inner and outer surfaces. Subsequently, selectively removal of PS by dissolving in tetrahydrofuran (solvent) resulted in the formation of double-shelled polypyrrole hollow particles with a structure resembling that of a thermal bottle. Niu et al [316] used iron oxide hollow microspheres as both the sacrificial template and initiator in acidic solution to prepare double-shelled polypyrrole hollow microspheres. According to Gu et al,[317] MnO_2 nanorods is selected as a self-sacrifice template formed double shelled hollow polypyrrole nanotubes by in-situ polymerization of pyrrole monomer in the presence of hydrochloride acid and sodium p-styrene sulfonate.

4.5 Synthesis of Hollow Nanocomposites of ICPs and Core-Shell Structures

Recently, hollow and core@shell composites have been receiving considerable attention due to the effective combination and displayed interesting properties with great promise for their broad range of applications in many fields.[67] In this regard, intrinsically conducting polymer derived composites have gained significant recognition due to their unique properties, such as environmental stability, processability, and less corrosive with

View Article Online
DOI: 10.1039/D5LP00230C

tunability.[72,73] In addition, such ICP based binary and ternary core-shell nanocomposites offer the advantage in its properties due to the combination of the core and the shell.[75] Core–shell nanostructured materials can be prepared by the physical and chemical methods. However, the chemical synthesis of hollow and core-shell ICP nanostructures are well recognised compared to physical methods. This is mainly due to the their greater versatility, precise control, and ability to use templates unlike in physical methods which invariably requires complex equipment's. In view of this, preparative methods of these hollow and core-shell composites are ICP are described in the subsequent sections under their applications in the field of electromagnetic interference shielding/microwave absorption, removal of metal ions/dyes and supercapacitors.

Recently, the electrodeposition is a promising method in fabricating the ICP based core-shell materials, though, its potential is yet to be harnessed. as superior electrode in supercapacitors.[145,318] This is ascribed to the superior control over morphology, enhanced performance through binder-free synthesis, and improved interface between the polymer and substrate., Chen et al [319] synthesized polypyrrole (binder-free) on the carbon cloth acting (working electrode). Core-Shell nanorod arrays with polyaniline was successfully electrodeposited into mesoporous $NiCo_2O_4$ support.[320] Wu et al.[321] polypyrrole-coated low-crystallinity Fe_2O_3 supported on carbon cloth by a combination of chemical reduction and electrodeposition methods. The preparation of free-standing Graphene/Polyaniline/MnO_2 ternary composite by the sequential electrodeposition on carbon cloth as working electrodes.[322] In another work, electrodeposition of PANI on the surface of GO/α-MnO_2 has been used to prepare hierarchical GO/α-MnO_2/PANI composites.[323] This electrodeposition technique has also been used in fabricating $CoCrFeMnNi)_3O_4$@CC-PPy,[324] $LaMnO_3$@CC-PPy,[325] porous PPy/black phosphorus oxide composites electrodeposited on CNT.[326] In

View Article Online
DOI: 10.1039/D5LP00230C

another approach, Fauzi et al [327] used oxidative chemical vapor deposition to deposit the submicrometer thick layer of PPy on the carbon fabric.

5. Application of Hollow ICPs, their Cire-Shell Nanocomposites

5.1 Electromagnetic Interference Shielding and Microwave Absorption

In recent decades, uses of rapid and extensive devices have contributed in the electronic pollution due to the electromagnetic interference. limiting their applications and also threating the human life **(Figure 15)** [328] In this regard, development of electromagnetic shielding and microwave absorbing materials have recently been receiving considerable attention When an electromagnetic (EM) wave perforates through the shielding material, primarily, it involves primarily three processes namely reflection, absorption, and multiple reflection occur.[2] The shielding performance of a materials is expressed by term electromagnetic interference shielding effectiveness (EMI SE). The total EMI SE (SE_T) measures the ability of a material to block the EM waves and expressed in decimal (dB) as a function of the logarithm of the ratio of the power P, electric E, or magnetic H field intensities before and after EM attenuation, i.e.

$$SE_T(dB) = 10\log\left(\frac{P_1}{P_2}\right) = 20\log\left(\frac{E_1}{E_T}\right) = 20\log\left(\frac{H_1}{H_T}\right) \quad (1)$$

, where I and T represent the incident and transmitted components.[203,204]

Further, SE_T is sum of shielding efficiency originating from absorption (SE_A), reflection (SE_R) and multiple reflections (SE_M),[9] i.e.,

$$SE_T = SE_R + SE_A + SE_M \quad (2)$$

The factors affecting the shielding effectiveness include permeability, permittivity, skin depth and thickness, external physical properties, eddy current loss, magnetic loss, dielectric loss, size and morphology etc.[54] The impedance matching ratio, $|Z_M Z_0|$ (Z_{in}: input impedance, Z_0; free space impedance) is also another important factor that provides infomation on EM waves entering the shield. It may be noted that the reflection loss (R_L) of a shielding material is

View Article Online
DOI: 10.1039/D5LP00230C

closely related to the input impedance (Z_{in}) and free space impedance (Z_0). According to the transmission line theory, both Z_{in} and R_L are expressed as shown below.[9] $Z_{in} = Z_0$

$$Z_{in} = Z_0 \sqrt{\frac{\mu_r}{\varepsilon_r}} \tanh\left[i \frac{2\pi f t}{c} \sqrt{\varepsilon_r \mu_r}\right] \quad (3)$$

$$R_L = 20\log 10\left|\frac{Z_{in} - Z_0}{Z_{in} + Z_0}\right| \quad (4)$$

, where t, ε_r and c represent thickness of the absorber relative dielectric permittivity and velocity of light in free space, respectively.

The methods commonly used to measure the electromagnetic shielding efficiency (also referred as effectiveness) of a material could be based on the space transmission, shield box, shield room and coaxial transmission line approach.[75]

In this regard, more interest has been focused recently in developing electromagnetic wave (EMW) shielding materials undergoing absorbing mechanism.[9] This is because EMW following the reflection mechanism undergoes secondary pollution due to their reflection to the environments. Accordingly, conductive polymers have been receiving considerable attention guided by their choice due to their conductivity, light weight, corrosion resistance and processibility.[9] In this regard, morphology of the intrinsically conducting polymer remains one of the materials is considered as vital parameter in their functioning as EMW absorbers. This is ascribed to successive internal reflection (multiple internal reflections of incident EM waves.[204,329-333] The hollow microhemisphere like polypyrrole and carbon dielectric materials could act as promising high-performance microwave absorbers with strong reflection loss and wide absorption frequency bandwidth.[332]

According to available literature, electromagnetic-wave absorption materials has proven to be a very effective in mitigating electromagnetic pollution and interference.[9] The choice of an ideal microwave absorber materials is guided by lightweight, good thermal stability, antioxidation capability, multi-interfaces, impedance matching, synergistic effects,

strong absorption properties wide bandwidth simultaneously.[54,333-335] In addition, other important features that affect the absorption of microwaves include complex permittivity/permeability, impudence matching and morphology of these materials.[9] In such studies, choice of ICPs in improving the microwave absorbing properties is guided by its low cost of synthesis and great environmental stability as hollow core or as film on the magnetic (Co, Ni, Fe_2O_3, Fe_3O_4 etc) and dielectric (carbon, carbon nanotubes, graphene, graphene oxides, SiO_2 etc) materials in forming core-shell composites could be most benefitting owing to high electric and magnetic losses, respectively.[334]

Among these, Fe_3O_4 has drawn a great deal of attentions because of its low cost, easy synthesis, saturation magnetization value and high Curie temperature.[9,] However, several drawbacks of Fe_3O_4 such as ease of oxidation, high density, dramatic decrease of permeability in high frequency range due to the Snoek's limit, weak interfacial compatibility and substrate dispersion difficulty need to be addressed.[9,334,335] In view of this, combining ICPs with magnetic materials could be more effective in enhancing the electromagnetic wave attenuation synergistically.[329] Further, outstanding performance can also be achieved by combining dielectric and magnetic components together.[336]Accordingly, most studies are focused on Fe_3O_4 in the form of binary composites with ICP or its ternary nanocomposites involving ICPs and carbonaceous materials. It may be noted that hollow structures of Fe_3O_4 nanospheres and PANI reduces the weight of the composites. In addition, they also prolong the transmission path of microwaves as result of multiple reflection and scattering loss.

5.1.1 Hollow ICP Micro-/Nanospheres

Self-assembled 3D helical hollow superstructures of polyaniline (20 wt%) filled with epoxy to (thickness: 2.0 mm) exhibited the lowest R_L value (-51.60 dB at 13.95 GHz) and the effective absorbing bandwidth ($R_L < -10$ dB) reached 5.12 GHz (12.03–17.15 GHz).[337] Wan et al [332] fabricated hollow polypyrrole microhemisphere (HPMs) and hollow carbon

View Article Online
DOI: 10.1039/D5LP00230C

microhemispheres (HCMs) by sol-gel method using SiO_2 microspheres as the templates and investigated its microwave absorption properties. The studies have shown the better microwave absorption properties in HCMs (reflection loss, R_L: -63.9 dB at 8.0 GHz, thickness:5 mm) compared to the HPMs (R_L: -23.8 dB at 7.3 GHz, thickness:4.2 mm) owing to the enhanced conductive loss and optimized impedance matching. It is anticipated that the multiple reflection/scattering derived from hollow hemispherical microstructures could account for such enhanced microwave absorption performance. Xu et al [338] prepared hollow polypyrrole aerogel by modulating the proportion of hollow PPy nanofibers seeds and pyrrole. In their study, 8 % paraffine filled PPy sample (thickness: 2.69 mm) attained the minimum reflection loss value of −58.73 dB at 16.48 GHz and wide effective absorption bandwidth of 7.28 GHz (thickness: 2.69 mm). Further studies revealed EMI shielding effectiveness of the composite loaded with 20 wt% of hollow PPy nanofibers aerogels in paraffin reaching 68.92 dB (thickness: 3.0 mm). Such performances have been explained considering the multireflection, interfacial polarization and formation of the conductive network.

Guo et al [339] studied electromagnetic waves absorption of the hollow polypyrole nanorods fabricated by using the self-assembly template that can be easily removed. These findings have shown the tuning the wall thickness facilitates control of the dielectric constant of HPPy. The variation of reflection loss with frequency in the range of 2-18 GHz with filler loading of 10 wt% indicated the minimum reflection of - 54.94 dB with the largest effective absorption bandwidth of 7.36 GHz (thickness: 3.4 mm). The possible EMA mechanism of HPPy nanorods could be ascribed to the impedance matching, multiple reflection, good conductive network and enhances polarization loss. In another method, hollow or partially collapsed bowls of polyaniline, polypyrrole, polythiophene and poly(3,4-ethylenedioxythiophene), have successfully been synthesized by surfactant-free Ouzo emulsion.[307] Subsequently, EMI shielding performance of the three samples PEDOT

View Article Online
DOI: 10.1039/D5LP00230C

sphere/bowl film (thickness: 6.5 μm), composite film of PEDOT hollow spheres/bowls film (thickness: 6.3 μm) with infiltrated PH1000 and pure PH1000 film (thickness: 6.2 μm) have been investigated in X-band (8–12 GHz). It is noted that EMI SE of the corresponding samples over the X-band follow the order: PEDOT hollow spheres/bowls film with infiltrated PH1000 (~75 dB)> PEDOT:PSS with infiltrated PH1000 film (~70 dB) > PEDOT hollow spheres/bowls film (very low). The low electrical conductivity of pure PEDOT hollow spheres/bowls film accounts for its inferior EMI performance, In contrast, composite comprising the PEDOT hollow spheres/bowls film with infiltrated PH1000 exhibited enhanced EM absorption as evident from the total EMI SE (SE_T) due to the larger contribution from the absorption compared to the reflection. Ni et al [308] observed maximum R_L of -24 dB at 15.9 GHz for sample (thickness: 2 mm) of PEDOT hollow microspheres.

5.1.2 ICP Micro-/Nanotubes

Polyaniline microtubules prepared by template free method following the doping (β-naphthelene sulfonic acid) and codoping (D-Glucose) could find potential application as microwave absorbing materials in the frequency range of 1-18 GHz.[340] Moučka et al [341] used methyl orange as a soft-template to synthesize polypyrrole nanotubes (dia:~100–400 nm, length: in μm range) and investigated its application in the electromagnetic interference shielding in the microwave region. EMI shielding studies of polypyrrole nanotubes and nanobelts (thickness: 2 mm) have displayed shielding of almost 80% of incident radiation in the C-band at very low loading of conductive filler in the silicone (5% w/w). PANI microtubes (dia: 3.0 μm, length: 12.0 μm) were successfully synthesized in in the presence of toluene-p-sulfonic acid via a self-assembly process assisted by excess ammonium persulfate showed the reflection loss of about -15.5 dB (0-6000 MHz).[342] Yang et al [343] synthesized nanorod-coated PANI hierarchical microtubes by sodium dodecylsulfate/HCl (7.5 mM) assisted oxidative polymerization method. Subsequent studies have shown that 50 wt% of the fabricated

View Article Online
DOI: 10.1039/D5LP00230C

hierarchical 1D hollow structure in with molten paraffin exhibited stronger absorption (- 43.6 dB) and a wide absorption band of 5.84 GHz, smaller sample thickness (1.55 mm) and wider bandwidth (5.84 GHz). It is suggested that 1D hierarchical, hollow structure, and conductivity (0.08 S cm^{-1}) accounts for such excellent performance by contributing to the enhanced permittivity, multiple resonances, strong attenuation capability, multiple scattering and EM radiation.

5.1.3 Binary Nanocomposites of Hollow ICPs

Panigrahi [203] and Srivastava synthesized polyaniline hollow microspheres (PnHM)/Ag nanocomposites by emulsion polymerization of aniline and Tollen's reagent as a source for Ag nanoparticles. The variation of SE versus frequency corresponding to the different thickness samples in S-and X band regions showed SE to be remarkably higher in PnHMAg (19.5 dB: 11.2 GHz) compared to PnHM (12 dB:8.5 GHz). It is anticipated that the Ag nanoparticles present in PnHMAg acts as interconnecting particles between the micro-sized PnHM in forming the continuous linkages to account for the enhanced EMI shielding efficiency. In another work, they reported a novel approach for the trapping of microwave radiation in hollow polypyrrole microsphere ~~through~~ enhanced internal reflection.[204] In their work, the hollow polypyrrole (HPPY) was synthesized by in-situ chemical oxidative copolymerization of pyrrole (Py) using polystyrene as spherical. In addition, HPPy/Ag nanocomposites were prepared using Tollen's. SEM and TEM of HPPy/Ag nanocomposites in **Figure 16(a,b)** shows the presence of Ag nanoparticles (<40 nm) on the surface of HPPy shell. Further investigations showed significantly higher electromagnetic interference (EMI) shielding efficiency (SE) of HPPy (34.5-6 dB) compared to PPy (20-5 dB) in the frequency range of 0.5-8 GHz (**Figure 17 a).** EMI shielding efficiency is further enhanced to 59–23 in 10 wt% Ag loaded HPPy/Ag-10 This is attributed to the trapping mechanism of EM wave through enhanced internal reflection in HPPy/Ag as displayed in (**Figure 17 b).**

View Article Online
DOI: 10.1039/D5LP00230C

Microwave absorption of milled carbon fiber (4 wt %) and hollow polyaniline spheres (1 wt %) impregnated in the epoxy matrix (thickness: 1.8 mm) exhibited maximum absorption (−49.3 dB) and the effective bandwidth of 1.7 GHz −10 dB in. the X band region.[344] The observed reflection loss of EM waves in the given frequency range is attributed to the improves the impedance matching, multiple reflections and scattering of EM waves. According to Wang et al, [345] hollow polyaniline derived N/S co-doped carbon nanoflakes possessed R_L^{min} of − 53.5 dB (10.2 GHz) and corresponding effective absorption band of 4.5 GHz at 2.9 mm. This could be accounted on the basis of the conductivity loss, interfacial polarization relaxation and the impedance matching from hollow structure synergistically determine excellent microwave absorption performance.

Chu et al [346] fabricated well-designed structure of sandwich-like composite films based on hollow polyaniline and cellulose nanofiber (CNF) in the surface layers and MXene/CNF in the intermediate layer. This displayed EMI SE as 35.3 dB for proportion of MXene and PANI achieved at a less filler loading than compared to many others. It is suggested that the formation of such sandwich structure effectively reduces the reflection of the EM wave and make the absorption more dominant. Hollow polyaniline/Fe_3O_4 microsphere (7.33 wt%) composites showed the maximum reflection loss of -15.6 dB and maximum bandwidth of 8.0 GHz over −10 dB in the frequency range of 2–18 GHz.[347] Double-shelled hollow polypyrrole nanotubes was synthesized by using the reactive MnO_2 template.[317] It exhibited the optimasl reflection loss of –50.4 dB and a wide EAB of 7.7 GHz in presence of 5 wt% in a paraffin wax matrix. Such performance is ascribed to the synergistic effects of interfacial polarization and conduction loss.

View Article Online
DOI: 10.1039/D5LP00230C

5.1.4 Core@Shell Nanocomposites of ICPs

5.1.4.1 Binary Core@Shell Nanocomposites

Guo et al [348] observed maximum reflection loss (R_L^{max}) and EAB are −52.01 dB and 2.72 GHz in the Hollow core-shell structured Fe_3O_4@Polypyrrole (Fe_3O_4: 60.0 wt%) synthesized by in situ polymerization method, Such performance is attributed to the synergistic effect on account of dielectric as well as magnetic losses. The broadband electromagnetic wave absorption properties of Fe_3O_4/PPy double-carbonized core-shell-like composites (Thickness: 1.6 mm) exhibited R_L^{min} and EAB of −26 dB and 4.64 GHz, respectively.[349] The observed performance is ascribed to the synergistic effects of conductive loss, dielectric loss, magnetic loss, multiple reflection loss. Tang et al.[350] synthesized Fe_3O_4@PPy with hollow core–shell structures by solvothermal process followed by in situ polymerization. For this purpose, 170 μL, 180 μL, 190 μL of pyrrole were taken and corresponding nanocomposites referred as FP-170, FP-180 and FP-190 acted as an efficient microwave absorber as indicated by its observed performance from its minimum reflection loss of -63.82 dB (4.55 mm), −84.92 dB (3.87 mm), and −71.25 dB (2.64 mm) at low frequencies, respectively. The maximum effective absorption bandwidth of the corresponding composites were found to be 3.48 GHz (2.39 mm), 4.20 GHz, 2.38 mm and 4.96 GHz (2.16 mm). The excellent microwave absorption performance of hollow core-shell Fe_3O_4@PPy could be due to the good impedance matching, strong magnetic loss, including natural resonance and eddy current loss, excellent conductivity, defects and polar groups in h-Fe3O4 and PPy acting as polarization centers, presence of abundant heterogeneous interfaces. and interfacial polarization. Further, presence of hollow structure of Fe_3O_4 in the nanocomposite contribute to the multiple reflection and scattering losses and also enhance the impedance matching.

View Article Online
DOI: 10.1039/D5LP00230C

Promlok et al [351] reported the formation of the hollow magnetic polyaniline by in-situ polymerization in one-pot for EMI applications, In another work, Fe_3O_4–polyelectrolyte modified polyaniline (Fe_3O_4–PE@PANI) were prepared by the self-assembly approach. [352] TEM image of the product clearly established the formation of hollow Fe_3O_4-Polyelectrolyte (PE)@PANI nanocomposites (average size~500 nm), with Fe_3O_4 nanoparticles tightly and completely attached to the PANI hollow sphere surfaces. The 50 wt% of Fe_3O_4–PE@PANI loaded in paraffin exhibited a minimum reflection loss of -6.5 dB (14.3 GHz) and the frequency bandwidth (<-5 dB) from 12.5 to 15 GHz and ascribed it to the impedance matching and dielectric/magnetic loss abilities. Hou et al [353] prepared hollow-structure Fe_3O_4/PANI microspheres based on three steps namely, preparation of Fe_3O_4 nanoparticles, hollow PANI microspheres and subsequently investigated the effects of the mass ratio of aniline/PS (template) on its EMW absorption properties. Fe_3O_4/PANI microspheres corresponding to the mass ratio of aniline/PS of 1:6 and thickness of 1.5 mm attained R_L^{min} of -24.3 dB and the bandwidths below −10 dB corresponds to 4.64 GHz 11.04-15.68 GHz) for 2 mm thickness of the sample. It is suggested that dielectric loss, magnetic loss (2-7 GHz) and eddy current loss (7-18 Ghz) play important role. In addition, hollow Fe_3O_4/PANI microspheres act as potential absorber in the absorption of microwave due to strong destructive interference and eddy current loss. Hollow poly(aniline-co-pyrrole)–Fe_3O_4 (0.06 g) composite nanospheres were prepared via the oxidative polymerization of a mixture of aniline and pyrrole in the presence of a magnetic fluid.[354] The reflection loss calculations showed the best microwave absorbing property between 0.5-10 GHz for the hollow poly(aniline-co-pyrrole) filled with 0.06 g of Fe_3O_4. These studies also revealed that both dielectric and magnetic loss, significantly affect the efficiency of microwave absorption.

In another work, Fe_3O_4/PANI [355] composite was fabricated with hollow Fe_3O_4 nanospheres and polyaniline nanotubes by the hydrothermal treatment and chemical oxidative

View Article Online
DOI: 10.1039/D5LP00230C

polymerization and studied its micro absorption properties by varying the ratio of PANI and the loading amount of the composites in paraffin. These findings have shown remarkable performances (R_L^{min}: − 55.03 dB, EAB: 4.88 GHz) for its thickness of 1.84 mm in the frequency range of 2-18 GHz. Such excellent performance was attributed to the interfacial polarization loss, multiple reflectionm scattering loss and synergistic effect of hollow Fe_3O_4 (magnetic) and 1 D PANI (dielectric material). Fe_3O_4 microspheres core (size: 300 nm)/PANI shell (thickness: 100 nm) synthesized by in- situ polymerization reached R_L^{max} of -37.4 dB at 15.4 GHz.[356] Such enhanced microwave absorption properties arise due to the improved impedance, dielectric loss, interfacial loss and synergistic effect. Core–shell Fe_3O_4–PEDOT microspheres (EDOT)/(Fe_3O_4 molar ratio=20) were also prepared by two-step method in the presence of polyvinyl alcohol (stabilizer) and p-toluenesulfonic acid (dopant) **(Figure 18(a)**.[357] TEM studies displayed in **Figure 18(b)** established Fe_3O_4 microspheres coated by PEDOT and the thickness of the shell corresponds to 90 nm. The variation of reflection losses of Fe_3O_4/PEDOT with frequency in **Figure 18(c)** showed excellent microwave absorbing property (R_L^{min}:-30 dB at 9.5 GHz, thickness: 4 mm) due to the impact of layer thickness, volume fraction and conductivity.

`Fe_3O_4-Polyaniline,[358] Fe_3O_4@Polypyrrole,[359,360] and $BaFe_{12}O_{19}$@PANIn[361] core–shell structured materials have also been studied for their electromagnetic wave absorption, Hosseini et al [362;] used core–shell approach to fabricate polythiophene nanofiber coated on $MnFe_2O_4/Fe_3O_4$ through the combined co-precipitation and in situ polymerization methods. The micro absorption properties of the 1.5-mm nanocomposite showed minimum R_L of -21 dB (12 GHz) in the frequency range 8.0–12.0 GHz. $CoSe_2$@polythiophene [363] and $rGO/Ni_{0.5}Co_{0.5}Fe_2O_4$@PEDOT [364] core-shell composites were also synthesized and studied for its electromagnetic, microwave absorbing properties. Fe_3O_4 microspheres @PPy anchored on 3D graphene aerogel (GO to Fe_3O_4@Ppy wt. ratio: 1:3) of 2.5 mm thickness reached

View Article Online
DOI: 10.1039/D5LP00230C

minimum reflection loss of −40.53 dB at 6.32 GHz and the effective bandwidth of 5.12 GHz (11.12–16.24 GHz).[365] Such enhanced microwave absorption properties of ternary composite could be accounted on the basis of abundant interfaces, enlarged dielectric properties, enhanced conductivity and synergistic effect.

Excellent microwave absorption performance has been shown by PANI decorated on prism-shaped hollow carbon (thickness: 2.5 mm) synthesized by in-situ polymerization.[366] It showed the minimum reflection loss of –64.0 dB (11.1 GHz), and EAB corresponding to 5.0 GHz (9.5–14.5 GHz) and attributed to the high impedance matching, dielectric loss and geometric effect. Gai et al [367] constructed PPy nanotubes@MoS_2 core-shell and observed the optimal R_L of −49.1 dB at 6.1 GHz and the widest bandwidth up to 6.4 GHz from 11.5 to 17.5 GHz (R_L < −10 dB corresponding to its thickness of 2.5 mm. Such enhanced microwave absorption properties of PPy@MoS_2 composite are ascribed to the morphology, attenuation capacity and the impedance matching.

Tian et al [368] fabricated PPy@PANI of tunable shell thickness (30-120 nm) by direct polymerization of aniline on the surface of PPy microspheres. The fabricated PPy@PANI composite showed maximum reflection loss of -34.8 dB at 13.9 GHz and bandwidths exceeding −10 dB corresponds to 11.9−16.6 GHz (4.7 GHz), In another studies, hollow $Zn_xFe_{3-x}O_4$@Polyaniline [369] core-shell composites acted as high-performance microwave absorbers and high reflection loss, respectively. In-situ polymerized grown polyaniline nanorod arrays on the surface of carbon (C@PANI) microspheres exhibited waxberry-like shape.[370] Subsequently, its microwave absorption performance has been evaluated and displayed considerable reflection loss (samples thickness: 2.2 mm), impedance matching ratio of samples and 3 D reflection loss with different thickness as referred in **Figure 19 (a),(b) and (c)** respectively. It is noted that C@PANI exhibited superior microwave absorption performance (Sample thickness: 2.2 mm, R_L^{min}: −59.6 dB at 15.5 GHz, effective bandwidth

View Article Online
DOI: 10.1039/D5LP00230C

for R_L<−10 dB: 5.4 GHz (12.6 to 18 GHz) compared to pure PANI and carbon microsphere. This is suggested that dielectric loss ability, synergistic effect and defects present in C microspheres contribute to such high microwave absorption performance of C@PANI microspheres. In addition, relatively low electrical conductivity owing to amorphous structure of C@PANI could be favourable in the impedance matching. The variation of 3 D reflection loss of C@PANI micro-spheres with the sample thickness in the range of 2-3 mm showed the shifting of R_L^{min} peak from the high to low frequency region. Based on the observations, the absorption mechanism of C@PANI microsphere has also been proposed. In another work, PANI shell fabricated on the surfaces of CNTs (CNT/aniline mass ratio = 1:2) acted as an excellent microwave absorber (R_L^{min}: ~41.5 dB at 9.5 GHz and EB for $R_L \leq$ - 10 dB: 5.1 GHz for 2 mm thickness) as a result of the microwave dissipation ability of CNTs and good impedance matching.[371]

Liu et al [372] reported excellent microwave absorption performance (R_L^{max}: -38.1 dB at 11.6 GHz) in the frequency range of X-band for the pyrrole as the shell on the core of carbon microspheres. The microwave absorption studies have been made on core shell type PEDOT (outer shell) nanocomposite with barium ferrite (center) synthesized by in situ emulsion polymerization in the frequency range of 12.4−18 GHz.[373] The subsequent findings on microwave have shown its absorption value (SE_A) of 22.5 dB (>99% attenuation) owing to the higher dielectric and magnetic loss contributions. The effective electromagnetic shielding performance (EMI SE: 28.8 dB) has also been achieved in core–shell heterostructure comprising polyaniline-coated bagasse fiber.[374] According to Saini et al, [375] TEM studies established coating of PANI deposited via in situ polymerization on the surface of individual MWCNT and contributed towards the absorption dominated total shielding effectiveness (-27.5 to -39.2 dB) in the frequency range of 12.4–18.0 GHz). In another work,

View Article Online
DOI: 10.1039/D5LP00230C

Polyaniline@Helical CNTs with dual chirality exhibited enhanced microwave absorption synergistically.[376]

5.1.4.2 Ternary and Quaternary Core@Shell Composites of ICPs

Zhang et al [377] used spray-dry method to fabricate ternary composite comprising hollow microspheres of PPy@Fe_3O_4/CNTs microspheres by combining the conductive PPy, strong magnetic Fe_3O_4 and high-conductivity CNTs components. It showed the maximum reflection loss of -51.8 dB (8.8 GHz) at the thickness of 2.38 mm. Such performance of PPy@Fe_3O_4/CNTs as an excellent microwave absorber is attributed to the dielectric, magnetic and conductive loss due in achieving the synergistic absorption. Hollow Polypyrrole/Ni/PVDF microspheres prepared by spray phase inversion acted as an efficient electromagnetic microwave absorber (R_L^{min}: -47.2 dB at 25.36 GHz) and R_L^{min}: -39.8 dB at 31.30 GHz).[378] Further studies on the variation in the absorber thickness (1.0-3.5 mm) resulted in the tuning of the effective absorption bandwidth in the range of 18–40 GHz. PPy@FeCo@PPy nanotubes exhibited R_L^{min} of - 50.5 dB and an EAB of 5.7 GHz at a thickness of 2.0 mm.[379] The excellent microwave absorption performance are also reported in the trilaminar composite comprising double-shell PPy@Air@MnO_2 nanotubes,[380] double-shell hollow poly(acrylonitrile) microspheres@polyaniline@Ag,[381] Ge et al [382] prepared hollow-spherical composites of PANI/CoS/(carbon nanodots) CDS under the applied magnetic field of 0.5 T and observed strong electromagnetic wave absorbing characteristics (R_L^{max}:−24 dB at 14 GHz). According to this, magnetic field induced ferromagnetic nanodomains of Co^{2+}clusters greatly enhance Maxwell-Wagner relaxation as well as ionic orientation polarization in the composite leading to the dielectric loss. This in combination with magnetic loss contribute to EMW absorption of PANI/CoS/CDs-0.5T in low frequency range of 2–12.5 GHz.

View Article Online
DOI: 10.1039/D5LP00230C

Kunal and Srivastava [383] motivated by the role of dual interface in the microwave absorption and shielding performance reported the fabrication of Fe_3O_4@C@PANI according to Scheme in **Figure 20 (a)** by varying the aniline: Fe_3O_4@C as 9:1, 8:2, 7:3 with aniline monomer under identical reaction condition and products designated as PFC-10, PFC-20 and PFC-30, respectively. HRTEM image of trilaminar PFC-10 composite in **Figure 20 (b)** clearly shows the formation of highest outermost thickness of nonmagnetic polyaniline shell (~30 nm) on Fe_3O_4@C corresponding to the aniline: Fe_3O_4@C ratio of 9:1. Further investigations revealed the decrease in complex permittivity and increase in complex permeability on encapsulating of Fe_3O_4@C by PANI due to the impedance matching. **Figure 20 (c)** shows the highest shielding efficiency for PFC-10 composite predominantly due to absorption (SE_A: ~47 dB) than reflection (SE_R: ~15 dB) in the frequency range of 2−8 GHz. Such findings in Fe_3O_4@C@PANI are unique owing to the dual interfaces compared to Fe_3O_4@C and Fe_3O_4/PANI due to their applicability limited to a discrete frequency. In addition, such remarkable EM wave attenuation in Fe_3O_4@C by PANI trilaminar core@shell composite was also indorsed by impedance matching and dielectric and magnetic loss.

Motivated by this, trilaminar they extended their work on core@shell@shell-type Fe_3O_4@SiO_2@PPy anticipating the aggregation of Fe_3O_4 in the PPy matrix could be prevented by introducing SiO_2 as first shell (dielectric) the between the interfaces of Fe_3O_4 and PPy in comparision to Fe_3O_4 alone.[384] Their findings indicated Fe_3O_4@SiO_2@PPy (Fe_3O_4@SiO_2/pyrrole wt/wt=1:9) exhibited the highest total shielding efficiency (SE_T:~32 dB) in the frequency range of 2−8 GHz **(Figure 21 a)** following the reflection as the dominant shielding mechanism. It is attributed to role of dual interfaces, poor impedance matching between the PPy (conducting)/SiO_2 (insulating) and high electrical conductivity of Fe_3O_4@SiO_2@PPy and interfacial polarization, reflection/scattering of EM waves, These findings clearly established that switching of the dominating shielding mechanism from

absorption to reflection could be achieved by tuning C@ PANI compared to SiO_2@PPy shells in Fe_3O_4@C@PANI and Fe_3O_4@SiO_2@PPy trilaminar composites, respectively **(Figure 21b)**. Such switching over of the shielding mechanism has also been supported by the impedance mismatch and impedance matching in Fe_3O_4@ SiO_2@PPy and Fe_3O_4@C@PANI.

Ji et al [385] synthesized hollow γ-Fe_2O_3@PEDOT (FP) and γ-Fe_2O_3@SiO_2@PEDOT (FSP) core-shell nanocomposites**.** The corresponding SEM images of FSP and FP clearly established removal of SiO_2 layer from γ- Fe_2O_3@SiO_2@EDOT to form hollow γ-Fe_2O_3@PEDOT. Further investigations on the frequency (2–18 GHz) dependence of reflection loss revealed remarkable microwave absorption properties hollow γ-Fe_2O_3@PEDOT (R_L^{min}: -44.7 dB: 12.9 GHz, EAB: 4.3 GHz in 10.8–15.1 GHz range) compared to the γ-Fe_2O_3@SiO_2@PEDOT (R_L^{min}: −21.3 dB: 14.1 GHz, EAB: 3.8 GHz:12.6–16.4 GHz range) for thickness 2.0 mm. This is ascribed to the synergistic effect between the magnetic and dielectric components and its core-shell structure. The reports are also available on enhanced electromagnetic wave absorption of Co@Hollow carbon nanospheres @PANI [386] and FeNi@C@PANI.[387] Panigrahi and Srivastava[388] fabricated rubber (EPDM, NBR, and NR)@Polystyrene@Polyaniline blends and observed high shielding efficiency (>30 dB:1–8 GHz). Such high performance of rubber blends is attributed to the trapping of EM waves through enhanced internal reflection due to the typical core-shell morphology of PS@PANI. PPy nanotubes/NR/NBR [389] core-shell composites also displayed excellent electromagnetic wave absorption properties.

γ-Fe_2O_3/$(SiO_2)_2$–SO_3H/PPy composite (thickness: 2.0 mm) core/shell/shell microspheres displayed substantially improved microwave absorption properties (R_L^{max}:−43.1 dB (15.1 GHz), EAB: 6.1 GHz (11.9–18.0 GHz) **(Figure 22a)**.[390] This is ascribed to impedance matching, unique core/shell/shell structures, synergistic interaction, dielectric loss (SiO_2 and PPy layers) and magnetic loss (γ-Fe_2O_3). A model has been proposed in **Figure 22**

View Article Online
DOI: 10.1039/D5LP00230C

(b) to account the effects of core/shell/shell structures on the microwave absorption. Core/shell/shell-structured Ni/C/PANI nanocapsule prepared by two-step process involving the modified arc-discharge and chemical polymerization exhibited optimal R_L value of -9.3 dB at 6.2 GHz (Thickness: 3 mm) with broad -5 dB- (3.4–18 GHz) bandwidth.[391] Wang et al [392] prepared hierarchical Fe_3O_4@Graphene@PANI following the hydrothermal and in-situ polymerization. The composite exhibited favourable microwave absorption properties as evident from R_L^{max} of - 43.7 dB (at 10.7 GHz) and the EAB <10 dB of 5.4 GHz (6.8-12.2 GHz) with a matching thickness of 3 mm. These findings are explained on the basis of impedance matching, enhanced interfacial polarization and orientation polarization.

Ding et al [393] fabricated core@shell hierarchical cable-like TiO_2@Fe_3O_4@PPy (Thickness: 3.2 mm) and observed maximum reflection loss of −61.8 dB owing to the magnetic–dielectric synergy. CoNi@SiO_2@Polypyrrole nanocomposites displayed enhanced microwave absorbing capacity as evident from its minimum reflection loss of −34.19 dB at 9.59 GHz (thickness: 2.12 mm) and the EAB with R_L< −10 dB in the entire X-band.[394] In another work, core-shell SiC_{NWs}@MnO_2@PPy prepared through multistep showed the minimum reflection loss of −50.59 dB (matching thickness: 2.41 mm) and the effective absorption bandwidth of 6.64 GHz (matching thickness: 2.46 mm).[395] Such excellent electromagnetic wave absorption performances is ascribed to the advantage of the interfacial polarization and dipole polarization displayed by core-shell SiCNWs@MnO_2@PPy.Several other ternary composites are also reported as efficient microwave absorbers, such as Ni/PANI/RGO,[396] Fe_3O_4@PEDOT microspheres/RGO,[397] $NiCo_2O_4$ (hollow)@PPy nanofibers/RGO,[398] encapsulation of γ-Fe_2O_3 decorated RGO in PANI core-shell tubes,[399] RGO/Fe_3O_4/PANI,[56] N-doped Graphene@PANI nanorod modified by Fe_3O_4 nanoclusters.[400] Polyaniline/Graphene oxide/Fe_3O_4,[401] magnetite nanoparticles decorated CNT/PANI,[402] PANI/CIP/Fe_3O_4,[403] and Fe_3O_4@SiO_2@PPy.[404] Shukla [405] prepared dual core–shell structured

View Article Online
DOI: 10.1039/D5LP00230C

Fe_3O_4/C/PPy (Fe_3O_4/C:PPy:2:8 wt/wt) composites via hydrothermal and chemical oxidative polymerization method and observed its absorption dominated excellent EMI shielding efficiency (>28) dB in the range of 1 to 8.5 GHz **(Figure 23 a)**. The probable mechanism in **Figure 23 (b)** shows the attenuation of electromagnetic waves by trilaminar Fe_3O_4/C/PPy composite. It is also suggested that spin motion plays a decisive role in in such performance. In addition, excellent electromagnetic absorption properties have also been reported in PANI@Natural graphite flakes (NGF)/MWCNT,[406] and PEDOT/RGO/Co_3O_4. [407]

According to available literature, very limited amount of work has been reported on quaternary core-shell composites in general are reported or their applications in microwave absorption. In one such work quaternary MWCNT/CuO/Fe_3O_4/PANI nanocomposites following the weight ratio of CuO/Fe_3O_4/PANI to MWCNT in the 1:3, 1:4 and 1:5 showed minimum reflection losses -45.7, -85.4, and -87.4 dB, respectively.[408] The corresponding absorption bandwidths ($R_L \leq -10$ dB) of MWCNT/CuO/Fe_3O_4/PANI nanocomposites were found to be 6, 7.6, and 6 GHz. The higher value of loss constant (α) of MWCNT/CuO/Fe_3O_4/PANI nanocomposites indicated both magnetic and dielectric loss tangent playing key role in influencing the microwave absorption efficiency.

Wang et al [409] fabricated 3D heterostructure of Gaphene@Fe_3O_4@WO_3@PANI involving hydrothermal method and chemical oxidation polymerization and studied its performance in microwave absorption. In addition, presence of WO_3 decrease permittivity facilitating in the better impedance matching. The synthesized quaternary nanocomposite displayed maximum R_L value (−46.7 dB at 9.4 GHz and the maximum absorbing bandwidth exceeding −10 dB as 1.8 GHz (12.4 to 14.2 GHz) corresponding to the thickness of 4 mm and 1.5 mm, respectively. EM wave absorption mechanism involved the contributions originating from enhanced interfacial polarization, better impedance matching, multiple reflection, and synergistic effect, In another work, Liu et al [410] investigated

View Article Online
DOI: 10.1039/D5LP00230C

electromagnetic wave absorption properties of Graphene (GN@Fe_3O_4@PANI) decorated with TiO_2 prepared by hydrothermal method and in situ polymerization as described in **Figure 24(a)**. The corresponding TEM image in **Figure 24 (b) and (c)** indicated TiO_2 nanosheets oriented perpendicular to GN@Fe_3O_4@PANI and TiO_2 nanosheets forming hierarchical structures. The EM wave absorption properties of graphene@Fe_3O_4@PANI@TiO_2 nanosheets loaded in 50 wt% paraffin is displayed in **Figure 24 (d).** According to this, GN@Fe_3O_4@PANI@TiO_2 nanosheets showed R_L^{max} of -41.8 dB at 14.4 GHz (thickness: 1.6 mm) and absorption bandwidth of R_L < -10 dB ~3.5 GHz. The attenuation of EM waves is attributed to the interfacial polarization and improved impedance matching of the nanocomposites.

Table 1. Microwave absorbing properties of hollow ICPs, hollow ICP nanocomposites and ICP based core-shell nanocomposites

5.2 Removal of Heavy Metals in Water

Heavy metals with atomic weights between 63.5 and 200.6, and a specific gravity greater than 5.0.[411] These are considered as utmost important environmental toxic environmental pollutants on their discharge from tanneries, fertilizers, mining, metal plating, batteries, pesticides, paper industries and many more into lakes, rivers, ocean or in open environments and endangering the life of human being and other living systems owing to their toxicity. Some heavy metals such as Cu, Zn, Fe, Mn are essential for the working of human metabolic system, but could lead harmful effects when its concentration is very high.[62] **Table 2** highlights the sources as well as the health effects of the heavy metals on the human beings.[412]

In view of this, heavy metal ions can be removed from wastewaters/aqueous solution by using different adsorbents. Intrinsically conducting polymers, specially, polyaniline and polypyrrole have played excellent role as an adsorbent in removal of different heavy metal

View Article Online
DOI: 10.1039/D5LP00230C

ions from the contaminated aqueous solution. [81-85,413] This is ascribed to the several advantages, such as simple synthesis, excellent environmental stability, chemical versatility, biocompatibility, low cost, presence of functional group that enable them to facilitate their modification and functionalization by doping and composite formation to favors the adsorption process by tuning its properties as an attractive alternative to the several naturally occurring waste materials,[85,414] Further, hollow morphology of ICPs, specially polyaniline, could be effective for the adsorption of various pollutants such as heavy metals and dyes due to larger surface area. In addition, hollow ICP based composites and core-shell nanomaterials been reported as good adsorbents to remove heavy metals pollutants from wastewater due to their unique physical and chemical properties.

5.2.1 Chromium

Among all heavy metals, hexavalent chromium (Cr (VI)) is considered a seriously hazard in water due to its high toxicity compared to Cr (III).[415] The source of Cr originates from the discharge coming out of chrome plating, textile, leather tanning, metal finishing industries, paint pigment industries into water system. In this regard, review related to the removal of Cr(VI) using hollow ICPs and core-shell (ICP) as adsorbent are described as below.

5.2.1.1 Hollow ICPs

Recently, hollow spherical polyaniline synthesized using poly(styrene-co-acrylic acid) sphere as the template showed high adsorption of Cr(VI) as evident from 601.3, 347.8 and 235 mg g^{-1} at pH corresponding to 1, 2, and 3, respectively.[416] Further, the adsorption of Cr(VI) followed pseudo second-order equation and Redlich–Peterson isotherm models including excellent regeneration. According to Wu et al,[417] hollow polyaniline micro/nanospheres (10 mg) achieved maximum removal capacity of 127.88, 43.20 and 25.6 mg g^{-1} at the 1.2 mmol L^{-1} initial concentration of Cr (VI) corresponding to the solution pH of

View Article Online
DOI: 10.1039/D5LP00230C

3, 4 and 5, respectively. The kinetic studies fitted well with second order model and removal of Cr (VI) could be described by Langmuir isotherm. 1D-Polyaniline nanowire/tubes removed Cr(VI) rapidly and affectively from aqueous solution over a suitable pH range and adsorbent could be easily regenerated for its reuse.[418] Hollow tubular structure comprising the amino acid-doped polyaniline by in situ chemical polymerization method exhibited removal capacity toward Cr(VI) (60.0 mg,g^{-1}).[419] Li et al [420] prepared bamboo-like polypyrrole nanotubes following the reactive-template vapor phase polymerization method using electrospun V_2O_5 nanofibers acting as templates as well as the oxidant. These findings indicated the maximum adsorption capacity of 9.281 mmol g^{-1} for Cr (VI) in aqueous solution with the adsorption data fitting well with Langmuir model and followed pseudo-second-order kinetics (k:0.0031 g $mmol^{-1}$ min^{-1}).

5.2.1.2 Binary Core-Shell Composites of ICPs

Polyaniline/Polystyrene core-shell nanocomposite showed the ~95 % removal of Cr (VI) corresponding to the initial concentration of Cr (VI), adsorbent dose, volume of the medium and pH of 100 mg L^{-1}, 250 mg, 50 mL and 2, respectively.[421] The maximum adsorption capacity of PANI/PS for Cr (VI) was found to be 19 mg g^{-1}. The possible mechanism involved the complexation between Cr (VI) ions and the N atoms of the –N=C– groups through sharing of their lone pair of electrons. In addition, polyacrylonitrile/polyaniline core/shell nanofiber mat, [422] sulfonated Poly(arylene ether nitrile)/Polypyrrole core/shell nanofibrous mat,[423] Ag-P/Ppy core-shell composite,[424] polypyrrole wrapped oxidized MWCNTs,[425] polyaniline coated ethyl cellulose, [426] and polypyrrole-coated halloysite nanotube clay nanocomposite [427] have also been used as adsorbents in the efficient removal of toxic Cr(VI) from aqueous solution.

Fe_3O_4/PANI microspheres fabricated through the interfacial polymerization removed about 94 % of Cr(VI) ions from water.[428] The adsorption isotherm followed Langmuir

View Article Online
DOI: 10.1039/D5LP00230C

isotherm mode (q_m: 200 mg g^{-1}), and pseudo-second-order kinetics. Fe_3O_4/PANI microspheres. In addition, Fe_3O_4/PANI has been evaluated for its regenerability and reusability to remove the adsorbed Cr(VI) ions using NaOH aqueous solution. These studies have shown the adsorption capacity of Fe_3O_4/PANI microspheres retained 90% of the initial value after reusing five times. It may be interesting to mention that the regeneration of Fe_3O_4/PANI microspheres using hydrochloric acid is not possible as it degrades the polyaniline and dissolves the Fe_3O_4. In another study, Fe_3O_4/Polypyrrole nanotubes prepared by one-pot process exhibited Cr(VI) adsorption capacity of ~ 451.45 mg·g^{-1}.[429] This is suggested that adsorption process take place due to the ion exchange and chelation. Futter, the existence of $-NH^+$ on the Fe3O4/PPy nanotubes partially reduce Cr(VI) to Cr(III). Fe_3O_4/PPy nanotubes also retained about 90% of the initial removal efficiency after 5 adsorption/desorption cycles. According to this, adsorption of Cr(VI) on the Fe3O4/PPy nanotubes involve the ion exchange and chelation. As a resuly where Cr(VI) was partially reduced to Cr(III) due to the existence of −NH+ on the Fe3O4/PPy nanotubes.

In another work, Fe_3O_4 coated polypyrrole (Initial concentration:200 mg/L) showed 100% adsorption for 200 mg L^{-1} Cr(VI) aqueous solution corresponding to the pH 2.[430] The proposed mechanism for removal of Cr(VI) is guided by the ion exchange and reduction on the surface of the nanocomposite. The kinetics studies indicated pseudo-second-order rate model and Langmuir model inevitable from the fitting of isotherm data. The maximum adsorption capacity of Polypyrrole/Fe_3O_4 magnetic nanocomposite increases from 169.4 to 243.9 mg/g corresponding to the temperature from 25 ^{0}C to 45 °C, respectively. The possible mechanism was elucidated based on the XPS studies. According to this, the possible mechanism for Cr(VI) removal by the PPy/Fe_3O_4 could be due to the ion exchange and reduction on the surface. Several other adsorbents comprising magnetite arginine functionalized polypyrrole,[431] magnetic particle coated PPy and PANI,[432] polypyrrole coated

View Article Online
DOI: 10.1039/D5LP00230C

Fe_3O_4,[433] polypyrrole modified natural corncob-core sponge,[434] polyaniline coated protonic titanate nanobelt,[435] and MnO_2 coated polyaniline nanofibers [436] also successfully removed hexavalent chromium from water.

Du et al [437] synthesized core-shell Polypyrrole/Hollow mesoporous SiO_2 particles by in-situ polymerization to study the removal of Cr(VI) from aqueous solution exhibited the maximum adsorption capacity of Cr(VI) of ~322 mg g^{-1} at 25 ^{0}C following the quasi-second-order kinetic model and the Langmuir isotherm model. In another study, deposition of PANI on the surface of ThO_2 surface has been validated by TEM analysis.[438] Further investigations revealed the adsorption of Cr(VI) on this core shell composites to be dependent on the solution pH. The kinetic model and adsorption process fitted well with the pseudo-second-order and Langmuir model (q_m: 141 mg g^{-1}). Polyacrylonitrile/Polypyrrole core/shell nanofiber mat exhibited high selectivity for Cr (VI) compared to the Ni(II), and Cu(II) ions in the solution.[439] The high removal efficiency of hexavalent chromium has also been reported on L-cystine doped glucose carbon sphere (GCS)@PPy,[440] PANI@Nano hollow carbon sphere,[441] Polypyrrole@Attapulgite,[442] copper slag@polyaniline,[443] polyaniline@$Ni(OH)_2$,[444] PPy@$MgFe_2O$,[445] Polypyrrole/Graphene oxide,[446] and PANI@Almond shell biocomposite. [447]

5.2.1.3 Ternary Core-Shell Composites of ICPs

Dutta et al [448] prepared polypyrrole–polyaniline coated rice husk ash (termed as PPy PANI@RHA) by in situ polymerization and used it in the removal of Cr(VI) from the aqueous solution and corresponding findings are shown in **Figure 25 (a-d)**. It revealed about 98% of Cr(VI) removal at room temperature (303 K) under optimum conditions (adsorbent dose: 0.8 g L^{-1}, adsorbate concentration: 50 mg L^{-1}, pH of ~2, contact time: 300 min). The adsorption studies indicated Elovich kinetics and is better described using the Freundlich isotherm model with a maximum adsorption capacity of 769.15 mg g^{-1}. The possible Cr(VI) adsorption

View Article Online
DOI: 10.1039/D5LP00230C

mechanism by the PPy–PANI@ RHA adsorbent has been described in **Figure 26** on the basis of ion-exchange, strong electrostatic attraction and reduction of Cr(VI). Their findings also indicated the removal efficiency of of Cr(VI) remains more or less unaltered in the presence of moderate concentrations of co-existing ions (Ca^{2+}, Na^{+}, Mg^{2+}, and Cl^{-}, NO^{3-}, PO_4^{3-}). The regenerated adsorbent on subjecting to adsorption of Cr(VI) for 5 desorption/adsorption cycles have shown the removal efficiency of 94% and 80% in the first and second cycles respectively.

In another work, adsorption of Cr (VI) in aqueous solution on polypyrrole decorated graphene-silica (Graphene/SiO_2@Polypyrrole) composite exhibited the maximum adsorption capacity corresponding to 429.2 mg g^{-1} (298 K) at pH 2.[449] The adsorption of Cr (VI) on graphene/SiO_2@ polypyrrole fitted well with the pseudo-second-order kinetic and Langmuir isotherm model. The simultaneous removal of methyl orange and Cr (VI) from water has also been evaluated based on PPy@Magnetic chitosan adsorbent.[450] Da Rocha et al [451] reported the formation of PPy chains layer on the PMMA/Rice husk ash (RHA) fibers and observed Cr(V) removal capacity q_e of 363.63 mg/g (after 150 min) at pH 2. In another work, core-shell PS/PANI-Fe_3O_4 adsorbent removed 100% Cr (VI) corresponding to pH: 2, adsorbent: 0.05 g, initial concentration of Cr (VI): 5 mg L^{-1}, total volume:30 mL and 120 min, respectively.[452] The removal of hexavalent chromium from water has also been studied using Polyaniline/Wood sawdust/Polyethylene glycol composite.[453] Yao et al [454] prepared Fe_3O_4@Polypyrrole nanospheres with hierarchical porous structure anchored on graphene nanosheets and noted excellent adsorption capability in the Cr (VI) removal (q_m:~348.4 mg g^{-1}) due to the synergic effect between graphene and Fe_3O_4@polypyrrole. The adsorption kinetics has been explained on the basis of pseudo-second-order kinetics. In addition, the fabricated adsorbent was found to be stable and retained ~ 72.2% removal efficiency after six cycles.

View Article Online
DOI: 10.1039/D5LP00230C

The large specific surface area of γ-Fe_2O_3@Chitosan@PPy accounted for the maximum Cr (VI) adsorption capacity of 301.2 mg. g^{-1}.[455] The magnetic nanocomposite removed 100% Cr (VI) in aqueous solution and described this based on exchange and chelation as the dominant interaction mechanisms.

5.2.2 Lead

The source of lead pollution in water mainly comes from steel plants, battery factories, and several other industries. This could lead serous health related issues owing to its non-degradable characteristics and bioaccumulation presence of even if present at low level of concentrations. In view of this, removal of Pb in water based on hollow ICPs and core-shell (ICP) as adsorbent is described as below.

5.2.2.1 Hollow ICPs

Han et al [456] fabricated hollow structure comprising PANI nanospheres with incontinuous multicavities by chemical polymerization using chloroaurate acid as oxidant and citric acid as dopant. Subsequently PANI nanospheres exhibiting in continuous multicavities were formed by dissolving Au particles in excess saturated KI/I_2 solution. The adsorption capacity and adsorptivity of PANI in the removal of Pb in water correspond to 1589 mg g^{-1} and 93%, respectively.

5.2.2.2 Binary and Ternary Core-Shell ICPs based Composites

γ-Fe_2O_3 coated with proton acid doping polyaniline nanocomposites (γ-Fe_2O_3@PANI) showed high adsorption capacity for arsenic(V) removal in water (pH: 4 to 11) and explained this based on the electrostatic interaction and hydrogen bonding.[457] Mehdinia et al [458] investigated the effects of transformation of core-shell Fe_3O_4@PPy to its rattle type (yolk shell) on removal of heavy metals Pb^{2+} and Cu^{2+} from water. PANI/TiO_2 adsorbent prepared by the chemical oxidative polymerization of aniline on the surface of TiO_2 hydrate showed adsorption capacities of Cr(VI) in water to be 394.43 mg g^{-1} with excellent reusability.[459]

View Article Online
DOI: 10.1039/D5LP00230C

Further, the adsorption of Cr(VI) oxyanions involved the electrostatic attraction, hydrogen bonding and anion-π interactions.

Vatani and Eisazadeh [460] coated polythiophene on polystyrene and poly(vinyl chloride) to investigate its role as adsorbents in the removal of Pb(II) from aqueous solution. They observed the higher removal efficiency of PTh/PVC compared to PTh/PS nanocomposites under the optimum conditions (pH: 2, initial concentration of cations 100 mg^{-1}, equilibrium time:30 min). Chen et al [461] prepared PTh/MnO_2 composite with MnO_2 as the core and PTh as the shell for the selective adsorption towards Pb^{2+}, Zn^{2+} and Cu^{2+} from the industrial wastewater in the aqueous medium. These findings showed the adsorption capacities of Pb^{2+}, Zn^{2+} and Cu^{2+} (within 30 min) were found to be 82.10, 30.72 and 60.79 mg g^{-1}, respectively. These findings have been explained on the basis of synergetic effect between PTh and MnO_2. Binary composites have been prepared following the coating of polyaniline for their applications in removal of Pb (II) ion in water. Fe_3O_4 particles coated with polyaniline showed the maximum lead adsorption capacity of Pb (II) as 114.9 mg g^{-1}.[462] Pb (II) ions were found to be almost completely removed under the optimum conditions (initial concentration of lead (II): 50 ppm, adsorbent dosage: 3 mg, pH: 9,3).

According to Shakhsari et al, [463] $CoFe_2O_4$@PANI removed 98% of Pb at 25 ^{0}C from water under optimum condition of initial concentration of metal ions (17 mg L^{-1}), adsorbent dose (1 g), pH (7) and time (120 minutes). The adsorption kinetics followed the quasi-first-order model, and data fitted well with the Freundlich isotherm. Polypyrrole-coated ZnO-NiO nanocomposites has also been investigated as adsorbents for enhanced removal of Pb(II) in aqueous solution and wastewater.[464] The possible mechanism of Pb(II) adsorption on the PPy/ZnO-NiO adsorbent has been explained based on the ion exchange, electrostatic attraction, and formation of metal complexes. The reusability and regeneration experiments after six adsorption-desorption cycles have shown decrease in the adsorption and desorption

View Article Online
DOI: 10.1039/D5LP00230C

of Pb(II) from 98.7 % to 77.8 % and 92 % to 67 %, respectively. Naphthalene sulfonic acid doped polyaniline@Ni^0 composite (0.5 g L^{-1}) achieved 90.9% removal efficiency of Pb(II) ions in aqueous solution (pH: 5).[465] The findings based on the isotherm data supported Langmuir isotherm model with maximum Pb(II) removal capacity of 414.6 mg/g at 25 ^{0}C. Fe_3O_4/polyaniline hollow microspheres has been fabricated and used as adsorbent in the uptake of Pb^{2+} from aqueous solution.[466] It followed the pseudo second order kinetics and adsorption data agreed well with the Langmuir isotherm.

Zare et al [467] used a poly (aniline-co-3-aminobenzoic acid)-based magnetic core–shell nanocomposite and observed maximum adsorption capacity of Pb(II) to be 138.31 mg g^{-1} in the aqueous solution. The findings are also found to be in agreement with the pseudo-first order and Freundlich isotherm. Pomegranate-like MnO_2@PANI using 0.1 mol L^{-1} of $KMnO_4$ have been successfully synthesized according to the procedure described in **Figure 27 (a)**.[468] Subsequently, the variation of removal ratios (q) of Pb(II) ions with PANI nanoflowers (NF), commercial MnO_2, PANI sphere prepared with cavities and pomegranate-like MnO_2@PANI spheres have been studied as adsorbents and findings are displayed in **Figure 27(b) and (c).** It is noted that respective removal ratios (q) values correspond to 36.1 %, 54.9 %, 71.2 %, and 99.2 %, respectively. MnO_2@PANI showed the maximum sorption capacity of 309.6 mg g^{-1}. Such excellent adsorbability of MnO_2@PANI spheres is ascribed to the presence of mesoporous structures of PANI spheres with more exposed adsorption sites towards Pb (II) ions. Alternatively, enhancing the sorption ability of Pb (II) ions could be ascribed to the interaction (chelation/physisorption) between MnO_2 and PANI contribute in synergistically. The removal ratios of different heavy metal ions on PANI and PANI@MnO_2 as adsorbents were also tested for Ni(II), Cd(II), Cu(II), Zn(II) heavy metal ions. Subsequent findings revealed higher removal ratios of these heavy metals for the MnO_2@PANI hybrids compared to PANI nanospheres and also agreed well with the earlier results on Pb(II) ions adsorption.

View Article Online
DOI: 10.1039/D5LP00230C

Chemically modified polythiophene with copper nanoparticles and polyvinylpyrolidine-sulfonic acid [469] and polypyrrole-iron oxide–seaweed [470] exhibited the adsorption capacity of lead from aqueous solution to be 111 mg g^{-1} and 333.33 mg g^{-1}, respectively.

PANI/Jute fiber composites exhibited effective Cr(VI) and Cd(II) ions decontamination from water.[471] Core/shell like structure of the PTh/SiO_2 composite exhibited superior selectivity to separate and recycle Zn^{2+} among the multiple ions (Pb^{2+}, Zn^{2+}, Cu^{2+}) in the wastewater due to the synergetic effect.[472] Sun et al [473] studied the adsorption of Cu(II), Pb(II) and Ni(II) on PANI@Aminopropyltriethoxysilane (APTS)-Fe_3O_4/Attapulgite composite and observed the maximum adsorption capacity of 189.03, 270.27 and 142.86 mg g^{-i}, respectively. The reusability performance of PANI@APTS-Fe_3O_4/Attapulgite after 5 times use showed slight decrease for all the heavy metals (Cu(II):84% to 79%, Pb(II):87% to 81%, Ni(II):63% to 56%). SiO_2-coated magnetic graphene oxide modified with a pyrrole-thiophene copolymer showed maximum adsorption capacity of Cu(II), Pb(II), Zn(II), Cr(III) and Cd(II) in aqueous solution corresponding 201, 230, 125, 98 and 80 mg g^{-1}, respectively.[474] High-temperature hydrothermally prepared polypyrrole-derived N-doped carbon nanotube decorated with fish scale-like MoS_2 nanosheets showed significantly much higher removal capacity of Pb(II) (q_m:381.87 mg g^{-1}) in waste water.[475] Based on XPS studies, following possible mechanism for the adsorption of Pb(II) adsorption on the C-Ppy@MoS_2 has been proposed:

$$Mo(IV) + 2H^+ + 4e^- + 4H_2O\ (aq) \rightarrow 5H_2\ (g) + MoO_4^{2-}(VI)$$

$$MoO_4^{2-}(VI) + Pb^{2+} + S \rightarrow PbMoO_{4-x}S_x\ (s)$$

It is believed that the protons produced in the above reaction may have a driving effect on the adsorption process. The unique structure of the fish scale-like MoS_2 nanosheets on the C-PPy nanotubes account for the adsorption of Pb(II).

View Article Online
DOI: 10.1039/D5LP00230C

5.2.3 Other Metal Ions

Dutta et al [476] fabricated hollow polyaniline microsphere (PNHM)/Fe_3O_4-40 (Fe_3O_4 content: 40 wt.%) magnetic nanocomposites**.** Subsequent investigations in **Figure 28(a-d)** and adsorption studies revealed about 98–99% removal of As(III) and As(V) from the contaminated water in the presence of PNHM/Fe_3O_4-40 and followed pseudo-second-order kinetics and Freundlich isotherm. The maximum adsorption capacity of As(III) and As(V) correspond to 28.27 and 83.08 mg g^{-1}, respectively. The adsorption of arsenic species on the surface of PNHM/Fe_3O_4-40 could be attributed to the formation of monodentate-mononuclear/bidentate-binuclear As-Fe surface complex. The probable schematic representation of arsenic adsorption mechanism in aqueous solution is deduced based on X-ray photoelectron spectroscopy analysis and displayed in **Figure 29**. The reusability studies of the PNMH/Fe_3O_4-40 demonstrated ~83% removal efficiency of As(III) in the third adsorption cycle and was found to be much higher than many other reported adsorbents./Fe_3O_4-40 composite was also found to be very effective adsorbent in removal of arsenic from naturally contaminated groundwater samples.

Further studies have shown increase in the adsorption of As (III) and As (V) on the surface of PNHM/Fe_3O_4-40 on increasing temperature from 293 K to 313 K.[477] In another work, Fe_3O_4/PANI was prepared by the chemical polymerization method.[478] SEM studies confirmed the formation of PANI on the surface of Fe_3O_4 grains. Such core-shell structure of Fe_3O_4/5%PANI exhibited the highest arsenic adsorption ability at pH 7 and 300 K. According to Muhammad et al.[479] Fe_3O_4/PANI core-shell composite can be applied as effective adsorbents for the removal of hexavalent chromium and divalent nickel from water. Polyaniline/Fe^0 [480] and iron-functionalized polythiophene (PTh@Fe) [481] also reported as excellent adsorbent for the removal of arsenic from aqueous solutions**.** In addition, heavy metals from aqueous solution have also been removed by polyaniline coated on sawdust,[482]

View Article Online
DOI: 10.1039/D5LP00230C

Fe_3O_4-embedded poly(thiophene),[483] PAN/PANI-Nylon.[484] 2-aminopyridine functionalized magnetic core–shell Fe_3O_4@Polypyrrole composite,[485] and Fe_3O_4/SiO_2/PANI-SDBS nanocomposite.[486] Fe_3O_4@PPy core-shell functionalized with tetrakis (4-carboxyphenyl) porphyrin (TCCP) prepared in multiple steps displayed 100 % efficiency of Hg (II) removal in water.[487] The investigations have been also been reported on the adsorptive removal of Hg^{2+} by Polyaniline/Attapulgite [488] Ren et al [489] prepared Fe_3O_4@Polypyrrole@Sodium dodecyl sulfate core@shell composite and observed the selective removal of Mn (VII) and other dyestuffs from wastewater.

Table 3 Performance data of hollow ICPs, hollow ICP nanocomposites and ICP based core-shell adsorbents in removal of heavy metal ions in water medium.

5.3. Removal of Dyes

These dyes are primarily used by leather, paint, varnish, pharmaceutical, textile, printing, pulp and paper, food and several other industries.[60-64] **Figure 30** depicts the sources and pathways of various dye pollutants in water bodies.[88] However, the discharge of these highly toxic, carcinogenic and non-biodegradable toxic dye from these sources including their improper disposal in the agricultural land without proper treatment even in extremely small amounts is dangerous to aquatic life, microorganism, and human health.[61] The details are already described on the classification, examples, applications, solubility in water, and ecotoxicological effects of dyes on living organisms.[88] Therefore, issue of toxic dye present in wastewater remains major challenge to the existing conventional water treatment systems. As a consequence, the environmental remediation of these water-soluble dyes presence in wastewater is mandatory before it is released into water bodies to avoid negative effects, In view of this, adsorption process among the different available technologies is considered as one of the most studied one.

View Article Online
DOI: 10.1039/D5LP00230C

In this regard, polyaniline has been reported as one of most studied cost-effective adsorbents in the decontamination processes of wastewater treatment owing to its easy synthesis with a possibility of doping, exhibiting environmental stability, mechanical flexibility and good physicochemical properties and presence of presence of amine and imine groups.[64,489] However, conventional PANI powder has low surface area that limits its ability to adsorb dye. In this regard, hollow and core-shell structured conducting polymers, specially, polyaniline have been used in the effective adsorption of dyes owing to its high surface area and other properties.

From this perceptive, hollow structure polyaniline is more advantageous in the removal of dye due to high surface area and porous structure. In addition, core-shell structured polyaniline also offers several advantages that include enhanced adsorption capacity, improved selectivity, better stability and in achieving the as increased surface area and the ability to incorporate different materials for specific interactions with dye molecule.[64,68] Accordingly, the adsorption performance by hollow conducting polymers, hollow conducting polymers composites and conducting polymer based their core-shell composites have been reviewed below for the removal different dyes from water.[490-550]

5.3.1 Rhodamine

5.3.1.1 Hollow ICPs

Wu et al [491] used functionalized polystyrene sphere as the template to fabricate hollow spherical polyaniline (average dia: 300 nm, shell thickness: 100 nm) and observed its high adsorption capacity of RhB (61.75 mg g^{-1}). According to Chen et al .[492] hollow polyaniline helical nanobelts have been prepared through the generation of hollow oligoaniline helical nanobelts acting as sacrificial templates during the chemical oxidation method. It was inferred that the presence of the large number of adsorption sites comprising several amino and imino groups in hollow PANI helical nanobelts facilitated the effective adsorption of rhodamine 6G.

View Article Online
DOI: 10.1039/D5LP00230C

5.3.1.2 Binary Core-Shell Composites of ICPs

The investigations have also been made on the removal of Rhodamine B dye in aqueous solutions by using polyaniline-coated on filter papers,[493] PANI/Sawdust,[494] and PANI@Carbonized tea waste material.[495] Rachna et al [496] studied the removal of RHB dye using PANI@Zn ferrite and observed maximum removal at pH 2. The adsorbent was also found to be effective even also after desorption. Thermodynamics studies indicated adsorption process to be spontaneous and exothermic in nature. Dhanavel et al [497] prepared α-MoO_3/Polyaniline by the chemical oxidative polymerization method. Further, these findings showed the maximum adsorption capacity of 36.36 mg g^{-1} and 76.22 mg g^{-1} corresponding to RhB and CR dyes, respectively. Ovando-Medina et al [498] coated polypyrrole (dia:200–300 nm) on coffee grounds waste (CGD) by in-situ pyrrole polymerization using potassium persulfate as oxidant. Subsequent studies have shown that the removal of the RhB dye from aqueous solution is favoured by basic pH due to its adsorption on CGD/PPy. It is also noted that the adsorption isotherm followed the Redlich–Peterson and Langmuir models with q_m of 50.59 mg g^{-1}.

5.3.1.3 Ternary Core-Shell Composites of ICPs

Ren et al [499] used Fe_3O_4@polypyrrole@4-vinylpyridine composites for the removal of rhodamine B and few other dyes (methylene blue, malachite green, alizarin red). The investigations on the adsorption kinetics and isotherm studies of rhodamine B fitted well with pseudo-second-order model and Langmuir model (q_m: 58.72 g mg^{-1}), respectively. The removal of RhB after five adsorption–desorption cycles of rhodamine B was found to be to 97.87%. According to the proposed mechanism, the adsorption of different dye on ternary composite could be related to the synergy effect of electrostatic interaction, hydrogen-bonding interaction, and $\pi-\pi$ interaction. Thermodynamic studies indicated spontaneous endothermic behavior for all the four dye. Xu et al [500] used Polyaniline/Attapulgite-supported

View Article Online
DOI: 10.1039/D5LP00230C

nanoscale Fe^0 to study the removal property and degradation mechanism of Rhodamine B including alizarin yellow R, methyl red, chrome black T, methyl orange and methylene blue. Their findings indicated relatively better removal performance of composite adsorbent on azo dyes compared to non-azo dyes. Polyaniline modified magnetic nanocomposites coated with dicationic ionic liquid was used to remove Rhodamine B from water sample.[501] The overall findings indicated best fitting of the kinetic data and adsorption studies to the pseudo-second order and Temkin's models, respectively.

In another study, the maximum adsorption capacity of rhodamine B, methylene blue, malachite green, and crystalline violet present on Fe_3O_4@polypyrrole@2-acrylamido-2-methyl-1-propanesulfonic acid composite in the aqueous solution were found to be 215.054 mg g^{-1}, 183.486 mg g^{-1}, 144.718 mg g^{-1} and 194.175 mg g^{-1}, respectively.[502] Trilaminar composite maintained removal efficiency exceeding 95 % after going through the 5 cycles. The kinetic, adsorption isotherm and thermodynamic studies indicated pseudo-second-order, Langmuir model and endothermic spontaneous adsorption process, respectively. In addition, mechanism has also been proposed on the adsorption of dyes by Fe_3O_4@PPy@AMPS composite based on the electrostatic interactions between dyes and adsorbent, formation of hydrogen bonding involving O (in AMPS) and H (dyes), π-π interactions between the benzene rings (AMPS) and in dye including the hydrophobic interactions. Sayeed et al [503] prepared PANI/C hybrid by in-situ chemical oxidation method under ultrasonic vibration. The scanning electron microscopy of the composite revealed the PANI network formation of intersecting nanorods. They also was reported that the uptake of Rhodamine B. by free form of the employed polyaniline take place due to the hydrogen binding, electrostatic altercations, and pi−pi interaction.

Varghese et al [504] prepared PEG capped PANI/TiO_2/CuO composite by in situ chemical oxidative polymerization to study its adsorption performance in the removal Rhodamine B

View Article Online
DOI: 10.1039/D5LP00230C

and other organic dyes in water. TEM studies of the trilaminar composite) confirmed the incorporation of TiO_2/CuO int CuO into the tubular-shaped fibrous network of PANI**.** The adsorption efficiency of MB, MG, CR, RhB, and CV on PANI/TiO_2/CuO after 120 minutes correspond to the removal efficiency of 98%, 67.7%, 95.1%, 64.4%, and 97.3%, respectively **(Figure 31 (a)**. The effect of the variety of materials on the adsorption of RhB dye has also been studied and corresponding findings are displayed in **Figure 31 (b)**. These findings revealed the superior removal performance by PANI/TiO_2/CuO (PTC) (89.7%) compared to PANI, (64.9%) TiO_2 (63.9%), CuO (44.3%), PANI/TiO_2 (PT):72.9%), PANI/CuO (PC):60.4%, and TiO_2/CuO (TC): 52.7% in 240 min due to its more negative zeta potential value. **Figure 31 (c)** shows effect of adsorbent (PANI/TiO_2/CuO) amounts on the adsorption of RhB for 120 min. According to this, the maximum adsorption efficiency was inevitable at 05 g of adsorbent. The variation of initial dye concentration in **Figure 31 (d)** indicated the maximum removal efficiency of 89.7% (adsorbent: 0.2 g, dye: 5 mg L^{-1}). The temperature dependence of the adsorption studies in **Figure 31 (e)** showed the removal efficiency decreasing from 89.7% (25 ^{0}C) to 78% (50 ^{0}C). The dependence of the pH displayed in **Figure 31 (f)** showed removal efficiency of RhB increasing from 78.5% to 89.7% on increasing pH from 4 to 6, respectively. Furthermore, the adsorption process followed the Langmuir adsorption isotherm (q_m: 3.53 mg g^{-1}). pseudo second order kinetics. **Figure 32** shows the effect of pH on the adsorption efficiency of PANI/TiO_2/CuO.

5.3.2 Congo Red

5.3.2.1 Hollow ICPs

A natural amino acid-doped polyaniline hollow tubular morphology [419] and hollow spherical polyaniline shell [491] exhibited removal capacity of Congo red of from the aqueous solution corresponding to 955.6 mg·g^{-1} and 60 mg g^{-1}, respectively. Benhaddad et al [505] synthesized hollow sea urchin-shaped polypyrrole in acidic medium using nanostructured

View Article Online
DOI: 10.1039/D5LP00230C

MnO_2 powder acting as oxidizing agent and sacrificial template. Subsequently, they studied its comparative performance in the adsorption of Congo red and methylene blue in aqueous solutions**.** These studies indicated that adsorption and removal of Congo red and methylene blue to be favoured under acidic and basic pH conditions, respectively. The adsorption followed Langmuir isotherm and pseudo-second-order kinetics for both the dyes. Mondal et al,[506] prepared network of polyaniline nanotubes by in-situ polymerization of aniline in the presence of ammonium persulfate and different aromatic carboxylic acids acting as a dopant (referred as B4CA). Subsequent investigations on its application in wastewater treatment led the following maximum adsorption capacity order for CR and other dyes: Indigo carmine (300 mg g^{-1}) ⩾ Eriochrome Black T (288 mg g^{-1}) > Methyl orange (285 mg g^{-1}) >Congo red (194 mg g^{-1})> *N,N'*-Bis (4-benzosulfonic acid)-perylene-3,4,9,10-tetracarboxylbisimide (192 mg g^{-1}). It may be noted that the adsorption of the dye is guided here by the electrostatic interaction between dye molecules and the PANI surface.

5.3.2.2 Binary Core-Shell Composites

PANI@ZnO nanocomposite were synthesized by oxidation chemical process and evaluated its time dependence performance on the adsorption of Congo red from aqueous solution keeping pH:5.0, C_0: 150 mg L^{-1}, adsorbents dose: 10 mg at 298 K.[507] These findings suggested 81.37 % removal of CR at 60 min. The kinetic model and isotherm data fitted well with the pseudo-second-order model (k: 0.0004 g mg^{-1} min^{-1}) and Langmuir (q_m: 76.92 mg g^{-1}), respectively. The regeneration efficiency of PANI@ZnO was found to be adequate even after five repeated cycles. Tanweer et al [508] prepared 3D-Polyaniline/Activated silica gel by the in-situ polymerization and used as potential adsorbent in the successful removal of Congo red, brilliant green, crystal violet, methyl orange. In another approach, hollow electrospun Polypyrrole@Cellulose fibrous membrane has been prepared by the

electrospinning followed by a dip-coating approach achieved 99.4 % rejection of anionic Congo red.[509]

Teng et al [510] observed 89.62% removal of CR from aqueous solution on PANI coated Fe_3O_4 nanoparticles (PANI/Fe_3O_4:70/30). These studies also indicated slightly enhanced dye removal by PANI/Fe_3O_4 compared to PANI alone. The adsorption of CR on PANI/Fe_3O_4 adsorbent could be ascribed to the possible bond formation between the -OH functional group (Fe_3O_4) and CR, electrostatic interactions between the $–NH^+$ of PANI (Emeraldine Salt form) and anionic sulfonic group of CR dye and hydrogen bonding interaction between CR and PANI/Fe_3O_4 surface. The regeneration studies have shown 77.4% removal retained after fifth cycle of adsorption-desorption, Singh et al [511] confirmed the coverage of in situ prepared PANI over the zinc titanate surface by FESEM. This showed the dramatically enhanced Congo red adsorption (q_m: 64.51 mg g^{-1}) compared to that of PANI and zinc titanate.

5.3.2.3 Ternary Core-Shell Composites

Recently, several works have been reported on ternary core-shell composites comprising Fe_3O_4 as a magnetic material. In one such work, Fe_3O_4/Polypyrrole/Carbon black nanocomposite fabricated by encapsulating Fe_3O_4 nanoparticles in PPy/Carbon black exhibited 96.9% removal of Congo red under given experimental conditions.[512] The findings matched well with Langmuir isotherm (q_m: 500 mg g^{-1}) and pseudo-second order kinetics. Dutta et al [513] fabricated polyaniline hollow microsphere (PNHM)/MnO_2/Fe_3O_4 composites by in situ deposition of MnO_2 and Fe_3O_4 nanoparticles on the surface of PNHM. Subsequently, they used it as adsorbent to study the removal of methyl green and Congo red in water. In view of this, the effect of pH on MG and CR dye removal efficiency (inset: change of wavelength of the dye solutions at different solution pH) are presented in **Figure**

View Article Online
DOI: 10.1039/D5LP00230C

33 (a) and (b) respectively. In addition, variation of zeta potential of PNHM/MnO_2/Fe_3O_4 with the variation of pH, effect of adsorbent dose, contact time, and initial dye concentration on MG and CR dye removal efficiency are respectively. described in **Figure 33 (c), (d), (e) and (f)**. It is noted that ternary composite showed 98% and 88 % adsorption efficiency in the removal of CR and MG under optimum conditions. The adsorption mechanism of MG and CR dye removal on the surface of PNHM/MnO_2/Fe_3O_4 at pH ~6.75 is schematically displayed in **Figure 34**. This has been explained on the basis of electrostatic interaction, ion exchange and the formation of the covalent bonds.

PANI@ZnO-SiO_2 hybrid material displayed better adsorption efficacy for CR 83.82 mg g^{-1} and MB (71.19 mg g^{-1}) in aqueous solution.[514] According to Weng et al [515], ultrathin Mg silicate nanosheets were grown on Fe_3O_4@PPy and subsequently used as adsorbent to remove Congo red from aqueous solution. These findings revealed applicability of Langmuir isotherm model with maximum monolayer adsorption capacities of 540.5 mg^{-1} and kinetic data fitting to the pseudo second-order model (k:0.9030 $g \cdot mg^{-1} \cdot min^{-1}$).Adsorptive removal of CR on L-cysteine/rGO/PANI nanocomposite have been made at room temperature to find out the optimum conditions.[516] These findings indicated the data fitting well with Langmuir model (q_m:56.57 mg g^{-1}) and kinetics validating pseudo-second-order. Further, the adsorption process was found guided by the via intra-particle diffusion and thermodynamic studies indicated adsorption process of CR to be endothermic and spontaneous.

5.3.3 Methylene Blue

5.3.3.1 Hollow ICPs

The contamination of toxic, carcinogenic, and non-biodegradable methylene blue in water is remain threat to human health as well as environmental safety and needs urgent attention. [517] Ayad et al [518] observed the adsorption capacity of PANI nanotubes to be about

View Article Online
DOI: 10.1039/D5LP00230C

8 times higher compared to PANI powder. In addition, the adsorption data of MB best fitted with Langmuir isotherm (monolayer saturation capacity: 9.21 mg g^{-1} and followed pseudo-second-order kinetics (k: 0.03595 g mg^{-1} min^{-1}). In another work, polyaniline hollow nanotubes (external dia: 50-60 nm, internal dia: 5–10 nm) have been in situ synthesized by using acid green crystal as structure directing agent as well as template and used it in the adsorption of methylene blue from aqueous media.[519] The experimental data supported fitting of pseudo first order kinetic model (k: 0.001 mon^{-1}) and maximum monolayer of 69.4 mg g^{-1}. Amer et al [520] reported acid-free synthesis of polyaniline nanotubes via the aniline oxidation using ammonium peroxydisulfate as an oxidant in the presence of methyl orange as structure-guiding agent in the dual removal of MB and AG dyes from aqueous solution. The kinetic studies confirmed the second-order model, while, adsorption data fitted well to the Langmuir isotherm. Furthermore, the calculated value of maximum monolayer capacity for MB and AG were found to 91.1 and 58 mg g^{-1}, respectively.

5.3.3.2 Binary Core-Shell Composites

PPy@MoS_2 hollow microtubes prepared through the combination of multistep successfully removed CR and MB from aqueous solution with kinetic data fitted well the pseudo-second-order.[521] Further, the adsorption process followed Langmuir model and Freundlich model for MB (q_m:121.3 mg g^{-1}) and CR (q_m:598.7 mg g^{-1}). The observed performance of dye removal is ascribed to its 1D hierarchical hollow structure and the synergistic effect between the MoS_2 nanoflakes and PPy coating. Ayad et al [522] observed complete adsorption of methylene blue displayed by the polyaniline nanotubes base/silica composite (0.05 g in 10 min corresponding to the 0.95 mg L^{-1} initial concentration of the dye. According to their findings, rate of adsorption increased in the following order: PANI NTs base/silica composite > PANI NTs base > conventional PANI base/silica composite > conventional PANI base. The experimental data was applied to study the kinetics (pseudo

View Article Online
DOI: 10.1039/D5LP00230C

first order, pseudo-second order) and the intraparticle diffusion models. Further, MB adsorption data filled best with the Langmuir isotherm. PANI partially covering the TiO_2 hydrate in water (pH 3-11) exhibited high maximum adsorption capacity (458.10 mg g^{-1}).[523] Further investigations have shown its 99% regeneration capability achieved after 10 cycles. It is suggested that the adsorption performance of MB onto PANI/TIO_2 is guided by the hydrogen bonding and electrostatic interaction on amino site, π-π stacking hydrophobic effect on benzene ring site and synergistic effect.

El-Sharkaway et al [524] synthesized transparent layered and wrinkled wavy structure of GO covered with PANI and used it subsequently in the preparation of PANI-RGO and used it to study the adsorption ability of MB in water. The kinetic studies of the PANI/GO and PANI/RGO indicated the pseudo first order kinetics and adsorption data best suited to the Langmuir model. The estimated maximum dye adsorption capacity of MB on PANI/GO and PANI/RGO adsorbents were found to be 14.2 and 19.2 mg g^{-1}, respectively. These findings affirmed PANI/RGO to be more effective compared to the PANI/GO in the removal of MB. Ayad et al [525] prepared coating of polypyrrole on the cotton textile by in situ oxidative polymerization of pyrrole monomer and subsequently used as adsorbent of methylene blue in alkaline solutions. the adsorption process followed Freundlich isotherm model and the adsorption kinetics fitted well with pseudo-second-order. They also extended their work on the removal of Acid Green 25 in acidic medium and observed some affinity.

5.3.3.3 Ternary Core-Shell Composites

Fe_3O_4@Polypyrrole@Sulfamica Acid Composite prepared by the hydrothermal method and in situ polymerization have been evaluated for its performance in the adsorption of MB and other dyes MG, CV, and RhB).[526] The adsorption kinetics and adsorption isotherms of all the dyes were found to fitting with pseudo-second-order and Langmuir adsorption isotherm, respectively. The thermodynamic study of the adsorption process

View Article Online
DOI: 10.1039/D5LP00230C

indicated spontaneous heat absorption behavior. Wang et al [527] fabricated core–shell Fe_3O_4@Polypyrrole@Sodium dodecyl benzene sulfonate (SDBS) composite following the combination of different methods and studied the effect of different parameters on the adsorption of MB and MG from aqueous solutions. These findings indicated kinetic and adsorption following the pseudo-second order and Langmuir isotherm (q_m^{MB}: 124.07 mg g^{-1}, q_m^{MG}: 73.10 mg g^{-1}), respectively. Further, cyclic stability of the adsorbent was also assessed by carrying out adsorption–desorption experiment for five cycles. These findings have shown remarkable removal efficiencies of MB (80 %) and MG (90 %) following the five desorption-adsorption cycles. The excellent adsorption performance of dye on the ternary coew-shell composite is assigned to the synergistic effect of the electrostatic interactions, hydrogen bonding, and π-π interactions mediated by PPy and SDBS,

Polypyrrole/GO@Fe_3O_4 has been prepared by one-step and used as magnetic adsorbent in the removal of methylene blue dye from aqueous solution (pH: 8).[528] This adsorbent exhibited adsorption capacity of 323.2 mg g^{-1} for MB. A super-paramagnetic architecture comprising of Fe_3O_4@PPy@RGO ternary nano-adsorbents was fabricated to remove the methylene from wastewater.[529] The choice of Fe_3O_4 hollow spheres, polypyrrole layers and, graphene sheets were guided by their role in contributing towards the abundant hydrophilic groups, protecting hollow spheres from acid corrosion/surface oxidation and in enhance the removal performance of Fe_3O_4@PPy. HRTEM studies of Fe_3O_4@PPy@RGO established the formation of a ternary nano-architecture comprising wrapping of Fe_3O_4@PPy by RGO sheets. **Figure 35 (a)** shows Fe_3O_4@PPy@RGO exhibiting superior removal efficiency of MB compared to Fe_3O_4 and Fe_3O_4@PPy in neutral solution (pH: 7). Further, Fe_3O_4@PPy@RGO remained about 96% removal efficiency after five cycles of adsorption–desorption process **Figure 35 (b).** In addition, removal efficiency of these adsorbents in acidic solution (pH: 2) and alkaline solution (pH 10) are also displayed in

View Article Online
DOI: 10.1039/D5LP00230C

Figure 35 (c) and (d), respectively. Graphene modified magnetic polypyrrole,[530] and Fe_3O_4/Polypyrrole/Phytic acid [531] also efficiently removed methylene blue from aqueous solution.

5.3.4 Methyl Orange

Methyl orange (MO) ably used in the textile, food, paper, cosmetics and for several other purposes.[532] However, its release into the industrial effluents deteriorate the water quality with hazard impact on public health effecting the human's eye, skin irritation, nausea, diarrhea and respiratory tract irritation. The high-water solubility, high stability towards heat, and temperature of MO makes the removal of this dye from aqueous solution not exciting.[533]

5.3.4.1 Hollow ICPs and its Composites

A very limited work has been reported on the removal of methyl orange using hollow sphere and one dimensional ICPs as adsorbents. According to Zhao et al,[419] amino acid-doped polyaniline nanotubes exhibited the following order towards the adsorption capacity of different dye: Congo red (112.0 mg g^{-1}) > Orange yellow (69.2 mg g^{-1}) ≥ Indigo carmine 66.8 mg g^{-1}) > Methyl orange 54.8 mg g^{-1}) > Crystalline violet 50.0 mg g^{-1}). Yildirim et al [534] carried out the removal of methyl orange using polyaniline nanotube-filled sodium alginate bio-composite to study the effect of adsorbent dose, pH, time, and concentration of MO. Based on the applicability of Langmuir isotherm, maximum adsorption capacity (q_m) was found to be 370.4 mg g^{-1} at 25 ^{0}C under optimum conditions.

5.3.4.2 Binary and Ternary Core-Shell Composites

TEM studies of PANI-MWCNTs (4 wt%) composite prepared by in-situ oxidative polymerization showed spherical PANI covering the tubular structure of MWCNT nonuniformly. [535] The adsorption studies of methyl orange using PANI-MWCNTs as adsorbent agreed with the second-order kinetics (k: 5.265 × 10^{-4} g mg^{-1} min^{-1} at 30 °C) and

View Article Online
DOI: 10.1039/D5LP00230C

Langmuir equilibrium model (q_m:149.25 mg g^{-1}). Polyaniline (skin)/polyamide 6 (core) composite fiber prepared via a facile in situ oxidation polymerization was tested for the removal of methyl orange. [536] These findings revealed the adsorption/desorption kinetics and isotherms following the pseudo-second-order and Langmuir models (q_m:58.7 mg g^{-1}), respectively. Waterborne poly vinyl pyrrolidone stabilized polyaniline core (dia: 85–90 nm)–shell (dia: 20–22 nm) composite also effectively removed MO in aqueous solution.[537]

Zhang et al [538] fabricated halloysite nanotubes/Polypyrrole nanocomposites by in situ polymerization of pyrrole monomer in the presence of HNTs. Subsequently, its adsorption efficiency was evaluated in the removal of methyl orange as a function of adsorbent dose, contact time, initial concentration MO, temperature on the adsorption efficiency. The adsorption kinetics fitted to the pseudo-second-order and adsorption isotherms validated by Langmuir (q_m: 214,6 mg g^{-1}) and Freundlich models. The thermodynamic investigations pointed adsorption process of methyl orange onto HNTs/PPy to be spontaneous and exothermic. Furthermore, regeneration experiments have shown reusability of HNTs/PPy nanocomposites at least three times in removing methyl orange in aqueous solution.

Yao et al [539] prepared core–shell Fe_3O_4@C@polyaniline composite microspheres as separable adsorbent for the removal of MO dye from aqueous solution. the TEM images of the the product confirmed core-shell structure of Fe_3O_4@C@PANi composite microspheres. The adsorption isotherms and kinetics data supported the Langmuir and pseudo second order models, respectively. The trilaminar core-shell composite also exhibited excellent adsorption capability (q_m: 120.2 mg g^{-1}) and removal efficiency retained after 5 cycles (of was also inevitable an excellent adsorption capability (~81%) after five adsorption–desorption cycles.

6.3.5 Other Dyes

View Article Online
DOI: 10.1039/D5LP00230C

In addition, several work has also been reported using different core-shell adsorbents comprising conducting polymers (in the removal of several other dyes), such as: Polymethylmethacrylate/Rice husk ash)/Polypyrrole (E102, IC).[451] magnetic Fe_3O_4@Polypyrrole@Sodium dodecyl sulfate (MG, AR1),[489] magnetic core−shell Fe_3O_4@Polypyrrole@4-vinylpyridine (AR, MG),[499] Polyaniline/Attapulgite supported nanoscale zero-valent iron (AYR, MO, methyl red, chrome black T),[500] Magnetite@Polypyrrole@2-acrylamido-2-methyl-1-propanesulfonic acid microspheres (MG, CV),[502] 3D Polyaniline/Activated silica gel (BG,CV, MO),[508] Hollow Polyaniline microsphere/MnO_2/Fe_3O_4 (MG),[513] Polyaniline hollow nanotubes (AG),[519,520] Fe_3O_4@Polypyrrole@Sodium dodecyl benzene sulfonate (MG),[527] Fe_3O_4/Polypyrrole/Phytic acid (CV),[531] Polyaniline@TiO_2 and Polyaniline@SiO_2 (CV, R6G,BB,CV),[540] Graphene/Fe_3O_4/Polyaniline (MG,AR1),[541] Carbon nanotube/Polyaniline (MG),[542] Fe_3O_4@RGO@PANI (MG),[543] wheat straw-core hydrogel spheres with polypyrrole nanotubes (EY),[544] Polypyrrole/$Mn_{0.8}Zn_{0.2}Fe_2O_4$/Graphite Oxide (AR1),[545] Polyaniline coating chitosan-Graphene oxide-functionalized carbon nanotube (AR1,BG),[546] Polythiophene/ZnO/MWCNTs and Polythiophene/ZnO/ox-MWCNTs (BG),[547] and Fe_3O_4@PDA@PANI (TTZ, SY),[548]

Table 4 presents the removal of the various dye in aqueous solution based on hollow intrinsically conducting polymers, nanocomposites comprising hollow intrinsically conducting polymers and core-shell based ICP nanocomposites as adsorbents.

5.4. Supercapacitor Applications of Hollow ICPs

Supercapacitors are considered as energy storage devices storing and releasing energy through the movement of ions within the electrolyte.[549,550] Further, the carbonaceous materials, conducting polymers, and transition metal oxides attracted more attention as electrode material in this application. The comparison of their merit/demerits has been

View Article Online
DOI: 10.1039/D5LP00230C

highlighted in **Table 5**. These supercapacitors are regarded as more promising candidates for having very high-power density, long cyclic stability and excellent durability. The supercapacitors can be classified, into electrical double-layer capacitors (EDLCs), pseudocapacitors (PCs), and hybrid supercapacitors, as schematically based on the of mechanism involved in energy storage (**Figure 36)**.[551] EDLCs are non-faradic supercapacitors or ultracapacitor involves the storage of the charge taking place taking place in the electrical double layer formed at the electrode/electrolyte interface without any changes in the chemical properties of electrode materials. In case of PC, charge is stored electrochemically through highly reversible redox reactions at the electrode-electrolyte interface and offer more power and charge density compared to EDLCs. A hybrid supercapacitor, on the other hand, is a combination of an EDLC and a pseudocapacitor and allow for both faradaic and non-faradic charge storage.

In this regard, intrinsically conducting polymers are favoured in supercapacitor applications due to simple synthesis, tunable conductivity, large surface area, high flexibility, and pseudocapacitive properties.[7] These features enable them to store and release energy quickly thereby making conducting polymers as ideal candidate for high-power applications. The superior electrochemical performance of these ICPs is greatly guided by their morphology. In view of this, hollow-structured materials electrode can be better alternatives by offering higher specific surface area to facilitate the large electrode/electrolyte interface favorable for the fast transport of charges and ions as well as act as the ion reservoir to benefit the accumulation of ions Therefore, ICPs are considered as promising electrode materials due to their low production cost and their ability to possess redox pseudocapacitance and double-layer capacitance. However, application of ICPs is limited due to the inferior stability, therefore, ICP is combined with other active materials to

View Article Online
DOI: 10.1039/D5LP00230C

overcome this intrinsic disadvantage, Accordingly, the performance of ICP for hollow structured ICPs, their composites and core-shell based materials below.

5.4.1 Hollow ICPs Microsphere

Tan et al [552] prepared hollow polyaniline microspheres using sulfonated polystyrene microspheres as template. The electrochemical investigations of hollow polyaniline predicted increase in specific capacitance of hollow polyaniline microspheres with the feed ratio of aniline (ANI) to sulfonated polystyrene (SPS) referred as $r_{ANI/SPS}$ and attained a maximum value of 421 F g^{-1} corresponding to $r_{ANI/SPS}$ of 1.0. The cycle life performance of hollow polyaniline microspheres electrode was tested for 500 cycles (10 mA cm^{-2}). It decreased for the first 200 cycles most likely due to the swelling and shrinking of PANI and finally remained more or less unaltered. In another work, interfacial polymerization method was used to synthesize hollow polyaniline nano-capsule with the holes on the wall in absence of any template.[553] According to TEM studies, PANI nano-particles comprising the formation of nano-rods with uniform hollow capsule-like structure comprising the holes on the wall (capsule). The PANI nano-capsule electrode displayed high specific capacitance of 502 F g^{-1} (at the current density of 5 mA cm^{-2}) and excellent cycling stability. Such electrochemical performance of capsule-like PANI electrode has been attributed to the conductivity and hollow nanostructure that accounts for rapid electrolyte transport, shortened the ions diffusion paths within the active materials.

Polyaniline hollow microsphere (dia: 410 nm, thickness: 72 nm) doped by (poly (2-acrylamido-2-methylpropane sulfonic acid) (PAMPS) synthesized by a self-assemble method have shown excellent promise in the fields of supercapacitors.[554] Li et al [555] fabricated Ce^{3+}-doped polyaniline hollow microspheres by self-assembly method exhibited its high specific capacitance of 248.2 F g^{-1} (1 mA cm^{-2}) due to its enhanced conductivity

View Article Online
DOI: 10.1039/D5LP00230C

compared to PANI (201.6 F/g). In another approach, hollow PANI nanospheres prepared by in-situ chemical oxidative polymerization of aniline in presence of uniform poly(methyl methacrylate-butyl methacrylate-methacrylic acid) latex microspheres (self-sacrificial template) demonstrated specific capacitance (485.5 F g^{-1} at 1 A g^{-1}) and performance after 500 cycles (69%).[556]

Polypyrrole hollow nanospheres prepared using polystyrene (PS) as a template and subsequently removing it by dissolving it in DMF displayed high specific capacitances (350 F g^{-1} at 1 A g^{-1}).[557] The corresponding symmetric supercapacitor has shown the maximum energy density of 40 Wh kg^{-1} at a power density of 490 W kg^{-1}). The electrochemical studies were also made on hollow polypyrrole films prepared by deposing polypyrrole on 3D colloidal crystal template.[558] According to Li et al, [559] hollow capsular polypyrrole nanofibers with porous capsular acted as flexible, binder-free, self-supported supercapacitor electrode exhibiting specific capacitance of 203 F g^{-1} at 2 mV sec^{-1} and excellent capacitance retention (> 90% after 11000 charge–discharge cycles @10 A g^{-1}). This is attributed to the availability of enough free-space in the capsular walls of the hollow PPy film to facilitate the volume variation during doping/de-doping. Zhang et al [244] synthesized PEDOT hollow nanospheres by expulsion of SiO_2 from the SiO_2@PEDOT nanospheres by dissolving it hydrofluoric acid. The PEDOT hollow sphere film fabricated in this manner showed a high specific capacitance (121.6 F g^{-1}) at the current density of 0.5 A g^{-1} and sustained 65.7% of its initial specific capacitance at a current density of 8.0 A g^{-1}.

5.4.2 Nanotubes of ICPs

According to Cui et al.,[100] dual-colloid interface co-assembly approach in the synthesis of hollow mesoporous conducting polymers (mPPy-nb-4) delivered specific capacitance of 225 F g^{-1} (1 mV s-1) and also offered a power density of 343 mW cm^{-3} at energy density of 0.758 mWh cm^{-3}. In another work, Chen et al [492] prepared hollow polyaniline helical nanobelts

View Article Online
DOI: 10.1039/D5LP00230C

by using a synthetic template (oligomers) following in-situ chemical oxidation of aniline. They observed specific capacitance up to 688 F g^{-1} (scan rate: 5 mV s^{-1}) and 81.6% retention (1000 cycles). Subsequent studies on the fabricated symmetric supercapacitor showed energy density and power density of.14.37 Wh kg^{-1} and 500 W kg^{-1}, respectively. Fan et al [560] synthesized polyaniline nanotubes using natural tubular halloysite as hard template and subsequently subjected it to carbon coating by hydrothermal method **Figure 37 (a)**. The electrochemical performance of this electrode material indicated high specific capacitance (654 F g^{-1} at 1 A g^{-1}), excellent electrochemical stability with capacitance retentions (~87% after 10000 cycles). This is suggested that carbon coated PANI electrode acted as a constraint layer to prevent the tubular structured PANI from expanding outward during the charge-discharge process. ZnO nanorod arrays (sacrificial templates) have been used to fabricate polyaniline nanotube arrays and studied its electrochemical polymerization for supercapacitor applications **(Figure 37 (b).**[561] Jyothibasu and Lee [562] fabricated polypyrrole tubes using curcumin (template) as schematically shown in **Figure 37(c)** and combined it with functionalized carbon nanotubes (*f*-CNTs) to form freestanding electrodes **(**referred as PPyC3T2/f-CNT**).** It showed excellent areal capacitance of 11830.4 mF cm^{-2} at a current density of 2 mA cm^{-2} thick freestanding PPyC3T2/*f*-CNT-electrode at a high mass loading of 30 mg cm^{-2}. Further, symmetric supercapacitor assembled by using the PPyC3T2/*f*-CNT displaced areal capacitance, cycling stability, high energy density and maximum power density of 2732 mF cm^{-2} at 2 mA cm^{-2}, 118.18% retention after 12,500 cycles, 242.84 μW h cm^{-2} and 129.35 mW cm^{-2}, respectively.

Hollow PANI nanotubes (inner dia: 80 nm, outer dia:180 nm) prepared via one-step polymerization attained specific capacitance of 436 F g^{-1} (0.5 A g^{-1}) in H_2SO_4 (1 mol L^{-1}) solution with good cycling stability (89.2%: 500 cycles at a current density of 0.5 A/g) [563] Crystalline tetragonal hollow polyaniline nanotubes prepared by using methyl orange as self-

View Article Online
DOI: 10.1039/D5LP00230C

degraded template showed the specific capacitance of 590 ± 36 F g^{-1} at a scan rate of 5 mV/s.[564] The assembled symmetrical device exhibited maximum energy density and power density of 14.56 Wh kg^{-1} and 250 W kg^{-1}, respectively. Ahn et al [565] prepared PPy hollow nanoparticles with controlled diameters were through surfactant-templated chemical oxidation polymerization **(Figure 37 (d)**. The specific capacitance of PPy hollow nanoparticles (326 F g^{-1}) fabricated in this manner was found to be approximately twice as large as that of solid PPy nanospheres. The high-performance supercapacitors performance has also been displayed by PANI nanofibers, nanotubes, and nanospheres [566] hollow polyaniline nanofibers fabricated by electrospinning, [312] Hryniewicz and Vidotti [567] form the first time electrodeposited PEDOT nanotubes onto stainless steel mesh electrodes in the presence of methyl orange template and observed enhanced supercapacitive and electrocatalytic properties.

5.4.3 Hollow ICPs Nanocomposites

Zhang et al [569] prepared hollow Polypyrrole/Cellulose hydrogels to study their performance as flexible supercapacitor. The assembled symmetrical supercapacitor device delivered high specific capacitance (255 F g^{-1} at 0.25 A g^{-1}), good rate capability (77% capacitance retention at 30 A g^{-1}), cyclic stability (80% after 10000 cycles at 10 A g^{-1}) and energy density (20.4 Wh kg^{-1}) at a power density of 194 W kg^{-1}. Wang and others [570] investigated the electrochemical performance of mesoporous MnO_2/Polyaniline composite with unique morphology of hierarchical hollow submicron spheres synthesized by an interfacial approach. The electrochemical studies revealed its superior electrochemical properties as indicated by its specific capacitance (262 F g^{-1}) and higher capacitance retention (93% of its initial capacitance after 800 cycles) owing to its microstructure and polyaniline/MnO_2 coexisting together.

View Article Online
DOI: 10.1039/D5LP00230C

3D hollow balls of graphene–polyaniline hybrids were prepared fabricated through the self-assembly of graphene oxide and PMMA followed by the polymerization of polyaniline and demonstrated high specific capacitance and good cycle stability.[571] Luo et al [572] used **by** layer-by-layer assembly for the preparation of Graphene–Polyaniline hollow microsphere for supercapacitor application. It displayed excellent specific capacitance (381 F g^{-1}: 4.0 A g^{-1}) and good cycling stability (83 % after 1000 cycles) in 1 M H_2SO_4 solution due to synergistic effect. The hierarchical Ti_3C_2/PANI nanotubes have shown excellent specific capacitance performance (596 F g^{-1} at 0.1 A g^{-1} with 94.7% retention after 5000 cycles (at 1 A g^{-1}).[573] Further, symmetric supercapacitor device based on this showed excellent performance (energy density: 25.6 Wh kg^{-1} at 153.2 W kg^{-1}), power density: 1610.8 W kg^{-1} at 13.2 Wh kg^{-1}, capacitance retention 81.1% after 4000 cycles).

Devi and Kumar [574] prepared nanocpmposites of reduced graphene oxide/polyaniline nanotubes in presence as well as absence of irradiation high energetic ions and performed electrochemical investigations as supercapacitor. They observed the relatively enhanced specific capacitance (482 F g^{-1} at 0.5 A g^{-1}) and cyclic stability (92%) compared to unirradiated nanocomposite. This is ascribed to the increased surface energy and porosity as a result of irradiation. Yang et al [575] tested electrochemical performance polypyrrole hollow nanosphere intercalated graphene-based flexible supercapacitor and observed its area specific capacitance and capacitance retention of 381.54 mF cm^{-2} (at 2 mA cm^{-2}) and 93.94% after 1000 cycles, respectively. Graphene–polypyrrole hollow sphere,[576] hollow polypyrrole nanosphere embedded in N-doped graphene layers,[577] 3D-arrayed polyaniline hollow nanospheres encaging RuO_2 nanoparticles,[578] polyaniline hollow fibers decorated by graphene,[579] graphene-polypyrrole nanotube,[580] 3D metal−organic frameworks with conductive polypyrrole tubes,[581] and hollow PPy nanospheres decorated on the CNT [582] were synthesized and also used as electrode material for electrochemical supercapacitor applications.

5.4.4 Core-Shell based ICP Nanocomposites

5.4.4.1 Binary Core-Shell Nanocomposites

Tian et al [583] wrapped polyaniline nanowires on the polypyrrole hollow nanotubes by the chemical method and observed its high specific capacitance (~ 765 F g^{-1} at a scan rate of 10 mV s^{-1}) and the capacitance loss of~ 13.7% after 1000 charging/discharging cycles. Such performance has been explained on the basis of the synergistic effect of PANI and PPy. Core-shell polyaniline functionalized carbon quantum dots exhibited high specific capacity of 264.6 F g^{-1} (2.5 A g^{-1}) and high stability indicated by 5000 charge–discharge cycles.[584] The sea urchin-like polyaniline grown on the surface of polypyrrole displayed (referred as PPy@PANI) with a core-shell structure by dilute solution polymerization according to the **Figure 38 (a).**[585] The variation of the specific capacitance versus the scan rate is displayed in **Figure 38 (b**). According to this, the specific capacitance of PPy@PANI corresponds to 510 F g^{-1} (scan rate: 10 mV s^{-1}) compared to PPy (87 F g^{-1}) electrode and of pure PANI. (256 F g^{-1}) electrodes. PPy@PANI also showed the good cycle stability as evident from 12.4% loss of specific capacitance after 1000 charge/discharge as evidenced from **Figure 38 (c).** Such electrochemical performance of PPy@PANI electrodehas been assigned to the ascribed to the synergistic effect between cored PPy and shelled PANI layer.

Li et al [586] used hollow microsphere (MS) and microtubes (MT) as PPy core using polystyrene microspheres and methyl orange as hard and soft templates. Subsequently, they prepared respective poly(1,5-diaminoanthraquinone) (referred as PDAAQ) with MS and MT and observed the following order for specific capacitance at a current density of 1 A g^{-1}:

PPy@PDAAQ MTs (533 F g^{-1}) > PPy@PDAAQ MSs (471 F g^{-1}) > PDAAQ, 348, F g^{-1}) >PPy MTs (322 F g^{-1}) > PPy (MSs 235 F g^{-1}).

View Article Online
DOI: 10.1039/D5LP00230C

The hollow morphology of PPy could account for the observed high specific capacitance of PPy@PDAAQ MTs.

The. specific capacitance retention after 10,000 cycles followed the following trend: PDAAQ (146.0%)> PPy@PDAAQ MTs (107.4%), PPy@PDAAQ MSs (98.0%), PPy MTs 43.6%), and PPy MSs (27.3%).

Fan et al [587] prepared core-shell hybrid comprising PS@PANI, Polyaniline hollow spheres (PANI-HS)@GO and PANI-HS@ ERGO (Electrochemical reduced graphene oxide) according to the procedure as illustrated in **Figure 39 (a)**. The morphology and structure of the PANI-HS36@GO (36: shell thickness of PANI-HS) hybrid has been studied by SEM and displayed in **Figure 39 (b).** PANI-HS36@ERGO hybrids indicated its significantly high specific capacitance corresponding to 614 F g^{-1} at 1 A g^{-1} current density **(Figure 39 c)** and maintained 90% after 500 charging/discharging cycles at a current density of 1 A g^{-1} **(Figure 39(d)** due synergistic effect.

Du et al [588] used MnO_2 nanotubes as the reactive template for the preparation of PANI nanotubes following used in-situ polymerization process and exhibited excellent specific capacitance (455.7 F g^{-1} at 0.5 A/g), rate capability of 63.2% even up to 30 A/g. However, it showed poor cycle stability due to the swelling and shrinking of PANI during intercalating/deintercalating. Therefore, they fabricated hierarchical carbon layer encapsulated PANI nanotubes by hydrothermal method and observed its superior performance compared to PANI nanotubes. In addition, the assembled symmetric supercapacitors based on this delivered high energy density (42.32 Wh kg^{-1}) and power density (16.44 kW kg^{-1}) and good cycle stability. Mini and Devendrappa[589] prepared core/shell Polyaniline/NiO nanocomposite and studied its use electrochemical performance as electrode is supercapacitor applications. These findings revealed its specific capacitance, energy density, power density and Coulombic efficiency corresponding to 362 F g^{-1} (1 A g^{-}

View Article Online
DOI: 10.1039/D5LP00230C

^{1}), 50.2 Wh kg^{-1}, 0.50 kW kg^{-1} and 99% (at 4 Ag^{-1}) respectively. The enhanced specific capacitance performance is ascribed to the nanosized effect of NiO and the synergic effect between NiO and PANI.

Polypyrrole nanosphere (dia: ~70 nm)/Graphene oxide synthesized via in situ surface-initiated polymerization exhibited specific capacitance of 370 F g^{-1} @.5 A g^{-1}, and capacitance retention of 91.2% even after 4000 cycles owing to the core-shell structure and synergistic effect.[590] Qi et al [591] reported preparation of core-shell structured tubular graphene nanoflakes-coated polypyrrole nanotubes and observed its large capacitance, high capacitance retention and stable cycling performance. The energy density and cycling stability of the symmetric supercapacitor device based on this correspond to 11.4 μWh cm^{-2} at 720 μW cm^{-2} and over 80% capacitance retention after 5000 cycles, respectively.

In recent years, considerable interest has aroused to study the capacitive properties of MoS_2 for its application in the supercapacitor.[592-597] However, despite many advantages, its aggregation, poor electrical conductivity and specific capacitance of MoS_2 limit its practical application in energy storage electrode material.[592] As a result, MoS_2 is combined with conducting polymers to overcome this problem. In view of this, Chen et al [593] prepared urchin-like MoS_2@PANI (MoS_2:25 wt%) by hydrothermal method and observed its maximum capacitance of 645 F g^{-1} at 0.5 A g^{-1} due to the synergistic effect. In addition, excellent cycling stability (89% capacitance retention) has been observed after 2000 cycles at a current density of 10 A g^{-1}).

Zhang et al [594] fabricated core/shell microspheres comprising hollow MoS_2/PANI-5 (5 represents the mass ratio of aniline to hollow MoS_2 microspheres). The electrochemical studies of this electrode material displayed the specific capacitance of 633 F g^{-1} @0.5 A g^{-1} and retention of the capacitance up to 86.0% after 1000 cycles at 10 A g^{-1} benefitting from

View Article Online
DOI: 10.1039/D5LP00230C

polyaniline confined firmly on the microspheres of. MoS_2. In addition, MoS_2/PANI-5 composite the energy density can deliver 31.7 W h kg^{-1} at the power density is 0.3 kW kg^{-1}.

A template-assisted method has been employed to synthesize the MoS_2/PANI (mass ratio=1:2) hollow microsphere and used aa a promising electrode for supercapacitor.[595] SEM images clearly established the coating of PANI on the surface of hollow structure of MoS_2 microspheres (dia: ~2 μm). The specific capacitance was found to be 299 F g^{-1} at a scan rate:10 A g^{-1} and attributed to the synergistic effect of MoS_2 core and PANI coating shell. MoS_2/PANI microspheres electrode materials also delivered the excellent cycle stability as evident from its retention of 84.3% after 8000 cycles. The investigations also indicated the energy density reaching 23.1 Wh kg^{-1} at a power density of 8320 W/kg. The specific capacitances of fabricated symmetric supercapacitor based on MoS_2/PANI microspheres electrodes corresponds to 231, 139, 97, 79 F g^{-1} at the current density of 0.2 A g^{-1}. Further, assembled symmetric supercapacitor also exhibited high cyclic stability (80.4% after 5000 cycle at1 A g^{-1}). These findings highlighted potential application of MoS_2/PANI hollow microspheres for supercapacitor.

Ansari et al reported [596] the formation of mechanically exfoliated MoS_2 sheet coupled with polyaniline. TEM studies of the product indicated PANI coated on the MoS_2 sheet and displayed the specific capacitance of 510.12 F g^{-1} at a current of 1 A g^{-1} due to the synergistic effect and interfacial interaction. The hierarchical PEDOT@MoS_2 showed high specific capacitance (2540 mF cm^{-2} at 1 mA cm^{-2}) and excellent capacitance retention (98.5% after 5000 cycles at a high current density of 100 mA cm^{-2}. This ia ascribed to the hierarchical core/shell structure of the electrode material and the synergic effect.[597] In addition, assembled asymmetric supercapacitor delivered the high energy density (937 Wh m^{-2}) at 6500 W m^{-2} and excellent cycling stability with capacitance retention of 100% (5000 cycles).

View Article Online
DOI: 10.1039/D5LP00230C

According to Liang et al,[598] V_2O_5@PPy displayed high conductivities and synergic effect accounted for the specific capacitance of 307 F g^{-1} and good cycling life (82 % capacity retention up to 1000 cycles). Such performance of V_2O_5@PPy is benefited from the enhanced conductivity, synergistic effect, and the stability of the composite. The symmetric V_2O_5/PPy device exhibited a maximum energy density of 37 Wh Kg^{-1} at a power density of 161 W kg^{-1}. In addition, polyaniline-carbon nanotube core-shell,[599] pistil-like $MnCo_2O_{4.5}$@PANI,[600] and CuO@NiO/Polyaniline/MWCNT are also examined as high-performance electrode for Supercapacitor.[601] Ni ferrite@Polypyrrole,[602] core/sheath structured ultralong MnO_x/PPy nanowires,[603] and CuS@PANI [604] also displayed superior performance as electrodes in supercapacitor applications. The performance of MWCNT coated with PANI (core dia: ~80–150 nm) by has been also been evaluated for supercapacitor application.[605] These findings showed maximum specific capacitance (552.11 F g^{-1} at a 4 mA cm^{-2}) for PANi/MWCNT (10 wt%) in 1 M H_2SO_4.

Xia et al [606] prepared core-shell PANI/CNTs nanostructured hybrid by chemical vapor and electrochemical deposition methods according to the **Figure 40**. Subsequent findings based on galvanostatic charge/discharge (GCD) curves of CNTs and PANI/CNTs with and without the addition of 0.02 M Fe^{3+}/Fe^{2+} are displayed in **Figure 41 (a).** It is inferred that discharge time is extended on the addition of Fe^{3+}/Fe^{2+} redox couple. The following order for discharge time is observed: PANI/CNTs (0.02 M Fe^{3+}/Fe^{2+}) > PNI/CNTs > CNT ((0.02 M Fe^{3+}/Fe^{2+}) > CNTs. GCD curves of PANI/CNTs at different current density in 1 M H_2SO_4 in **Figure 41 (b)** confirmed the ideal capacitive mechanism of the core–shell hybrid. GCD curves of PANI/CNTs in 1 M H_2SO_4/0.02 M Fe^{3+}/Fe^{2+} electrolyte at different current densities displayed in **Figure 41 (c).** These findings affirmed non-ideal triangular pattern corresponding to the redox reactions behavior of Fe^{3+}/Fe^{2+} redox couple**.** The specific capacitance curves of PANI/CNTs at different current densities in **Figure 41 (d)** showed improvement in the

View Article Online
DOI: 10.1039/D5LP00230C

specific capacitance of PANI/CNTs (1005 F g^{-1}) on adding 0.02 M Fe^{3+}/Fe^{2+} (1547 F g^{-1}) at 2 A g^{-1} in 1 M H_2SO_4. Such superior performance is attributed to the synergistic effect originating from contribution of the Fe^{3+}/Fe^{2+} redox couple and the PANI/CNTs core–shell structure. In addition, specific capacitance of the assembled symmetric architecture device was calculated and found to be 412 F g^{-1} at 0.5 A g^{-1}. In addition to energy density (22.9 Wh kg^{-1}) reached at a power density of 700.1 W kg^{-1} and the capacitance retention of 97% (2000 charge–discharge cycles) using PVA/H_2SO_4/Fe^{3+}/Fe^{2+} gel as redox electrolyte. These findings justify the role of core–shell PANI/CNT hybrid electrode and Fe^{3+}/Fe^{2+} redox additive electrolyte in achieving such enhanced electrochemical performance.

The enhanced electrochemical performance has been reported for the hierarchical $NiCo_2S_4$@PANI core-shell nanowires grown on carbon filter.[607] The specific capacitance of the electrode fabricated in this manner showed enhanced areal capacitance of 4.74 F cm^{-2} (1823 F g^{-1}) at 2 mA cm^{-2} and a capacitive retention of 86.2% (5000 cycles) compared with $NiCo_2S_4$/CF due to the availability of the more electrochemically active sites and faster ionic diffusion. The excellent cycling stability of $NiCo_2S_4$@PANI/CF is suggested to be induced by the presence of the PANI shell. The assembled asymmetric supercapacitor (positive electrode: $NiCo_2S_4$@PANI/CF, negative electrode (graphene/CF) delivered high energy density of 64.92 Wh kg^{-1} at a power density of 276.23 W kg^{-1}. This was found to be significantly higher compared to the asymmetric and symmetric supercapacitors based on $NiCo_2S_4$ and ascribed to the core/shell heterostructure of $NiCo_2S_4$@PANI/CF.

Pan et al [608] displayed more surface capacitive contribution and enhanced electrochemical performance benefiting from the unique heterostructure in $NiCo_2O_4$@Polyaniline nanotubes anchored on carbon. Their finding showed specific capacitance of 720.5 C g^{-1} at 1 A g^{-1} and found to be much better than that of $NiCo_2O_4$. In addition, cyclic performance and coulombic efficiency has also been investigated of the

View Article Online
DOI: 10.1039/D5LP00230C

$NiCo_2O_4$@PANI electrode. These findings showed sample retaining 99.64% of its initial gravimetric capacity following 10000 cycles with 100% of coulombic efficiency due to the high efficiency of rapid electron transfer for charge storage and delivery. They also suggested that unique coaxial structure $NiCo_2O_4$@Polyaniline increases the interface area of the electrode/electrolyte and facilitates a shorter diffusion path for ions and electrons

Mu et al [609] used polystyrene sulfonate microsphere as template to fabricate graphene/polyaniline hybrid hollow microspheres in two steps involving the layer-by layer assembly technique followed by in situ oxidative chemical polymerization**.** Subsequent studies have indicated specific capacitance of graphene/polyaniline hybrid hollow microsphere of ~633 F g^{-1} in a 1.0 M H_2SO_4 electrolyte as well as the excellent cycle stability (with 92 % of its original specific capacitance in all probability due to the synergistic effect. Alternatively, the contribution of the unique structure facilitating the reduced transport lengths for both mass and charge transport also cannot be ruled out. The energy density has also been calculated led and found to be 382.97 Wh kg^{-1} at a current density of 10 mA cm^{-2}.

In another work, the hierarchical polyaniline/NiCo-layered double hydroxide (PANI/NiCo-LDH) core-shell composite nanofiber network has been prepared by a two-step strategy (in-situ oxidative polymerization and electrochemical deposition) on the carbon cloth.[610] The choice of LDH nanosheets shell grown on the PANI network in this work was guided by its role in facilitating the ion and electron transport and also in relieving the strain change of the electrode during redox reaction. The electrode fabricated in this manner delivered specific capacitance of 1845 F g^{-1} at 0.5 A g^{-1} and excellent cycling stability (82% after 5000 cycles at 10.0 A g-1) benefiting from rapid electron transport and ion diffusion, the well-defined. In addition, assembled asymmetric device (positive electrode: PANI/NiCo-LDH, negative electrode: activated carbon) displayed excellent energy density (46.0 Wh kg^{-1}) at a power density of 351.6 W kg^{-1} and good cycling performance. Polyaniline/Graphene

View Article Online
DOI: 10.1039/D5LP00230C

nanosheets,[611] $Co(OH)_2$-Polyaniline,[612] Polyaniline/$NiCo_2S_4$,[613] carbon nanotube@polypyrrole core–shell, [614,615] and Janus-type α-Fe_2O_3/PEDOT nanoparticles core/shell [616] also functioned as high-performance supercapacitive electrode materials.

5.4.4.2 Ternary and Quaternary Core-Shell ICP Nanocomposites

Vellakkat and Hundekkal [617] reported the formation of chitosan mediated synthesis of core/double shell ternary polyaniline/Chitosan/Cobalt oxide nano composite for their application as high energy storage electrode material in supercapacitors. In another work, in-situ chemically prepared polyaniline film wrapped Ag decorated MnO_2 nanorod (PANI/Ag@MnO_2) showed specific capacitance of 1028.66 F g^{-1} at a current density of 1 A g^{-1} synergistically.[618] Further, assembled asymmetric supercapacitor (PANI/Ag@MnO_2//AC) device in 1 M H_2SO_4 displayed high energy density (49.77 Wh kg^{-1} at power density of 1599.75 W kg^{-1}. According to Iqbal et al,[619] ternary composite comprising porous Polyaniline@CNT-MnO_2 nanorods prepared by hydrothermal method and in-situ oxidative polymerization of aniline in 0.1 M KOH electrolyte achieved specific capacity, cycle life, energy density and power density of 143.26 C g^{-1}at 3 mV s^{-1}, 119% (3500 cycles) at 0.3 A g^{-1}, 27.17 Wh kg^{-1} and 298 W kg^{-1}, respectively. MWCNT@MnO_2@PPy supercapacitor electrodes attained specific capacitance of 272.7 F g^{-1} and reasonable cycling performance.[620] Ho et al [621] synthesized PPy/Multilayer graphene-wrapped copper nanoparticles (MLG-Cu NPs) composite by a two-step process on a flexible carbon cloth substrate. This displayed excellent specific capacitance performance (845.38 F g^{-1} at the current density of 1 A g^{-1}.

Moreno et al [622] recorded the cyclic voltammetry (CV) of vertically aligned ZnO@CuS@PEDOT core@shell nanorod arrays decorated with MnO_2 nanoparticles at different scan rates in 1 M $LiClO_4$ aqueous electrolyte. The appearance of more or less quasi-

View Article Online
DOI: 10.1039/D5LP00230C

rectangular with symmetric shape of CV indicated the fast reversible reaction and an ideal capacitor type behaviour. Further, ZnO@CuS@PEDOT exhibited excellent electrochemical performance as evident from its high specific areal capacitance of 19.85 mF cm^{-2}, good rate capability and cycling stability. Such stimulating capacitive behavior is attributed to the unique hierarchical core–shell hybrid nanorod configuration and the synergistic effects. Core@shell hollow Bi_2O_{3-x}@Carbon fiber@PEDOT electrode fabricated through the multistep exhibited specific capacitance of 460 F g^{-1} (1 A g^{-1}) and reasonably good cyclic stability.[623] It is also noted that energy density, power density and remarkable cycling performance in the assembled symmetric supercapacitor correspond to 16.4 Wh kg^{-1}, 500.34 W kg^{-1}) and remarkable cycling performance (i.e., 99 % capacitance retention after 8500 cycles).

The coaxial core-sheath shaped supercapacitor based on polypyrrole functionalized graphene/carbon nanotubes hollow fibers exhibited ultrahigh length specific capacitance and energy density.[624] According to Ghosh et al,[625] asymmetric supercapacitor comprising 3-D urchin shaped coaxial MnO_2@PANI composite a self-assembled 3-D pillared graphene foam exhibited energy density of 37 Wh kg^{-1} at a power density of 386 W kg^{-1} and stable cycling performance. In another report, Graphene carbon sphere@PANI@RGO composites reached specific capacitance of 446.19 F g^{-1} (scan rate: 5 mV s^{-1}) in 1 M H_2SO_4 solution with 93.4% capacitance retentions after 1000 cycles.[626] Wang et al [627] prepared core–shell MoS_2/PPy/PANI ternary hybrid with 'pizza-like' nanostructure. It achieved the high specific capacitance (1273 F g^{-1} at 0.5 A g^{-1}) with good cyclic performance (83% after 3000 charge/discharge cycles). This is ascribed to the synergistic effect, improved electrical conductivity and enhanced electrolyte/electrode interaction. Recently, Liu et al [628] synthesized poly (3,4-propylenedioxythiophene)-OH/CoNi-SeS@Hollow carbon sphere via a sulfurization/selenization ion exchange method and in- situ oxidation and showed excellent

View Article Online
DOI: 10.1039/D5LP00230C

electrochemical performance (mass specific capacity: 775.1 C g^{-1} at 1 A g^{-1}). The assembled asymmetric supercapacitor device possesses a good energy density (84.8 Wh kg^{-1}) and excellent power density (8000 W kg^{-1}), and the capacity retention rate of 82.85 % at 4 A g^{-1} (after 20,000 cycles). It is suggested that synergistic effect of the conductive polymer, the hollow structure, and modified electronic structure contributed in achieving the better capacitance performance.

Polypyrrole-coated low-crystallinity Fe_2O_3 supported on carbon cloth[321] Graphene/Polyaniline/MnO_2,[322] GO/α-MnO_2/PANI,[323] $CoCrFeMnNi)_3O_4$@CC-PPy,[324] $LaMnO_3$@CC-PPy,[325] PPy/black phosphorus oxide/ CNT [3,26] CuO@NiO/PANI/CNT [629] and PANI-coated CuO–ZnO–MnO [630] have also been investigated as electrodes for their supercapacitor performance.

Table 6 Electrochemical per.formance of various supercapacitors fabricated based on polyaniline electroactive material.

6. Future scope and Perspectives

Conducting polymers, in spite of promising cost-effectiveness and tunable properties, have certain limitations such as lower conductivity compared to the metals, poor mechanical strength, processability, solubility and environmental stability remain the key issues to be addressed in their high demand applications.[1,2] These challenges are very critical to future ongoing research in order to harness their full potential of conducting polymers in different applications. Further, advancements through innovative synthesis methods including new materials compositions and material design are likely to play key role in developing scalable and cost-effective hollow conducting polymers, its nanocomposites and core-shell materials with significantly enhanced performance in their applications in electrical/environmental remediation and energy storage devices. Recently, research is also emerging on the electrodeposition technique as a promising approach in developing the effective electrode

View Article Online
DOI: 10.1039/D5LP00230C

materials in supercapacitor applications.[154,321-325] In this regard, the unique insight gained by focusing exclusively on hollow and core-shell morphologies in present review article across the three distinct applications (EMI shielding, adsorption, supercapacitors complement the existing literature.

Electromagnetic interference creates electronic pollution that is very harmful to human health and the functioning of electronic devices and remains a critical challenge for researchers.[9] The practical application of the electromagnetic interference/microwave absorption materials is limited by the complex synthetic procedures and expensive raw materials. In this regard, lightweight hollow ICPs and their binary and ternary composites and core-shell structured materials are reported in trapping/absorbing electromagnetic waves to enhance dielectric loss, multiple internal reflection, and scattering of EM waves.[9] However, challenges require researchers to develop thermally and mechanically stable hollow structured ICPs, their composites, and core-shell based materials with superior electrical conductivity, dielectric/magnetic, and corrosion-resistance properties, and their applicability to a wide range of frequencies and absorption bandwidth.[54] The conducting blends with simultaneously enhanced mechanical properties could also be interesting for their future applications in EMI shielding and microwave absorption.[388]

The removal of heavy metals and organic dye in wastewater remains a critical challenge for the researchers.[84,88] In this regard, their polyaniline and polypyrrole attracted considerable attention as promising adsorbents in the separation of dye and metal ions from wastewater. In view of this, hollow conducting polymer [60-64] and core-shell materials[66,67] hold great promise in the adsorptive removal of metal ion from wastewater due to their enhanced surface area, tunability, and potential for synergistic effects.[88] The challenges exists in developing low-cost, high-performing adsorbents with significantly enhanced activity and long-term stability for the separation of the mixture of individual dye, metal ions, dye/metal ions including other

View Article Online
DOI: 10.1039/D5LP00230C

types of pollutants present in wastewater. Further, regeneration of the spent adsorbents is still challenging and needs more attention in developing cost-effective regeneration methods for their reusability with high economic viability and environmental sustainability.[631] Further, safe disposal or reuse of spent/exhausted adsorbents also need to be considered.

Hollow ICPs have emerged as a promising electrode material in supercapacitor applications. Its larger surface area and shorter ion diffusion path facilitate faster charging and discharging. [72,73] However, the future scope of hollow conducting polymer as electrode material is limited due to its poor structural stability, which results in lower cyclability and capacity retention of the assembled supercapacitor.[632] This problem can be mitigated by fabricating its nanocomposites by integrating different components, such as carbonaceous, metal oxides, metal chalcogenides, and MXene base materials through an inexpensive and facile synthesis approach. Attention is also focused on achieving enhanced mechanical stability of hollow ICPs to prevent degradation during repeated charging and discharging cycles. In addition, the fabrication of hollow copolymers of ICPs remains another area not well addressed so far.[633] In addition, core-shell nanostructured electrode materials fabricated by the coating of ICPs on a conducting core have been very promising due to the short ion transport pathways and abundant active sites. Recently, the electrodeposition method has also received more attention, though there exist several challenges in real-world applications.

The future research also needs to be focused on the development of new cost-effective synthetic core-shell methods. This can be realized by utilizing naturally driven green and sustainable biomass,[634] plant waste, [635] marine bio-waste, [636] marine plastic waste, [637] biomass waste, [638-642] cotton, [643] fly ash of coal waste [644] and agricultural by-products [645] as a source of carbon in realizing the fabrication of conducting polymer coated core-shell materials across the three distinct application fields.

7. Summary and Conclusion

View Article Online
DOI: 10.1039/D5LP00230C

The hollow conducting polymers (such as hollow microspheres, nanotubes, etc) have attracted great attention for their wide multifaceted applications guided by their properties. In this regard, polyaniline and to some extent polypyrrole has received much attention owing to their good processability, excellent environmental stability, unique properties, such as controllable internal structures, low density, high surface areas, permeability including surfaces and interfaces, properties controllable by oxidation and protonation states, and its ability to exist in a number of intrinsic redox state. In view of this, present article is dealt with the general method reported on the preparation of conducting polymers fabrication of hollow (PANI<PPy, PTh and PEDOT) structured and their mechanism. This is followed by the review on the synthetic strategies on the fabrication of their hollow morphologies, such as nanotubes, nanocapsules, nano and microspheres etc by utilizing hard templates (Al_2O_3, SiO_2, polystyrene etc), soft templates, sacrificial templates and template free methods, The article father describes the formation of nanocomposites comprising hollow and core–shell structure of ICPs and their applications in protection of environments and harnessing energy. The choice of hollow morphology of conducting polymers is considered as a novel approach in the trapping of microwave radiation through enhanced internal reflection and their remarkable performance has been reviewed. In addition, review on hollow structured conducting polymers demonstrated great structural advantages as efficient adsorbents in the removal of toxic metal ions and dyes present in waste water, Review final concludes with future perceptive of the hollow and core-shell ICPs for their application as microwave absorbers, adsorbents and electrode materials in the absorption of electromagnetic waves and removal of metals ions/dyes in wastewater. It is also anticipated that present provide a significant inspiration to the researchers working on hollow and core-shell ICP for their application several other fields.

Acknowledgement

View Article Online
DOI: 10.1039/D5LP00230C

The author, formerly a Professor in the Department of Chemistry at the Indian Institute of Technology Kharagpur, expresses sincere appreciation to all who made this work possible. He gratefully acknowledges his former research scholars-Dr. R. Panigrahi, and Dr. S. Dutta, and Dr. Rakesh Manna for their valuable contributions to this field. Special thanks are also extended to Dr. Brahma Gupta, Mr. Akash Rawat, Mr. Adarsh Singh from the Department of Civil Engineering, IIT Kharagpur, and Mr Anjan A Chakraborty from Electric Mobility and Tribology Research Group, Central Mechanical Engineering Research Institute, Durgapur, India for their assistance at various stages of preparing this article.

References

1. A. Varghese, K. R. P. Sunajadevi and D. Pinheiro, Energy Adv., 2025, 4, 743.

2. S. K. Srivastava, Nanostructured Materials for Environmental Applications (Eds: S. Balakumar, V. Keller, M. V. Shankar), Springer, 2021, 167–215.

3. M. B. Hasan, M. M. Parvez, A. Y. Abir and M. F. Ahmad, Heliyon, 2015, **11**, e42375.

4. H. H. Al-Refai, A.A. Ganash and M.A. Hussein, Mater. Today Commun., 2021, **26**, 101935.

5. M. A. H. Bayan, F. A. Taromi, M. Lanzi and F. Pierini, Sci, Rep., 2021,**11**, 21144.

6. H. Zhang, X. Wang, H. Ma and M. Xue, Adv. Energ. Sust. Res., 2021, **2**, 2100088

7. E. Dhandapani, S. Thangarasu, S. Ramesh, K. Ramesh, R. Vasudevan and N. Duraisamy, J. Energy Storage, 2022, **52** 104937.

8. X. Gao, Y. Bao, Z. Chen, J. Lu, T. Su, L. Zhang,and J. Ouyang, Adv. Electron. Mater. 2023, **9**, 2300082.

9. S K Srivastava and K. Manna, J. Mater. Chem. A., .2022, **10**, 7431-7496.

10. C. Van Le and H. Yoon, Int. J. Mol. Sci. 2024, **25**, 1564.

View Article Online
DOI: 10.1039/D5LP00230C

11. H. Kazim, M. Sabri, A. AlOthman and M. Tawalbeh, Nano-Struct. Nano-Objects., 2024, **40**, 101371.

12. T. Nezakati, A. Seifalian, A. Tan and A.M. Seifalian, Chem. Rev., 2018, **118**, 6766–6843.

13. A. Puiggalí-Jou, L.J. del Valle and C. Alemán, J. Contr. Release., 2019, **309**, 244-264.

14. S.K Srivastava, RSC Appl. Interf., 2024, **1**, 340-429.

15. J. Kumari, A. Singh, A. Rawat, S.K. Srivastava, A.K. Gupta, RSC Sustain., Submitted 2025.

16. M. S. Tamboli, A. A. Gupta, H. S. Avchat, S. S. Bhosale and D. S. Shrikant. Webology (ISSN: 1735-188X), 2020, 17, 761-771.

17. M. Ayad, G. El-Hefnawy and S. Zaghlol, Chem. Eng. J., 201, **217**, 460-466.

18. M. Aleahmad, H. G. Taleghani and H Eisazadeh, Asian J. Chem., 2010, **22**, 7353-7360.

19. Y. Gao, Z-H. Kang, X. Li, X-J. Cui and J. Gong, CrystEngComm, 2011, **13**, 3370-3372.

20. E. Saracino, S, Zuppolini, V. Guarino, V. Benfenati, A. Borriello, R. Zamboni and L. Ambrosio, RSC Adv., 2021,**11**, 11347-11355.

21. K. Huang, Y. Zhang, Y. Long, J. Yuan, D. Han, Z. Wang, L. Niu and Z. Chen, Chem. Eur. J., 2006, **12**, 5314-5319.

22. Md Moniruzzaman Sk and C. Y. Yue, J. Mater. Chem. A, 2014, **2**, 2830.

23. S. Virji, J.X. Huang, R.B. Kaner and B.H. Weiller, Nano Lett.. 2004, **4**, 491-496.

24. E. Song and J-W. Choi, Nanomaterials, 2013, **3**, 498-523.

25. G. Li, H. Peng, Y. Wang, Y. Qin, Z. Cui and Z. Zhang, Macromol. Rapid Commun., 2004, **25**, 1611-1614.

26. J. Jang, J. Bae and K. Lee, Polymer, 2005, **46,** 3677-3684.

27. X-G. Li, A. Li and M-R. Huang, Chem. Eur. J., 2008, **14**, 10309-10317.

28. H. Wang and Y. Lu, Synthetic Metals 2012, **162**, 1369–1374.

29. Q. Zhang, W. Li, X. Liu, J. Ma, Y. Gu, R. Liu and J. Luo, ACS Appl. Mater. Interfaces, 2024, **16**, 1461-1473.

30. D. Zhang, X. Fan, X. Hao and G. Dong, Ind. Eng. Chem. Res., 2019, **58**, 1906-1913

31. H. Wang, Y. Liu, L. Kong, S. Yin, X. Shen and S. Premlatha, Colloids Surf. A Physicochem. Eng. Asp., 2023, **665**, 131234.

32. M. Shi, Y. Zhang, M. Bai and B. Li, Synth. Met., 2017, **233**, 74-78.

33. C. Yu, J. Zhai, X. Gao, M. Wan, L. Jiang, T. Li and Z. Li, J. Phys. Chem. B., 2004, 108, 4586-4589.

34. B. Butoi, A. Groza. P. Dinca, A. Balan and V. Barna, Polymers, 2017, **9**, 732.

35. S. J. T. Rezaei, Y. Bide and M. R. Nabid, Synth. Met., 2011,**161**, 1414–1419.

36. G.M. Neelgund and A. Oki, Polym. Int. 2011, **60**, 1291-1295

37. H-W. Park, T. Kim, J. Huh, M. Kang, J.E. Lee and H. Yoon, ACS Nano 2012, **6**, 7624–7633.

38. Namsheer K, Reneesha V B, and C.S. Rout, ACS Symposium Series, 2023, Vol.1438, Chapter 2, pp 9-27, DOI: 10.1021/bk-2023-1438.ch002

39. L. Yu, X. Y. Yu and X. W. (David) Lou, Adv. Mater., 2018, **30**, 1800939.

40. L. Yu, H. Hu, H. B. Wu and X. W. (David) Lou, Adv. Mater., 2017, **29**, 1604563.

41. X. Wang, J. Feng, Y. Bai, Q. Zhang and Y. Yin, Chem. Rev., 2016, **116**, 10983–11060.

42. P. Liu and L. Zhang, Crit. Rev. Solid State Mater. Sci., 2009, **34**, 75–87.

43. Y. Xue, S. Chen, J. Yu, B. R. Bunes, Z. Xue, J. Xu, B. Lu and L. Zang, J. Mater. Chem. C, 2020, **8**, 10136–10159.

44. I. Hussain, S. Sahoo, M.S. Sayed, M. Ahmad, M. S.Javed, C. Lamiel, Y. Li, J-J. Shim, X. Ma and K. Zhang, Coord. Chem. Rev., 2022, **458**, 214429.

45. X. W (David). Lou, L. A. Archer and Z. Yang, Advanced Materials, 2008, 20, 3987-4019.

46. K. An and T. Hyeon, Nano Today, 2009, **4**, 359-373.

47. M. Zhu, Y. Cheng, Q. Luo, M. El-khateeb and Q. Zhang, Mater. Chem. Front., 2021, 5, 2552-2587.

48. L. Yang, H. Xu, G. He and H. Chen, Dalton Trans., 2022,**51**, 13559-13572.

49. J. Qi, X. Lai, J. Wang, H. Tang, H. Ren, Y. Yang, Q. Jin, L. Zhang, R. Yu, G. Ma, Z. Su, H. X. Zhao and D. Wang, Chem. Soc. Rev., 2015, **44**, 6749-6773.

50. K. Zhang, K. Song and K. Clays, Nanophotonics 2018, **7**, 693-671.

51. X. Zhu, J. Tang, H. Huang, T. Lin, B. Luo and L. Wang, Sci. Bull., 2020, 65,496–512.

52. A. Venkataraman, E.V. Amadi, Y. Chen and C. Papadopoulos, Nanoscale Res. Lett., 2019, **14**, 220.

53. G. Ma, Z. Wen, J. Jin, Y. Lu, X. Wu, M. Wu and C. Chen, J. Mater. Chem. A, 2014, **2**, 10350-10354.

54. C. Kuila, A. Maji, N. C. Murmu, T. Kuila and S. K. Srivastava, Carbon, 2023, **210**, 118075.

55. R. Manna, K. Ghosh and S. K. Srivastava, Langmuir, 2021, **37,** 7430-7441.

56. R. Manna and S. K. Srivastava, ACS Omega, 2021, **6**, 9164-9175.

57.D. Xu, M. Zhang, C. Wang, Z. Shen, M. Wang, J. Zhang, Z. Han, L. Li, X. Xiong and P. Chen, Polymer, 2025, **317**, 127900.

58. K Manna and SK Srivastava, J. Phys. Chem. C., 2018, 122, 19913-19920.

59. S. Kumari, J. Dalal, A.Kumar, R. Pal, R. Chahal and A. Ohlan, RSC Adv., 2024, **14**, 662-676.

60. S. Senguttuvan, P. Senthilkumar, V. Janaki and S. Kamala-Kannan, Chemosphere, 2021, **267**, 129201.

61. E. N. Zare, A. Motahari and M. Sillanpää, Environ. Res., 2018, **162**, 173-195.

62. P. Rana, B. Kaur, K. Poonia, V. Soni, P. Singh, S. Thakur, C-W. Huang, V-H. Nguyen and P. Raizada, Inorg. Chem. Commun., 2025, **172**, 11365.

View Article Online
DOI: 10.1039/D5LP00230C

63.A. Taghizadeh, M. Taghizadeh, M. Jouyandeh, M.K. Yazdi, P. Zarrintaj, M.R Saeb, E.C. Lima, V. K. Gupta, J. Mol. Liq., 2020, **312**, 113447.

64. S. Dutta, Fabrication od sustainable nano adsorbents in removal of toxic pollutants from contaminated water, Ph.D Thesis, Indian Institute of Technology, Kharagpur, 2022.

65. X. Y. Lai, J. E. Halpert and D. Wang, Energy Environ. Sci. 2012, 5, 5604−5618.

66. C. F. Jones, L. Resina, F. C. Ferreira, P. Sanjuan-Alberte and T. Esteves, J. Phys. Chem. C 2024, **128**, 11083–11100

67. Y. Bhattacharjee and S. Bose, ACS Appl. Nano Mater., 2021, **4**, 949–972.

68. M. K. Goswami, A.Srivastava, R. K. Dohare, A. K. Tiwari and A. Srivastav, Environ. Sci. Pollut. Res., 2023.https://doi.org/10.1007/s11356-023-27458-4

69. L. Wang, X. Li, X. Shi, M. Huang, X. Li, Q. Zeng and R. Che, Nanoscale, 2021, **13**, 2136.

70. L. Liu, S. Liu, L. Zhao, G. Su, X. Liu, H. Peng, J. Xue and A. Tang, J. Mol. Liq., 2020, **313**, 113593.

71 A. Muhammad, A-U.H. Ali Shah, S. Bilal and G. Rahman, Materials 2019, **12**, 1764.

72. C. Xia, W. Chen, X. Wang, M.N. Hedhili, N. Wei and H. N. Alshareef, Adv. Energy Mater., 2015, 1401805.

73.. D Khalafallah, D.E.E. Refaay, X. Gu, A.M.A. Henaish and Q. Zhang, Energy Stor. Mater., 2025, **78**, 104284

74. N. Maruthi, M. Faisal and N. Raghavendra, Synth. Met., 2021, **272**, 116664.

75. B. G. Soares, G. M. O. Barra and T. Indrusiak, J. Compos. Sci., 2021, **5**, 173.

76. M. Zahid, R. Anum, S. Siddique, H. M. F. Shakir and Z. A. Rehan, J. Thermoplast. Compos. Mater., 2021, **36**, 1717-1761.

77. X. Su, Y. Liu, Z. Liao, Y. Bi, M. Ma, Y. Chen, Y. Ma, F. Wan and K. L. Chung, Synth. Met., 2022, **291**, 117190.

78. N. Biçer, I. T. Çelik and I. A. Kariper, J. Ind. Text., 2022, **51**, 36S-64S

View Article Online
DOI: 10.1039/D5LP00230C

79. A. Kausar and I. Ahmad, J. Compos. Sci., 2023, **7**, 240.

80. J. Wang, Q. Sun, J. Li, Y. Guo, W. Tian, Y. Liu, B. Wu, L. Deng, N. Mahmood and X. Jian, Mater. Today Phys., 2023, **31**, 100981.

81. H. Hajjaoui, A. Soufi, W. Boumya, M. Abdennouri and N. Barka, J. Compos. Sci., 2021, **5**, 233.

82. A. Samadi, M. Xie, J. Li, H. Shon, C. Zheng and S. Zhao, Chem. Eng. J., 2021, **418**, 129425.

83. S. Jadoun, J.P. Fuentes, B.F. merUrbano and J. Yáñez, J. Environ. Chem. Eng., 2023, **11**, 109226.

84 A. Samadi, Z. Wang, S. Wang, S.K. Nataraj, L. Kong and S. Zhao, Chem. Eng. J., 2023, **478**, 147506.

85. M. M. Talukder, M. M. R. Khan and M. K. Amin, S. Afr. J. Chem. Eng., 2023, **44**, 276-282.

86. A-N. Chowdhury, S. R. Jesmeen, M. M. Hossain, Polym. Adv. Technol., 2004, **15**, 633-638.

87. A. Nasar and F. Mashkoor, Environ. Sci. Pollut. Res. Int., 2019, **26**, 5333–5356.

88. S. Dutta, B. Gupta, S. K. Srivastava and A. K. Gupta, Mater. Adv., 2021, **2**, 4497–4531.

89. R. Rehman, A. Raza, F. Yasmeen, A. Dar, Z. T. Al-thagaf, and Z. Meraf, Adsorpt. Sci. Technol., 2022, Article ID 7047832, https://doi.org/10.1155/2022/7047832

90. J. Stejskal, Polymers 2022, **14**, 4243.

91. M.L. Sall, A.K.D. Diaw, D..Gningue-Sall, S. E. Aaron and J-J. Aaron, Environ. Sci. Pollut. Res., 2020, **27**, 29927–29942.

92. Y. Han and L. Dai, Macromol. Chem. Phys. 2019, 1800355. DOI: 10.1002/macp.201800355

View Article Online
DOI: 10.1039/D5LP00230C

93. L. Fu, Q. Qu, R. Holze, V. V. Kondratiev and Y. Wu, J. Mater. Chem. A, 2019, **7**, 14937-14970.

94. M. I. Ul Hoque and R. Holze, Polymers, 2023, **15**, 730.

95. S. Ahmed, A. Ahmed, D. B. Basha, S. Hussain, I. Uddin and M. A. Gondal, Synth. Met., 2023, **295**, 117326.

96. M. G. Tadesse, A. S. Ahmmed and J. F. Lübben, J. Compos. Sci., 2024, **8**, 53.

97. V.J.V. Vinayak., K. Deshmukh, V.R.K. Murthy, S.K.K. Pasha, J. Energy Storage, 2024, **100**, 113551.

98. O. B. Okafor, A. P. I. Popoola, O. M. Popoola, S. O Adeosun, Next Materials. 2025, **6**, 100389.

99. E. N. Zare, P. Makvandi, B. Ashtari, F. Rossi, A. Motahari and G. Perale, J. Med. Chem., 2019, **63**, 1-22.

100. J. Cui, F-F. Xing, H. Luo, J-Q. Qin, Y. Li, Y. Zhong, F. Wei, J. Fu, C. Jing, J. Cheng, Z-S. Wu and S. Liu, J. Energy Chem., 2021, **62**,145–152.

101. M. Halvaee, K. Didehban, V. Goodarzi, M. Ghaffari, M. Ehsani and M. R. Saeb, J. Appl. Polym. Sci., 2017, **134**, 45389.

102. T-H. Le, Y. Kim and H. Yoon, Polymers 2017, **9**, 150.

103. A.G. MacDiarmid, R.J. Mammone, R.B. Kaner, S.J. Porter, R. Pethig, A.J. Heeger; and D.R. Rosseinsky, Phil. Trans, R. Soc. Lond. A 1985, 314. Doi: 10.1098/rsta.1985.0004

104.J.V. Yakhmi, V, Saxena and D.K. Aswal, Functional Materials, 2012, 61-110. https://doi.org/10.1016/B978-0-12-385142-0.00002-7

105. A K Bakhshi, Bull. Mater. Sci., 1995, **18**, 469-495.

106.P. C. Maity, M.Tech. Thesis,.Indian Institute of Technology, Hyderabad, 2016. https://raiithold.iith.ac.in/2718/1/MS14METCH11003.pdf

107. C-C. Hung and T-C. Wen, J. Taiwan Inst. Chem. Eng., 2011, **42**, 371-376.

108. S. Qian, H.A. Lin, Q. Pan, S. Zhang, Y. Zhang, Z. Geng, Q. Wu, Y. He and B. Zhu, Bioact Mater. 2023, **26**, 24-51.

109.. N. A. Kukhta, A. Marks and C. K. Luscombe, Chem. Rev. 2021, **122**, 4325–4355.

110. G. G. Wallace, G. M. Spinks, L. A. P. Kane-Maguire and P. R. Teasdale, Conductive Electroactive Polymers, Third Edison, CRC Press, 2008.

111. J. Stejskal, Chemical Papers, 2019, **74**, 1-54.

112. K. Namsheer and C. S. Rout, RSC Adv., 2021, **11**, 5659-5697.

113. B. Qiu, J. Wang, Z. Li, X. Wang and X. Li, Polymers 2020, **12**, 310.

114. S. P. Armes and J. F. Miller, Synth. Met., 1988, **22**, 385-393.

115**.** J. Stejskal, A. Riede, D. Hlavatá, J. Prokeš, M. Helmstedt and P. Holler, Synth. Met.,1998, **96**, 55-61.

116. R. Manna, Functionalized Graphene Based Nanocomposites as Flexible Dielectric Materials and Microwave Absorber, Ph.D Thesis, Indian Institute of Technology, Kharagpur, 2021.

117. J. Yang, Y. Ding, G. Chen and C. Li, Euro. Polym. J, 2007, **43**., 3337-3343.

118. **S.** Budi, Yusmaniar, A Juliana, U Cahyana, A Purwanto, A Imaduddin and E Handoko, IOP Conf. Series: Journal of Physics: Conf. Series, 2018, **983** 012162 doi :10.1088/1742-6596/983/1/012162

119. A. H. Majeed, L. A. Mohammed, O. G. Hammoodi, S. Sehgal, M. A. Alheety, K. K. Saxena, S. A. Dadoosh, I. K. Mohammed, M. M. Jasim and N. U. Salmaan, Inter. J. Polym. Sci.,

2022, Article ID 9047554, https://doi.org/10.1155/2022/9047554

120. J. Mahmood, N. Arsalani, S. Naghash-Hamed, Z. Hanif and K. E. Geckeler, Sci. Rep., 2024, **14**, 11653.

121. J.C. Thieblemont, M.F. Planche, C. Petrescu, J.M. Bouvier and G. Bidan, Synth. Met., 1993, **59**, 81-96.

122.Y. Sood, K. Singh, H. Mudila, P.E. Lokhande, L. Singh, D. Kumar, A. Kumar, N.M. M ubarak, M. H. Dehghani, Heliyon, 2024, **10,** e33643.

123. M. Omastová, J. Pionteck, M. Trchová, Synth. Met.. 2003, **135–136**, 437-438.

124. Y. Kudoh, Synth. Met., 1996, **79**, 17–22.

125. Y. Kudoh, K. Akami and Y. Matsuya, Synth. Met., 1998, **95**, 191–196.

126. A. Yussuf, M. Al-Saleh, S. Al-Enezi and G. Abraham, Int. J. Polym. Sci., 2018 Article ID 4191747. https://doi.org/10.1155/2018/4191747

127. Y. Tan and K. Ghandi, Synth. Met., 2013, **175**, 183-191.

128. A. Kausaite-Minkstimiene, V. Mazeiko, A. Ramanaviciene and A. Ramanavicius, Colloids Surf. A Physicochem. Eng. Asp., 2015, **483**, 224–231.

129. V. Bocchi, L. Chierici, G.P. Gardini and R. Mondelli, Tetrahedron, 1970, **26**, 4073-4082.

130. T V Vernitskaya, O N Efimov, Russ. Chem. Rev.,1997, 66, 443-457.

131. A.F. Diaz, J. Bargon, Handbook of Conducting Polymers, Marcel Dekker, NewYork, 1986.

132. T. P. Kaloni, P. K., Giesbrecht, G. Schreckenbach and M.S. Freund, Chem, Mater., 2017, 29, **24**, 10248–10283

133. D. Thanasamy, D. Jesuraj, S. K. K. Kannan and V. Avadhanam, Polymer, 2019,**175**, 32-40.

134. M. Jaymand, M. Hatamzadeh and Y. Omidi, Progress in Polymer Science, 2015, **47**, 26-69.

135. S. Das, D.P. Chatterjee, R. Ghosh and A. K. Nandi, RSC Adv., 2015, **5**, 20160.

136. S. Nie, Z. Li, Y. Yao and Y. Jin, Front. Chem., 2021, **9**, 803509.

137. G. Heywang and F. Jonas, Adv. Mater., 1992, **4**, 116-118. doi:10.1002/adma.19920040213

View Article Online
DOI: 10.1039/D5LP00230C

138. Y. Jiang, T. Liu, and Y. Zhou, Adv. Funct. Mater., 2020, 2006213

139. R. Corradi and S. Armes, Synth. Met., 1997, **84**, 453-454.

140. N. Paradee and A. Sirivat, Polym. Int., 2014; **63**, 106–113.

141. S. G. Im, D. Kusters, W. Choi, S. H. Baxamusa, M.C.M. Van de Sanden and K. K. Gleason, ACS Nano, 2008, **2**, 1959-1967.

142. D. Bhattacharyya, R M. Howden, D. C. Borrelli and K. K. Gleason, J. Polym. Sci., Part B: Polym. Phys., 2012, **50**,1329-1351.

143. Y-H. Ha, N. Nikolov, S.K. Pollack, J. Mastrangelo, B.D. Martin and R. Shashidhar, Adv. Funct. Mater., 2004, **15,** 615-622.

144. M. A. Ali, H. Kim, C Lee, H Nam and J. Lee, Synth. Met., 2011, **161**, 1347-1352.

145**.** J. M. Bone and J. L. Jenkins, J..Chem. Educ., 2023, **100**, 10, 4062–4071.

146. S. A. Kumar, S. Sahoo, G. K. Laxminarayana and C. S. Rout, Small, 2024, **20,** 2402087.

147. J. Liao, S. Wu, Z. Yin, S. Huang, C. Ning, G, Tan and P.K. Chu, ACS Appl. Mater. Interfaces 2014, **6**, 10946−10951.

148 S. A. Campbell, Y. Li, S. Breakspear, F. C. Walsh and J. R. Smith, Transactions of the IMF, 2007, **85**, 237-244.

149. X. Luo X and X.T. Cui, Acta Biomater. 2011, **7**, 441-446.

150**.** J. Tietje-Girault, C. Ponce de Leó and F.C. Walsh, Surf. Coat. Technol., 2007, **201**, 6025-6034.

151.J. Li, L. Zhao and P, Liu, Langmuir 2023, **39**, 40, 14297–14307.

152. K. K. Shiu, F-Y. Song and K-W. Lau, J. Electroanal. Chem., 1999, **476**, 109–117.

153. S. S. Shah, M. A. Aziz, A-R. Al-Betar and W. Mahfoz, Arab. J. Chem., 2022, **15**, 104058.

View Article Online
DOI: 10.1039/D5LP00230C

154. J. E. Nady, A. Shokry, M. Khalil, S. Ebrahim, A. M. Elshaer and M.Anas, Sci. Rep., 2022,3611. https://doi.org/10.1038/s41598-022-07483-y

155. K. M. Cheung, D. Bloor and G. C. Stevens, J. Mater, Sci,, 1990, **25**, 3814–3837.

156. R. Menon and A.K. Mukherjee, Encycl. Nanosci. Nanotechnol. 2004, **8**, 715−729.

157. S.V. J. Siti, A. Ulianas, and S. Aini, Journal of Physics: Conference Series, Volume 1788, Issue 1, article id. 012004 (2021). DOI: 10.1088/1742-6596/1788/1/012004

158. X. Gong, L. Dai, A. W. H. Mau and H. J. Griesser, J. Polym. Sci., Part A: Polym. Chem.. 1998, **36**, 633-643.

159. T. Yamamoto, J. Organomet. Chem., 2002, **653**, 195-199.

160. M. Mueller, M. Fabretto, D. Evans, P. Hojati-Talemi, C. Gruber and P. Murphy, Polymer, 2012, **53**, 2146-2151.

161. R. Brooke, P. Cottis P. Talemi, M, Fabretto, P. Murphy and D. Evans, Prog. Mater. Sci., 2017, **8**6, 127–146.

162. S. P. Armes, Synth. Met., 1987, **20**, 365–371.

163. Y. Cao, A. Andreatta, A. J. Heeger and P. Smith, Polymer, 1989, **30**, 2305-2311.

164. Y. Li and J. Yang, J. Appl. Polym. Sci., 1997, **65**, 2739–2744.

165. S. Sinha, S. Bhadra and D. Khastgir, J. Appl. Polym. Sci., 2009. **112**. 3135–3140.

166. T. Yonehara, K. Komaba and H. Goto, Polymers, 2020, **12**, 375.

167. C. A. Ferreira, S. Aeiyach, M. Delamar and P. C. Lacaze, J. Electroanal. Chem., 1990, **284,** 351-369.

168. G. Ciric-Marjanovic, M. Trchova and J. Stejskal, J. Raman Spectrosc., 2008, **39**, 1375–1387.

169. A. Kaur, B. Bajaj, A. Kaushik, A. Saini and D. Sud, Mater. Sci. Eng. B., 2022, **286**, 116005.

View Article Online
DOI: 10.1039/D5LP00230C

170. S. Zhang, B. Cheng, Z. Jia, Z. Zhao, X. Jin, Z. Zhao and G. Wu, ACHM, 2022, **5**,1658-1698.

171. Y. Xie, D. Kocaefe, C. Chen and Y. Kocaefe, J. Nanomater., 2016, Article ID 2302595. https://doi.org/10.1155/2016/2302595

172. Q. Zhang, W. Wang, J. Goebl and Y. Yin, Nano Today, 2009, **4**, 494–507.

173. Y. Bao, C. Shi, T. Wang, X. Li and J. Ma, Micropor. Mesopor. Mater., 2016, **227**, 121-136.

174. A-G. Schiopu, D.M. Iordache, M. Oproescu, L.M. Cursaru and A.-M. Iota, Crystals 2024,14, 899.

175. R. R. Poolakkandy and M. M. Menamparambath, Nanoscale Advan., 2020, **2**, 5015–5045.

176. Y. Boyjoo, M. Wang, V. K. Pareek, J. Liu and M. Jaroniec, Chem. Soc. Rev., 2016, **45**, 6013–6047.

177. T. He, D. Chen, X. Jiao, Y. Xu and Y. Gu, Langmuir, 2004, **20**, 8404–8408.

178. T. Cheng, Y. Xiang, X. He, J. Pang, W. Zhu, L. Luo, Y. Cao and R. Pei, J. Mater. Chem. B, 2025,**13**, 4739-4769

179. A. Bai, C-C. Hu, Y-F. Yang and C-C. Lin, Electrochim. Acta, 2008, **53**, 2258-2264

180. C. Mijangos and J, Martin, Polymers 2023, **15**, 525.

181. S. Xiong, Q. Wang, H. Xia, Mater. Res. Bull., 2004, 1569-1580.

182. B. H. Kim, D. H. Park, J. Joo, S. G. Yu and S. H. Lee, Synth. Met., 2005, **150**, 279-284.

183. L. Liu, C. Zhao, Y. Zhao, N. Jia, Q. Zhou, M. Yan and Z. Jiang, Euro. Polym J., 2005, **41**, 2117-2121.

184. F-L. Cheng, M-L. Zhang and H. Wang, Sensors, 2005, **5**, 245–249.

185. N. Esman and J-P. Lellouche, Polym. Chem., 2010, **1**, 158–160.

186. J. Jang and J. H. Oh, ChemCom, 2004, 882-883.

View Article Online
DOI: 10.1039/D5LP00230C

187. S. Chuanyu and W. Yu, OAM-RC, 2012, **6**, 1037-1040.

188. S. Das, A. Kumar and K. S. Narayan, Phys. Rev. Mater., 2022, **6**, 025602.

189. R. Liu, S.I. Cho and S.B Lee, Nanotechnology 2008, **19**, 215710.

190. P.P. Pednekar, S.C. Godiyal, K.R. Jadhav, V.J. Kadam, Chapter 23 - Mesoporous silica nanoparticles: a promising multifunctional drug delivery system, in: A. Ficai, A.M.B.T.-N. for C.T. Grumezescu (Eds.), Micro Nano Technol, Elsevier, 2017, pp. 593–621,

191. G. D. Fu, J. P. Zhao, Y. M. Sun, E. T. Kang, and K. G. Neoh, Macromolecules, 2007, **4**0, 2271-2275,

192. Y Hao, L. Song and Y Zhang, Prog. Org. Coat., 2022, **168**. 106912.

193. Y. Li, Y. Chang, M. Jin, Y. Liu and G. Han, J. Appl. Polym. Sci., 2012, **126**, 1316-1321.

194. W. Wang, L. Lu, T. Chen and M. Rao, J. Appl. Polym. Sci., 2012, **12**6, 974-979.

195. J. Ge, L-H. Rong, X. Cheng, Y. Tang, D. J. Pochan, E. B. Caldona, and R. C. Advincula, Macromolecules 2025, **58**, 3289−3297

196. M. N. Gorsd, M. N. Blanco and L. R. Pizzio, Procedia Materials Science, 2012, **1**, 432-438.

197. A. B. D. Nandiyanto, A. Suhendi, T. Ogi, R. Umemotoa and K. Okuyama, Chem. Eng. J., 2014, **256**, 421-430.

198. Y-C. Kuo, S-S. Wang, K-C. Chang and H. Chen, J. Thermoplast. Compos. Mater., 2013, **28**,1091-1109.

199. Z. Zhong, Y. Yin, B. Gates, and Y. Xia, Adv. Mater., 2000, **12**, 206–209.

200. M-Y. Bai, Y-J. Cheng, S. A. Wickline and Y. Xia, Small, 2009, **5**, 1747–1752.

201. Y. Yang, Y. Chu, F. Yang and Y. Zhang, Mater. Chem. and Phys., 2005, **92**, 164–171.

202. Z. Niu, Z. Yang, Z. Hu, Y. Lu and C. C. Han, Adv. Funct. Mater., 2003, **13**, 949–954.

203. R. Panigrahi and S. K. Srivastava, Mater. Res. Bull., 2015, **64**, 33-41.

204. R. Panigrahi and S. K. Srivastava, Sci. Rep., **5**, 7638, DOI:10.1038/srep07638.

View Article Online
DOI: 10.1039/D5LP00230C

205. M. Saraf, A. Deep and A. Sharma, Conference: EMSI-2014, University of Delhi, DOI:10.13140/2.1.4400.0009

206. C. Mangeney, S. Bousalem, C. Connan, M.-J. Vaulay, S. Bernard and M. M. Chehimi, Langmuir, 2006, **22**, 10163–10169.

207. X. Shi, A. L. Briseno, R. J. Sanedrin and F. Zhou, Macromolecules 2003, 36, 4093-4098.

208. C. Sun and D. Sheng, Chem. Lett., 2011, **40**, 153–155.

209. B.H. Sung, Y.G. Ko, and U.S. Choi, Colloids Surf. A Physicochem. Eng. Asp., 2007, **292**, 217-223.

210. X. Feng, C. Mao, G. Yang, W. Hou and J-J. Zhu, Langmuir, 2006, **22**, 4384-4389

211. Y. Gao, F. Wang, J. Gong, Z. Su and L. Qu, J. Nanosci. Nanotechnol., 2008, **8**, 5972-5976.

212. L. Zhang and P. Liu, Mater. Lett., 2010, **64**, 1755–1757.

213. S. Zuo, W. Liu, C. Yao, X. Li, Y. Kong, X. Liu, H. Mao and Y. Li, Chem. Eng. J., 2013, **228**, 1092–1097.

214. Y. Gao, X. Li, J. Gong, B. Fan, Z. Su and L. Qu, J Phys. Chem. C, 2008, **112**, 8215–8222.

215. C-L. Zhu, S-W. Chou, S-F. He, W-N. Liao and C-C, Chen, Nanotechnology, 2007, **1**8, 275604.

216. Z. Zhang, J. Deng, J. Sui, L. Yu, M. Wan and Y. Wei, Macromol. Chem. Phys., 2006, **207**, 763-769.

217. Z. Zhang, J. Sui, L. Zhang, M. Wan, Y. Wei, and L Yu, Adv. Mater., 2005,**17**, 2854-2857.

218. G. Li, Y. Li, Y. Li, H. Peng, and K. Chen, Macromolecules 2011, **44**, 9319–9323.

219. W. Liu, A. L. Cholli, R. Nagarajan, J. Kumar, S.t Tripathy, F. F. Bruno and L. Samuelson, J. Am. Chem. Soc. 1999, 121, 11345-11355.

220. S-R. Yun, G-O. Kim, C. W. Lee, N-J Jo, Y Kang, K-S. Ryu, J. Nanomat., 2012, Article ID 894539, doi:10.1155/2012/894539

View Article Online
DOI: 10.1039/D5LP00230C

221. A. Madani, B. Nessark, R. Brayner, H. Elaissari, M. Jouini, C. Mangeney and M. M. Chehimi, Polymer, 2010, **51**, 2825–2835.

222. C. H. Chang, P. S. Son, J-A. Yoon and S-H. Choi, J. Nanomat., 2010, Article ID 168025, DOI:10.1155/2010/168025.

223. S. Li, M. Zhou, Y. Zhang, X. Zhang and L. Ding, J. Macromol. Sci., Part A, 2018, **55**, 98-105.

224. K. Manna, Fabrication of Carbonaceous/Magnetic Nanomaterial filled Polymer Nanocomposites in Electromagnetic Interference Shielding Applications, Ph. D Thesis, Indian Institute of Technology Kharagpur, 2020.

225. J. Zhang, T. Qiu, S. Ren, H. Yuan, L. He and X. Li, Mater. Chem. Phys., 2012, **134** 1072-1078.

226. T-L. Hsieh, P-S. Hung, C-J. Wang, Y-S. Chou and P.W. Wu, SN Appl. Sci., 2019. **1**, 319

227. S. M. Marinakos, D. A. Shultz, and D. L. Feldheim, Adv. Mater., 1999, **11**, 34-37.

228. F. Yin, D. Wang, Z. Zhang, C. Zhang and Y. Zhang, Mater. Lett., 2017, **20**7, 225-229.

229. D. Su, J. Zhang, S. Dou and G. Wang, ChemCom., 2015, **51**, 16092–16095.

230. C.H. Chang, P.S. Son, J-A Yoon and S-H. Choi, J. Nanomater., 2010, https://doi.org/10.1155/2010/168025

231. L. Qu and G. Shi, J. Polym. Sci., Part A: Polym. Chem., 2004, **42**, 3170-3177.

232. J. Huang, B. Quan, M. Liu, Z. Wei, L. Jiang, Macromol. Rapid Commun., 2008, **29**, 1335–1340.

233. L. Piraux, V-A. Antohe, E. Ferain and D. Lahem, RSC Adv., 2016, **6**, 21808-21813.

234. A. Kros, R. J. M. Nolte and N. A. J. M. Sommerdijk, Adv. Mater., 2002, **14**, 1779–1782.

235. X. Lixin, L. Guangye, L. Jingfu, and S. Mengtao, Kinet. Catal., 2011, **52**, 716–722.

236. D. P. Dubal, Z. Caban-Huertas, R. Holze and P. Gomez-Romero, Electrochim. Acta, 2016, **191**, 346–354.

237. X. Zhang and S. K. Manohar, J. Amer, Chem. Soc., 2005, **127**, 14156-14157.

238. L. Benhaddad, M-C. Bernard, C. Deslouis, L. Makhloufi, B. Messaoudi, A. Pailleret and H. Takenouti, Synth. Met, 2013, **175**, 192-199.

239. C. Wang, Z. Liu, Q. Wang, J Guo, Q. Zhao and Y. Lu, J. Electroanal. Chem., 2021, **901**, 115780.

240. J. Zhao, Z. Li, J. Wang, Q. Li and X. Wang, J. Mater. Chem. A, 2015, **3**, 15124–15132.

241. J. Wu, Y. Liu, and L. Bao, Chem. Lett., 2015, **44**, 557–559.

242. T. Yao, T. Cui, X. Fang, J. Yu, F. Cui and J. Wu, Chem. Eng. J., 2013, **225,** 230–236.

243. J. Rehmen, T. Pathirana, L. Garcia-Quintana, R. Kerr, P. C. Howlett, K. Zuber, C. Pozo-Gonzalo and D. R. Evans, ACS Appl. Nano Mater., 2020, **3**, 3820–3828

244. S. Zhang, J. Ren, Y. Zhang, H. Peng, S. Chen, F. Yang and Y. Cao, Org. Electron., 2020, **77**, 105497.

245. S-C. Luo, H-H. Yu, A. C. A. Wan, Y. Han and J. Y. Ying, Small, 2008, **4**, 2051-2058

246. X. Zhang, D. Xin, Z. Yu, J. Sun, Q. Li, X. He, Z. Liu and Z. Lei, J, Colloid Interface Sci., 2025, **677**, 472–481.

247. C-W. Kung, Y-H. Cheng, H-W. Chen, R. Vittal and K-C. Ho, J. Mater. Chem. A, 2013, 10693-10702.

248. Y-H. Cheng, C-W. Kung, L-Y. Chou, R. Vittal and K-C. Ho, Sens. Actuators B: Chem., 2014, **192**, 762–768.

249. C. R. Martin, Acc. Chem. Res., 1995, **28**, 61-68.

250. F-L. Li and H-J. Zhang, Materials, 2017 **10**, 995.

251. L. Pan, H. Qiu, C. Dou, Y. Li, L. Pu, J. Xu and Y. Shi, Int. J. Mol. Sci., 2010, **11**, 2636-2657.

View Article Online
DOI: 10.1039/D5LP00230C

252. Z. Zhang, T. Sun, M. Shao and Y. Zhu, in Functional Nanomaterials: Synthesis, Properties, and Applications, W-Y. Wong, Q. Dong (Editors.), Chapter 8, 2022, pp 303-336, Wiley. https://doi.org/10.1002/9783527828562.ch8

253. A. Ali, R. Jamal and T. Abdiryim, RSC Adv., 2021, **11**, 33425–33430.

254. Z. Zhang, Z. Wei and M. Wan, Macromolecules, 2002, **35**, 5937–5942.

255. E.N. Konyushenko, M. Trchová, J. Stejskal and I. Sapurina, Chem. Pap., 2010, **64**, 56–64. https://doi.org/10.2478/s11696-009-0101-z

256. J Han, J. Dai, C. Zhou and R. Guo, Polymer Chemistry, 2013, **4**, 313-321.

257. G. H. Lim and H. J. Choi, J. Ind. Eng. Chem., 2017, **47**, 51-55.

258. L. Zhang, Y. Long, Z. Chen and M. Wan, Adv. Funct. Mater., 2004, **14,** 693–698.

259. Z. Zhang, M. Wan and Y. Wei, Adv. Funct. Mater., 2006, **16**, 1100-1104.

260. L. Zhang, H. Peng, Z. D. Zujovic, P. A. Kilmartin and J. Travas-Sejdic, Macromol. Chem. Phys., 2007, **208**, 1210–1217.

261. U. Rana, K. Chakrabarti and S. Malik, J. Mater. Chem. 2012, **22**, 15665-15671.

262. J. Huang and M. Wan, J. Polym. Sci., Part A: Polym. Chem., 1999, **37**, 1277-1284.

263. J. Wu, Y. Li and W. Feng, Synth. Met., 2007,**157**, 1013-1018.

264. X. Wu, Y. Wang, Y. Xiao, Y. Han, T. Li and Y. Ma, Synth. Met., 2022, **291**, 117212.

265. Y. Long, Z. Chen, N. Wang, Y. Ma, Z. Zhang, L. Zhang and M. Wan, Appl. Phys. Lett., 2003, **83**, 1863–1865.

266. L. Zhang, H. Peng, J. Sui, P. A. Kilmartin and J. Travas-Sejdic, Curr. Appl. Phys., 2008, **8**, 312–315.

267. W. Wu, D. Pan, Y. Li, G. Zhao, L. Jing and S. Chen, Electrochim. Acta, 2015, **152**, 126 -134.

268. J. Mu, G. Ma, H. Peng, J. Li, K. Sun and Z. Lei, J. Power Sources, 2013, **242**, 797-802.

269. L. Zhang and M. Wan, Thin Solid Films, 2005, **477**, 24–31.

View Article Online
DOI: 10.1039/D5LP00230C

270. R. Panigrahi and S. K. Srivastava, RSC Adv., 2013, **3**, 7808-7815.

271. Z. Zhang, Z. Wei, L. Zhang and M. Wan, Acta Mater., 2005, **53**, 1373-1379.

272. Q. Sun and Y. Deng, Mater. Lett., 2008, **62**, 1831-1834.

273. H. Qiu and M. Wan, Macromolecules 2001, **34**, 675-677.

274. H. Xia, D. Cheng, P. Lam, H. S. O. Chan, Nanotechnology, 2006, **17**, 3957–3961.

275. Y. Li, Z. Li and F. Zheng, Mater. Lett., 2015, **148**, 34-36.

276. K. Huang, X-H. Meng and M. Wa4n, J. Appl. Polym. Sci., 2006, **100**, 3050–3054.

277. Y. Zhu, D. Hu, M. X. Wan, L. Jiang and Y. Wei, Adv. Mater., 2007, **19**, 2092-2096.

278. L. Zhang and M. Wan, Adv. Funct. Mater., 2003, **13**, 815-820.

279. W. Liang, S. Rhodes, J. Zheng, X. Wang, J. Fang, ACS Appl. Mater. Interfaces, 2018, **10**, 37426–37433.

280. M. Liu, C. Luo, R. Huang, H. Peng, Y. Wang, and J. Travas-Sejdic, Int. J. Polym. Mater. Polym. Biomater., 2014, **63**, 602–608.

281. L. Zhang, H. Ping, J. Sui, C. Soellar, P.A. Kilmartin and J. Travas-Sejdic, J. Phys. Chem. C, 2009, **113**, 9128-9134.

282. N. P. Tavandashti, M. Ghorbani and A. Shojaei, Polym. Int., 2015, **64**, 88-95.

283. H. Ding, J. Shen, M. Wan and Z. Chen, Macromol. Chem. Phys., 2008, **209**, 864-871.

284. C. Zhou, J. Han, G. Song and R. Guo, J. Polym. Sci., Part A: Polym. Chem., 2008, **46**, 3563–3572.

285. R. Yuan, H. Wang, T. Ji, L. Mu, L. Chen, Y. Zhu and J. Zhu, J. Mater. Chem. A, 2015, **3**, 19299-19303.

286. L. Ren, K. Li and X. Chen, Polym. Bull., 2009, **63**, 15–21.

287. S. Pang, W. Chen, Z. Yang, Z. Liu, X. Fan and D. Fang, Polymers, 2017, **9**, 510.

288. K. P. D. Orellana and M. E. Roberts, Meet. Abstr. MA2014-01, 2014 page 266. https://iopscience.iop.org/issue/2151-2043/MA2014-01/2

289. S. Wang, Q, Lu, Y. K, Kwon and H. J. Choi, J. Mol. Liq., 2025, 437, 128554.

290. N-R. Chiou, L. J. Lee and A. J. Epstein, Chem Ma.ter., 2007, **19**, 3589–3591.

291. Y-S. Zhang, W-H. Xu, W-T. Yao and S-H. Yu, J. Phys. Chem. C, 2009, **113**, 8588–8594.

292. H. Zhang, Y. Li, X. Wang, J. Li and F. Wang, Polymer, 2011, **52**, 4246-4252.

293. Z. Wei and M. Wan, Adv. Mater., 2002, **14**, 1314–1317.

294. C. Gao, M. Ai, X. Li and Z. Xu, J. Polym. Sci., Part A: Polym. Chem., 2011, **49**, 2173-2182

295. Y. Zhu, G. Ren, M. Wan and L. Jiang, Macromol. Chem. Phys., 2009, **210**, 2046–2051

296. P. Liu, Y. Zhu, J. Torres, S. H. Lee and M. Yun, Polym. Sci., Part A: Polym. Chem. 2017, **55**, 3973–3979.

297. B. Sim and H. J. Choi, RSC Adv., 2015, **5**, 11905.

298. A. Tajima, Y. Ogawa, K. Nakabayashi and M. Atobe, Proceedings of the Annual Meeting of the Japan Society of Sonochemistry, 2015, Volume 24, Session ID P10, Pages 39-40, 2017. https://doi.org/10.20577/pamjss.24.0_39

299. D. P.Bhattarai, A. P. Tiwari, B. Maharjan, B. Tumurbaatar, C. H. Park and C.S. Kim, J. Colloid Interf. Sci., 2019, **534**, 447-458.

300. X. Yang, Z. Zhu, T. Dai and Y. Lu, Macromol. Rapid Commun., 2005, **26,** 1736-1740.

301. J. Wang, Y. Xu, F. Yan, J. Zhu and J. Wang, J. Power Sources, 2011, **196**, 2373–2379.

302. Y. Xia, M. Wei and Y. Lu, Synth. Met., 2009, **159**, 372-376.

303. Y. Bian, C. Yang, Q. Gu, X. Zhu, Y. Wang and X. Zhang, J Polym Sci Pol Chem., 2019, **57**, 1550–1555.

View Article Online
DOI: 10.1039/D5LP00230C

304. X. Zhang, J-S. Lee, G. S. Lee, D-K. Cha, M. J. Kim, D. J. Yang and S. K. Manohar, Macromolecules, 2005, **39**, 470–472.

305. Z. Guo, Y. Qiao, H. Liu, C. Ding, Y. Zhu, M. Wan and L. Jiang, J. Mater. Chem., 2012, **22**, 17153-17158.

306. A. Ali, R. Jamal, T. Abdiryim and X. Huang, J. Electroanal. Chem., 2017, **787**, 110-117.

307. J. Lee, S-B. Cho, K. C. Dimitrov, Y. Lee and D-Y. Khang, Eur. Polym J., 2024, **206**, 112771.

308. X. Ni, X. Hu, S. Zhou, C. Sun, X. Bai and P. Chen, Polym. Adv. Technol., 2011, **22**, 532–537.

309. J. Sui, L. Zhang, J. Travas-Sejdic and P. A. Kilmartin, Macromol. Symp. 2010, **290**, 107-114.

310. M. Acosta, M. D. Santiago, J.A. Irvin. Materials. 2022, **15**, 8820.

311.X. Karagiorgis, S. Sandhu, P. J. Skabara and R. Dahiya, Polym. Int., 2025. https://doi.org/10.1002/pi.70026

312. Y-E, Miao, W. Fan, D. Chen and T. Liu, ACS Appl. Mater. Interfaces 2013, **5**, 4423-4428.

313 Z-Q. Feng, J. Wu, W. Cho, M. K. Leach, E. W. Franz, Y. I. Naim, Z-Z. Gu, J. M. Corey and D. C. Martin, Polymers, 2013, **54**, 702–708.

314. M. Zhu, J. Tang, W. Wei and S. Li, Mater. Chem. Front., 2020, **4**, 1105-1149.

315. M-Y. Bai and Y. Xia, Macromol. Rapid Commun., 2010, **31**, 1863-1868.

316. C. Niu, B. Zou, Y. Wang, L. Chen, H. Zheng and S. Zhou, Chem. Com, 2015, **51**, 5009–5012.

317. H. Gu, J. Huang, N. Li, H. Yang, G. Chen, C. Dong, C. Gong and H. Guan, J. Mater. Sci. Technol., 2023, **146**, 145–153.

View Article Online
DOI: 10.1039/D5LP00230C

318. H. Lv, Q. Pan, Y. Song, X-X. Liu and T, Liu, Nano-Micro Lett.,. 2020, **12**, 118.

319. Z. Chen, X. Zhao, R. Lu, R. Hong and X.Yang, Synt. Met., 2023, **296**, 117378.

320. N. Jabeen, Q. Xia, M. Yang and H. Xia, ACS Appl Mater Interfaces. 2016, **8**, 6093–6100

321. C**.** Wu, Z. Pei, M. Lv, D. Huang, Y. Wang and S. Yuan, Molecules, 2023 **28**, 434.

322. A. Xu, Y. Yu, W. Li, Y. Zhang, S. Ye, Z. Zhao and Y. Qin, Electrochim. Acta, 2022, **435**, 141378.

323.D. Liu, L. Zhou, Y. Liu, C. Xia, J. Ouyang and A. A. Adesina, J Environ. Chem. Eng., 2025, **12**, 113450

324.X. Hu, Y. Duan, Z. Hao, Z. Meng, B. Wang, Z. Kang, S. Liu and H. Tian, J. Alloys Compd., 2024, **1009,**176851.

325.X. Sun, Z. Hao, F. Zeng, J. Xu, H. Nan, ZMeng, J.Yang, W. Shi, Y. Zeng, X. Hu and H. Tian, J. Colloid Interf. Sci., 2022, **610**, 601-609.

326. Z. Lv, Y. Tang, Z. Zhu, J. Wei, W. Li, H. Xia, Y. Jiang, Z. Liu, Y. Luo, X. Ge, Y. Zhang, R. Wang, W. Zhang, X. J. Loh and X. Chen, Adv. Mater., 2018, **13**, 1805468.

327. F. Fauzi, Y. Di, D. M. Morales and R. K. Bose, ACS Appl. Energy Mater. 2025, **8**, 4656-4668.

328. P. Yin, D. Lan, C. Lu, Z. Jia, A. Feng, P. Liu, X. Shi, H. Guo, G. Wu, J. Wang, J. Mater. Sci. Technol., 2025, **204**, 204-223.

329 Y. Li, G. Chen, Q. Li, G. Qiu and X. Liu, J. Alloys Compd,, J. Alloys Compd., 2011, **509**, 4104-4107.

330. C. Cui, Y. Du, T. Li, X. Zheng, X. Wang, X. Han and P. Xu, J. Phys. Chem. B, 2012, **116**, 9523−9531.

331. L. Wang, J. Zhu, H. Yang, F. Wang, Y. Qin, T. Zhao and P. Zhang, J. Alloys Compd,, 2015, **634**, 232–238.

332. Z. Wan, H. Ma, S. Hou, Y. Wang, J. Ho and H. Ge, J. Mater. Sci.: Mater. Electron., 2021, **32**, 10991-11003.

333.S. Chhetri and T. Kuila, RSC Appl. Polym., 2024, **2**, 507-533

334. S. K. Srivastava and V. Mittal, Hybrid Nanomaterials: Developments in Energy, Environments and Polymer Nanocomposites, S.K.Srivastava and V. Mittal (Eds), Scrivener-Wiley, page 241-320, 2017.

335.R. Che, J. Gu, J. Kong, W. Lu, Y. Huang, H. Lv, X. Liu, X.i Qi, G. Wu and H. Wu, Cell Rep. Phys. Sci., 2025, **6**, 102502.

336. P. Saini, V. Choudhary, N. Vijayan and R. K. Kotnala, J Phys. Chem. C 2012, **116**, 13403–13412.

337. Y. Yang, J. Zhang, W. Zou, S. Wu, F. Wu, A. Xie and Z. Wei, Macromol. Rapid Commun., 2018, **39**, 1700591.

338. C. Xu, F. Wu, A. Xie, L. Duan, Z. Yang, Y. Xia, M. Sun and Z. Xiong, Ind. Eng. Chem. Res., 2020, **59**, 7604-7610.

339. R. Guo, L. Wu, J. Shi, F. Wu and A. Xie, Synth. Met., 2022, **290**, 117161.

340. M. Wan, J. Li and S. Li, Polym. Adv. TXechnol., 2001, **12**, 651–657.

341. R. Moučka, M. Sedlačík, H. Kasparyan, J. Prokeš, M. Trchová, F. Hassouna and D. Kopecký, Int. J. Mol. Sci., 2020, **21**, 8814.

342. Y. Sun, G. Guo, B. Yang, M. He, Y. Tian, J.C. Cheng and Y. Liu, J. Mater. Res., 2012, **27**, 457–462.

343. X. Yang, B. Fan, X. Wang, X. Tang, J. Wang, G. Tong, X. Wang and W. Tian, J. Environ. Chem. Eng., 2021, **9**, 105672.

344. S. K. Singh, M. J. Akhtar and K. K. Kar, Ind. Eng. Chem. Res., 2020, **5**9, 9076-9084.

345. H. Wang, K. Zhang and Y. Zhu, J. Mater. Sci.: Mater. Electron., 2024, **35**, 1063.

346. Q. Chu, W. Tao, H. Lin, M. Ma, S. Chen, Y. Shi, H. He and X. Wang, Ind. Crop. Prod., 2023, **194**, 116299.

347. C. Yang, H. Li, D. Xiong and Z. Cao, React. Funct. Polym., 2009, **69**, 137–144.

348. J. Guo, Y. Sun, X. Li, S. Xi, M. M. Ibrahim, H. Qiu, G. A. M. Mersal, Z. M. El-Bahy, V. Murugadoss, W. Abdul, F. Zhou, J. Ren, Z. Guo and J. Zhu, Compos.Sci. and Technol., 2024, **258**, 110917.

349. A. Elhassan, X. Lv, I. Abdalla, J. Yu, Z. Li and B. Ding, Polymers, 2024, **16**, 1160.

350. P. Tang, J. Du, M. Li, X. Zhao. H. Ren, X. Zhang, G. Wu and X. Wang, ACS Appl. Nano Mater., 2024, **7**, 10325-10337.

351. D. Promlok, W. Wichaita, S. Phongtamrug, C. Kaewsaneha, P. Sreearunothai, T. Suteewong and P. Tangboriboonrat, Prog. Org. Coat., 2024, **186**, 108002.

352. Y-F. Zhu, Q-Q. Ni, Y-Q. Fu and T. Natsuki, J. Nanopart. Res.,2013, **15**,1988.

353. J. Hou, L. Zhang, H. Qiu, W. Duan, X. Wang, X. Wan and X. Du, J. Mater. Sci. Mater. Electron., 2017, **28**, 9279-9288.

354. Y-F. Zhu, L. Zhang, T. Natsuki, Y-Q. Fu and Q-Q. Ni, Synth. Met., 2012, **162,** 337-343.

355. P. Tang, M. Li, J. Du, Y. Gong, X. Zhang, G. Wu and X. Wang, Appl. Surf. Sci., 2024, **649**, 159183.

356. B. Zhang, Y. Du, P. Zhang, H. Zhao, L. Kang, X. Han and P. Xu, J. Appl. Polym. Sci., 2013, **130**, 1909-1916.

357. W. Zhou, X. Hu, X. Bai, S. Zhou, C. Sun, J. Yan and P.ep Chen, ACS Appl. Mater. Interfaces, 2011, **3**, 3839-3845.

358. Y. Sun, F. Xiao, X. Liu, C. Feng and C. Jin, RSC Adv., 2013, **3**, 22554-22559.

359. Z. Wu, D. Tan, K. Tian, W. Hu, J. Wang, M. Su and L. Li, J. Phys. Chem. C, 2017, **121**, 15784–15792.

360. M. Wang, Y. L in, Y. Liu and H. Yang, J. Mater. Sci. Mater. Electron., 2019, **3**0, 14344–14354.

View Article Online
DOI: 10.1039/D5LP00230C

361. M. Qiao, X. Lei, Y. Ma, L. Tian, K.H. Su and Q. Zhang, Ind. Eng. Chem. Res., 2016, **55**, 6263–6275

362. S. H. Hosseini, A. Moghimi and M. Moloudi, Mater. Sci. Semicond. Process., 2014, **24**, 272–277.

363. C. Dong, D. Li, H. Wang, B. Cai, Y. Xin, H. Peng, Y. Zhao, N. Wang, Z. Cui and G. Wang, Carbon, 2023, **215**, 118459.

364. S. Kumari, J. Dalal, A. Kumar and A. Ohlan, Adv. Eng. Mater., A 2022, **24**, 2200635.

365. J. Li, H. Ji, Y. Xu, J. Zhang and Y. Yan, JMRT, 2020, **9**, 762-772.

366. X. Li, L. Yu, W. Zhao, Y. Shi, L. Yu, Y. Dong, Y. Zhu, Y. Fu, X. Liu and F. Fu, Chem. Eng. J., 2020, **379**, 122393.

367. L. Gai, Y. Zhao, G. Song, Q. An, Z. Xiao, S. Zhai and Z. Li, Compos. - A: Appl. Sci. Manuf., 2020, **136**, 105965.

368. C. Tian, Y. Du, P. Xu, R. Qiang, Y. Wang, D. Ding, J. Xue, J. Ma, H. Zhao and X. Han, ACS Appl. Mater. Interfaces, Interfaces, 2015, **7**, 20090–20099.

369. Q. Shang, H. Feng, J. Liu, Q. Lian, Z. Feng, N. Chen, J. Qiu and H. Wu, J. Colloid. Interface Sci., 2021, **584**, 80–91.

370. L. Yu, Y. Zhu and Y. Fu, Appl. Surf. Sci., 2018, **42**7, 451–457.

371. Y-Y. Wang, W-J. Sun, H. Lin, P-P. Gao, J-F. Gao, K. Dai, D-X. Yan and Z-M. Li, Composites Part B, 2020, **199**, 108309.

372. J. Liu, Z. Wang, S. Rehman and H. Bi, RSC Adv, 2017, **7**, 53104–53110.

373. A. Ohlan, K. Singh, A. Chandra and S. K. Dhawan, .ACS Appl. Mater. Interfaces, 2010, **2**, 927–933.

374. Y. Zhang, M. Qiu, Y. Yu, B.Y. Wen and L. Cheng, ACS Applied Materials & Interfaces 2016, **9**, 809–818.

View Article Online
DOI: 10.1039/D5LP00230C

375. P. Saini, V. Choudhary, B. P. Singh, R. B. Mathur and S. K. Dhawan, Mater. Chem. Phys,, 2009, **113**, 919–926.

376. X. Tian, F. Meng, F. Meng, X. Chen, Y. Guo, Y. Wang, W. Zhu and Z. Zhou, ACS Applied Materials and Interfaces, 2017, **9**, 15711-15718.

377. M. Zhang, X. Qian, Q. Zeng, Y. Zhang, H. Cao and R. Che, Carbon, 2021, **175**, 499–508.

378. F. Liu, J. Sui, G. I. N. Waterhouse, W. Zhou, X. Jiang, Z. Zhang and L. Yu, J. Mater. Svi., 2022, **57**, 7570-7586.

379. J. Shu, L. Wang, Y. Dai, A. Chen, X. Wang and Z. Deng, J. Alloys Compd, 2024, **1001**, 175030.

380. L. Yang, M. Liu, G. Liang, X. Xiong, W. You, H. Cheng and R. Che, J. Mater. Chem. C, 2024, **12**, 15501-15509.

381. B. Zhang, J. Wang, J. Peng, J. Sun, X. Su, Y. Zou and Y. Zhou, J. Mater. Sci.: Mater. Electron., 2019, **30**, 9785-9797.

382. C. Ge, X. Zhang, J. Liu, F. Jin, J. Liu and H. Bi, Appl. Surf. Sci., 2016, **378**, 49–56.

383. K. Manna and S. K. Srivastava, ACS Sustain. Chem. Eng., 2017, **5**, 10710-10721.

384. K. Manna and S. K. Srivastava, Langmuir, 2020, **36**, 4519-4531.

385. S. Ji, C. Li, Z. Zhang, X. Jiang and L. Yu, Synth. Met., 2018, **239**, 59–65.

386. L. Meng, J. Li, X. Li, Z. Wang and W. Zhou, J. Alloys Compd., 2023, **966**, 171528.

387. D. Han, N. Xiao, H. Hu, B. Liu, G. Song and H. Yan, RSC Advances, 2015, 5, 97944-97950.

388. R. Panigrahi, S. K. Srivastava and J. Pionteck, Rubber Chem. Technol., 2018, **91**, 97-119.

389. H. Yang, A. Wang, X. Feng, H. Dong, T. Zhuang, J. Sui, S. Zhao and C. Sun, Polymers, 2023, **15**, 1866.

View Article Online
DOI: 10.1039/D5LP00230C

390. C. Li, Y. Zhang, S. Ji, X. Jiang, Z. Zhang and L. Yu, J. Mater.Sci., 2018, **53**, 5270-5286.

391. X. Liu, S. W. Or, C. M. Leung and S. L. Ho, J. Appl. Phys., 2014, **115**, 17A507.

392. Y. Wang, X. Wu, W. Zhang, C. Luo, J. Li, Q. Wang and Q. Wang, Mater. Chem. Phys., 2018, **209**, 23-30.

393. J. Ding, L. Wang, Y. Zhao, L. Xing, X. Yu, G. Chen, J. Zhang and R. Che, Small, 2019, **15**, 1902885.

394 J. Zhang and X. Wang, J. Mater. Sci.: Mater. Electron., 2018, **29**, 1592-1599.

395. M. Zhang, L. Zhao, W. Zhao, T. Wang, L. Yuan, Y. Guo, Y. Xie, T. Cheng, A. Meng and Z. Li, Nano Res., 2023, **16**, 3558-3569.

396. Y. Wang, X. Wu, W. Zhang and S. Huang, Synth. Met., 2015, **210**, 165-170.

397. X. Liu, X. Zhao, J. Yan, Y. Huang, T. Li and P. Liu, Carbon, 2021, **178**, 273-284.

398. H. Wang, S. Feng, M. Sun, X. Li, C. Wang, Z. Lin, M. Ma, T. Li and Y. Ma, J. Colloid Interface Sci., 2024, **658**, 889-902.

399. A. P. Singh, M. Mishra, P. Sambyal, B. K. Gupta, B. P. Singh, A. Chandra and S. K. Dhawan, J. Mater. Chem. A, 2014, **2**, 3581-3593.

400. L. Wang, Y. Huang, C. Li, J. Chen and X. Sun, Synth. Met., 2014, **198**, 300-307.

401. J. Zhao, J. Lin, J. Xiao and H. Fan, RSC Adv., 2015, **5**, 19345-19352.

402. D. Zhang, J. Cheng, X. Yang, B. Zhao and M. Cao, J. Mater. Sci., 2014, **49**, 7221–7230.

403. Z. He, Y. Fang, X. Wang and H. Pang, Synth. Met., 2011, **161**, 420-425.

404. T. Liu, N. Liu, S. Zhai, S. Gao, Z. Xiao, Q. An and D. Yang, J. Alloys Compd, 2019, **779**, 831-843.

405. V. Shukla, J. Mater. Sci., 2020, **55**, 2826=2835.

406. T. K. Gupta, B. P. Singh, R.h B. Mathur and S. R. Dhakate, Nanoscale, 2014, **6**, 842-851.

View Article Online
DOI: 10.1039/D5LP00230C

407. P.B. Liu, Y. Huang and X. Sun, ACS Appl. Mater. Interfaces, 2013, **5**, 12355-12360.

408. S-S. Afzali, S. H. Hekmatara, J. Seyed-Yazdi and S. M. B. M. Hosseini, Sci. Rep., 2022, **12**, 9590.

409. Y. Wang, X. Wu, W. Zhang, C. Luo, J. Li and Q. Wang, Synth. Met., 2017, **231**, 7-14.

410. P. Liu, Y. Huang, Y. Yang, J. Yan and X. Zhang, J. Alloys Compd., 2016, **662**, 63-68.

411. D. Lakherwal, IJERD, 2014, **4**, 41-48.

412. Rama Jyothi N. Heavy Metal Sources and Their Effects on Human Health, in Heavy Metals - Their Environmental Impacts and Mitigation, M.K. Nazal and H. Zhao (eds.), , IntechOpen, 2021, Chapter 2, http://dx.doi.org/10.5772/intechopen.95370

413. M. Chigondo, B. Nyamunda, M. Maposa and F. Chigondo, WST, 2022, **85**, 1600-1619.

414. M. I. Khan, M.K. Almesfer, A. Elkhaleefa, I. Shigidi, M.Z. Shamim, I. H. Ali and M. Rehan, Polymers, 2021,**13**, 3810.

415. A Olad and R. Nabavi, J. Hazard. Mater., 2007,147, 845–851.

416.. H. Chang, Q. Meng, D. Liu, Y. Wu, Z. Yang, B. Sun, F. Liu and Y. Liu, J. Appl. Polym. Sci., 2022, **139**, e52822.

417. H. Wu, Q. Wang, G. T. Fei, S. H. Xu, X. Guo and L. D. Zhang, Nanoscale Res. Lett., 2018, **13**, 401.

418. X. Guo, G. T. Fei, H. Su and L. D. Zhang, J. Phys. Chem. C, 2011, **115**, 1608-1613.

419. Z. Zhao, Y. Yang, L. Xu, Z. Qiu, Z. Wang, Y. Luo and K. Du, J. Chem., 2022, Article no. 2041512, https://doi.org/10.1155/2022/2041512

420. S. Li, X. Lu, X. Li, Y. Xue, C. Zhang, J. Lei and C. Wang, J. Colloid Interface Sci., 2012, **378**, 30-35.

DOI: 10.1039/D5LP00230C

421. M. S. Lashkenari, B. Davodi, M. Ghorbani and H. Eisazadeh, High Perform. Polym., 2012, **24**, 345-355.

422. J. Wang, K. Pan, E. P. Giannelis and B. Cao, RSC Adv., 2013, **3**, 8978-8987.

423. Y. Zhan, X. Wan, S. He and Y. He, J. Chem. Technol. Biotechnol., 2018, **93**, 1432–1442.

424. A. H. Bhat, H and T.N Chisti., J. Chem. Eng., 2023, **11**, 110664.

425. M. Bhaumik, S. Agarwal, V.K. Gupta and A. Maity, J. Colloid Interface Sci., 2016, 470, 257-267.

426 B. Qiu, C. Xu, D. Sun, H. Yi, J. Guo, X. Zhang, H. Qu, M. Guerrero, X. Wang, N. Noel, Z. Luo, Z. Guo and S. Wei, ACS Sustain. Chem. Eng., 2014, **2,** 2070–2080.

427. N. Ballav, H. J. Choi, S. B. Mishra and A. Maity, Appl. Clay Sci., 2014, **102**, 60–70.

428. X. Han, L. Gai, H. Jiang, L. Zhao, H. Liu and W. Zhang, Synth. Met., 2013, **171**, 1–6.

429. W. Zhang, Y. Wang, Y. Fei, Y. Wang, Z. Zhang, M. Kou, Q. Feng, S. Wang and X. Du, Adv. Mater. Sci. Eng., 2021, ID 7068003, DOI:10.1155/2021/7068003.

430. M. Bhaumik, A. Maity, V. V. Srinivasu and M. S. Onyango, J. Hazard. Mater., 2011, **190**, 381–390.

431. M. Chigondo, H. K. Paumo, M. Bhaumik, K. Pillay and A. Maity, J. Mol. Liq., 2019, **275**, 778–791.

432. A. E. Chávez-Guajardo, J. C. Medina-Llamas, L. Maqueira, C. A. S. Andrade, K. G. B. Alves and C. P. de Melo, Chem. Eng. J., 2015, **281**, 826–836.

433. A. M. Muliwa, T. Y. Leswifi, M. S. Onyango and A. Maity, Sep. Purif. Technol., 2016, **158**, 250–258.

434. J. Zhang, H. Chen, Z. Chen, J. He, W. Shi, D. Liu, H. Chi, F. Cui and W. Wang, RSC Adv., 2016, **6**, 59292–59298.

435. T. Wen, Q. Fan, X. Tan, Y. Chen, C. Chen, A. Xu and X. Wang, Polym. Chem., 2016, **7**, 785–794.

View Article Online
DOI: 10.1039/D5LP00230C

436. K.V. Brungesh, B.M. Nagabhushana, M.N.K. Harish and R, H. Krishna, J. Environ. Anal. Toxicol., 2017, **7**, 1000442.

437. L. Du, P. Gao, Y. Liu, T. Minami and C. Yu, Nanomaterials, 2020, **10**, 686.

438. S. Sahu, U. K. Sahu and R. K. Patel, J. Chem. Eng. Data., 2019, 64, 1294-1304.

439. J. Wang, K. Pan, Q. He and B. Cao, J. Hazard. Mater., 2013, **244-245**, 121-129.

440. Y. Li, I. Peng, J. Guo and Z. Chen, Langmuir, 2020, **36**, 11508–11516.

441. F. Wang, Y. Zhang, Q. Fang, Z. Li, Y. Lai and H. Yang, Chemosphere, 2021, **263**, 128109.

442. Y. Chen, H. Xu, S. Wang and L. Kang, RSC Adv., 2014, **4**, 17805-17811.

443. Y. Wu, H. Li, Z. Zhao, X. Yi, D. Deng, L. Zheng, X. Luo, Y. Cai, W. Luo and M. Zhang, J. Alloys Compd., 2021, **851**, 156741.

444. M. Bhaumik, V. K. Gupta and A. Maity, J. Environ. Chem. Eng., 2018, **6**, 2514–2527.

445. P. Karthikeyan, S. S. Elanchezhiyan, S. Meenakshi and C. M. Park, J. Hazard. Mater., 2021, **408**, 124892.

446. S. Li, X. Lu, Y. Xue, J. Lei, T. Zheng and C. Wang, PLoS One, 2012, **7**, e43328.

447. A. Hsini, A. Essekri, N. Aarab, M. Laabd, A. A, Addi, R. Lakhmiri and A. Albourine, Environ. Sci. Pollut. Res. Int., 2020, **27**, 15245–15258.

448. S. Dutta, S. K. Srivastava and A. K. Gupta, Mater. Adv., 2021, ***2***, 2431–2443.

449. W. Fang, X. Jiang, H. Luo and J. Geng, Chemosphere, 2018, **197**, 594–602.

450. N. S. Alsaiari, A. Amari, K. M. Katubi, F. M. Alzahrani, F. B. Rebah and M. A. Tahoon, Processes, 2021, **9**, 576.

451. H. D. da Rocha, E. S. Reis, G. P. Ratkovski, R. J. da Silva, F. D. S. Gorza, G. C. Pedro and C. P. de Melo, J. Taiwan Inst. Chem. Eng., 2020, **110**, 8–20.

452. M. K. Debnath, M. A. Rahman, H. Minami, M. M. Rahman, M. A. Alam, M. K. Sharafat, M.K. Hossain and H. Ahmad, J. Appl. Polym. Sci. 2019, **136**, 47524.

View Article Online
DOI: 10.1039/D5LP00230C

453. M. R. Samani and D. Toghraie, J. Environ. Health Sci. Eng., 2019, **17**, 53–62.

454. W. Yao, T. Ni, S. Chen, H. Li and Y. Lu, Compos. Sci. Technol., 2014, **99**, 15-22.

455. E. da S. Reis, F. D. S. Gorza, G. da C. Pedro, B. G. Maciel, R. J. da Silva, G. P. Ratkovski and C. P. de Melo, J. Environ. Chem. Eng., 2021, **9**, 104893.

456. J. Han, P. Fang, J. Dai and R. Guo, Langmuir, 2012, **28**, 6468–6475.

457. Y. Zhang, D-B. Jiang, Y. Wang, T. C. Zhang, G. Xiang, Y-X. Zhang and S. Yuan, Ind. Eng. Chem. Res., 2020, **59**, 7554–7563.

458. A. Mehdinia, R. Niroumand and A. Jabbari, Int. J. Environ. Sci. Technol., 2020, **17**, 2721–2730.

459. N. Wang, J. Feng, W. Yan, L. Zhang, Y. Liu and R. Mu, Front. Environ. Sci. Eng., 2022, **16**, 105.

460. Z. Vatani and H. Eisazadeh, Polym. Plast. Technol., 2013, **5**2, 1621-1625.

461. J. Chen, R. Dong, S. Chen, D. Tang, X. Lou, C. Ye, T. Qiu and W. Yan, J. Clean. Prod., 2022, **338**, 130536.

462. A. S. Rad, J. Water Wastewater, 2020, **31**, 169-183.

463**.** P. Shakhsari, P. A. Azar, F. Z. Hargalani, and M. H. Givianrad IOSRJEN, 2021, **11**, 06-15.

464. L. I. A. Ali, H. F. Alesary, H. K. Ismail, W. H. Hassan, A. A. Kareem and B. K. Nile, **J.** Water Process Eng**.**, 2024, **64**, 105589.

465. M. Bhaumik, A. Maity and H. G. Brink, Chem. Eng. J., 2021, **417**, 127910.

466. F. Wang, L. Huang, J. Li, L. Lin, Z. Liu and Z. Dong, Polym. Chem., 2014, **5**, 4332–4338.

467. E. N. Zare, M. M. Lakouraj and A. Ramezani, New J. Chem., 2016, **40**, 2521–2529.

468. C. Cui, X. Sun, C. Zhou, Y. Liu, H. Xiong, Y. Li and J. Han, Colloids Surf. A: Physicochem. Eng. Asp., 2021, **616**, 126336.

469. M. Karegar and M. M. Khodaei, Journal of Appl. Polym. Scie., 2022, **139**, 51489. View Article Online
DOI: 10.1039/D5LP00230C

470. G. Sarojini, S. Venkateshbabu and M. Rajasimman, Chemosphere, 2021, 278, 130400.

471. Q. Huang, D. Hu, M. Chen, C. Bao and X. Jin, J. Mol. Liq., 2019, **285**, 288–298.

472. J. Chen, J. Zhu, N. Wang, J. Feng and W. Yan, Chem. Eng. J., 2019, **360**, 1486–1497.

473. P. Sun, W. Zhang, B. Zou, X. Wang, L. Zhou, Z. Ye and Q. Zhao, Appl. Clay Sci., 2021, **209**, 106151.

474**.** K. Molaei, H. Bagheri, A. A. Asgharinezhad, H. Ebrahimzadeh and M. Shamsipur, Talanta, 2017, **167**, 607–616.

475**.** H. Zhang, X. Ding, S. Wang, Y. Huang, X-F. Zeng, S. Maganti, Q. Jiang, M. Huang, Z. Guo, and D. Cao, Eng. Sci., 2022, **18**, 320-328.

476. S. Dutta, K. Manna, S. K. Srivastava, A. K. Gupta and M. K. Yadav, Sci. Rep., 2020, **10**, 4982.

477. S. Dutta, A.K. Gupta, S.K. Srivastava, M.K. Yadav, Arsenic in the Environment: Bridging Science to Practice for Sustainable Development As2021, Proceedings of the 8th International Congress and Exhibition, 2021, The Netherlands, CRC Press.

478. V. Q. Trung, N. T. H. Trang, T. M. Thi, K. Vorayuth, N. M. Nghia and M. A. Tuan, Mater. Trans., 2018, **59**, 1095-1100.

479. A. Muhammad, A.u.H.A. Shah and S. Bilal, Appl. Sci. 2020, 10, 2882.

480. M. Bhaumik, C. Noubactep, V. K. Gupta, R. I. McCrindle and A. Maity, Chem. Eng. J., 2015, **271**, 135-146.

481. R. Chetia, S. Devi, N. Shukla, A. Hazarika, S. Bordoloi, B. Pokhrel, B. K. Saikia, A. Gogoi and S. Konwer, ACS Omega, 2024, **9**, 37012–37024.

482. M. S. Mansour, M. E. Ossman and H. A. Farag, Desalination, 2011, **272**, 301–305.

483. Y. Sadeghipour, F. Mojoudi and G. Behbudi, AANBT, 2020, **1**, 20–27.

484. A. Almasian, M. Giahi, G. Chizari Fard, S. A. Dehdast and L. Maleknia, Chem. Eng. J., 2018, **351**, 1166–1178.

485. M. Zheng, Y. Wei, J. Ren, B. Dai, W. luo, M. Ma, T. Li and Y. Ma, Sep. Purif. Technol., 2021, **277**, 119455.

486. M.M. Youssif and M. Wojnicki, Materials 2025, **18**, 2083.

487. J. Shokraiyan, M. Asadi, V. Jahed, T. Sahraeian and M. Rabbani, Desalin. Water. Treat., 2021, **231**, 244–253.

488. H. Cui, Y. Qian, Q. Li, Q. Zhang and J. Zhai, Chem. Eng. J., 2012, **211–212**, 216–223.

489 J. Ren, C. Wang, H. Zhang, X. Liu, T. Yang, W. Zheng, T. Li and Y. Ma, Langmuir, 2023, **39**, 10098-10111.

490. W. Wang, Y. Lv, H. Liu and Z. Cao, Sep. Purif. Technol., 2024, **33**0, 125265.

491. Y. Wu, H. Chang, J. Peng, Y. Liu, B. Sun, Z. Yang, S. Gao and F. Liu, Polym. Bull., 2023, **80**, 3675–3688.

492. S. Chen, D. Xu, L. Chen, Y. Zhang, C. Hu, L. Zhang and J. Chen, ACS Appl. Polym. Mater, 2023, **5**, 10303–10314.

493. S. Majumdar, U. Saikia, and D. Mahanta, J. Chem. Eng. Data, 2015. **60**, 3382–3391.

494. M. H. Fekri, M.B. Keivani, M. R. Mehr and B. Akbari-adergani, JMIUMS, 2019, **29**,166-179.

495. P. L. Meena, J. K. Saini, A. K. Surela, K. Poswal and L. K. Chhachhia, Biomass Convers Biorefin,, 2024, **14**, 1711–1730.

496. K. Rachna, A. Agarwal and N.B Singh, Environ. Nanotechnol. Monit. Manag., 2018, **9**, 154-163.

497. S. Dhanavel, E. A. K. Nivethaa, K. Dhanapal, V. K. Gupta, V. Narayanan and A. Stephen, RSC Adv., 2016, **6**, 28871–28886.

View Article Online
DOI: 10.1039/D5LP00230C

498. V. M. Ovando-Medina, N. E. Dávila-Guzmán, N. V. Pérez-Aguilar, H. Martínez-Gutiérrez, I. D. Antonio-Carmona, S. Y. Martínez-Amador and A. Dector, Iran. Polym. J., 2018, **27**, 171–181.

499. J. Ren, C. Wang, J. Ding, T. Li and Y. Ma, ACS Appl. Polym. Mater., 2022, **4**, 9449–9462.

500. H. Xu, Y. Zhang, Y. Cheng, W. Tian, Z. Zhao and J. Tang, Adsorpt. Sci. Technol., 2019, **37**, 217–235.

501. M. S. Shahriman, N. N. M. Zain, S. Mohamad, N. S. A. Manan, S M. Yaman, S. Asmand and M. Raoov, RSC Adv., 2018, **8**, 33180-33192.

502. C. Wang, B. Liang, H. Gao, T. Yang, T. Li, Y. Ma, H. M. Abo-Dief, G. Roymahapatra, J. Zhang, K. M. Abualnaja, Z. M. El-Bahy and Z. Guo, Colloids Surf. A Physicochem. Eng. Asp. , 2024, **700**, 134659.

503. M.A. Sayed, A. Mohamed, S.A. Ahmed, A.M. El-Sherbeeny, W.A. Zoubi, M.R. Abukhadra, ACS Omega 2023, **8**, 47210–47223.

504. A. Varghese, S. Devi K.R and D. Pinheiro, Mater. Today Commun., 2023, **35**, 105739.

505. L. Benhaddad, N. Belhouchat, A. Gueddouri, M. L. Hammache and H. Saighi, Russian J. Gen. Chem., 2023, **93**, 2378–2392.

506. S. Mondal, U. Rana, P. Das and S. Malik, ACS Appl. Polym. Mater., 2019, **1**, 1624-1633.

507. I. Toumi, H. Djelad, F. Chouli and A. Benyoucef, J. Inorg. Organomet. Polym. Mater., 2021, **32**, 112–121.

508. M. S. Tanweer, Z. Iqbal and M. Alam, Langmuir, 2022, **38**, 8837–8853.

509. C. Ao, B. Zhang, L. Yuan, J. Li, D. Wu, R. Xu and B. Pan, J. Membr. Sci., 2024, **708**, 123020.

510. X.P. Teng, M.Y.K. Bryan, P.V. Chai and J.Y. Law, Mater. Today Proc., 2021, **46**, http://dx.doi.org/10.1016/j.matpr.2021.01.766

511**.** S. Singh, S. Perween and A. Ranjan, J. Environ. Chem. Eng., 2021, **9**, 105149.

512. H. Ali and A. M. Ismail, J. Polym. Environ., 2023, **31**, 976–998.

513**.** S. Dutta, S. K. Srivastava, B. Gupta and A. K. Gupta, ACS Appl. Mater. Interfaces, 2021, **13**, 54324-54338.

514. I. Benchikh, S. Lahreche, Y. Benmimoun and A. Benyoucef, Research Square, 2022, DOI: https://doi.org/10.21203/rs.3.rs-1479466/v1

515. Y. Weng, Z. Jin, S. Xie and M. Zhang, Colloids Surf. A: Physicochem. Eng. Asp., 2024, **681**, 132745.

516**.** S. Razzaq, M. Akhtar, S. Zulfiqar, S. Zafar, I. Shakir, P. O. Agboola, S. Haider and M. F. Warsi, J. Taibah Univ. Sci., 2021, **15**, 50–62.

517. I. Khan, K. Saeed, I. Zekker, B. Zhang, A.H. Hendi, A. Ahmad, S. Ahmad, N. Zada, H. Ahmad, L.A. Shah, et al., Water 2022, **14**, 242.

518. M. M. Ayad and A. A. El-Nasr, J. Phys. Chem. C, 2010, **114**, 14377-14383**.**

519. W. A. Amer, M. M. Omran, A. F. Rehab and M. M. Ayad, RSC Adv., 2018, 8, 22536–22545.

520. W. A. Amer, M. M. Omran and M. M. Ayad, Colloids Surf. A: Physicochem. Eng. Asp., 2019, **562**, 203–212.

521. Y. Zhang, S. He, Y. Zhang, Y. Feng, Z. Pan and M. Zhang, Colloids Surf. A: Physicochem. Eng. Asp., 2022, **632**, 127765.

522. M. M. Ayad, A. Abu El-Nasr and J. Stejskal, J. Ind. Eng. Chem., 2012, **18**, 1964-1969.

523. N. Wang, J. Chen, J. Wang, J. Feng and W. Yan, Powder Technology, 2019, **347**, 93–102.

524. E. A. El-Sharkaway, R. M. Kamel, I. M. El-Sherbiny and S. S. Gharib, E. A. El-Sharkaway, R. M. Kamel, I. M. El-Sherbiny and S. S. Gharib, Environ. Technol., 2019, **41**, 2854–2862.

525. M. M. Ayad, W. A. Amer, S. Zaghlol, I. M. Minisy, P. Bober and J. Stejskal, Chem. Pap., 2018, **72**, 1605–1618.

526. Y. Wang, J. Appl. Organomet. Chem., 2025, **39**, e7977.

527. C. Wang, B. Zhang, X. Sun, Y. Zhang, W. Li, T. Yang, Y. Ma, Z. Sun and T. Li, Sep. and Purif. Technol., 2024, **329**. 125140.

528. A. A. Nezhad, M. Alimoradi and M. Ramezani, Mater. Res. Express, 2018, **5**, 025508.

529. W. Zhang, L. Hao, Y. Wang, Q. Lin, C. Lu and Z. Xu, J. Environ. Chem. Eng., 2016, **4**, 882-890.

530. L. Bai, Z. Li, Y. Zhang, T. Wang, R. Lu, W. Zhou, H. Gao and S. Zhang, Chem. Eng. J., 2015, **279**, 757-766.

531. N. Mohanty, S. Behera and B N. Patra, Ind. Eng. Chem. Res., 2025, **64**, 2274–2282.

532. K. O. Iwuozor, J. O. Ighalo, E. C. Emenike, L. A. Ogunfowora and C. A. Igwegbe, CRGSC, 2021, **4**, 100179.

533. S. Radoor, J. Karayil, A. Jayakumar, J. Parameswaranpillai and S. Siengchin, Colloids Surf. A: Physicochem. Eng. Asp., 2021, **611**, 125852.

534. S. Yildirim, B. Isik and V. Ugraskan, Mater. Chem. Phys., 2023, **307**, 128083.

535. S. Pete and R. A. Kattil and L. Thomas, Diam. Relat. Mater., 2021, **117**,108455.

536. Y**.** Xia, T. Li, J. Chen and C. Cai, Synth. Met., 2013, **175**, 163–169.

537. A.R. Prasad and A. Joseph. RSC Adv., 2017, **7**, 20960.

538. M. Zhang, L. Chang and Z. Yu, Desalin Water Treat., 2018, **110**, 209–218.

539. W. Yao, C. Shen and Y. Lu, Compos. Sci. Technol., 2013, **87**, 8–13.

540. M. Maruthapandi, L. Eswaran, J.H.T. Luong and A. Gedanken, Ultrason. Sonochem. 2,020, **62**, 104864.

541. N. Sadegh, H. Haddadi, F. Sadegh and A. Asfaram, Polyhedron, 2024, **248,**116671.

542. Y. Zeng, L. Zhao, W. Wu, G. Lu, F. Xu, Y. Tong, W. Liu and J. Du, J. Appl. Polym. Sci., 2013. **12**7, 2475-2482.

543. Z. Tang, M. Ai, and J. Peng, J. Comput. Theor. Nanosci., 2017, **14**, 1965-1969.

544. F. Huang, X. Tian, W. Wei, X. Xu, J. Li, Y. Guo and Z. Zhou, J. Clean. Prod., 2022, **344**, 131100,

545. M. A. Gabal, E. A. Al-Harthy, Y. M. Al Angari, M. Abdel Salam, A. Awad, A. A. Al-Juaid and A. Saeed, Catalysts, 2022, **12**, 1624.

546. H. K. Alzahrani and D. F. Katowah, Nanocomposites, 2023, **9**, 183-202.

547. S. A. Alqarni, Nanocomposites, 2022, **8**, 47–63.

548. Z. Miri, S. Elhami, V, Zare-Shahabadi and H. J. Jahromi, Spectrochim Acta A Mol Biomol Spectrosc., 2021, **262**, 120130.

549. P. Roy and S. K. Srivastava, Nanomaterials for Electrochemical Energy Storage Devices, Scrivener Publishing, 2020.

550.S. Raj, S.K. Srivastava, P. Kar and P. Roy, RSC Adv., 2016, 6, 95760-95767.

551. N. Swain, B. Saravanakumar, M. Kundu, L. Schmidt-Mende and A. Ramadoss, J. Mater. Chem. A 2021, 9, 25286–25324.

552. Y-T. Tan, F. Ran, L-R. Wang, L-B. Kong and L. Kang, J, Applied. Polym. Sci., 2012, **127**, 1544-1549.

553. W. Yang, Z. Gao, N. Song, Y. Zhang, Y. Yang and J. Wang, J. Power Sources, 2014, **272**, 915-921.

554. Z. Li, Y. Shen and Y. Li, J. Electrochem. Soc., 2018, **165**, G75–G79.

555. Z. Li, J. Hu, Y. Li and J. Liu, ChemistrySelect, 2018, **3**, 6737-6742.

556. Z. Wang, H. Qiang, C. Zhang, Z. Zhu, M. Chen, C. Chen and D. Zhang, J. Polym. Res., 2018, **25**, 129.

View Article Online
DOI: 10.1039/D5LP00230C

557. R. Hong, X. Zhao, R. Lu, M. You, X. Chen and X. Yang, Molecules, 2024, **29**, 2331.

558. M. S. Kim, J. H. Moon, P. J. Yoo and J. H. Park, J. Electrochem. Soc., 2012, **15**9, A1052–A1056.

559. Z. Li, J. Cai, P. Cizek, H. Niu, Y. Du and T. Lin, J. Mater. Chem. A, 2015, **3**, 16162–16167.

560. P. Fan, S. Wang, H. Liu, L. Liao, G. Lv and L. Mei, Electrochim. Acta, 2020, **331**, 135259.

561. Z-L. Wang, R. Guo, G-R. Li, H-L. Lu, Z-Q. Liu, F-M. Xiao, M. Zhang and Y-X. Tong, J. Mater. Chem., 2012, **22**, 2401-2404.

562. J. P. Jyothibasu and R.-H. Lee, J. Mater. Chem. A, 2020, **8**, 3186–3202.

563. H-H Huang, Y-H. Wu, M-Z. Wang and X-W. Ge, Chin. J. Chem. Phys., 2018, **31**, 827-832.

564. D. Xu, A. Chen, Q. Sheng, G. Hu, L. Chen, Y. Zhang, S. Chen, and C. Hu, J. Power Sources, 2025, **638**, 236627.

565. K-J. Ahn, Y. Lee, H. Choi, M-S. Kim, K. Im, S. Noh, and H. Yoon, Sci. Rep., 2015, **5**, 14097, DOI: 10.1038/srep14097

566. S. Xiong, Y. Zhang, Y. Wang, B. Wu, J. Chu, X. Wang, R. Zhang, M. Gong, Z. Li, and Z. Chen, High Perform. Polym., 2019, **32**, 600-608.

567. B. M. Hryniewicz and M. Vidotti**,** ACS Appl. Nano Mater**.** 2018, 1, 3913–3924.

568. Y. Wang, X. Wu, Y. Xiao, Y. Han, T. Li and Y. Ma, Synth. Met., 2023, **299**, 117483.

569. X. Zhang, J. Zhao, T. Xia, Q. Li, C. Ao, Q. Wang, W. Zhang, C. Lu and Y. Deng, Energy Storage Mater., 2020, **31**, 135–145.

570. J-G. Wang, Y. Yang, Z-H. Huang and F. Kang, J. Power Sources, 2012, **204**, 236–243.

571. N. B. Trung, T. V. Tam, H. R. Kim, S. H. Hur, E. J. Kim and W. M. Choi, Chem. Eng. J., 2014, **255**, 89–96.

572. J, Luo, Q. Ma, H. Gu, Y. Zheng and X. Liu, Electrochim. Acta, 2015, **173**, 184-192.

573. W. Wu, C. Wang, C. Zhao, D. Wei, J. Zhu and Y. Xu, J. Colloid Interface Sci., 2020, **580**, 601–613.

574. M. Devi and A. Kumar, Polym. Compos., 2020, **41**, 653–667.

575. Y. Yang, P. Zhu, L. Zhang, T. Li, Q. Wang, R. Sum and C. Wong, 19th International Conference on Electronic Packaging Technology (ICEPT), Shanghai, China, 2018, pp. 270-274, doi: 10.1109/ICEPT.2018.8480452.

576. S. Wu, J. Tian, X. Yin and W. Wu, Nano, 2019, **14**, 1950056.

577. Z. Wang, C. Zhang, C. Xu, Z. Zhu and C. Chen, Ionics, 2016, **23**, 147–156.

578. H. Kwon, D. Hong, I. Ryu and S. Yim, ACS Appl. Mater. Interfaces, 2017, **9**, 7412–7423.

579. F. A. Tabar, F. Sharif and S. Mazinani, Polymer, 2018, **15**4, 80–89.

580. J. Liu, J. An, Y. Ma, M. Li and R. Ma, J. Electrochem. Soc., 2012, **159**, A828–A833.

581. X. Xu, J. Tang, H. Qian, S. Hou, Y. Bando, Md. S. A. Hossain, L. Pan and Y. Yamauchi, ACS Appl. Mater. Interfaces, 2017, **9**, 38737–38744.

582. P. Liu, X. Wang and H. Li, Synth. Met., 2014, **189**, 173-176.

583. D. Tian, H. Cheng, Q. Li, C. Song, D. Wu, X. Zhao, S. Hu, S. Chen and C. Hu, Electrochim. Acta, 2021, **398**, 139328.

584. K. Kakaei, S. Khodadoost, M. Gholipour and N. Shouraei, J. Phys. Chem. Sol., 2021, **148**, 109753.

585. S. Chen, H. Cheng, D. Tian, Q. Li, M. Zhong, J. Chen, C. Hu and H. Ji, ACS Appl. Energy Mater., 2021, **4**, 3701–3711.

586. J. Li, X. Li, W. Wei, D. Wang and P. Liu, Electrochim. Acta, 2021, **395**, 139193.

587. W. Fan, C. Zhang, W. W. Tjiu, K. P. Pramoda, C. He and T. Liu, ACS Appl. Mater. Interfaces, 2013, **5**, 3382–3391.

View Article Online
DOI: 10.1039/D5LP00230C

588. P. Du, W. Wei, D. Liu, H. Kang and P. Liu, Chem. Eng. J., 2018, **335**, 373-383.

589. V. Mini and H. Devendrapp, Mater. Today Proc., 2018, **5**, 23148-23155.

590. W. Wu, L. Yang, S. Chen, Y. Shao, L. Jing, G. Zhao and H. Wei, RSC Adv., 2015, **5**, 91645–91653.

591. K. Qi, R. Hou, S. Zaman, B. Y. Xia and H. Duan, J. Mater. Chem. A, 2018, **6**, 3913–3918.

592. J. Zhu, W. Sun, D. Yang, Y. Zhang, H. H. Hoon, H. Zhang and Q. Yan, Small 2015, **1**1, 4123-4129.

593. Q. Chen, F. Xie, G Wang, K. Ge, H. Ren, M. Yan, Q. Wang and H. Bi, Ionics, 2021, **27**, 4083–4096.

594. X. Zhang, L. Ma, M. Gan, G. Fu, M. Jin and Y. Zhai, Appl. Surf. Sci., 2018, **460**, 48–57.

595. S. Zhang, X Song, S. Liu, F. Sun, G. Liu and Z. Tan, Electrochim. Acta 2019, **312**, 1-10.

596. S. A. Ansari, H. Fouad, S. G. Ansari, Md Palashuddin Sk and M.H. Cho, J. Colloid Interface Sci., 2017, **504**, 276-282.

597. Y. Cai, L. Xu, H. Kang, W. Zhou, J. Xu, X. Duan, X. Lu and Q. Xu, Electrochim. Acta, 2021, **370**, 137791.

598. Y. Liang, Z. Wei, X. Zhang, and R. Wang, ES Energy Environ., 2022, **18**, 101-110.

599. D. Thanasamy, D. Jesuraj, V. Avadhanam, K. Chinnadurai, S. Kumar and K. Kannan, J. Energy Storage, 2022, **53**, 105087.

600. Z. Li, Y. Sui, J. Qi, F. Wei, Y. He, Q. Meng, Y. Ren, X. Zhang, Z, Zhan and Z. Sun, Compos. Interfaces, 2019, **27**, 631–644.

601. I. Chakraborty, N. Chakrabarty, A. Senapati and A. K. Chakraborty, J. Phys. Chem. C 2018, **122**, 27180–27190.

602. S. S. Scindia, R.B. Kamble and J. A. Kher, AIP Adv., 2019 **9**, 055218.

603. J. Fu, Y. Zhang, H. Zhao, R. Jiang and R. Zhang, J. Colloid Interface Sci., 2020, **559**, 39-44.

604. C. Chen, Q. Zhang and C. Peng, Polym. Polym. Compos., 2017, **25**, 483-488.

605. A. Imani and G. Farzi, J. Mater. Sci.: Mater. Electron., 2015, **26**, 7438-7444.

606. C. Xia, M. Leng, W. Tao, Q. Wang, Y. Gao and Q. Zhang, J. Mater. Sci.: Mater. Electron., 2019, **30**, 4427–4436.

607. X. Liu, Z. Wu and Y. Yin, Chem. Eng. J., 2017, **323**, 330-339.

608. C. Pan, Z. Liu, W. Li, Y. Zhuang, Q. Wang and S. Chen, J. Phys. Chem. C, 2019, **123**, 25549-25558.

609. B. Mu, W. Zhang and A. Wang, J. Nanopart. Res., 2014, **16**, 2432.

610. X. Ge, Y. He, T. Plachy, N. Kazantseva, P. Saha and Q. Cheng, Nanomaterials 2019, **9**, 527.

611. X. Li, H. Song, Y. Zhang, H. Wang, K. Du, H. Li, Y. Yuan and J. Huang, Int. J. Electrochem. Sci., 2012, **7**, 5163–5171.

612. J. H. Shendkar, M. Zate, K. Tehare, V. V. Jadhav, R. S. Mane, M. Naushad, J. M. Yun and K. H. Kim, Mater. Chem. Phys., 2016, **180**, 226-236.

613. X. He, Q. Liu, J. Liu, R. Li, H. Zhang, R. Chen and J. Wang, Chem. Eng. J., 2017, 325, 134-143.

614. P. Li, E. Shi, Y. Yang, Y. Shang, Q. Peng, S. Wu, J. Wei, K. Wang, H. Zhu, Q. Yuan, A. Cao and D. Wu, Nano Res., 2014, **7**, 209-218.

615. Y. Yesi, I. Shown, A. Ganguly, T. T. Ngo, L-C. Chen and K-H. Chen, ChemSusChem, 2016, **9**, 370-378.

616. J. W. Park, W. Na and J. Jang, J. Mater. Chem. A, 2016, **4**, 8263–8271.

View Article Online
DOI: 10.1039/D5LP00230C

617. M. Vellakkat and D. Hundekkal, Mater. Res. Express, 2016, **3**, 015502.

618. M. B. Poudel, M. Shin and H. J. Kim, Int. J. Hydrogen Energy, 2021, **46**, 474-485.

619. J. Iqbal, M. O. Ansari, A. Numan, S. Wageh, A. Al-Ghamdi, M. G. Alam, P. Kumar, R. Jafer, S. Bashir and A. H. Rajpar, Polymers, 2020, **12**, 2918.

620. A.H. P. de Oliveira, M.LF. Nascimento and H. P. de Oliveira, Mater. Res., 2016, **19**, 1080-1087.

621. H-Y. Ho, H-I Chu, Y-J. Huang, D-S. Tsai and C-P. Lee, Nanotechnology, 2023, **34**, 125401.

622. J. Rodríguez-Moreno, E. Navarrete-Astorga, E. A. Dalchiele, R. Schrebler, J. R. Ramos-Barrado and F. Martín, Chem Com, 2014, **50**, 5652-5655.

623. Y. Huang, J. Wang, X. Ju, S. Zhang and X. Sun, J. Energy Storage, 2023, **72**, 108460.

624. R. Li, P. Song, Z. Ji, H. Zhou, Y. Xue, L. Kong and X. Shen, Appl. Surf. Sci., 2024, **649**, 159188.

625**.** K. Ghosh, C. Y. Yue, M. M. Sk and R. K. Jena, ACS Applied Materials and Interfaces, 2017, **9,** 15350-15363.

626. L. Liu, Y. Wang, Q. Meng and B. Cao, J. Mater. Sci., 2017, **52**, 7969–7983.

627. K. Wang, L. Li, Y. Liu, C. Zhang and T. Liu, Adv. Mater, Interfaces, 2016, **3**, 1600665

628. Y. Liu, X. Wang, T. Abdiryim, R. Jamal, A. Abdurexit, F. Xu, N. Fan, K. Song and H. Yang, J. Energy Storage, 2024, **94**,112530.

629. R Joy and S. Haridas, $SrTiO_3$/CNT/PANI Ternary Composite for Supercapacitor Applications. In: A. Dixit, V.K. Singh, S. Ahmad (eds), Energy Materials and Devices. E-MAD 2022. Advances in Sustainability Science and Technology. Springer, Singapore. (2024). https://doi.org/10.1007/978-981-99-9009-2_12

630. N. Boutaleb, G.M. Al-Senani, S. D. Al-Qahtani, A. Benyoucef and B. Dhygham Alkoudsi, Colloids Surf. A: Physicochem. Eng. Asp., 2025, **718**, 136867

631. A. V. Baskar, N. Bolan, S. A. Hoang, P. Sooriyakumar, M. Kumar, L. Singh, T. Jasemizad, L. P. Padhye, G. Singh, A. Vinu, B. Sarkar, M.B. Kirkham, J. Rinklebe, S. Wang, H. Wang, R. Balasubramanian and K. H.M. Siddique, Total Environment, 2022, **822**,153555.

632. O.B. Okafor, A.P.I. Popoola, O.M. Popoola, ***U.*** O. Uyor and V. E. Ogbonna**,** Polym. Bull.*,* 2024, **81**, 189–246.

633. N. Singh and U. Riaz, Polym. Bull., 2022, **79**,10377–10408.

534. S. Rawat, R.K. Mishra and T. Bhaskzar, Chemisphere, 2022, **2**, 131961.

635. G. Jiang, R.A. Senthil, Y. Sun, T.R. Kumar and Pan, J. Power Sources, 2022, **520**, 230886.

636. A.T.S.C. Brandão, S. State R. Costa P. Potorac J. A. VázquezJesus, Valcarcel A. F. Silva, L. Anicai, M. Enachescu and C.M. Pereira, ACS Omega 2023, **8**, 18782–18798.

637. D. Tashima, T. Kashio, T. Eguchi, S. Kumagai, T. Tsubota and J. D.W. Madden, Mater. Lett., 2023, **18**, 100193.

638. P. Manasa, S. Sambasivam and F. Ran, J. Energy Storage 2022, **54,** 105290.

639. K. Mensah-Darkwa, C. Zequine, P. K. Kahol, and R. K. Gupta, Sustainability 2019, **11**, 414.

640. X. Zhu, Y. Zeng, X. Zhao, D. Liu, W. Lei, and S. Lu, EcoEnergy, 2025. https://doi.org/10.1002/ece2.70000

641. B. R. Holla, M. Kanthraj, Vaishali, Namitha and Vishnumurthy K A, J. Ind. Che, Soc. 2025, 102, 101948.

642. P. H. Patil and Sushilkumar A. Jadhav, RSC Appl. Interfaces, 2024, **1**, 624

643. N. V. Challagulla, M. Vijayakumar, D. S. Rohita, G. Elsa, A. B. Sankar, T. N.a Rao and M. Karthik, Energy Technol., 2020, **8**, 2000417.

644. S. N. Karri, S. P. Ega, V. Perupogu and P. Srinivasan, ChemistrySelect, 2021, **6**, 2576-2589.

645. S. Rajput, V. Tyagi, Sonika, R. Nayak and S.K. Verma, Energy Technology, 2025, **13**, DOI: 10.1002/ente.202401977

View Article Online
DOI: 10.1039/D5LP00230C

Table 1. Microwave absorbing properties of hollow ICPs, hollow ICP nanocomposites and ICP based core-shell nanocomposites.

Conducting polymer/ Nanocomposites	Method of preparation	Filling (wt %) in the matrix selected	Frequency range	Shielding performance (Sample thickness)	Maximum Bandwidth (<10 dB) (GHz)	Ref.
Hollow Polyaniline/Ag	Emulsion polymerization	---	100 KHz-20 GH	SE_T: 19.5 dB	---	203
Hollow Polypyrrole/Ag	via in situ chemical oxidative copolymerization	---	100 KHz–20 GHz	SE_T: 34.5 dB	---	204
Fe_3O_4 (core: ~100 nm)/PPy (Shell: ~70 nm)	In situ polymerization	50 wt.% in Paraffine	2-18 GHz	R_L^{min}:-22.4 dB at 12.9 GHz (thickness: 2.3 mm)	~5 GHz in the range of 4-18 GHz (Thickness: 1.5-5.0 mm)	329
Fe_3O_4 microsphere @PANI	Two step oxi. polymerization	50 wt % in paraffin wax bn	2-16 GHz	R_L^{max}:-31.3 dB at 9.0 GHz (Thickness: 3 mm)	4.0−18 GHz (Thickness :1.5 to 5.0 mm)	330
Graphene@Fe_3O_4@SiO_2@PANI	Dilute polymerisation	25 wt % in paraffin wax	2-18 GHz	R_L^{max}:-40.7 dB at 12.5 GHz (thickness: 2.5 mm)	5.8 GHz (10.5-16.3 GHz)	331
3D Helical Hollow superstructure of PANI	Co-self-assembly process combined with emulsion droplets	20 wt% in paraffin	2-18 GHz	R_L^{min}:-51.60 dB at 13.95 GHz (Thickness:2.0 mm)	5.12 GHz (12.03–17.15 GHz)	337
Hollow PPy nanofibers based self-assembled aerogel (seeds and Py proportion =1:0.5)	Self-assembly	8% in paraffin	2-18 GHz	R_L^{min}: -58.73 dB at 16.48 GHz (Thickness: 2.30 mm)	7.28 GHz (Thickness: 2.69 mm)	338

Hollow PPy nanorods	Via self-assembly template sacrificial strategy	10 wt% in paraffin	2-18 GHz	R_L^{min}: -54.94 dB at 13.2 GHz (Thickness: 3.4 mm)	7.36 GHz	339
PANI microtubes	Via a self-assembly process assisted by excess APS	---	0 to 6000 MHz.	R_L: -15.5 dB	----	342
PANI hierarchical microtubes	SDS/HCl (7.5 mM) assisted oxidative polymerization method	50% in paraffin	2-18 GHz	-43.6 dB: Absorption (Thickness: 1.55 mm)	5.84 GHz	343
Polyaniline 3D hollow spheres integrated milled carbon fibers (MCF)	PANI 3D hollow spheres are synthesized by removing the polystyrene (PS) core from PS/PANI composites	4 wt% MCF+1 wt % PANI in epoxy	8-12 GHz	Max. absorption −49.3 dB (Thickness: 1.8 mm)	1.7 GHz (Thickness: 1.8 mm)	344
Polyaniline-mediated N and S co-doped carbon nanoflakes	In-situ polymerization method and carbonization process with oxygen limitation.	Paraffin wax (80 wt%) and samples (20 wt%)	2-18 GHz	R_L^{min}:− 53.5 dB at 10.2 GHz (Thickness: 2.9 mm)	4.5 GHz at 2.9 mm	345
Hollow PANI /CNF in the surface layers and MXene/CNF in the intermediate layer	Alternating vacuum-assisted filtration method	MXene: 8 wt% and Hollow PANI : 24 wt% in CNF matrix	8-12.4 GHz	EMI SE: 35.3 dB	---	346
Hollow Fe_3O_4 (7.33 wt%)@ PANI (Magnetic fluid: 15 ml)	Hollow PANI prepared by using PS microspheres as hard template and decorating FeO4 on its surface.	Paraffin filled with with a sample (loaded with 7.33 wt% Fe_3O_4) content of 75%	2-18 GHz	R_L^{max}:- 15.6 dB	8.0 GHz	347
Fe_3O_4@PPy	In situ polymerization method	60 wt% of composites blended with paraffin wax	2-18 GHz	R_L^{max}: - 52.01 dB in 25 wt% of paraffin wax loaded sample of 3.1 mm thickness	2.72 GHz (Thickness: 3.1 mm)	348
Fe_3O_4/PPy Double-carbonized core-shell-like composite	Rapid microwave assisted carbonization process	---	2–18 GHz.	R_L^{min}: −26 dB at 16 GHz (Thickness: 1.6 mm.	4.64 GHz (Thickness: 1.6 mm.)	349

Hollow core–shell Fe_3O_4@ PPy	Solvothermal process, followed by in situ polymerization (aniline monolere:170 μL)	50% of nanocomposite by wt in paraffin	2-18 GHz	R_L^{min}: −84.92 dB at 3.87 mm	4.20 GHz at 2.38 mm,	350
Fe_3O_4–PE@PANI Hollow sphere	Electrostatic self-assembly approach	50 wt% in paraffin	0.5–15 GHz	R_L^{min}: -6.5 dB at 14.3 GHz	Frequency bandwidth at less than -5 dB (12.5 to 15 GHz)	352
Hollow structure Fe_3O_4/PANI microspheres (aniline:PS=1:6)	Three-step synthesis 1.5 and 2.0 mm, the bandwidth below and 4.64 GHz (11.04–15.68 GHz),	50 wt% in paraffin	2-18 GHz	R_L^{min}: −24.3 dB at 18 GHz (Thickness: 1.6 mm)	2.48 GHz (15.52–18 GHz for 1.5 mm thickness, 4.64 GHz (11.04–15.68 GHz) for 2 thickness	353
Hollow Poly(aniline-co-pyrrole)– (0.6 g Fe_3O_4	Oxidized polymerisation of aniline and pyrrole in presence of Fe_3O_4 (0.06 g) using non-ionic surfactant as a template.	50 wt% in paraffin	0.5–10 GHz	R_L^{min} : −3 dB at 9 GHz and 10 GHz (Thickness: 2 mm)	---	354
Fe_3O_4/PANI (Hollow 0D/1D)	Hydrothermal treatment and chemical oxidative polymerization	40 % in wax	2-18 GHz	R_L^{min}: -55.03 dB (thickness: 1.84 mm)	4.88 GHz (thickness: 1.84 mm)	355
Fe_3O_4/Polyaniline Core/Shell microspheres (PANI shell thickness: 100 nm)	In situ polymerization method	50 wt % in paraffin	1–18 GHz,	R_L^{max}: -37.4 dB at 15.4 GHz	----	356
Fe_3O_4-PEDOT microspheres (EDOT/Fe_3O_4 vol. fraction:20%)	Two-step method	Paraffin wax	2-18 Ghz	R_L^{min}: ~ -30 dB at 9.5 GHz (thickness: 4 mm)	---	357
Core–shell Fe_3O_4–Polyaniline	In situ polymerization of aniline in the presence of dodecyl benzenesulfonic acid	40% Fe_3O_4–polyaniline in paraffin wax	0.03–18 GHz	$R_L^{optimal}$: -35.1 dB at 16.7 GHz (thickness: 1.7 mm)	---	358
Core-Shell Fe_3O_4@ Polypyrrole	Process comprising of etching (time: 5 min), polymerization and replication	50 wt % filler in paraffin	2-18 GHz	R_L^{max}: −41.9 dB (.99.99%) at 13.3 GHz (thickness: 2.0 mm)	6.0 GHz (12.0−18.0 GHz).	359

Core-shell Fe_3O_4 @Polypyrrole microspheres (Pyrrole/Fe_3O_4 ratio=20)	Chemical oxidative polymerization in the presence of polyvinyl alcohol and p-toluenesulfonic acid.	50% filler in paraffin wax	2-18 GHz-	R_L^{max}: -31.5 dB (99.99%) at 15.5 GHz (thickness: 2.5 mm)	5.2 GHz (12.8-18 GHz)	360
Core–shell structure $BaFe_{12}O_{19}$@ PANI	30 vol% paraffin wax and 70 vol% powdered filler	In situ polymerization method (aniline: 400 μL)	2-18 GHz	R_L^{max}:− 65.354 dB at 17.28 GHz (Thickness: 1.47 mm.)	2.3 GHz	361
Polythiophene nanofibers coated on $MnFe_2O_4$/ Fe_3O_4 (core–shell)	Co-precipitation and in situ polymerization	----	8.0–12.0 GHz	R_L^{min}: -21 dB at 12 GHz (Thickness: 1.5 mm)	Whole X-band	362
$CoSe_2$@Polythiophene core-shell	Hydrothermal followed by in-situ polymerization	10 wt% mixed with PVDF	2-18 GHz-	R_L^{min}: -55.40 dB (Thickness: 1.76 mm)	5.8 GHz (Thickness: 1.76 mm)	363
rGO/$Ni_{0.5}Co_{0.5}Fe_2O_4$@PEDOT	In situ oxidative polymerization	--	12.4–18.0 GHz	SE_T: 38.79 dB	Broad absorption bandwidth	364
3D graphene supported Fe_3O_4 coated by polypyrrole	One-step chemical reduction method (GO to Fe_3O_4@PPy wt ratio=1:3	Composites soaked into molten paraffin	2−18 GHz	R_L^{min}: −40.53 dB at 6.32 GHz (Thickness:2.5 mm)	5.12 GHz (Thickness:2.5 mm)	365
Prism-shaped hollow carbon decorated with polyaniline	Carbonization and in-situ polymerization	30 wt% filler in wax	2-18 GHz	R_L^{min}:−64.0 dB at 11.1 GHz (Thickness:2.5 mm)	5.0 GHz (9.5–14.5 GHz)	366
Core-Shell PPy@MoS_2	Combining chemical oxidative polymerization and hydrothermal process	40 wt% filler in paraffin	2-18 GHz	$R_L^{optimal}$:−49.1 dB at 6.1 GHz (Thickness:2.5 mm)	6.4 GHz (11.5–17.5 GHz) at 2.5 mm	367
PPy@PANI	Polymerization of aniline on the surface of PPy microspheres	50 wt% filler in paraffin	2-18 Ghz	R_L^{max}:−34.8 dB at 13.9 GHz (thickness: 2 mm)	4.7 GHz (11.9–16.6 GHz)	368
Hollow $Zn_xFe_{3-x}O_4$@Polyaniline	Solvothermal followed by in-situ chemical oxidation polymerization (ZnxFe3-xO4: Aniline ratio=0.5: 1)	50 wt % filler in paraffin wax	2-18 GHz	R_L^{min}: -59.44 dB at 11.04 GHz (thickness: 2.31 mm)	4.65 GHz (13.35–18.0 GHz) for thickness of 1.72 mm.	369
Waxberry-like Carbon@Polyaniline microspheres	Via dilute polymerization	30 wt filler in paraffin wax)	2-18 GHz	R_L^{min}:−59.6 dB at 15.5 GHz (thickness : 2.2 mm)	5.4 GHz (12.6 to 18 GHz) for thickness of 2.2 mm.	370

CNTs/Polyaniline (shell)	Hybrid powders with wax at 10 wt% loading	In-situ polymerization (mass ratio of CNTs/PANI:1:2)	2-18 GHz	R_L^{min}:– 41.5 dB at 9.5 GHz (thicknesses: f 2 mm)	5.1 GHz at thickness of 2.0 mm.	371
PPy (shell)@ Carbon microsphere (CMC)	In situ polymerization	40 wt% of composite corresponding to 0.6 g of CMC in paraffin wax	2–18 GHz.	R_L^{max}: - 38.1 dB at 11.6 GHz (thickness: 3.00 mm)	11.17 to 12.26 GHz (thickness of 3.00 mm)	372
Core shell PEDOT/Barium ferrite	In situ emulsion polymerization	----	12.4-18 GHz	SE_A: 22.5 dB at 15 GHz with minimal reflection loss of 2 dB	---	373
PANI-coated Bagasse Fiber (BF) Core-Shell Heterostructure	One-step in situ polymerization of aniline in the dispersed system of BF	Mass ratio of BF/PANI to paraffin = 40:60	8.2–12.4 GHz	EMI SE: 28.8 dB (Thickness: 0.4 mm)	---	374
Polyaniline coated MWCNT	In situ polymerization	---	12.4–18.0 GHz	SE_T: −27.5 to −39.2 dB	---	375
Polyaniline@Helical-CNTs with dual chirality	In-situ polymerization	Mass ratio of the samples to wax:3:7	2–18 GHz.	R_L^{max}:−32.5 dB at 8.9 GHz (thickness: 3.7 mm)	5.1 GHz (from 7.1 to 11.2 GHz).	376
Hollow PPy microspheres @ Fe_3O_4/CNTs	Spray-dry method	Mass ratio of powder with Paraffin: 1:4	2-16 GHz	R_L^{max}:– 51.8 dB at 8.8 GHz (thickness:2.38 mm	2.24 GHz (7.76 GHz to 10 GHz)	377
Hollow PPy /Ni/PVDF microspheres	Spray phase inversion method	Mixing samples with paraffin wax in a 1:8 wt ratio	18–40 GHz	R_L^{min}:−47.2 dB at 25.36 GHz and −39.8 dB at 31.30 GHz	18–40 GHz (Thickness: 1.0 - 3.5 mm)	378
PPy@FeCo@PPy nanotubes	Combination of electroless plating and oxidative polymerization.	Mass fraction of 15 wt % dispersed in the paraffin	2-18 GHz	R_L^{min}:−50.5 dB (Thickness: 2.0 mm)	5.7 GHz (Thickness: 2.0 mm)	379
1D double-shell PPy@Air@MnO_2 nanotubes	50 wt% in paraffin	Dispersion and self-assembly method	2-18 GHz	R_L^{max}:−52.49 dB at 8.88 GHz (thickness: 2.94 mm)	3.84 GHz (thickness: 2.94 mm)	380
Hollow-spherical composites of PANI/CoS/Carbon nanodots (molar ratio of 3:1:1)	30 wt % in paraffin wax	Via in situ polymerization in presence of magnetic field	2–18 GHz	R_L^{max}:−24 dB at 14 GHz under external applied field of 0.5T (thickness: 3 mm)	1.92 GHz	382
Fe_3O_4@Carbon @PANI (Fe_3O_4 @ C:Aniline	Multiple steps	----	2-8 GHz	R_L: ~33 dB SE_T: ~65 dB	-----	383

=1:9 wt/wt)						
Fe_3O_4@SiO_2@PPy	Multistep	Mass ratio of products and paraffin=3: 7	2-18 GHz	SE_T: ~32 dB (thickness: 1 mm)	---	384
γ-Fe_2O_3@ PEDOT	Reaction of hydrofluoric acid and and γ-Fe_2O_3@SiO_2@ PEDOT	Mass ratio of γ-Fe_2O_3@PEDOT and paraffin=3: 7	2-18 GHz	R_L^{min}: -44.7 dB at 12.9 GHz with a matching layer thickness of 2.0 mm	4.3 GHz (10.8–15.1 GHz)	385
Co@Hollow carbon nanospheres @ Polyaniline	Mixed with paraffin in mass ratio of 1:2	Soft template, switching liquid phase transport and in-situ polymerization method	2-18 GHz	R_L^{min}:-43.63 dB (Matching thickness: 2.8 mm)	9.75 GHz (8–17.5 GHz) at a matched thickness of 2.8 mm	386
FeNi@C@Polyaniline	Combining the arc-discharge process and an in situ chemical oxidative polymerization reaction	FeNi@C@Polyaniline (40 wt%) mixed with paraffin	2–18 GHz	R_L^{min}:-49.2 dB at 16.6 GHz for a thickness of 1.3 mm	5 GHz (13–18 GHz for the thickness of 1.4 mm	387
PS@PANI	Solution mixing	---	100 KHz–20 GHz	EMI SE:~ 32 dB at 8 GHz (thickness: 0.5 mm)	---	388
PPy nanotubes/NR /NBR (90/10)	5.24 wt% in paraffin	Mixing technology	8.2–12.4 GHz	R_L^{min}:- 56.67 dB (thickness:2.9 mm)	3.7 GHz (thickness:2.9 mm)	389
γ-Fe_2O_3/$(SiO_2)_x$–SO_3H/Polypyrrole core/ shell /shell microspheres	Sol–gel process and an in situ polymerization	70 % in paraffin wax	2–18 GHz	R_L^{max}:– 43.1 dB (15.1 GHz), Thickness: 4 mm)	6.1 GHz (11.9–18.0 GHz)	390
Core/shell/shell-structured Ni/C/Polyaniline	Modified arc discharge method and a chemical polymerization method	40 wt% in paraffin	2–18 GHz	$R_L^{optimal}$: -9.3 dB at 6.2 GHz (Thickness: 3 mm)	5 dB (3.4–18GHz)	391
Fe_3O_4 microsphere@Graphene nanosheets @PANI nanorods	Hydrothermal and in-situ polymerization methods	30% in paraffine	2–18 GHz	R_L^{max}: -43.7 dB at 10.7 GHz with a thickness of 3 mm	5.4 GHz (from 6.8 to 12.2 GHz)	392
TiO_2@Fe_3O_4@PPy	Sequential process of solvothermal treatment and polymerization	---	2-18 GHz	R_L^{max}: −61.8 dB (thickness: 3.2 mm)	6.0 GHz (X and Ku band) at 2.2 mm thickness	393
CoNi@SiO_2@PPy	Three-step reaction:	=--	8.2 to 12.4 GHz.	R_L^{min}: − 34.19 dB at 9.59 GHz	Entire X-band (8.2–12.4 GHz)	394

				(thickness 2.12 mm)		
SiC_{NWs}@MnO_2 @PPy hetrostructures	Chemical vapor deposition and two-step electrodeposition process	----	2-18 Ghz	R_L^{min}: −50.59 dB (Matching thickness: 2.41 mm)	6.64 GHz (Matching thickness: 2.46 mm)	395
Ni/PANI/RGO	Hydrothermal followed by the in situ polymerization	---	2-18 GHz	R_L^{max}: -51.3 dB at 4.9 GHz with 3.5 mm thickness	3.1 GHz (3.3 to 6.4 GHz)	396
Fe_3O_4@PEDOT microspheres/RGO	Multiple steps	50 wt% in paraffin	2.0-18.0 GHz	R_L^{max}: -48.8 dB at 9.12 GHz (Matching thickness:2.9 mm)	4.32 GHz (Matching thickness:2.9 mm)	397
Core-shell $NiCo_2O_4$@Polypyrrole nanofibers /RGO	50 wt% in paraffin	Combination of multiple steps	2.0-18.0 GHz	R_L^{min}: -61.20 dB at 14.26 GHz a(Thickness:1.56 mm)	4.90 GHz at 1.57 mm	398
γ-Fe_2O_3 decorated RGO in PANI core–shell tubes	Aniline to Fe_2O_3 decorated rGO weight ratios=1 : 3	Multiple steps	8.2-12.8 GHz	SE_T: ~51 dB) (thickness: 2.5 mm)	----	399
N-doped graphene@PANI nanorod arrays modified with Fe_3O_4	Hydrothermal reaction	25 wt% of the sample in paraffin	2 - 18 GHz	R_L^{max}: -40.8 dB at 14.8 GHz with thickness of 2.7 mm	5.1 GHz (10.4 to 15.5 GHz)	400
PANI/GO/Fe_3O_4	In-situ polymerisation	50 % in paraffin wax	2 - 18 GHz	R_L^{max}: -53.5 dB at 7.5 GHz (thickness: 3.91 mm)	2.8 GHz (thickness: 3.91 mm)	401
PANI/Carbonyl iron powder (CIP)/Fe_3O_4	Mechanical mixing PANI/CIP composite with PANI/Fe3O4 composite with mass ratio of 7:3.	---	0.5–18 GHz	R_L^{max}: -48.3 dB at 9.6 GHz (thickness: 1.76 mm)	--	403
Fe_3O_4@SiO_2@PPy	Microemulsion polymerization method	Composites mixed paraffin with 15 wt%	2-18 Ghz	R_L^{min}:-40.9 dB at 6 GHz (Thickness: 5 mm)	6.88 GHz (11.12-18 GHz)	404
Fe_3O_4/C/PPy (Fe_3O_4/C:PPy :2:8 wt/wt)	Hydrothermal and chemical oxidative polymerization method	---	1-8.5 GHz	EMI SE: >28 dB (thickness: 0.8 mm)	---	405
PANI@Natural graphitic flakes (NGF)/MWCNT	In-situ by ball milling	10 wt% of MWCNTs	12.4–18.0 GHz	EMI SE: -98 dB	----	406
PEDOT@RGO/ Co_3O_4	Two-step method	50 wt% of paraffin	2-18 GHz	R_L^{max}:-51.1 dB (10.7 GHz) at	3.1 GHz (9.4-12.5 GHz)	407

				thickness of 2.0 mm	View Article Online DOI: 10.1039/D5LP00230C	
MWCNT/CuO/Fe_3O_4/PANI (wt ratios of CuO/Fe_3O_4/PANI to MWCNT=1.5)	Step by-step approach	25 % filler in paraffin	8.2–18 GHz	R_L^{min}:-87.4 dB (Thickness: 3 mm)	6 GHz (12–18 GHz	408
Graphene@Fe_3O_4@WO_3@PANI	Simple hydrothermal method and chemical oxidation polymerization	Composite blended with 70 wt % wax	2–18 GHz	R_L^{max}:- 46.7 dB at 9.4 GHz (Thickness: 4 mm)	1.8 GHz (12.4 -14.2 GHz) at thickness of 1.5 mm	409
Graphene@Fe_3O_4@PANI@TiO_2	Hydrothermal method and in situ polymerization	50 wt% in paraffin	2-18 GHz	R_L^{max}:- 41.8 dB at 14.4 GHz (thickness: 1.6 mm)	3.5 GHz	410

View Article Online
DOI: 10.1039/D5LP00230C

Table 2. Sources and health effects of heavy metals.[412] Reproduced with permission from IntechOpen.

	Heavy metal	Sources	Health Effects
Essential heavy metal	Zinc (Zn)	Oil Refining Plumbing, Brass manufacturing	Gastrointestinal disorders, Kidney Liver abnormal functioning
	Copper (Cu)	Copper polishing Plating, Printing	Abdominal disorders, Metabolic activity abnormalities
	Iron (Fe)	High intake of iron supplements & Oral consumption	Vomiting Diarrhea, Abdominal pain Dehydration & lethargy
	Cobalt (Co)	Hip alloy replacement case	Haemotological, Cardiovascular Hepatic, Endocrine
Non Essential heavy metal	Chromium (Cr)	Steel fabrication Electroplating Textile	Lung disorders, bronchitis,cancer), Renal and reproductive system
	Lead (Pb)	Batteries Coal combustion Paint industry	Serious effect on mental health (Alzheimer's disease), Nervous system
	Arsenic (As)	Atmospheric deposition Mining pesticides	Highly effects dermal region (Cancer), Brain & Cardiac problems
	Mercury (Hg)	Coal combustion, Fish Mining, Paint industry, Paper industry, Volcanic eruption	Sclerosis, Blindness, Minamata disease, Deafness, Gastric problems, Renal disorders
	Cadmium (Cd)	Plastic Fertilizers pesticides	Osteo related problems, Prostate cancer, Lung diseases, Renal issues

View Article Online
DOI: 10.1039/D5LP00230C

Table 3 Performance data of hollow ICPs, hollow ICP nanocomposites and ICP based core-shell adsorbents in removal of heavy metal ions in water medium.

Metal Ions	Adsorbent used	Water type	Preparative method	Experimental conditions on removal of metal Ions	q_m (mg/g)	Removal isotherm fitted to	Kinetics data fitted to (k)	Ref.
Cr(VI)	Hollow PANI micro/nano sphere	Waste water	Monomer polymerization in alk solution with Triton X-100. as soft templates	[Cr(VI)]: 1.2 m mol L^{-1} Dosage: 10 mg (20 mL) pH 3.0 q_e (time): ~73 mg g^{-1} (180 min)	127.88	Langmuir	Pseudo sec. order	417
Cr(VI)	Amino acid doped PANI nanotubes	Aqueous solutions	In-situ chemical polymerization	Temp: 25 ^{0}C [Cr(VI)]:30 mg L^{-1} Dosage:0.25 g (10 mL) pH: 7 Removal (Time): ~ 100 % (120 min)	60	Langmuir	Pseudo sec. order	419
Cr(VI)	Bamboo-like PPy nanotubes	Aqueous solution	Reactive-template vapor phase polymerization method	[Cr(VI)]: 1.95 mmole L^{-1} Dosage: 3 mg (20 mL) pH: 3 Adsorption capacity (time): ~9 mmole g^{-1} (1400 min)	9.281 mmol g^{-1}	Langmuir	Pseudo sec. order (0.0031 g mmol-1 min-1)	420
Cr(VI)	Core-Shell Polyaniline /Polystyrene	Aqueous solutions	Microemulsion polymer. of polystyrene followed by in-situ polymer. of aniline monomer	Temp: 20 ^{0}C Cr(VI):100 mg L^{-1} Dosage:250 mg (50 mL) pH: 2 Removal (time): ~95 % (30 min)	19	Temkin	Pseudo sec. order (k: $6.27x10^{-3}$ mg L^{-1} min^{-1})	421
Cr(VI)	Polyacrylonitrile/Polyaniline core/shell nanofiber mat	Aqueous solution	Via electrospinning followed by in situ polymer,	Temp: 25 ^{0}C Cr(VI):207 mg L^{-1} Dosage:100 mg (30 mL) pH: 2 q_t (time): 53.4 mg g^{-1} (12 h)	71.28	Langmuir	Pseudo sec. order (k:$7.20x10^{-3}$ g mg^{-1} min^{-1})	422

Cr(VI)	Sulfonated poly(arylene ether nitrile)/Polypyrrole core/shell	Aqueous solution	Electrospinning technique followed by in situ polymerization	Temp: RT [Cr(VI)]: 50 ppm (50 mL) Doage: 20 mg pH: 2 Removal (time): 56.5% (4h)	165.3	Langmuir	Pseudo-second order (k:6.9×10^{-4} g mg^{-1} min^{-1})	423
Cr(VI)	Ag-P/PPy core-shell	Water	In-situ chemical oxidative polymerisation	Temp: RT [Cr(VI)]: 50 mg L^{-1} (50 mL) Doage: 0.05 g pH: 2 Removal (time): 99.4 % (55 min)	138.5	Temkin and Redlich Peterson	Pseudo-second order	424
Cr(VI) C	Polypyrrole wrapped oxidized MWCNTs	Aqueous solution	In situ chemical polymerization	Temp: 25 ^{0} C Cr(VI): 200 mg L^{-1} Dosage: 0.1g L^{-1} (50 mL) pH: 2 Removal (time): 100 % (300 min)	294	Langmuir	Pseudo sec. order (k: 0.0028 g mg^{-1} min^{-1})	425
Cr(VI)	PPy-coated Halloysite nanotube (HNT) clay	Deionized water	In situ polymerization of pyrrole in the dispersion of HNTs	Temp: 25 °C Cr(VI): 100 mg L^{-1} (50 mL) Dosage: 1.5 g L^{-1} pH: 2.0 Removal (time); ~ 100% (24 h)	149.25	Langmuir	Pseudo sec. order (k:0.019 g mg^{-1} min^{-1})	427
Cr(VI)	Core–shell Fe_3O_4/ PANI microspheres	Water	Interfacial polymerization	Temp: RT Cr(VI): 100 mg g^{-1} Dosage: 0.1 g (60 mL) pH: 2 Removal (time);~ 94% (90 min)	200	Langmuir isotherm	Pseudo sec. order	428
Cr(VI)	Fe_3O_4/PPy nanotubes	Aqueous solution	One-pot process.	Temp: 25°C Cr(VI): 20 mg·L^{-1} Dosage: 0.01 g (50 mL) pH:1 Removal (time); 94.62 % (24 h)	451.45	Langmuir	Pseudo sec. order	429
Cr(VI)	Fe_3O_4 coated PPy	Aqueous solution	In-situ polymer. of pyrrole monomer	Temp: 25 ^{0}C Cr(VI)**:** 200 mg L^{-1} Dosage:2 g L^{-1} (50 mL) pH: 2 Removal (time); 100% (24 h)	169.5	Langmuir	Pseudo-sec. order (k;0.037 g mg^{-1} min^{-1} for [Cr(VI)]: 150 mg L^{-1}	430
Cr(VI)	Fe_3O_4@ arginine-functionalized PPy	Deionised water	In-situ polymerization	Temp.: 25 °C). Cr(VI): 200 mg L^{-1} Dosage: 0.05 g (50 mL)	322.58	Langmuir	Pseudo sec. order {k:6.67 ×	431

				pH: 2 Removal (time); ~100% (1 h)			10^{-3} g mg^{-1} min^{-1})	
Cr(VI)	PPy/γ-Fe_2O_3	Aqueous media	Emulsion polymerization	Temp: RT Cr(VI): 2.5 mg L^{-1} Dosage: 2 mg (10 mL) pH: 2 Removal (time); ~100% (1 h)	208.8	Langmuir	Pseudo sec. order (k : 2.0.x10^{-2} g mg^{-1} min^{-1})	432
Cr (VI)	PANI/γ-Fe_2O_3	Aqueous media	Emulsion polymerization	Temp: RT Cr(VI): 2.5 mg L^{-1} Dosage: 2 mg (10 mL) pH: 2 Removal (time); ~100% (1 h)	195.7	Langmuir	Pseudo sec. order (k : 7.5.x10^{-4} g mg^{-1} min^{-1})	432
Cr(VI)	PPy modified corncob-core Sponge	Aqueous solution	Solution polymerization	Temp: 25ºC Cr(VI): 100 mg L^{-1} Dosage: 3 g L^{-} pH: 3.5 Removal (time);~100% (180 min)	84.7	Langmuir	Pseudo sec. order (k; 0.0023 g·mg^{-}1 min^{-1} :[Cr(VI)]: 50 mg/L	434
Cr(VI)	MnO_2 coated polyaniline nanofibers	Aqueous Solution	In-situ oxidative polymerization	Temp: 298 K Cr(VI): 10 mg L^{-1} Dosage: 10 mg (50 mL) pH: 1 Removal (time); ~96% (60 min)	158.2	Freundlich	Pseudo-sec. order (k: 0.0751 g. mg^{-1}. min^{-1})	436
Cr(VI)	PPy/Hollow mesoporous silica	Aqueous Solution	In-situ polymerization	Temp.:25^{0}C Cr(VI): 400 mg L^{-1} Dosage: 80 mg (25 mL) pH: 2 Removal (time);~100 % (24 h)	322	Langmuir	Quasi-second-order	437
Cr(VI)	Polyacrylonitrile/PPy core/ shell nanofiber mat	Aqueous solution	Electrospinning followed by in situ polymerization of pyrrole monomer	Temp: 25 ^{0}C Cr(VI): 200 ppm Dosage: 0.20 g (30 mL) pH: 2 Removal (time); 84.5% (12 h)	61.80	Langmuir	Pseudo sec. order (k: 1.77× 10^{-3} g mg^{-1} min^{-1})	439
Cr(VI)	L-cystine doped glucose carbon sphere @PPy	Water	In situ growth method	Temp: RT Cr(VI): 100 mg L^{-1} Dosage: 0.050 g (100 mL) pH: 1 Adsorption capacity, q_e (time); 209.18 mg g^{-1} (24 h)	108.41	Langmuir	Pseudo sec. order (k: 0.00014 g mg^{-1} min^{-1})	440

Cr(VI)	PANI @Nano hollow carbon sphere	Wastewater	In-situ polymerization method	Temp: 298 K Cr(VI): 100 mg L^{-1} Dosage: 10 mg (25 mL) pH: 1 Removal (time);100 % (300 min)	250	Langmuir	Pseudo sec. order (k:0.284 x10^{-3} g mg-1 min^{-1})	441
Cr(VI)	PPy/Attapulgite core–shell	Aqueous solutions	In-situ polymerization on the surface of attapulgite	Temp: 298 K Cr(VI): 50 mg L^{-1} Dosage: 0.2 g (100 mL) pH: 3 Removal (time): 99.27 % (10 min)	48.45	Langmuir	Pseudo sec. order (k:1069x10^{-5} mg^{-1} s^{-1})	442
Cr(VI)	Cu slag@ PANI	Aqueous solution	In-situ polymerization	Temp:303 K Cr(VI): 300 mg L^{-1} Dosage: 0.01 g (20 mL) pH: 2 Absorption capacity (time): 357.68 mg g^{-1} (24 h)	343.23 (303 K)	Langmuir	Pseudo sec. order (k: 0.00409 g mg^{-1} min^{-1})	443
Cr(VI)	PANI nanotubes @$Ni(OH)_2$	Aqueous solution	By depositing Ni(OH)2 on 2-napthalene sulfonic acid doped PANI nanotubes surface	Temp: 25 °C Cr(VI): 100 mg L^{-1} Dosage: 0.03-0.05 g (50 mL) pH: 4.0 Removal (time): ~100% (24 h)	625 (25 ^{0}C)	Langmuir	Pseudo-sec. order (k: 0.03008 g mg^{-1} min^{-1})	444
Cr(VI)	PPy@5% $MgFe_2O_4$	Water and wastewater	Oxidation method	Temp.: 25 ^{0}C). Cr(VI): 100 mg L^{-1} Dosage: 1 g L^{-1} (10 mL). pH: 3-6 Removal (time): ~93 mg g^{-1} (600 min)	138.6	Langmuir	Pseudo sec order (0.0021 g mg-1 min^{-1})	445
Cr(VI)	PANI@Almond shell	Aqueous solutions	In situ chemical polymerization	Temp: 298 K Cr(VI): 50 mg L^{-1} Dosage: 1.4 g L^{-1} pH: 5 Removal (time): 95.86% (120 min]	335.25	Freundlich	Pseudo sec. order (k: 0.0273 mg g^{-1} min^{-1})	447
Cr(VI)	PPy-PANI coated rice husk ash	Aqueous solutions	In situ chemical polymerization	Temp: RT Cr(VI): 50 mg L^{-1} Dosage: 0.8 g L^{-1} pH: 2 Removal (time): ~98% (300 min)	769.15	Freundlich	Pseudo sec. order (k: 0.009 mg g^{-1} min^{-1})	448
Cr(VI)	Graphene/SiO_2@PPy	Deionized water	In-situ polymerization	Temp: 298 K Cr(VI):100 mg L^{-1}	429.2	Langmuir	Pseudo sec. order (k: 1.852	449

				Dosage: 100 mg (250 mL) pH: 2 q_e (time): ~240 mg g^{-1} (5000 min)			$x10^{-5}$ min^{-1})	
Cr(VI)	PPy/Fe_3O_4/ Chitosan	Water	Co-precipitation followed by in-situ polymerization	Temp: 25 ^{0}C Cr(VI): 100 mg L^{-1} Dosage: 100 mg (50 mL) pH: 2 q (time):~84 % (40 min)	105	Langmuir	---	450
Cr(VI)	PMMA/Rice husk/PPy membrane	Water	Electrospinning and chemical polymerization	Temp: 283 K Cr(VI):10 mg L^{-1} Dosage (membrane): 0.02 mx0.02 m (wt: 0.6 mg) pH:2.0 Removal (time): ~95 % (24 h)	363.63	Langmuir	Pseudo sec. order (k: 49.90 mg g^{-1} min^{-1})	451
Cr(VI)	PS/PANI/ Fe_3O_4	Water	Simultaneous chem. oxidation polymerization and precipitation	Temp: 303 K Cr(VI): 5 mg L^{-1}1 Dosage: 0.05 g (30 mL) pH:2.0 Efficiency (time): 100 % (120 min)	23.753	Freundlich	Pseudo sec. order	452
Cr(VI)	PANI/Wood sawdust /PEG	Water	Oxidation polymerization	Temp.: RT Cr(VI): 50 ppm Dosage: 40 g L^{-1} (50 mL) pH: 5 Removal (time): ~98 % (30 min)	3.2	Langmuir	---	453
Cr(VI)	γ-Fe_3O_4 /Chitosan/PPy	Aqueous media.	Coprecipitation method + in-situ polymerization	Temp: RT Cr(VI): 10 mg L^{-1} Dosage: 2 mg (10 mL) pH:2 Removal (time): 100 % (720 min)	301.2	Freundlich	Pseudo sec. order (k: 7.12 × 10^{-5} min^{-1})	455
Cr (VI)	PANI/Jute fiber	Deionized water	in-situ polymerization	Temp: 25 ^{0}C Cr (VI)):100 mg L^{-1} Dosage: 1.0 g (200 mL) pH: 2 Removal (time): 98% (120 min)	50	Langmuir	Pseudo sec order (k: 0.0023 mg g^{-1} min^{-1})	471
Pb(II)	Amino acid doped PANI nanotubes	Aqueous solutions	In-situ chemical polymerization	Temp: 25 ^{0}C [Cr(VI)]:30 mg L^{-1} Dosage:0.25 g (10 mL)	---	--	---	419

				pH: 7 Removal (Time): ~ 68 % (120 min)				
Pb(II)	Hollow polyaniline nanosphere	Deionized water	Chemical polymerization	Temp: 30 ^{0}C [Pb(II)]: 20 mg L^{-1} Dosage: 20 mg (25 mL) pH: 7 Absorptivity (time): 97% (24 h)	1589	Freundlich	---	456
Pb(II)	Fe_3O_4/@Py york-shell	Water	Multi step	Pb (II): 1 mg L^{-1} Dosage:15 mg (100 mL) pH:6 Removal (time): ~96 % (30 min)	65.093	Langmuir, Freundlich	Pseudo sec. order (k:0.004 g $mg^{-1}h^{-1}$)	458
Pb(II)	PTh coated on PS	Deionized water	Chemical oxidative polymerization	Temp.: RT Pb (II): 100 mg L^{-1} Dosage: 0.25 mg (25 mL) pH:2 Removal (time): ~100 % (30 min)	-	--	--	460
Pb(II)	PTh coated on PVC	Deionized water	Chem. oxi. polymerization	Temp.: RT Pb(II): 100 mg L^{-1} Dosage: 0.25 mg (25 mL) pH:2 Removal (time): ~85 % (30 min)	--	--	--	460 a
Pb(II)	PANI/Fe_3O_4	Wastewater	In-situ polymerization	Temp: 25 ^{0} C Pb(II): 50 ppm Dosage: 3 mg (100 mL) pH: 9 Removal (time): 93% (60 min)	114.9	Langmuir	Pseudo sec. order (k:0.0074 $g.g^{-1}$ min^{-1}}	462
Pb(II)	$CoFe_2O_4$@ PANI	Water	Aniline polymerization	Temp: 25 ^{0} C Pb(II): 17 mg L^{-1} Dosage: 1 g (50 mL) pH: 7 Removal (time): 98% (120 min)	23.31	Langmuir	Quasi first order	463
Pb(II)	PPy coated ZnO-NiO	Wastewater	Chemical polymerization	Temp: 298 K Pb(II): 100 mg L^{-1} Dosage: 25 mg (100 mL) pH: 5 Removal (time): 98.7% (240 min)	436.48	Langmuir	Pseudo sec. order (k:0.00013 mg g^{-1} min^{-1})	464
Pb(II)	PANI nanotubes/ Ni^0	Aqueous solution	Immobilisation	Temp: 25 ^{0}C Pb(II): 100 mg L^{-1} Dosage: 0.5 g L^{-1} pH: 5	414.6	Langmuir	Pseudo sec. order (k:0.00798	465

				Removal (time): ~90 % (24 h)			mg g^{-1} min^{-1})	
Pb(II)	MnO_2@PANI	Water	Oxidation polymerization	Temp: 25 ^{0}C Pb(II): 60 mg/L Dosage: 0.5 g L^{-1} (20 mL) pH: 5 Removal (time): ~98% (12 h)	309.6	Langmuir	Pseudo sec. order (k: 17.52 g mg^{-1} min^{-1})	468
Pb(II)	PTP/Polyvinylpyrolidine (PVP) /Sulfonic acid/Cu	Aqueous solution	In-situ co-polymerization	Temp: 298 K Pb(II): 30 mg L^{-1} Dosage: 3.0 g L^{-1} (10 mL) pH: 7 Removal (time): ~109 mg g^{-1} (24 h)	111.11	Langmuir	Pseudo sec. order (k: 3.62x 10^{-4} g. g^{-1} min^{-1}}	469
Pb(II)	PPy/Fe_3O_4/ Seaweeds	Aqueous solution	In - situ chemical oxidative polymerization	Temp: 40 ^{0}C Pb(II): 100 mg L^{-1} Dosage: 10 mg (50 mL) pH: 5 Removal (time): 97.25% (20 min)	333.33	Langmuir	Pseudo sec. order (k:0.005535 g mg^{-1} min^{-1})	470
Pb(II)	Carbon-PPy@MoS_2	Wastewater	Template method involving five steps	Temp: 25 ^{0} C Pb(II): 54.26 ppm Dosage: 50 mg (100 mL) Removal (time): 100% (10 min)	381.87	Langmuir	Pseudo sec order (k: $1.75x10^{-4}$ g mg^{-1} min^{-1}))	475
Pb(II)	Fe_3O_4/SiO_2/ PANI-SDBS	Wastewater	Polymerization of aniline	Temp: 30 ◦C. Pb(II): 15 mg L^{-1}. Dosage: 30 mg pH: 7.0 Removal (time): 94.1% (120 min)	72.20	Freundlich model	Pseudo sec. order	486
As(V)	γ-Fe_2O_3 @PANI	Deionized water	In- situ polymerization	Temp.: 298 K As(V): 20 mg L^{-1} Adsorbent: 0.5 g L^{-1} (100 mL) pH: 5 q_e (time): 0.358 mg g^{-1} (5 h)	37.61	Langmuir	Pseudo sec. order (k:1.733 g $mmol^{-1}$ min^{-1})	457[1]
As (III)	Hollow PANI microsphere-F_3O_4 (Fe_3O_4: 40 wt%)	Water	Multiple steps	Temp: 300 K As(III): 1000 mg L^{-1} Dosage: 5 g L^{-1} (100 mL) pH:7 Removal (time): 98% (240 min)	28.27	Freundlich	Pseudo sec order (k: 0.363 g mg^{-1} min^{-1})	476

[1]

As(V)	Hollow Polyaniline miicrosphere/F_3O_4 (Fe_3O_4: 40 wt%)	Water	Multiple steps	Temp: 300 K As(III): 1000 mg L^{-1} Dosage: 2 g L^{-1} (100 mL) pH:7 Removal (time): 100% (240 min)	83.078	Freundlich	Pseudo sec order (k: 0.733 g mg^{-1} min^{-1})	476
As (V)	PANI/Fe^0	Aqueous solutions	Polyaniline nanofiber in polymerization media +$NaBH_4$	Temp.: RT As (V): 10 mg L^{-1} Dosage: 0.002 g (20 mL) pH: 3-10 Removal (time): 99.9-89% (24 h))	227.3	Langmuir isotherm	Pseudo sec. order (k: 0.01343 –0.01714 g $mg^{-1}min^{-1}$)	480
As (III)	PANI/Fe^0	Aqueous solutions	Polyaniline nanofiber in polymerization media +$NaBH_4$	Temp.: RT As (III)]: 10 mg L^{-1} Dosage: 0.002 g (20 mL) pH: 3-10 Removal (time): 99.3-93.5% (24 h)	232.5	Langmuir isotherm	Pseudo sec order (k: 0.0332 g $mg^{-1}min^{-1}$)	480
Cd (II)	PANI/Jute fiber	Deionized water	in-situ polymerization	Temp: 25 ^{0}C Cd (II)):100 mg L^{-1} Dosage: 1.0 g (200 mL) pH: 5 Removal (time): 99% (120 min)	140	Langmuir	Pseudo sec order (k: 0.0039 mg g^{-1} min^{-1})	471
Cd(II)	PANI coated Sawdudst	Waste water	Mixing method	Temp: 20.5 ^{0}C Cd(II): 40 mg L^{-1} Dosage: 0.75 g (750 mL) pH: 6 q_e (Time): ~500 mg g^{-1} (35 min)	430	Freundlich	Pseudo sec. order	482
Cd(II)	Fe_3O_4/SiO_2/ PANI-SDBS	Waste water	Polymerization of aniline	Temp: 30 ◦C. Cd(II): 15 mg L^{-1}. Dosage: 30 mg pH: 7.0 Removal (time): 77.47% (120 min)	67.84	Freundlich model	Pseudo sec. order	486
Mn (VII)	Functionalized-Fe_3O_4@ PPy	Aqueous solution	in-situ polymerization of pyrrole monomer on Fe_3O_4	Temp: 20 ^{0}C Mn (VII): 150 mg L^{-1} Dosage: 20 mg: (50 mL) pH: 2 Contact time:~90 % (240 min)	781.25	Freundlich	Pseudo sec. order (k: 4.8x10-^{4} g mg^{-1} min^{-1})	485

Mn(VII)	Core@Shell Fe_3O_4 @Polypyrrole@Sodium Dodecyl Sulphate	Complex Wastewater	Hydrothermal + in situ polymerization methods	Temp: 20 ^{0}C Mn (VII): 60 mg L^{-1} Dosage: 10 mg (50 mL) pH: 7 Removal (time):~ ~93.14%. (60 min)	175.75	Langmuir	Pseudo sec. order (k: 2.93×10^{-5} g mg^{-1} min^{-1})	489
Cu(II)	PPy/γ–Fe_2O_3	Aqueous media	Emulsion polymerization	Temp: RT Cr(VI): 2.5 mg L^{-1} Dosage: 2 mg (10 mL) pH: 2 Removal (time); ~100% (1 h)	170	Langmuir	Pseudo sec. order (k : 4.7 $x10^{-2}$ g mg^{-1} min^{-1})	432
Cu (II)	PANI/γ-Fe_2O_3	Aqueous media	Emulsion polymerization qm of the	Temp: RT Cr(VI): 2.5 mg L^{-1} Dosage: 2 mg (10 mL) pH: 2 Removal (time); ~100% (1 h)	106.8	Langmuir	Pseudo sec. order (k : 6.1 $x10^{-3}$ g mg^{-1} min^{-1})	432
Cu(II)	Fe_3O_4@PPy york-shell	Water	Multi step	Cu(II): 1 mg L^{-1} Dosage:15 mg (100 mL) pH:6 Removal (time): ~95 % (30 min)	25.179	Langmuir, Freundlich	Pseudo sec. order (k:0.035 g $mg^{-1}h^{-1}$)	458
Ni(II)	Amino acid doped PANI nanotubes	Aqueous solutions	In-situ chemical polymerization	Temp: 25 ^{0}C [Cr(VI)]:30 mg L^{-1} Dosage:0.25 g (10 mL) pH: 7 Removal (Time): ~ 68 % (120 min)	---	---	---	419

View Article Online
DOI: 10.1039/D5LP00230C

Table 4 Dye removal performance of various adsorbents based on hollow intrinsically conducting polymers, nanocomposites comprising hollow intrinsically conducting polymers and core-shell based ICP nanocomposites.*

Dye	Adsorbent (s) used	Water type	Preparative method	Experimental Conditions and findings	q_m (mg g^{-1})	Removal isotherm fitted to	Kinetics data fitted to	Ref.
CR	Amino acid doped PANI nanotubes	Aqueous solutions	In-situ chemical polymerization	Temp: 25 ^{0}C [CR]:30 mg L^{-1} Dosage:0.25 g (10 mL) pH: 7 Removal (Time): ~110 mg g^{-1} (90 min)	112	Langmuir	Pseudo first-order	419
OG	PANI@ Almond shell	Aqueous solutions	In situ chemical polymerization	Temp: 298 K [OG]: 50 mg L^{-1} Dosage: 0.8-1.0 g L^{-1} pH: 5 Removal (time): 94.69% (120 min)	190.98	Freundlich	Pseudo sec. order (k: 0.0008 mg g^{-1} $min^{-}1$)	447
MO	PPy/Fe_3O_4/Chitosan	Water	Co-precipitation and in-situ polymerization	Temp: 25 ^{0}C [MO]: 100 mg L^{-1} Adsorbent: 100 mg (50 mL) pH: 3 Removal efficiency (time):67 mg g^{-1} (40 min)	95	Langmuir	---	450
IC	PMMA/Rice husk/PPy membrane	Water	Electrospinning and chemical polymerization	Temp: 283 K [IC]: 5 mg L^{-1} Dosage (membrane): 0.02mx0.02 m (wt: 0.6 mg) pH:2.0 q_e (time): 142.9 mg g^{-1} (70 min)	144.93	Langmuir	Pseudo sec. Order {k: 0.002 g mg^{-1} min^{-1})	451
E102	PMMA/Rice husk//PPy membrane	Water	Electrospinning and chemical polymerization	Temp: 283 K [TZ]:5 mg L^{-1} Dosage (membrane): 0.02mx0.02 m^2 (wt: 0.6 mg) pH:2.0 q_e (time): 165.7 mg/g (60 min)	171.23	Langmuir	Pseudo sec. Order {k: 0.002 min^{-1})	451

RhB	Fe_3O_4@PPy @Sodium dodecyl sulphate	Complex Wastewater	Combination of a hydrothermal method in situ polymerization	Temp: 20 ^{0}C [RhB]:40 mg L^{-1} Adsorbent: 10 mg (50 mL) pH: 7 Removal (time): 94.83% (7 h)	127.55	Langmuir	Pseudo sec. order (k:3.027x10^{-3} g mg^{-1} min^{-1})	489
CR	Fe_3O_4@PPy @Sodium dodecyl sulphate	Complex Wastewater	Combination of hydrothermal method and in situ polymerization	Temp: 20 ^{0}C [CR]:40 mg L^{-1} Adsorbent: 10 mg (50 mL) pH: 7 Removal (time): 96.45% (7 h)	101.63	Langmuir	Pseudo sec. order (k:2.75x10^{-4} g mg^{-1} min^{-1})	489
MB	Fe_3O_4@PPy @Sodium dodecyl sulphate	Complex Wastewater	Combination of a hydrothermal method in situ polymerization	Temp: 20 ^{0}C [MB]:40 mg L^{-1} Adsorbent: 10 mg (50 mL) pH: 7 Removal (time): 93.27% (400 min)	135.50	Langmuir	Pseudo sec. order (k:1.71x10^{-4} g mg^{-1} min^{-1})	489
MG	Fe_3O_4@PPy @Sodium dodecyl sulphate	Complex Wastewater	Three step process	Temp: 20 ^{0}C [MG]:40 mg/L Adsorbent: 10 mg (50 mL) pH: 7 Removal (time): ~95 % (7 h)	182.82	Langmuir	Pseudo sec. order (k: 8.93×10^{-4} g mg^{-1} min^{-1})	489
AR1	Fe_3O_4@PPy @Sodium dodecyl sulphate	Complex Wastewater	Combination of a hydrothermal method in situ polymerization	Temp: 20 ^{0}C [AR1]:40 mg L^{-1} Adsorbent: 10 mg (50 mL) pH: 2 Removal (time): 92.99% (7 h)	181.16	Langmuir	Pseudo sec. order (k:2.66x10^{-4} g mg^{-1} min^{-1})	489
RhB	Hollow spherical PANI	Aqueous solution	In-situ polymerization on functionalized polystyrene template	[RhB]: 100 mg L^{-1} Adsorbent: 5 mg (50 mL) q_e (time): 61.75 mg g^{-1} (72 h)	61.75	--	---	491
CR	Hollow spherical PANI	Aqueous solution	Chemical polymerization	[CR]: 5 mg Adsorbent: 100 mg L^{-1} (50 mL) Q_e(time): 46.91 (72 h)	46.91	---	---	491
Rh6G	Hollow PANI helical nanobelts	Aqueous solution	Chemical oxidation of aniline	Temp: RT [Rh 6G]: 50 mg Adsorbent: 479 mg L^{-1} (100 mL) Removal (time): ~230 mg L^{-1} (120 min)	0.42 mg/mg	Langmuir	Pseudo sec. order	492

RhB	Coating of PANI onto carbonized tea waste	Aqueous solutions	Coating of polyaniline onto carbonized tea waste material	Temp: 30 °C [RhB]: 50 mg L^{-1} Adsorbent: 100 mg (100 mL) pH: 8.0 Removal (min):95.21% (60 min)	34.93	Langmuir	Pseudo-second-order (k: 0.0035 g mg^{-1} min^{-1})	495
RhB	α-MoO_3/ PANI	Water	Chemical oxidative polymerization using camphor sulfonic acid as dopant	Temperature:20 ^{0}C [RhB]:2.1×10^{-5} mol L^{-1} Adsorbent: 50 mg (50 mL) pH:3 % Removal (time): 91% (60 min)	36.36	Langmuir	---	497
CR	α-MoO_3/ PANI	Water	Chemical oxidative polymerization using camphor-10 sulfonic acid as dopant	Temperature:15 ^{0}C [CR]:1.5×10^{-5} mol L^{-1} Adsorbent: 50 mg (1000 mL) pH: 5 Removal (time): 94.6 (60 min)	76.22	Langmuir	---	497
RhB	PPy/Coffee grounds waste	Aqueous solution	Pyrrole polymerization	Temp.: 15 ^{0}C [RhB]: 200 mg L^{-1} Adsorbent: 125 mg pH: 9 Removal (time): 32 mg g^{-1} (60 min)	50.597	Redlich–Peterson and Langmuir	---	498
RhB	Fe_3O_4@ PPy@4-Vinylpyridine	Wastewater	Multiple steps	Temp: 20 °C [RhB]: 50 mg L^{-1} Adsorbent: 10 mg (30 mL) pH = 7 Removal (time): >85 % (500 min)	58.72	Langmuir	Pseudo sec. order (k: 9.728×10^{-4} g mg^{-1} min^{-1})	499
MB	Fe_3O_4@PPy @4 vinylpyridine	Wastewater	Multiple steps	Temp: 20 °C [MB]: 50 mg L^{-1} Adsorbent: 10 mg (30 mL) pH = 7 Removal (time): 99 % (500 min)	85.98	Langmuir	Pseudo sec. order (k: 3.704×10^{-3} g mg^{-1} min^{-1})	499
MG	Fe_3O_4@PPy @4-vinylpyridine	Wastewater	Multiple steps	Temp: 20 °C [MG]: 50 mg L^{-1} Adsorbent: 10 mg (30 mL) pH = 7 Removal (time): ~ 98 % (600 min)	36.114	Langmuir	Pseudo sec. order	499

AR	Fe_3O_4@PPy @4-vinylpyridine	Wastewater	Multiple steps	Temp: 20 °C [AR]: 200 mg L^{-1} Adsorbent: 10 mg (30 m) pH = 7 Removal (time): ~97 % (600 min)	55.90	Freundlich	Pseudo sec. order (k: 2.270×10^{-4} g mg^{-1} min^{-1})	499
MB	PANI/Attapulgite supported nanoscale zero-valent Fe	Aqueous solution	Liquid-phase chemical reduction method	Temp: 298 K. [MB]: 60 mg L^{-1} Adsorbent: 0.05 g (50 mL) pH:11 Removal (time): 30% (30 minutes)	23	Langmuir	---	500
AYR	PANI/Attapulgite supported nanoscale zero-valent Fe	Aqueous solution	Liquid-phase chemical reduction method	Temp: 298 K [AYR]: 60 mg/L Adsorbent: 0.05 g (50 mL) pH:3 Removal (time): 99.56% (10 min)	72	Langmuir	---	500
RhB	Polyaniline magnetic nanoparticles /dicationic ionic liquid	Tap/industrial and lake water	Coating aniline and dicationic ionic liquids on magnetic nanoparticle	Temp: 298 K [RhB]:10 mg g^{-1} Adsorbent: 20 mg (10 mL) pH: 1 Removal (time); ~94% (60 min)	109.90	Temkin	Pseudo sec. order (k:0.4172 g mg^{-1} min^{-1})	501
RhB	Magnetite@ PPy@2-acrylamido-2-methyl-1-propanesulfonic acid microspheres	Aqueous solutions	Two-step process	Temp: 293 K. [RhB]: 60 mg L^{-1} Adsorbent: 7 mg pH:7 Removal (time): >90 % (300 min)	215.054	Langmuir	Pseudo sec. order (k:2.441x10^{-3} g mg^{--1} min^{-1})	502
MB	Magnetite@ PPy@2-acrylamido-2-methyl-1-propanesulfonic acid microspheres	Aqueous solutions	Two-step process	Temp: 293 K. [MB]: 50 mg L^{-1} Adsorbent: 7 mg pH:7 Removal (time): ~100 % (240 min)	183.486	Langmuir	Pseudo sec. order	502
CV	Magnetite@ PPy@2-acrylamido-2-methyl-1-propanesulfonic acid microspheres	Aqueous solutions	Two-step process	Temp: 293 K. [CV]: 50 mg L^{-1} Adsorbent: 7 mg pH:7 Removal (time): ~100 % (300 min)	194.175	Langmuir	Pseudo sec. order (k: 3.156×10^{-3} g mg^{-1} min^{-1})	502
RhB	PEG capped PANI/TiO_2/CuO	Water	In situ polymerization of aniline in presence of TiO_2/CuO	Temp: 300 K. [RhB]: 5 mg L^{-1} Adsorbent: 0.2 g (50 mL) pH: 6 Removal (time): 89.7% (240 min)	3.53	Langmuir	Pseudo sec. order (k: 0.809 g. mg^{--1} min^{-1})	504

CR	PANI@ZnO	Deionized water	In-situ oxidation chemical process	Temp: 298 K. [CR]: 150 mg L^{-1} Adsorbent: 10 mg (25 mL) pH:5 q_e (time):~70 mg g^{-1} (120 min)	76.92	Langmuir	Pseudo sec. order (0.0004 g mg^{-1} min^{-1})	507
MO	3D PANI@ Activated SiO_2 gel	Aqueous solution	In-situ polymerization	Temp: 298.15 K [MO]: 50 mg L^{-1} Adsorbent:0.25 g (30 mL) pH: 3 Removal efficiency (time):~100 % (200 min)	161.29	Langmuir	Pseudo sec. order 0.036 g mg^{-1} min^{-1}	508
BG	3D PANI@ Activated SiO_2 gel	Aqueous solution	In-situ polymerization	Temp: 298.15 K. [BG]: 50 mg L^{-1} Adsorbent: 0.025 g (30 mL) pH: 8 Removal (time): 100% (200 min)	136.98	Langmuir	Pseudo sec. order (k: 1.34 g mg^{-1} min^{-1})	508
CR	PANI-$ZnTiO_3$	Aqueous solutions	Polymerization of aniline in the suspensions of ZTO	Temp: RT [CR]:50-150 ppm (100 mL) Adsorbent: 200 mg pH: Natural pH Removal (time): 90% (15 min)	64.51	Langmuir	Pseudo sec. order (k: 0.000509 g s^{-1} $mg^{=1}$)	511
CR	Fe_3O_4/PPy/Carbon black	Aqueous solution	Encapsulating Fe_3O_4 nano particles in PPy/Cabon black	[CR]: 120 mg L^{--1} Adsorbent: 0.5 g L^{-1} (40 mL) pH:7 Removal (time): 96.9% (240 min)	500	Langmuir	Pseudo sec. order (k: 0.007x10^{-2} g.mg^{-1} min^{-1})	512
MB	Fe_3O_4/PPy/Carbon black	Aqueous solution	Encapsulating Fe_3O_4 nano particles in PPy/Cabon black	[MB]: 40 mg L^{-1} Adsorbent: = 0.5 g L^{-1} pH:7 Removal (time): 95.9% (120 min)	90.9	Langmuir	Pseudo sec. order (k: 0.14x10^{-2} g.mg^{-1} min^{-1})	512
CR	PANI Microsphere/ MnO_2/Fe_3O_4	Aqueous solution	In situ deposition	Temp: 303 ± 3 K [CR]: 20 mg L^{-1} Adsorbent: 1 g L^{-1} pH: ~6.75 Removal (time): 98% (1500 min)	599.49	Elovich	Pseudo sec. order (k:0.25 g mg^{-1} min^{-1})	513
MG	PANI Microsphere/ MnO_2/Fe_3O_4	Aqueous solution	In situ deposition	Temp: 303 ± 3 K [MG]: 20 mg L^{-1} Adsorbent: 1g L^{-1} pH: ~6.75 Removal (time): 88% (1500 min)	1142.13	Freundlich	Pseudo sec. order (k:0,012 g mg^{-1} min^{-1})	513
CR	L-cysteine/ rGO/PANI	Aqueous solution	rGO + 0.1M L-cysteine	Temp: RT [CR]: 30 mg L^{-1}	56.57	Langmuir	Pseudo sec. order	516

			solution.+ aniline monomer +APS	Adsorbent: 0.025 g (10 mL) pH: Neutral Removal (time): 98% (10 min)				
MB	Polyaniline nanotubes	Aqueous solutions	In-situ polymerization	Temp: 25 ^{0}C [MB]: 0.95 mg L^{-1} Adsorbent: 0.05 g (100 mL) pH: Removal/time: 100 % (20 min)	9.21	Langmuir	Pseudo sec. order (k: 0.03595 g mg^{-1} min^{-1})	518
MB	Polyaniline hollow nanotubes	In situ synthesis	In-situ polymerization	Temp: RT [MB]: 6.2 mg L^{-1} Adsorbent: 10 mg (100 mL) pH: 11 Removal/time: ~92 % (600 min)	69.4	Langmuir	Pseudo sec. order (k:0.001 g mg^{-1} min^{-1})	519
AG	PANI hollow nanotubes	Aqueous media	Using acid green as a structure-directing agent and soft template	Temp: 298 K [AG]:6.1 mg L^{-1} Adsorbent: 10 mg pH: 3.0 Removal (time): 52% (6 h)	57.8	Langmuir	Pseudo sec. order (k:8.9x10^{-4} g mg^{-1} min^{-1})	519
MB	Polyaniline nanotubes	aqueous medium	Aniline oxidation in the presence of methyl orange	[MB] = 8.8 mg L^{-1} Adsorbent: 10 mg (0.1 L) pH: 9 Removal (time): >90% (350 min)	91.1	Langmuir	Pseudo sec. order (k: 0.00117 g mg^{-1} min^{-1})	520
AG	PANI nanotubes	Aqueous medium	Green approach via the aniline oxidation	Temp: 25 °C [AG]: 20 mgL^{-1} Adsorbent: 8 mg L^{-1} (100 ml) pH:3 Removal (time): 67% (320 min)	58	Langmuir	Pseudo sec.-order (k:0.002 g mg^{-1} min^{-1})	520
CR	PPy@MoS_2 hollow microtubes	Aqueous medium	Hydrothermal process, in-situ polymerization and sulfidation	Temp: RT [CR]: 60 mg L^{-1} Adsorbent:50 mg L^{-1} (5 mL) pH: Neutral Removal (time): 84,14% (120 min)	598.7	Freundlich	Pseudo sec. order (k:0.0030 g mg^{-1} min^{-1})	521
MB	PPy@MoS_2 hollow microtubes	Aqueous medium	Hydrothermal process and in-situ polymerization and sulfidation	Temp: RT [MB]:150 mg·L^{-1} Adsorbent: 50 mg (5 mL) L^{-1} pH: Neutral Removal (time): 41.1% (120 min)	121.3	Langmuir	Pseudo sec. order (k:0.0003 g mg^{-1} min^{-1})	521
MB	PANI nanotubes base/Silica	Distilled water.	In-situ polymerization	Temp: 25 ^{0}C [MB]: 0.95 mg L^{-1}	10.31	Langmuir	Pseudo sec. order	522

				Adsorbent: 0.05 g (100 mL) Removal (time): : 100% (10 min)			(k: 0.09 g mg^{-1} min^{-1})	
MB	PANI/TiO_2 hydrate	Distilled water	One-pot chemical oxidative polymerization	Temp: 298 K [MB]:100-200 mg L^{-1} Adsorbent: 2 g L^{-1} (10 mL) pH: 3-11 Removal(time): ~100% (12 h)	458.10	Freundlich model,	Pseudo sec. order (k: 0.0009 g mg^{-1} min^{-1})	523
MB	PPy-coated cotton textile	Aqueous solution	In situ oxidative polymerization of cotton textiles	Temp: 25 ^{0}C [MB]: 3.9 mg L^{-1} Adsorbent: 0.05 g (50 mL) pH: 7 Removal (time): 96% (24 h)	6.83	Freundlich	Pseudo sec. order (k: 0.083 g mg^{-1} min^{-1})	525
MB	Fe_3O_4@PPy @SDBS	Aqueous solutions	Through hydrothermal, *in situ* polymerization, and surface modification	Temp: 20 ^{0}C [MB]: 20-30 mg L^{-1} Adsorbent: 10 mg (30 mL) pH: 7 Removal (time): ~93% (200 min)	124.07	Langmuir	Pseudo sec. order (1.213x10^{-3} g mg^{-1} min^{-1})	527
MG	Fe_3O_4@PPy @SDBS	Aqueous solutions	Through hydrothermal, *in situ* polymerization, and surface modification	Temp: 20 ^{0}C [MG]: 20 mg L^{-1} Adsorbent: 8 mg (30 mL) pH: 7 Removal (time): ~96% (500 min)	73.10	Langmuir	Pseudo sec. order (1.445x10^{-3} g mg^{-1} min^{-1})	527
MB	PPy/GO@Fe_3O_4	Aqueous solutions	One step	Temp: RT [MB]: 100 mg L^{-1} Adsorbent: 10 mg (40 mL) pH: 8 Removal (time): ~80% (140 min)	323.2	Langmuir	Pseudo sec, order (k:0.00172 g mg^{-1} min^{-1})	528
MB	Fe_3O_4@PPy/ RGO	Aqueous solutions	Chemical route	Temp: 30 ^{0}C. [MB]:100 mg L^{-1} Adsorbent: 0.333 g L^{-1} (30 mL) pH: natural Removal (time): ~95% (60 min)	270.3	Langmuir isotherm	Pseudo-second-order (k: 0.0154 g mg^{-1} min^{-1})	530
MB	Fe_3O_4/Polypyrrole/Phytic Acid	Water	.In-situ polymerization	Temp: 35 ^{0}C [MB]: 100 ppm Adsorbent: 80 mg (50 mL) pH: 10 Removal (time): ~90% (120 min)	153.84	Langmuir	Pseudo sec. order (k: 0.001 g mg^{-1} min$^{=1}$)	531

CV	Fe_3O_4/Polypyrrole/Phytic Acid	Water	In-situ polymerization	Temp: 35 ^{0}C [CV]: 100 ppm Adsorbent: 80 mg (50 mL) pH: 10 Removal (time): ~85% (120 min)	181.82	Langmuir	Pseudo sec. order (k:0.001 g mg^{-1} min^{-1})	531
MO	PANI nanotubes filled sodium alginate	Distilled water	Mixing of PANI nanotubes in water +$CaCl_2$	Temp: 35 ^{0}C [MO]: 20 mg L^{-1} Adsorbent: 0.05 g (50 mL) pH: 2 Removal (time): ~76% (90 min)	370.4	Langmuir	Pseudo sec. order (k:0.001 g mg^{-1} min^{-1})	534
MO	PANI-MWCNT	Water	In-situ oxidative polymerization	Temp: 30 °C [MO]: 30 mgL^{-1} Adsorbent: 8 mg L^{-1} (100 ml) pH: Neutral Removal (time): ~94% (60 min)	149.25	Langmuir	Pseudo sec. order (k:5.265×10^{-4} g mg^{-1} min^{-1})	535
MO	PANI (skin)/Polyamide 6 (core)	Aqueous solution	In situ oxidation polymerization	Temp:298 K [MO]:10 ppm Adsorbent: 0.03g pH: 6 Removal (time): 58.7 mg g^{-1} (120 min)	58.7	Langmuir	Pseudo sec. order	536
MO	Waterborne poly vinyl pyrrolidone stabilized PANI core–shell	Tap water	Waterborne PVP stabilized PANI core–shell	Temp: 28 ^{0}C [MO]: 32.73 mg L^{-1} Adsorbent: 5 mg (20 ml) pH 7.02 Removal (time): 100 % (15 min)	---	Langmuir	---	537
MO	Halloysite nanotubes/PPy	Aqueous solution	In situ polymerization	Temp: 25°C [MO]: 90 mg L^{-1} Adsorbent: 0.15 g (50 mL) pH: Natural Removal (time): 98.6% (120 min)	214.6	Langmuir and Freundlich	Pseudo sec. order (k: 0.0037 g mg^{-1} min^{-1})	538
RB	PANI@TiO_2	Deionized water	Sonochemical method	Temp: 28 °C. [RB]: 100 mg L^{-1} Adsorbent: 50 mg (100 mL) pH: 6.7 q_t (time):~80 mg g^{-1} (120 min)	----	Langmuir and Freundlich	First order (k: 0.007 min^{-1}), Pseudo sec. order (k: 0.00008 g mg^{-1} min$^{-1/2}$)	540
RB	PANI@SiO_2	Deionized water	Sonochemical method	Temp: 28 °C. [RB]: 100 mg L^{-1} Adsorbent: 50 mg (100 mL) pH: 6	----v	Langmuir and Freundlich	First order (k: 0.024 min^{-1}), Pseudo sec. order (k:	540

				q_t (time):~30 mg g^{-1} (120 min)			0.00029 g mg^{-1} $min^{-1/2}$)	
R6G	PANI@TiO_2	Deionized water	Sonochemical method	Temp: 28 °C. [CR]: 50 mg L^{-1} Adsorbent: 5 mg (100 mL) pH: 6.7 q_t (time):~ 90 mg g^{-1} (120 min)	94	Langmuir and Freundlich	First order (k:0.023 min^{-1}), Pseudo sec. order (k:0.00 069 g mg^{-1} $min^{-1/2}$)	540
R6G	PANI@SiO_2	Deionized water	Sonochemical method	Temp: 28 °C. [CR]: 5 mg L^{-1} Adsorbent: 5 mg (100 mL) pH: 6.7 q_t (time):~ 60 mg g^{-1} (120 min)	61	Langmuir and Freundlich	First order (k:0.011 min^{-1}), Pseudo sec. order (k:0.00 006 g mg^{-1} $min^{-1/2}$)	540
CR	PANI@TiO_2	Deionized water	Sonochemical method	Temp: 28 °C. [CR]: 100 mg L^{-1} Adsorbent: 5 mg (100 mL) pH: 6.7 q_t (time):~~90 mg g^{-1} (120 min)	93	Langmuir and Freundlich	First order (k:0.020 min^{-1}), Pseud sec. order (k:0.00048 g mg^{-1} $min^{-1/2}$)	540
CR	PANI@SiO_2	Deionized water	Sonochemical method	Temp: 28 °C. [CR]: 100 mg L^{-1} Adsorbent: 5 mg (100 mL) pH: 6.7 q_t (time):~70 mg g^{-1} (120 min)	71	Langmuir and Freundlich	First order (k:0.0253 min^{-1}), Pseudo sec. order (k: 0.00034 g mg^{-1} $min^{-1/2}$)	540
MB	PANI@TiO_2	Deionized water	Sonochemical method	Temp: 28 °C. [MB]: 100 mg L^{-1} Adsorbent: 50 mg (100 mL) pH: 6.7 q_t (time):~ 90 mg g^{-1} (120 min)	89	Langmuir and Freundlich	Pseudo first order (k: 0.024 min^{-1}), Pseudo sec. order (k:0.00050 g mg^{-1} $min^{-1/2}$)	540
MB	PANI@SiO_2	Deionized water	Sonochemical Method	Temp: 28 °C [MB]: 50 mg L^{-1} Adsorbent: 50 mg (100 mL) pH: 6.7 q_t (time):~ 73 mg g^{-1} (120 min)	74	Langmuir and Freundlich	First order (k:0.037 min^{-1}), Pseudo sec. order (k: 0.00056 g mg^{-1} $min^{-1/2}$)	540
EB	PANI@TiO_2	Deionized water	Sonochemical method	Temp: 28 °C. [EB]: 50 mg L^{-1} (100 mL)	--	Langmuir and	First order (k: 0.008 min^{-1})	540

				Adsorbent: 5 mg pH: 6.7 q_t(time) ~ 55 mg g^{-1} (120 min)		Freundlich	Pseudo sec. order (k: 0.00011 g mg^{-1} $min^{-1/2}$)	
EB	PANI@SiO_2	Deionized water	Sonochemical method	Temp: 28 °C. [EB]: 50 mg L^{-1} (100 mL) Adsorbent: 5 mg pH: 6.7 q_t(time) ~ 55 mg g-1 (120 min)	--	Langmuir and Freundlich	First order (k: 0.013 min^{-1}) Pseudo sec. order (k: 0.00012 g mg^{-1} $min^{-1/2}$)	540
BB	PANI@TiO_2	Deionized water	Sonochemical Method	Temp: 28 °C. [BB]: 100 mg L^{-1} Adsorbent: 5 mg (100 mL) pH: 6.7 q_t (time):~ 42 mg g^{-1} (120 min)	---	Langmuir and Freundlich	Pseudo first order (k: 0.011 min^{-1}), Pseudo sec. order (k:0.00013 g mg^{-1} $min^{-1/2}$)	540
BB	PANI@SiO_2	Deionized water	Sonochemical Method	Temp: 28 °C. [BB]: 100 mg L^{-1} Adsorbent: 5 mg (100 mL) pH: 6.7 q_t (time):~ 42 mg g^{-1} (120 min)	86	Langmuir and Freundlich	Pseudo first order (k: 0.038 min^{-1}), Pseudo sec. order (k: 0.00060 g mg^{-1} $min^{-1/2}$)	540
MG	Graphene/Fe_3O_4/PANI	Aqueous solutions	Multiple steps	Temp: 25 ºC [MG]:16 mg L^{-1} Adsorbent: 30 mg (50 (mL) pH:6.5 Removal (after cycle 1): 97.72%	196.10	Langmuir	Pseudo sec. order (k:0.0022 g .mg^{-1} min^{-1})	541
AR1	Graphene/Fe_3O_4/PANI	Aqueous solutions	Multiple steps	Temp: 25 ºC [AR1]:16 mg L^{-1}) Adsorbent: 30 mg (50 mL) pH:6.5 Removal efficiency (after cycle 1): 97.013%	150.27	Langmuir	Pseudo sec. order (k:0.0021 g .mg^{-1}·min^{-1})	541
MG	CNT/PANI	Aqueous solution	Static interfacial polymerization technique	Temp: 20 ^{0}C [MG]: 8-12 mg L^{-1} Adsorbent: 0.1 g (100 mL) pH:7 Removal (time): ~95% (120 min)	15.45	Langmuir	Pseudo sec-order (k: $5.0x10^{-3}$ (mg g^{-1} $min^{-0.5}$)	542

AR1	PPy/$Mn_{0.8}Zn_{0.2}Fe_2O_4$/GO (PMG50)	Wastewater	In-situ Py polymerization	Temp: 298 K [AR1]:10 mg L^{-1} Adsorbent: 100 mg (10 mL) pH: 2 Removal (time): 98.8% (120 min)	---	---	Pseudo sec. order (0.320 $g.mg^{-1}\cdot min^{-1}$)	545
BG	Cross-linked PANI/chitosan-graphene oxide-oxidized SWCNT	Aqueous solution	Chemical oxidative copolymerization	Temp: 22 ^{0}C [BG]: 5 mg L^{-1} Adsorbent: 12.5 mg (25mL) pH 6 Removal efficiency (time): ~ 98.4% % (120 min)	21.27	---	Pseudo-second-order ($k:9.2x10^{-4}$ mg g^{-1} $min^{-0.5}$)	546
AR1	Cross-linked PANI/chitosan-graphene oxide-oxidized SWCNT	Aqueous solution	Chemical oxidative copolymerization	Temp: 22 ^{0}C [AR1]: 20 mg L^{-1} Adsorbent: 12.5 mg (25mL) pH 2 Removal efficiency (time): 99.7% (120 min)	90.91	---	Pseudo-second-order ($k:3.4x10^{-4}$ (mg g^{-1} $min^{-0.5}$)	546
BG	Core–shell polythiophene/ZnO/MWCNTs	Aqueous solutions	In-situ chemical polymerization (two-way method)	Temp: 25 ^{0}C. [BG]: 5 mg L^{-1} Adsorbent: 30 mg (20 mL) pH: 6 Removal efficiency (time): 94 % (90 min)	8.3	---	Pseudo second-Order (k: 1.9x10-3 mg g^{-1} min^{-1})	547

*q_m: maximum adsorption capacity. AG: Acid green, AR: Acid Red, AR1: Acid Red 1, AYR: alizarin yellow R, BB: Brilliant Blue, BG:Brilliant Green, CR: Congo red, CV: Crystal violet, E102 (Tartrazine:TTz), EB: Evans Blue, EY: Eosin Y, OG: Orange Green, IC: indigo carmine, MG: Malachite Green, MO: Methyl Orange, MB: Methylene Blue, MR: Methyl Red, OG: Orange Green, Rh: Rhodamine, RhB: Rhodamine B, Rh6B: Rhodamine 6B. Rh6G: Rhodamine 6G, SY: Sunset Yellow,

View Article Online
DOI: 10.1039/D5LP00230C

Table 5 Merits and demerits of different electrode materials.[7] Reproduced with permission from Elsevier.

Materials	Advantages	Disadvantages
Carbonaceous materials	High specific surface area High electrical conductivity Inexpensive Eco-friendly High electrochemical stability	Low energy density Poor cyclability
Conducting polymers	High specific capacitance Tunable electrical conductivity Unique solution processability High flexibility Easy fabrication	Low conductivity Poor electrochemical stability
Transition metal oxide	High specific capacitance Wide potential window High energy density	Low conductivity Poor electrochemical stability

View Article Online
DOI: 10.1039/D5LP00230C

Table 6 Preparative methods and electrochemical performance of hollow ICPs and ICP based core-shell materials in supercapacitor applications.

Electrode Material	Method of preparation	Electrolyte	Specific capacitance (current density	Cycling stability	Energy density (ED)	Power density (PD)	Ref
$Ppy_{1\%}/DBSA_{2\%}/NiO_{97\%}$-GS	Electrodepositio n at 4 mA cm^{-2} for 10 min.	0.1 M $LiClO_4$	679 at 1 A g^{-1}	83.9 % (1000 cycle) at 1 A g^{-1}	94.4 Wh kg^{-1}	94.4 W kg^{-1}	154
MnO_2@PPy	Hard template (PS) method.	1 M Na_2SO_4	295 F g^{-1} at of 1 A g^{-1}	100% (20,000 cycles) 10 A g^{-1}	42 Wh kg^{-1}	1100 W kg^{-1}	239
Core-shell nanorod arrays with PANI deposited into $NiCo_2O_4$	Electrochemical polymerization	1 M $H2SO_4$	901 F g^{-1} at1 A g^{-1}	91% (3000 cycles) at 10 A g^{-1}	81.77 Wh kg^{-1} at a PD of 399.3 W kg^{-1}.	---	320
D-Fe_2O_3@ PPy/CC	Chemical reduction and electrodeposition methods	1 M Na_2SO	640 F g^{-1} at 1 mA cm-1	79.3% of its (10 mA cm-2) after 5000 cycles	--	--	321
$CoCrFeMnNi)_3O_4$ @CC-PPy	Two-step electrodeposition	2 M H_2SO_4	791 F·g^{-1} at 0.5 A·g□ 1,	63 % (5000 cycles) at 10 A·g-1	49.2 Wh·kg^{-1} (PD: 800 W·kg^{-1}).	--	324
$LaMnO_3$@CC-PPy	Two-step electrodeposition		862 F g^{-1} at 1 A g^{-1}	66% (3000 cycles) at 10 A g^{-1}	73 Wh k^{-1}.	--	325
Hollow polyaniline helical nanobelts	By chemical oxidation of aniline	---	688 F g^{-1} at 5 mV s^{-1}	81.6% (1000 cycles)	14.37 Wh kg^{-1} at PD of 500 W kg^{-1}	---	492

Hollow polyaniline microspheres	In situ chemical oxidative polymerization with SPS spheres as the template.	1M H_2SO_4	421 F g^{-1}	45% (500 cycles) at 10 mA cm^{-2}	---	---	552
Hollow polyaniline nanocapsules	Interfacial polymerization method	1 M H_2SO_4	502 F g^{-1} at 5 mA cm^{-2}	83.1% (1000 cycles) at 10 mA cm^{-2}	---	---	553
Ce^{3+} doped polyaniline hollow microspheres	Self-assembly method	H_2SO_4	248.2 F g^{-1} at 1 mA cm^{-2})	41.6% (5000 cycles) at 5 mA cm^{-2}	----	----	555
Hollow polyaniline nanospheres	Self-sacrificial templates and emulsion polymerization	1 M HCl	485.5 F g^{-1} at 1 A g^{-1}	69% (500 cycles) at 5 A g^{-1}	----	----	556
Polypyrrole hollow nanospheres	Hard template method	1 M H_2SO_4	350 at 1A g^{-1}	---	40 Wh kg^{-1}	490 W kg^{-1}	557
Hollow Polypyrrole Films	E lectrochemical oxidative polymerization of pyrrole		~300 F g^{-1} at 3 A/g	No decrease in capacitance (1000)	---	---	558
Hollow capsular polypyrrole nanofiber	Vapor-phase polymerization	1 M H_2SO_4	203 F g^{-1} at 2 mV sec^{-1}	>90 % (11000 cycles) at 10 A g^{-1}	---	---	559
Nanotubular-polyaniline	Using natural tubular halloysite as hard template	1M H_2SO_4	654 F g^{-1} at 1 A g^{-1}	120% (until 2000 cycles) and 87% (10000) at 100 mV s^{-1}.	---	---	560
Polyaniline nanotube arrays	Electrochemical polymerization using ZnO nanorod arrays as sacrificial templates	1 M H_2SO_4	675 F g^{-1} at 50 mV sec^{-1}	Decrease in ~30 % of Csp value (100) at 50 mV s^{-1}	---	---	561
Polyaniline nanotubes (Inner dia: 80 nm, Outer dia: 180 nm)	One-step polymerization and acrylic acid in aqueous solution	1 mol/L H_2SO_4	436 F g^{-1} at 0.5 A g^{-1}	89.2% (500 cycles	----	----	563

				) at 0.5 A g^{-1}			
Crystalline tetragonal hollow PANI nanotubes	MO (self-sacrificial template) in acidic solutions to facilitate the growth of PANI nanotubes	1 mol/L H_2SO_4	~590 ± 36 1 F g^{-1} at 5 mVs^{-1}	Capacitance loss of 49.6 % (1000 cycles) at 10 A g^{-1}	14.56 Wh kg^{-1} at PD of 250 W kg^{-1}	---	564
PPy hollow nanoparticles	Surfactant-templated chemical oxidation polymerization	1 M Na_2SO_4	326 F g^{-1} at A g^{-1}	86% (10,000 cycles)	---	---	565
Hollow polyaniline nanofiber	Chemical oxidation polymerization	1 M H_2SO_4	290 F g^{-1} at 1 A g^{-1}	83% (1000 cycles) at 3 A g^{-1}	---	---	568
MnO_2/Polyaniline hollow sphere	Interfacial synthesis	0.5 M Na_2SO_4	262 F g^{-1} at 1.5 mA cm^{-1}	93% (800 cycles) at 9 mA cm^{-1}	---	---	570
3D-Hollow balls of graphene-polyaniline	Self-assembly method	1M H_2SO_4	331 F g^{-1} at 1 A g^{-1}	14 % loss of capacitance (500 cycles) at 1 A g^{-1}.	---	---	571
3D-graphene-polyaniline hybrid hollow spheres	Layer-by-layer assembly	1 M H_2SO_4	381 F g^{-1} at 4.0 A g^{-1}	83% (1000 cycles) at 0.5A g^{-1}	---	---	572
Hollow polyaniline nanotubes supported on Ti_3C_2 MXene	By exfoliating Ti_3C_2 followed by in-situ polymerization	1 M H_2SO_4	596.6 F g^{-1} at 0.1 A g^{-1}	94.7 % (5000 cycles) at 1 A g^{-1}.	25.6 Wh kg^{-1} at PD of 153.2 W kg^{-1}	1610 Wkg^{-1} at ED of 13.2 Wh kg^{-1}	573
RGO/Polyaniline nanotubes	In-situ reduction	1M-H_2SO_4	Unirradiated: 448 F g^{-1} at 0.5 A g^{-1},	Unirradiated: 89 % (1000),	Unirradiated: 30.52 Wh kg^{-1},	Unirradiated:174.96 W kg^{-1},	574
RGO/Polyaniline nanotubes	In-situ reduction	1M-H_2SO_4	Irradiated: 482 F g^{-1} at 0.5 A g^{-1}	Irradiated: 92% (1000 cycles)	Irradiated: 32.81 Wh kg^{-1}	Irradiated: 174.98 W kg^{-1}	574

Graphene–Polypyrrole hollow sphere	Pickering emulsion polymerization using	1M H_2SO_4	238 F g^{-1} at 1 A g^{-1}	90.7% (1500 cycles) at 1 A g^{-1}	---	---	576
N-doped graphene (NG)/hollow PPy	Hollow PPy nanospheres prepared by using a sacrificial template and embedded in NG layers	1M HCl	575 F g^{-1} at a current density of 1 A g^{-1}	90.1 (500 cycles) at 1 A g^{-1}.	47.92 Wh kg^{-1} at 1A g^{-1}	---	577
Polyaniline hollow nanospheres encaging RuO_2 nanoparticles	Polymerizing aniline monomers on 3D-arrayed PS nanospheres	1.0 M aqueous $HClO_4$	1570 F g^{-1} at 10 mV s^{-1}	77.6% (1000 cycles) at 10 mV s^{-1}	---	---	578
Polyaniline hollow fibers (PANI-HF)	In-situ polymerization of aniline in presence of electrospun PAN nanofibers	1M H_2SO_4	425 F g^{-1} at 20 mV s^{-1}	72% (500 cycles) at 100 mV s^{-1}	---	---	579
PANI- hollow fiber decorated by RGO	Self-assembling of GO sheets on PANI-HF followed by electrochemical reduction of GO	1M H_2SO_4	449 F g^{-1} at 20 mV s^{-1}	91% (500 cycles) at 100 mV s^{-1}	---	---	579
Graphene-polypyrrole nanotube	Multi steps	2M H_2SO_4 aqueous solution	324 F g^{-1} at 1.5 A g^{-1}	88% (200 cycles) at 1.5 A g^{-1}	---	---	580
MOF-PPy tubes (mass ratio % of PPy:28)	Dispersion and mixing method	1 M Na_2SO_4	554.4 F g^{-1} at 0.5 A g^{-1}	90.7 % (10,000 cycles) at 20 A g^{-1}	0.0113 mW h cm^{-2} with PD of 0.12 mW cm^{-2}	---	581
Hollow PPy nanospheres decorated on CNTs	Via in situ chem. oxid. Emulsion interfacial polymerization	1.0 M aqueous $NaNO_3$	33.9 F g^{-1} at 20 mV sec^{-1}	71 % (500 cycles)	---	---	582
Polyaniline nanowires wrapped on the polypyrrole nanotubes	Chemical synthesis method	1 M H_2SO_4	765 F g^{-1} at a scan rate of 10 mV s^{-1}	86.3 % (1000 cycles) at 10 mV s^{-1}	---	---	583
Core-shell polyaniline functionalized carbon quantum dots (CQDs)	Via adsorption of CQDs on PANI to be produced PANI	1M H_2SO_4	264.6 F g^{-1} at 2.5 A g^{-1}	High stability (5000 cycles)	---	---	584

PPy@PANI nanosphere	By dilute solution polymerization	H_2SO_4	510 F g^{-1} at 10 mV s^{-1}	87.6 % (1000 cycles) at 5 A g^{-1}	---	---	585
Polypyrrole@poly(1,5-diaminoanthraquinone)	Dispersion and sonication	1.0 M H_2SO_4	533 F g^{-1} at 1 A g^{-1}	107.4 % (10,000 cycles) at 100 mV s^{-1}.	7.5 Wh kg^{-1} (at a PD of 96.1 W kg^{-1})	1124.9 W kg^{-1} (at ED of 4.0 Wh kg^{-1})	586
Graphene-Wrapped Polyaniline Hollow Spheres	Solution-based coassembly process	1 M H_2SO_4	614 F g^{-1} at 1 A g^{-1}	90% (500 cycles) 1 A g^{-1}	---	----	587
Carbon layer encapsulated polyaniline nanotubes	In-situ polymerization+ hydrothermal method	1 M H_2SO_4	410.5 F g^{-1} at 1 A g^{-1}	63% (2000 cycles)	42.32 Wh kg^{-1}	16.44 kW kg^{-1}	588
Polyaniline/Nickel oxide core/shell	In-situ polymerization in presence of NiO nanoparticles	1 M H_2SO_4	372 F g^{-1} at 20 mV s^{-1}	---	50.2 Wh Kg^{-1} at 1 Ag^{-1}	0,50 kW Kg^{-1} at 1 Ag^{-1}	589
Core-shell nanospherical Polypyrrole/Graphene oxide	In situ surface-initiated polymerization method	1.0 M H_2SO_4	370 F g^{-1} at 0.5 A g^{-1}	91.2% (4000 cycles)	---	---	590
MoS_2@PANI (wt % of MoS_2 in :71.2% for sample react 24 h)	Chemical polymerization	0.5 M H_2SO_4	669 F g^{-1} at 1 A g^{-1}	91 % (4000 cycles) at 10 A g^{-1}	106 Wh kg^{-1} at a power density of 106 kW kg^{-1}	—	592
MoS_2@Polyaniline (with 25 wt% MoS_2	One-pot hydrothermal method energy density was 25.7 Wh kg	1 M H_2SO_4	645 F g^{-1} at 0.5 A g^{-1}	89% (2000 cycles) at 10 A g^{-1}	25.7 Wh kg^{-1} at PD of 779.9 W kg^{-1}	---	593
Hollow MoS_2/ PANI core/shell microsphere	In-situ oxidative polymerization	1 M H_2SO_4	633 F g^{-1} at 0.5 A g^{-1}	86.0% (1000 cycles) at 10 A g^{-1}	31.7 W h kg^{-1} at 0.3 kW kg^{-1}	----	594
MoS_2/Polyaniline hollow microsphere	Template-assisted method	1M H_2SO_4	364 F g^{-1} at a scan rate of 5 mV s^{-1}	84.3% (8000 cycles) at 10 A g^{-1}	32 Wh kg^{-1} at PD of 320 W kg^{-1}	---	595
Mechanically exfoliated MoS_2 sheet coupled with polyaniline	In-situ chemical oxidative polymerization	KOH	510.12 F g^{-1} at 1 A g^{-1}	~80% (2500 cycles)	---	---	596
PEDOT@MoS_2	Electrochemical co-deposition of	1 M H $_2SO_4$	2540 mF cm^{-2} at 1 mA cm^{-2}	98.5% (5000 cycles) at	937 Wh m^{-2} at PD	---	597

	EDOT and MoS_2			100 mA cm^{-2}	of 6500 W m^{-2}		
V_2O_5@Polypyrroe (V_2O_5 Sol: Pyrrole:SDBS= 40 ml:0.1 ml: 20 mg	Sol-gel with *in situ* polymerization method	1 M Na_2SO_4	307 F g^{-1} at 1 A g^{-1}	~60% (2000 cycles) at 3 A g^{-1}	37 Wh Kg^{-1} at PD of 161 W kg^{-1}	---	598
3D core-shell pistil-like $MnCo_2O_4$/ Polyaniline	Electrochemical deposition polymerization	2M KOH	1098 F g^{-1} at 1 A g^{-1}	83.2% (5000 cycles) at 10 A g^{-1}	—	---	600
Nickel ferrite/ Polypyrrole core-shell	In-situ chemical oxidation containing sodium dodecyl sulfate	0.1N H_2SO_4	721.66 F g^{-1} at1A g^{-1}	No significant change (1-1000 cycles)	51.95 Wh Kg^{-1}	6.18 kW Kg^{-1}:	602
Core/sheath structured ultralong MnO_x/Polypyrrole nanowires	In-situ polymerization	1.0 M Na_2SO_4,	1091.4 F g^{-1} at 1 A g^{-1})	97.4% (10,000 cycles) at 10 A g^{-1}	144 Wh kg^{-1} at PD of 1100 W kg^{-1}	---	603
CuS@Polyaniline microspheres	Chemical oxidative polymerization	Li_2SO_4	308.1 F g^{-1} at 0.5 A g^{-1}	71.6% (1000 cycles) at 1 A g^{-1}	—	---	604
Polyaniline/CNT core–shell	Chemical vapor deposition and electrochemical deposition	1 M H_2SO_4 electrolyte	823 F g^{-1} at 5.0 A g^{-1}	---	22.9 Wh kg^{-1} at PD of 700.1 W kg^{-1}	---	606
Hierarchical $NiCo_2S_4$@Polyaniline grown on carbon fiber	Hydrothermal method and potentiostatic deposition	6 M KOH	1823 F g^{-1} at 2 mA cm^{-2}	86.2% (5000 cycles)	64.92 Wh kg^{-1} at PD of 276.23 W kg^{-1}	---	607
$NiCo_2O_4$@PANI nanotubes anchored on C	Electrodeposition method	---	720.5 C g^{-1} at 1 A g^{-1}	99.64% (10000 cycles)	---	---	608
Graphene/Polyaniline hybrid hollow microspheres	Combination of layer-by layer assembly and in situ chemical oxidative polymerization	1.0 M H_2SO_4	633 F g^{-1} at 10 mA cm^{-2}	92 % (1,000 cycles) at at 80 mV s^{-1}.	382.97 Wh kg^{-1} at 10 mA cm^{-2}	----	609
PANI/NiCo-LDH) core-shell composite	Electrochemical deposition method	2.0 M KOH	1845 F g^{-1} at 0.5 A g^{-1}	82% (5000 cycles) at 0.5 A g^{-1}	46.0 Wh kg^{-1} at PD of 351.6 W kg^{-1}	---	610
Graphene nanosheets coating with polyaniline	In situ polymerization	6 M KOH	261.4 F g^{-1} at 100 mA g^{-1}	Capacitance decreased	---	---	611

				to 161.2 F g^{-1} after 500 cycles at 0.1 A g^{-1}			
Polyaniline coated $NiCo_2S_4$	Chemical oxidative polymerization	PVA-KOH gel	1879 F g^{-1} at 1 A g^{-1}	91.1 % (2000 cycles) at 8 A g^{-1}	54.06 Wh kg^{-1} at PD of 0.79 kW kg^{-1})	27.1 Kw kg^{-1} at ED of 15.9 Wh kg^{-1}	613
Hierarchical core/shell Janus-type a-Fe_2O_3/ PEDOT	Multistep process	PVA–H_2SO_4 Hydrogel	252.8 F g^{-1} at 0.1 A g^{-1}	92% (1000) at 0.6 A g^{-1}	136.3 Wh kg^{-1}	10526 W kg^{-1}	616
Core/Double Shell PANI/Chitosan /Cobalt oxide	In situ chemical oxidation method	1M H_2SO_4	1253 F g^{-1} at 5 mV s^{-1}	91% (5000) at of 1 A g^{-1}	95.42 Wh kg^{-1} at 1 A g^{-1}	1549 Wkg^{-1} at 3 A g^{-1}	617
Polyaniline-Ag-MnO_2 nanorod	Two steps process	2 M KOH	1028.6 F g^{-1} at 1 A g^{-1}	93.7% (5000 cycles) at 10 A g^{-1}.	49.77 Wh kg^{-1}	1599.75 W kg^{-1}	618
Polyaniline@CNTs –MnO_2	Hydrothermal and in-situ oxidative polymerization of aniline	0.1 M KOH	143.26 C g^{-1} at 3 mV sec^{-1}	119% (3500 cycles) at 3.0 A g^{-1}	27.17 Wh kg^{-1} at 0.3 A g^{-1}	298.00 W kg^{-1} at 0.3 A g^{-1}	619
MWCNTs@MnO_2 @Polypyrrole	Multiple steps	---	272.7 F g^{-1}	60% after 300 cycles	---	---	620
ZnO NRs@CuS @PEDOT@MnO_2	Multiple steps	1 M $LiClO_4$	19.85 mF cm^{-2} at 5 mV s^{-1}	18% loss of initial value (1500) at 100 mV s^{-1}	---	---	622
Hollow Bi_2O_3@ Carbon fibre@ PEDOT	Electrospinning technique using stabilization, pyrolyzation and polymerization	PVA-KOH g	460 F g^{-1} at 1 A g^{-1}	93.6 % (10,000 cycles) at 2 A g^{-1} .	16.4 Wh kg^{-1}	500.34 W kg^{-1}	623
Hierarchical graphene/polyaniline hollow microsphere	Multiple steps	1 M H_2SO_4	446.19 F g-1 at 5 mV s^{-1}	93.4% (1000 cycles) at 2 A g^{-1}, 8.7% (5000 cycles) at 2 A g^{-1}	---	---	626

"Pizza-like" MoS_2/Polypyrrole/Polyaniline architecture	Multistep process	0.5 m H_2SO_4	1273 F^{-1} g at 0.5 A g^{-}	~83% (3000 cycles) at 2 A g^{-1}	---	---	627

View Article Online
DOI: 10.1039/D5LP00230C

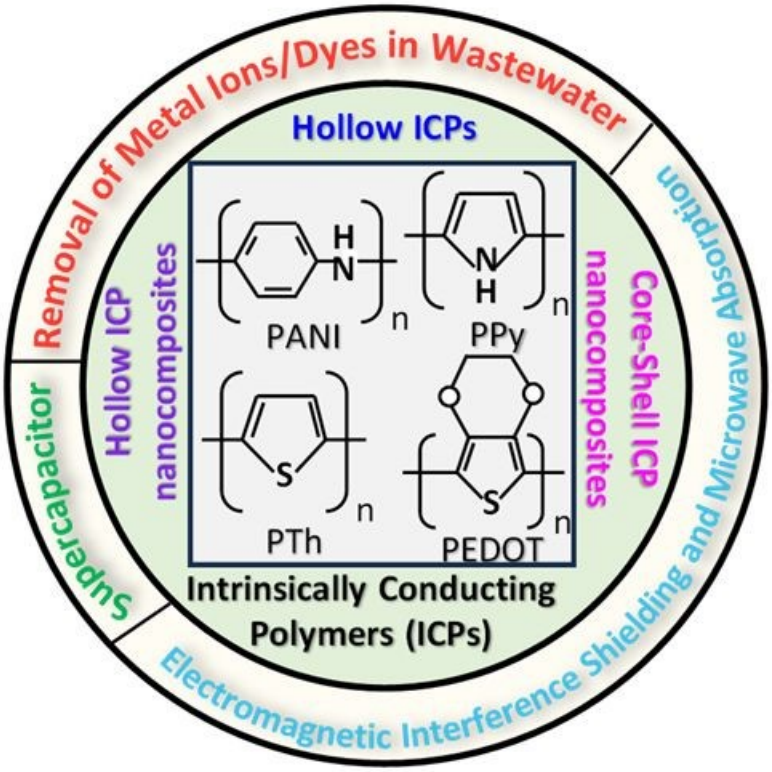

Figure 1 Hollow and Core-Shell Intrinsically conducting polymers (ICPs) and their applications (Inset: Structures of common ICPs.[2] Reproduced with permission from Elsevier).

View Article Online
DOI: 10.1039/D5LP00230C

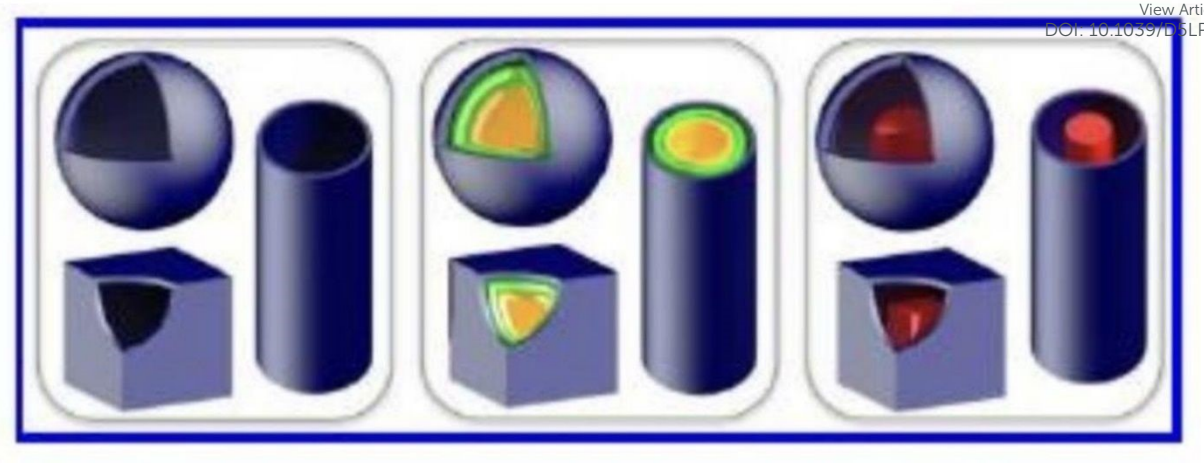

Figure 2. Schematic illustration showing various hollow structures: (left) hollow spheres/boxes/tubes; (middle) multi- shelled hollow spheres/boxes/tubes; (right) yolk−shell, cube-in-box, and wire-in-tube structures.[41]Reproduced with permission from ACS

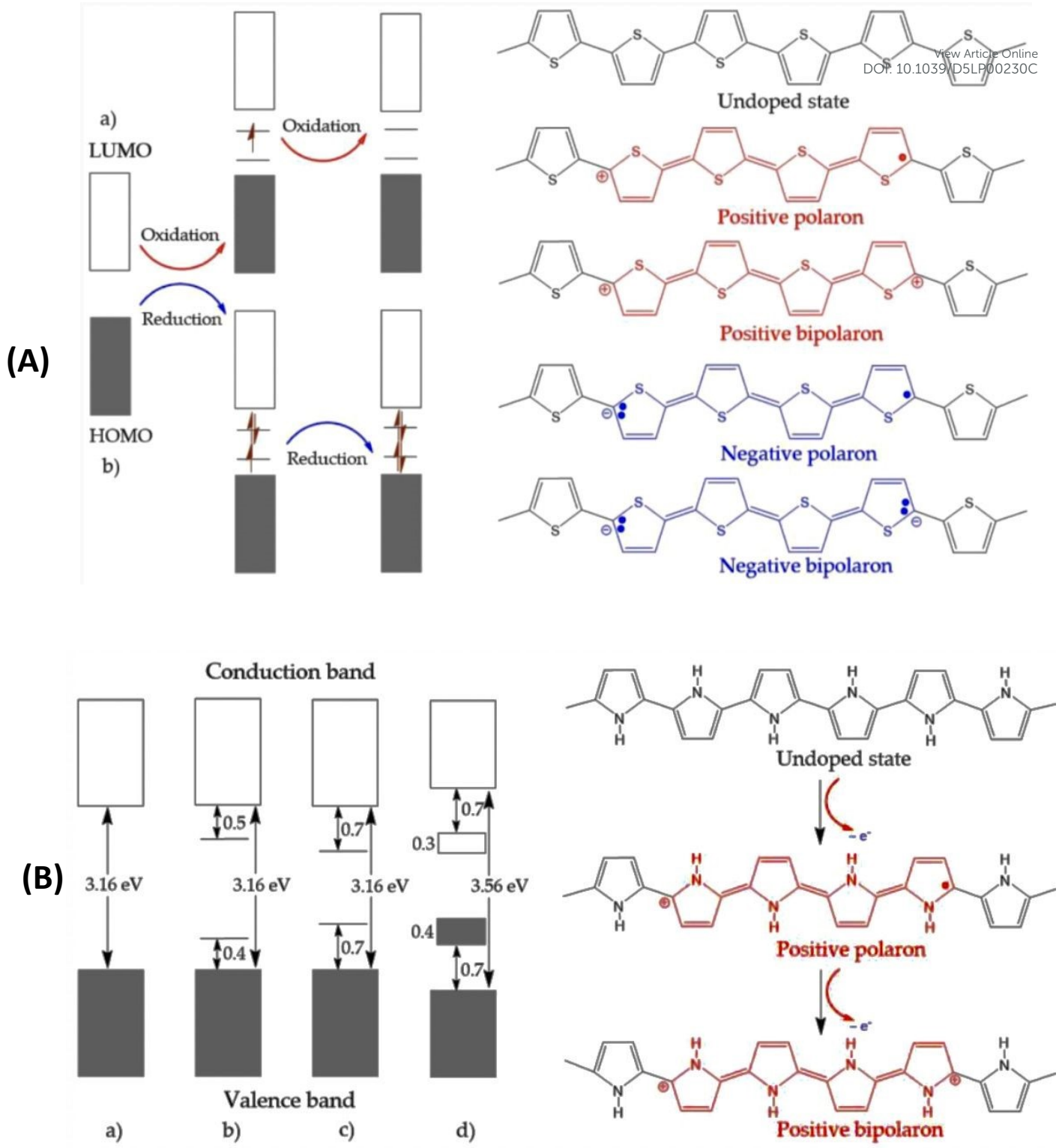

Figure 3 (A) The electronic band and chemical structures of polythiophene (PTh) with (a) p-type doping and (b) n-type doping, and (B) Electronic bands and chemical structures illustrating (a) undoped; (b) polaron; (c) bipolaron; and (d) fully doped states of polypyrrole.[102] Reproduced with permission from MDPI.

View Article Online
DOI: 10.1039/D5LP00230C

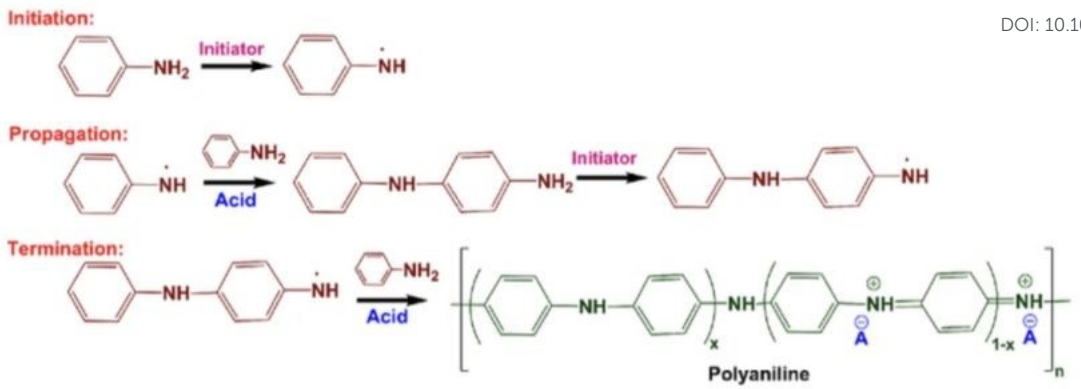

Figure 4 Chemical polymerization mechanisms of polyaniline. Chemical polymerization of polyaniline is carried out in acidic medium by using a common initiator such as ammonium persulfate and potassium persulfate.[99] Reproduced with permission from ACS.

View Article Online
DOI: 10.1039/D5LP00230C

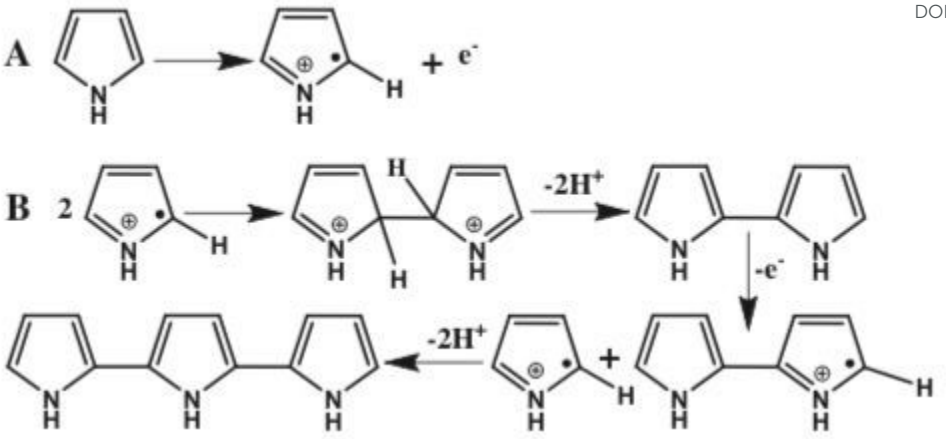

Figure 5 The oxidation of a pyrrole monomer (A) and formation of dimer and trimer of pyrrole (B).[128] Reproduced with permission from Elsevier.

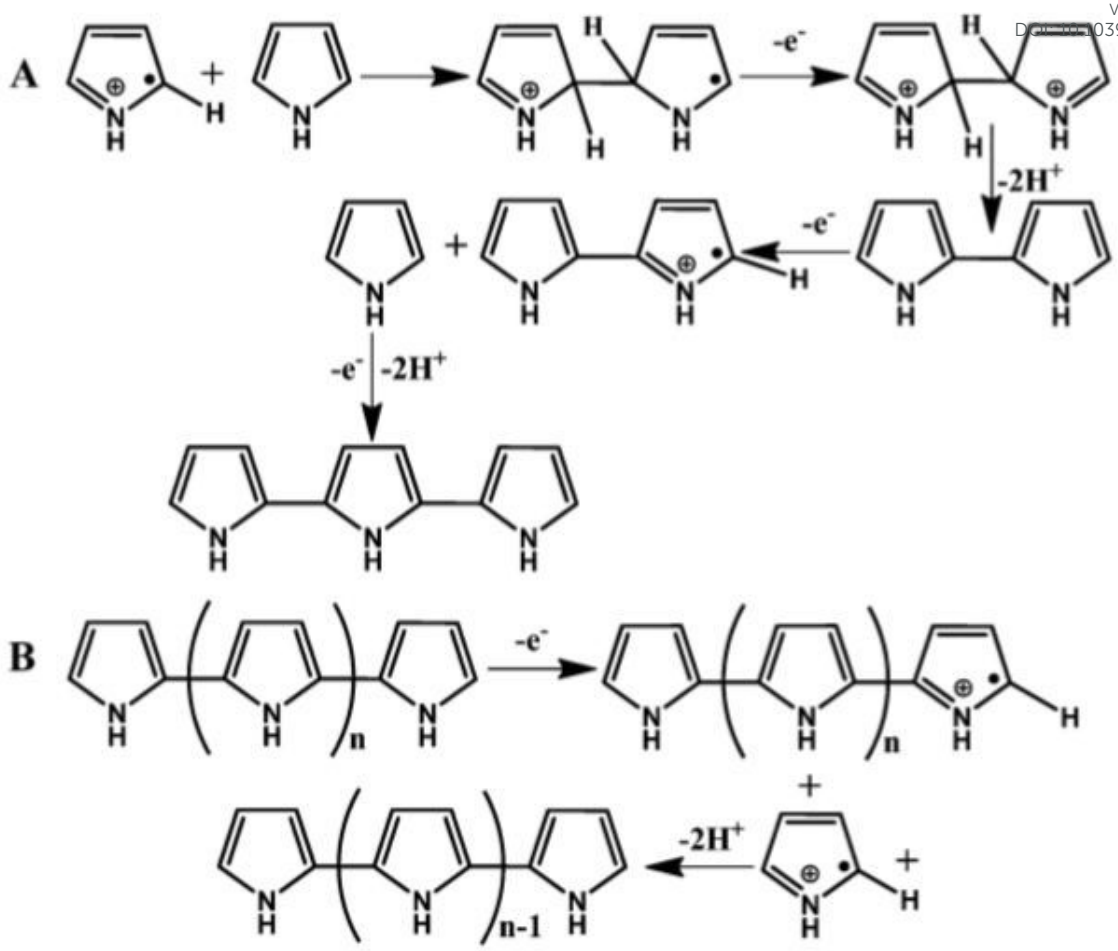

Figure 6. The formation of dimer and trimer of pyrrole (A) and further formation of the PPy (B).[128] Reproduced with permission from Elsevier.

View Article Online
DOI: 10.1039/D5LP00230C

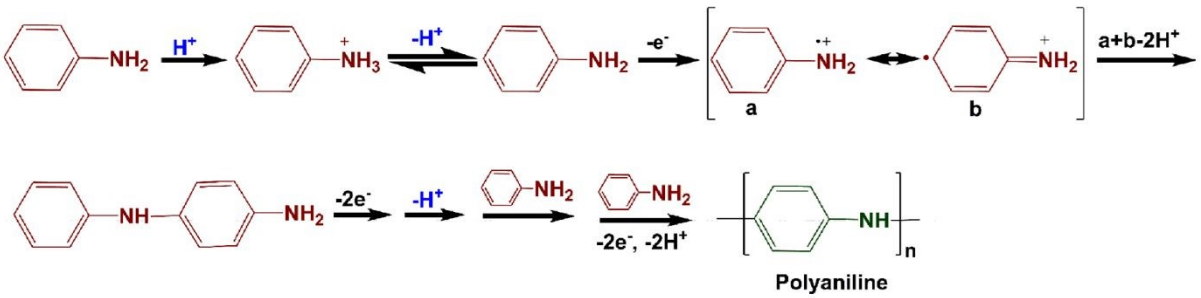

Figure 7 Electrochemical polarization mechanism of polyaniline. (electro-polymerization is carried out in the electrolyte solution of aniline and acid through applying a potential difference between the working and counter electrode).[99] Reproduced with permission from ACS.

View Article Online
DOI: 10.1039/D5LP00230C

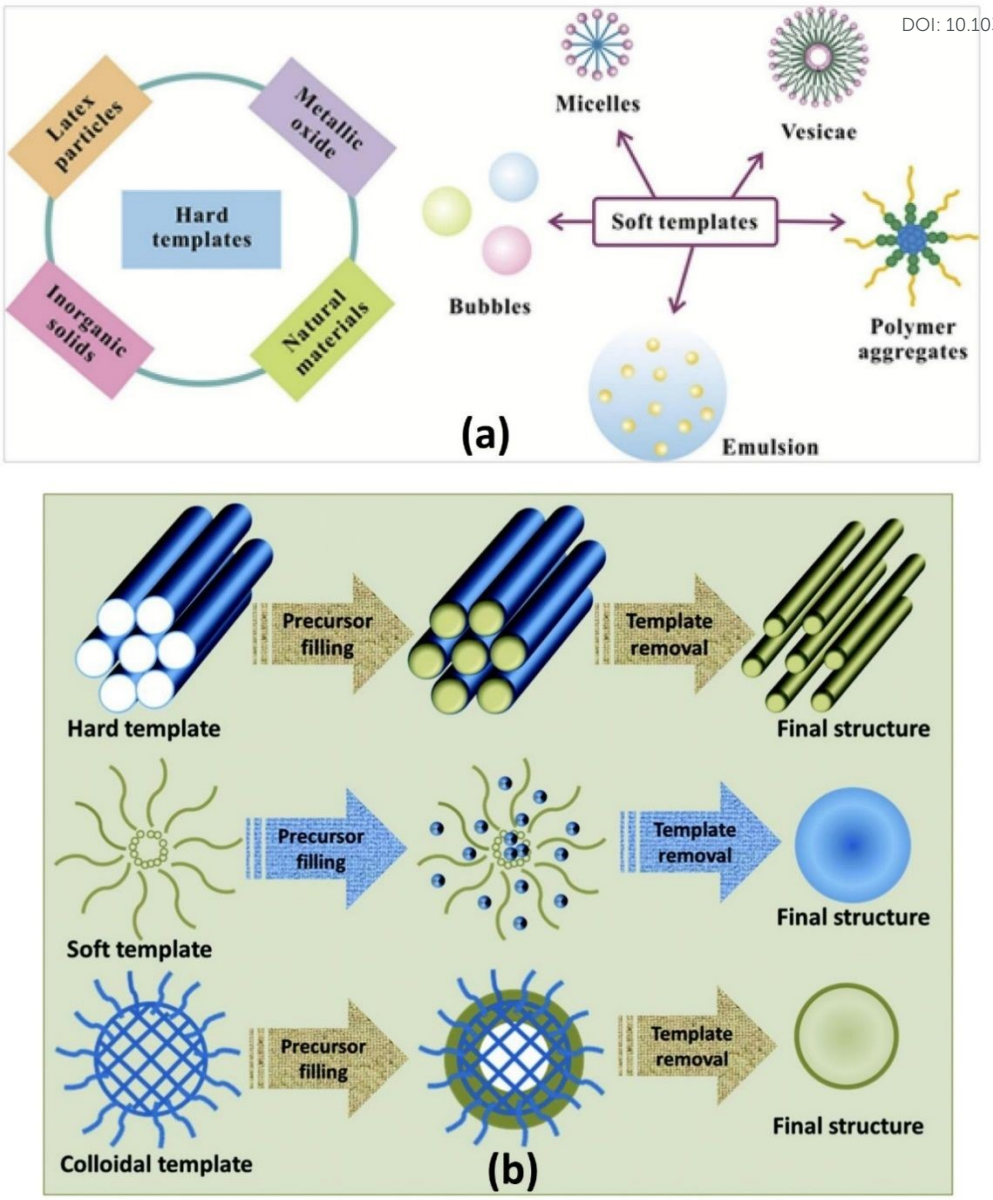

Figure 8 (a) Representative materials that can be used as templates.[173] Reproduced with permission from Elsevier, and (b) Schematic representation of the synthesis of materials using different types of templates.[175] Reproduced with permission from RSC.

View Article Online
DOI: 10.1039/D5LP00230C

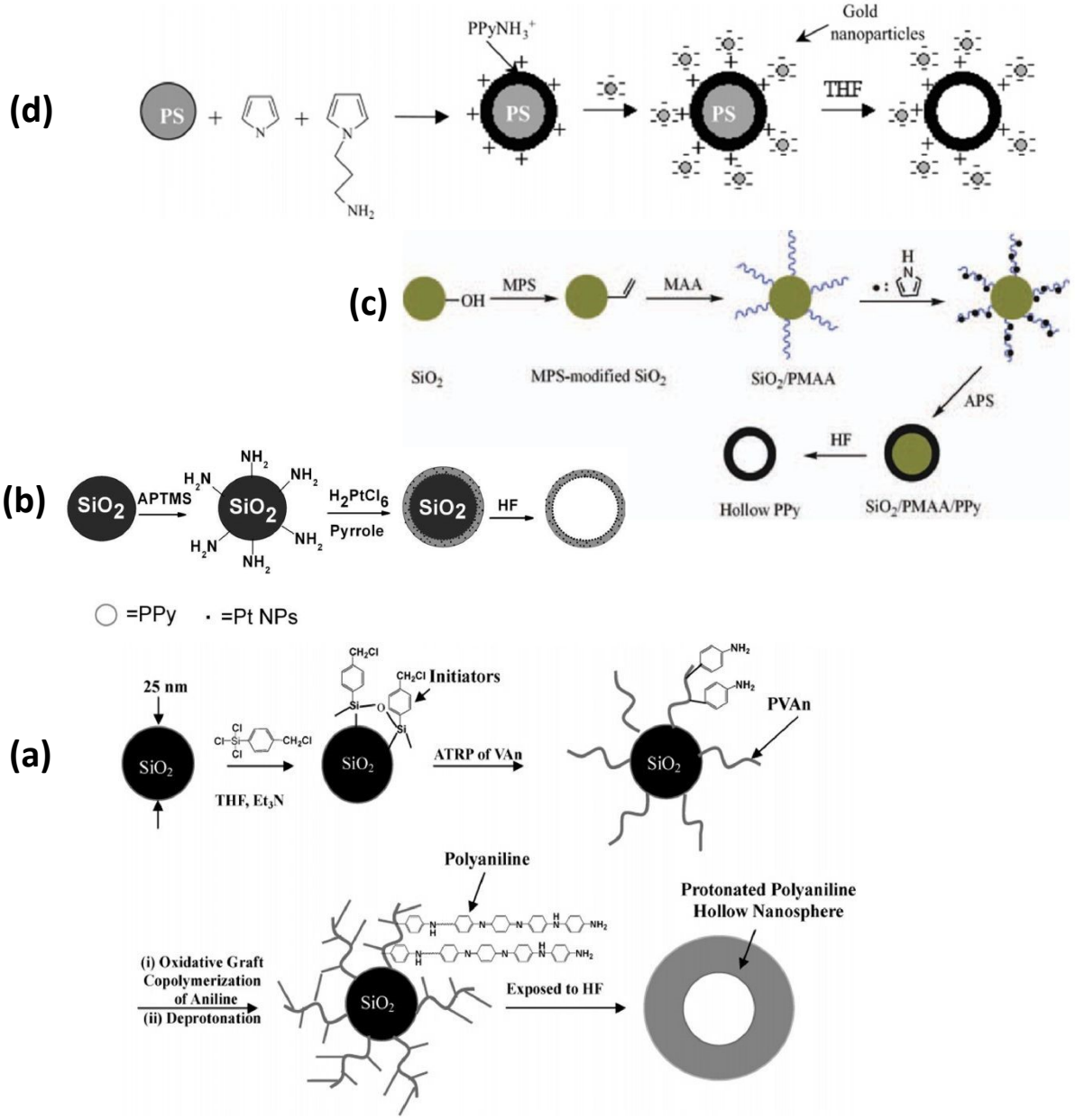

Figure 9 (a) Preparation of conductive poly(4-vinylaniline-graft-polyaniline), or P(VAn-g-PANI), hollow nanospheres via surface-initiated atom transfer radical polymerization (ATRP) and oxidative graft copolymerizationa.[191] Reproduced with permission from ACS, (b) The illustration of the formation of Pt/PPy hollow spheres.[193] Reproduced with permission from Wiley, (c) Formation of SiO_2/PMAA/PPy nanocomposite and PPy hollow spheres,[194] Reproduced with permission from Wiley, and (d) Schematic representation of the assembly of negatively charged gold nanoparticles on the surface of positively charged core-shell polypyrrole- polystyrene latex particles bearing surface-protonated N-propylamino groups.[206] Reproduced with permission from ACS.

View Article Online
DOI: 10.1039/D5LP00230C

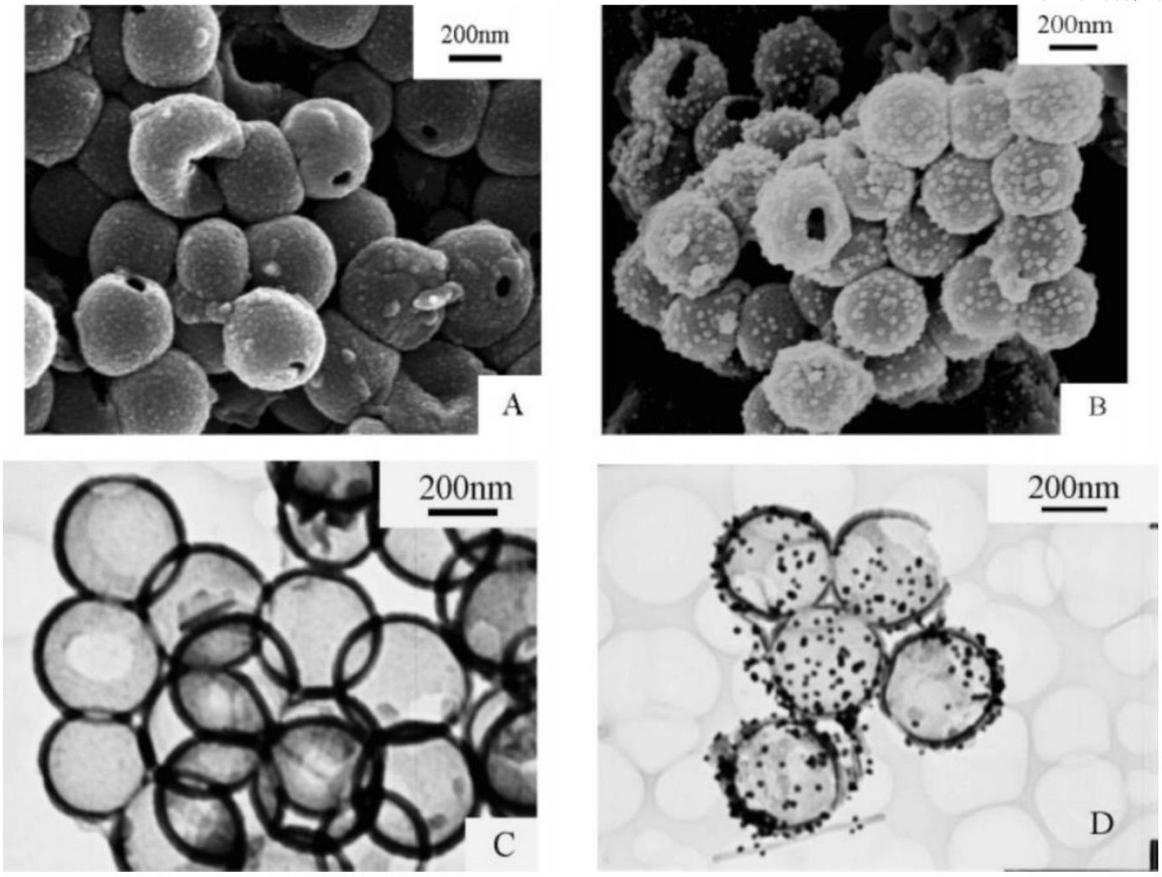

Figure 10 SEM and TEM images of PANI (A: SEM; C: TEM) and PANI/Au (B: SEM; D: TEM) composite hollow spheres (Synthetic conditions: aniline, 1 mmol, APS, 1 mmol, concentration of PANI in the Au colloid, 1.0 mg mL^{-1}).[210] Reproduced with permission from ACS.

View Article Online
DOI: 10.1039/D5LP00230C

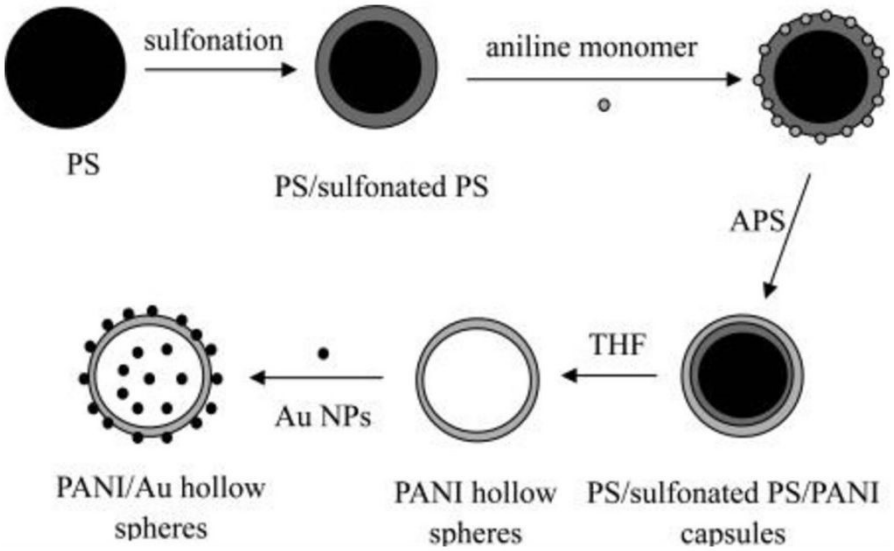

Figure 11 Scheme of the preparation of PANI and PANI/Au hollow spheres.[210] Reproduced with permission from ACS.

View Article Online
DOI: 10.1039/D5LP00230C

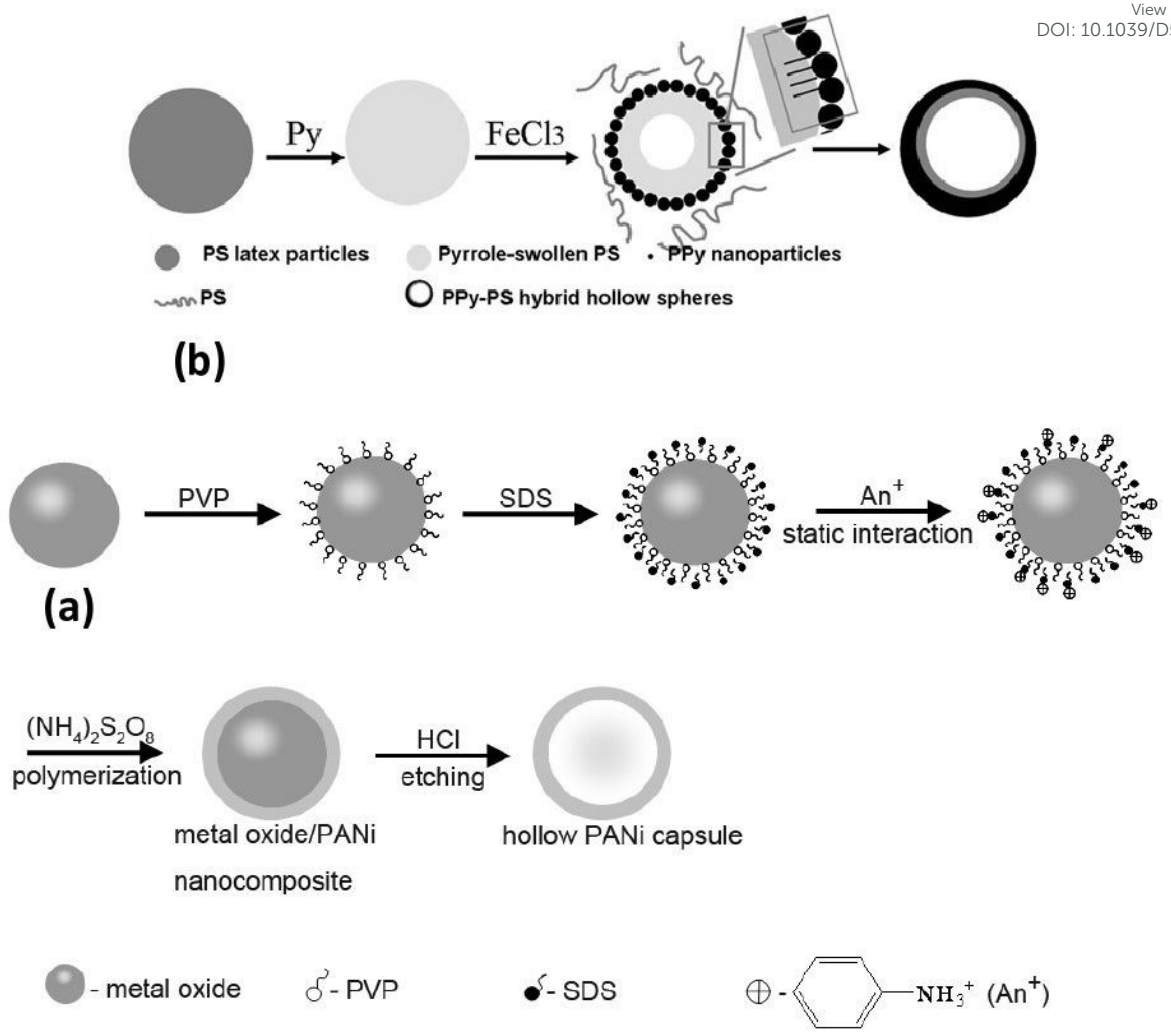

Figure 12 (a) Schematic illustration for the formation of well-controlled core/shell metal oxides/PANi nanocomposites and PANi capsules.[215] Reproduced with permission from IOP and (b) The fabrication process of PPy-PS hybrid hollow spheres.[225] Reproduced with permission from Elsevier

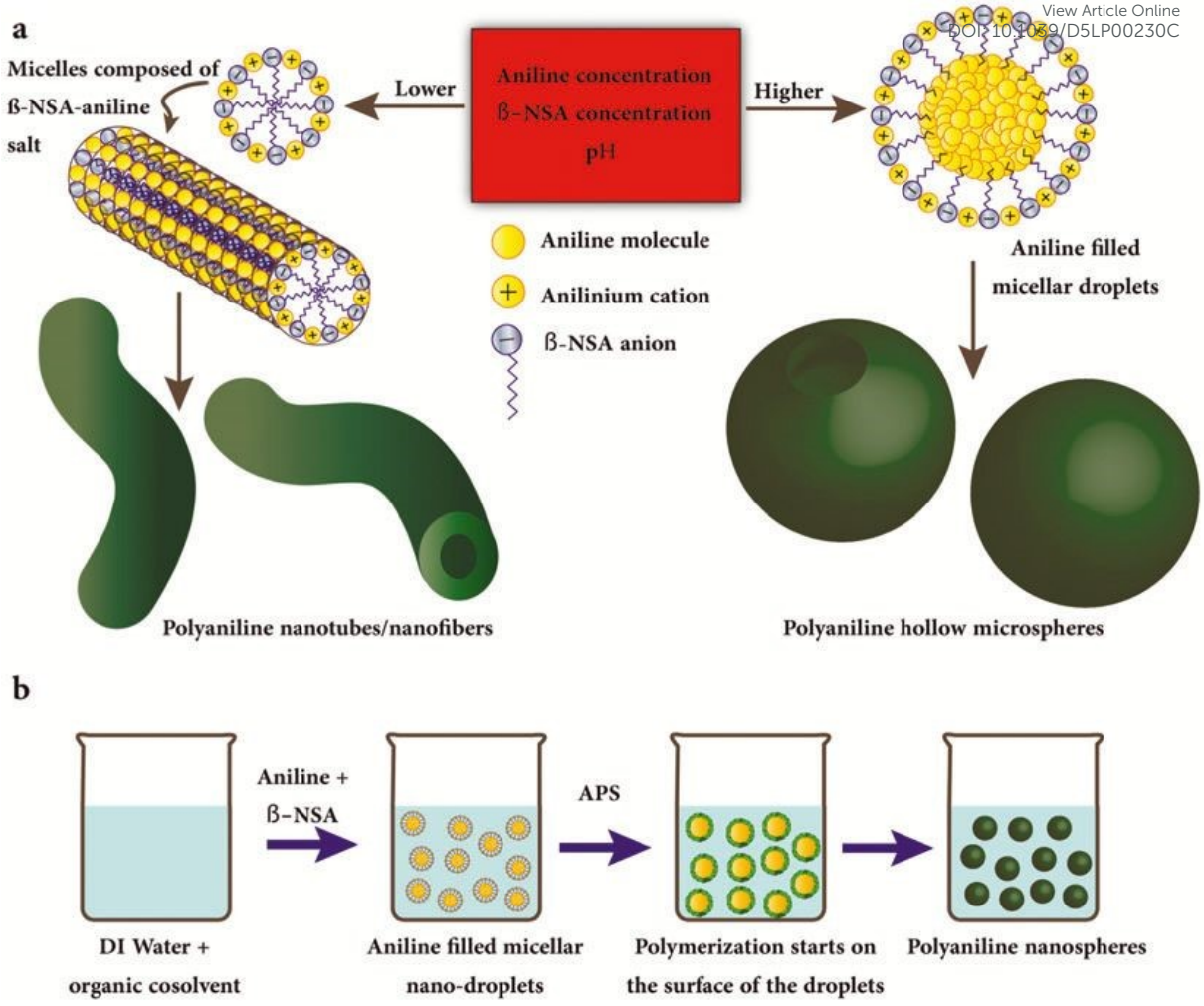

Figure 13. The schematics of the formation mechanisms of (a) PANI nanotubes/nanofibres and hollow microspheres and (b) PANI nanospheres.[282] Reproduced with permission from Wiley.

View Article Online
DOI: 10.1039/D5LP00230C

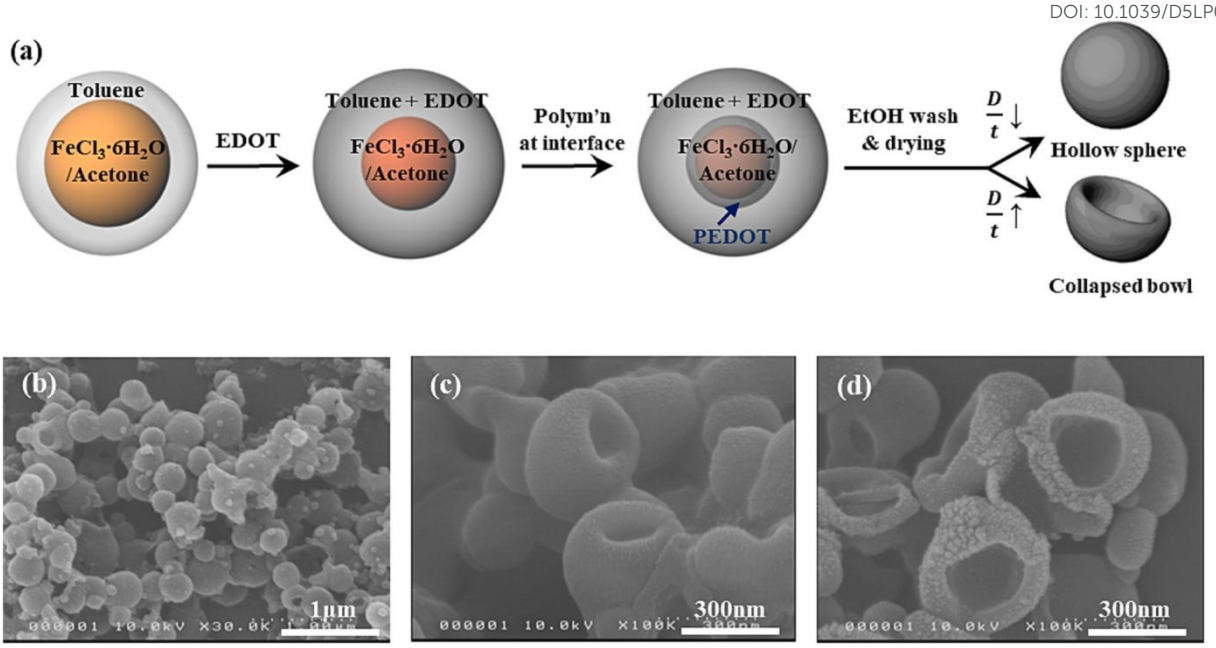

Figure 14 (a) Schematic illustration for the oxidative chemical polymerization of PEDOT hollow spheres/bowls. (b–d) SEM images of the synthesized PEDOT nanostructures, (b) PEDOT nanoparticles before wash-removal of oxidant, (c) after the removal of oxidant by ethanol washing, and (d) collapsed hollow bowls after the washing and drying.[307] Reproduced with permission from Elsevier

Figure 15 Electromagnetic radiation hazards and application of EWAMs around daily life.[328] Reproduced with permission from Elsevier.

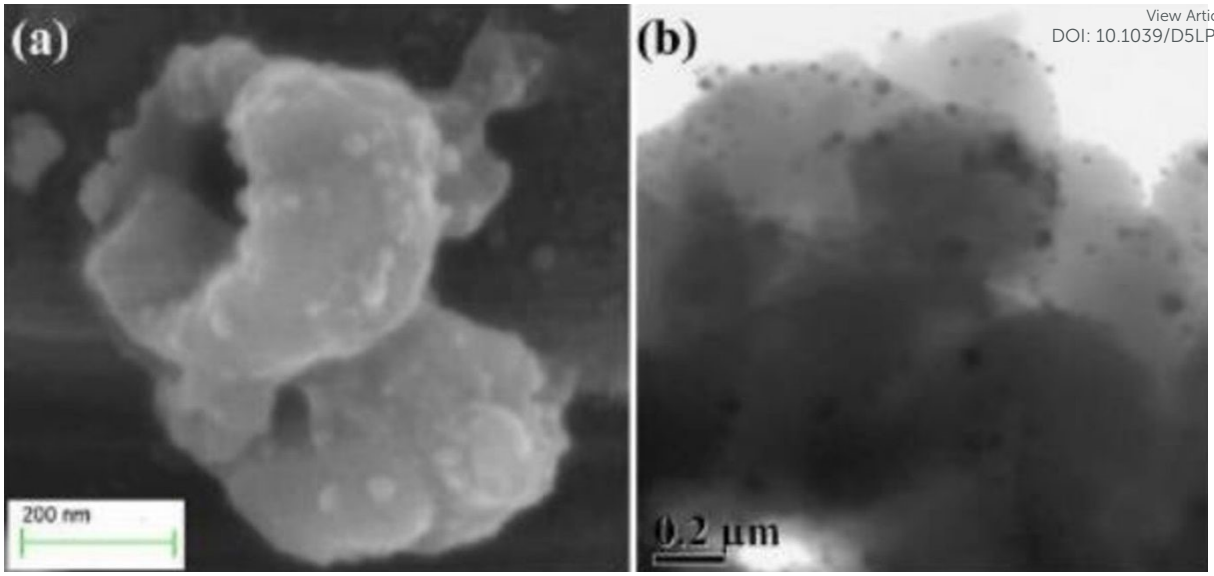

Figure 16 (a) SEM image and (b) TEM image of HPPy/Ag-10.[204] Reproduced with permission from Nature Publication.

View Article Online
DOI: 10.1039/D5LP00230C

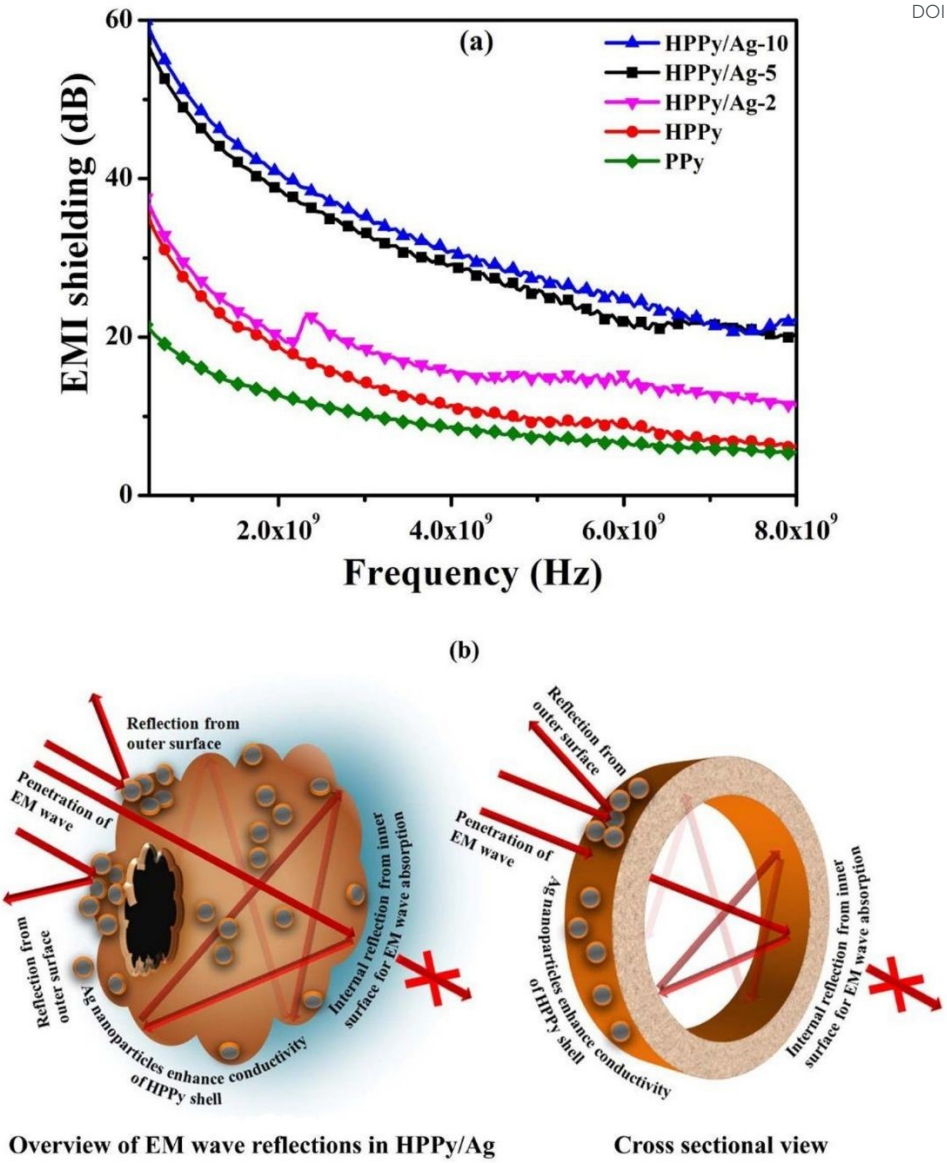

Figure 17 (a) Variation of EMI shielding of PPy, HPPy, HPPy/Ag-2, HPPy/Ag-5, HPPy/Ag-10 with varying frequency at 0.5-8 GHz, and (b) Trapping mechanism of EM wave through enhanced internal reflection in HPPy/Ag: An anticipated scheme.[204] Reproduced with permission from Nature Publication.

View Article Online
DOI: 10.1039/D5LP00230C

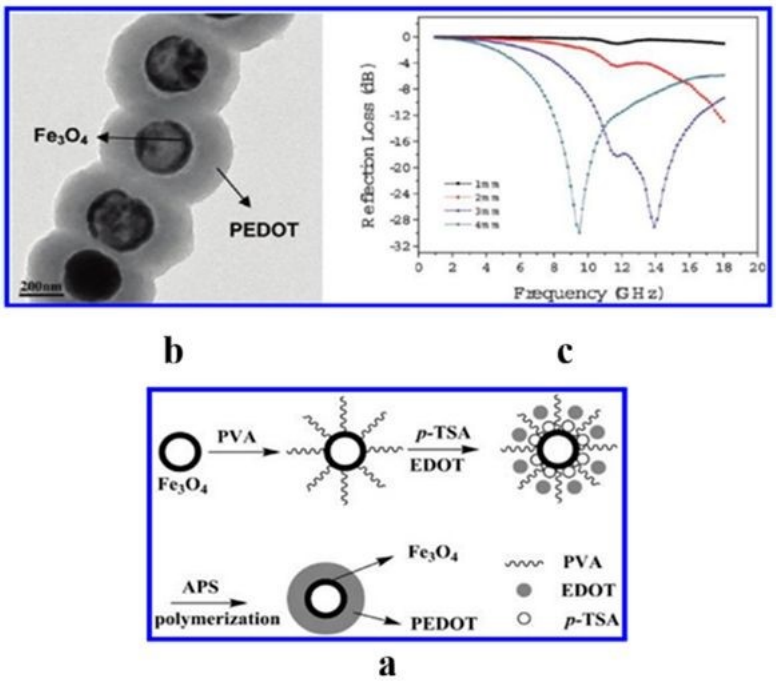

Figure 18 (a) Formation mechanism of Fe_3O_4@PEDOT core-shell microspheres, (b) TEM images of Fe_3O_4@PEDOT core-shell microspheres prepared with (EDOT)/(Fe_3O_4) ratios: 20, and (c) Reflection losses in different thickness of Fe_3O_4@PEDOT composites with (EDOT)/(Fe_3O_4) = 20.[357] Reproduced with permission from ACS.

View Article Online
DOI: 10.1039/D5LP00230C

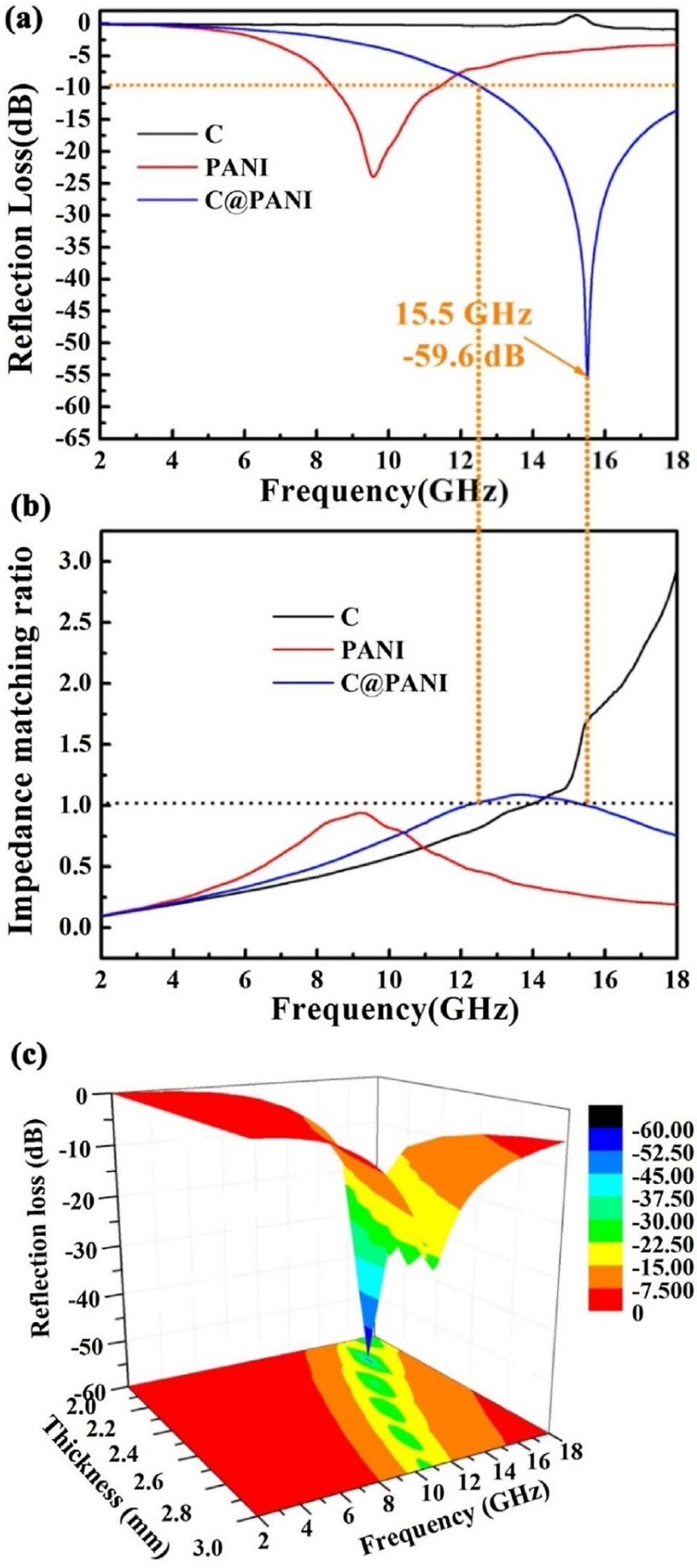

View Article Online
DOI: 10.1039/D5LP00230C

Figure 19 (a) Reflection loss of samples with the thickness of 2.2 mm; (b) impedance matching ratio of samples; (c) three-dimensional reflection loss of C@PANI micro-spheres with different thickness.[370] Reproduced with permission from Elsevier

View Article Online
DOI: 10.1039/D5LP00230C

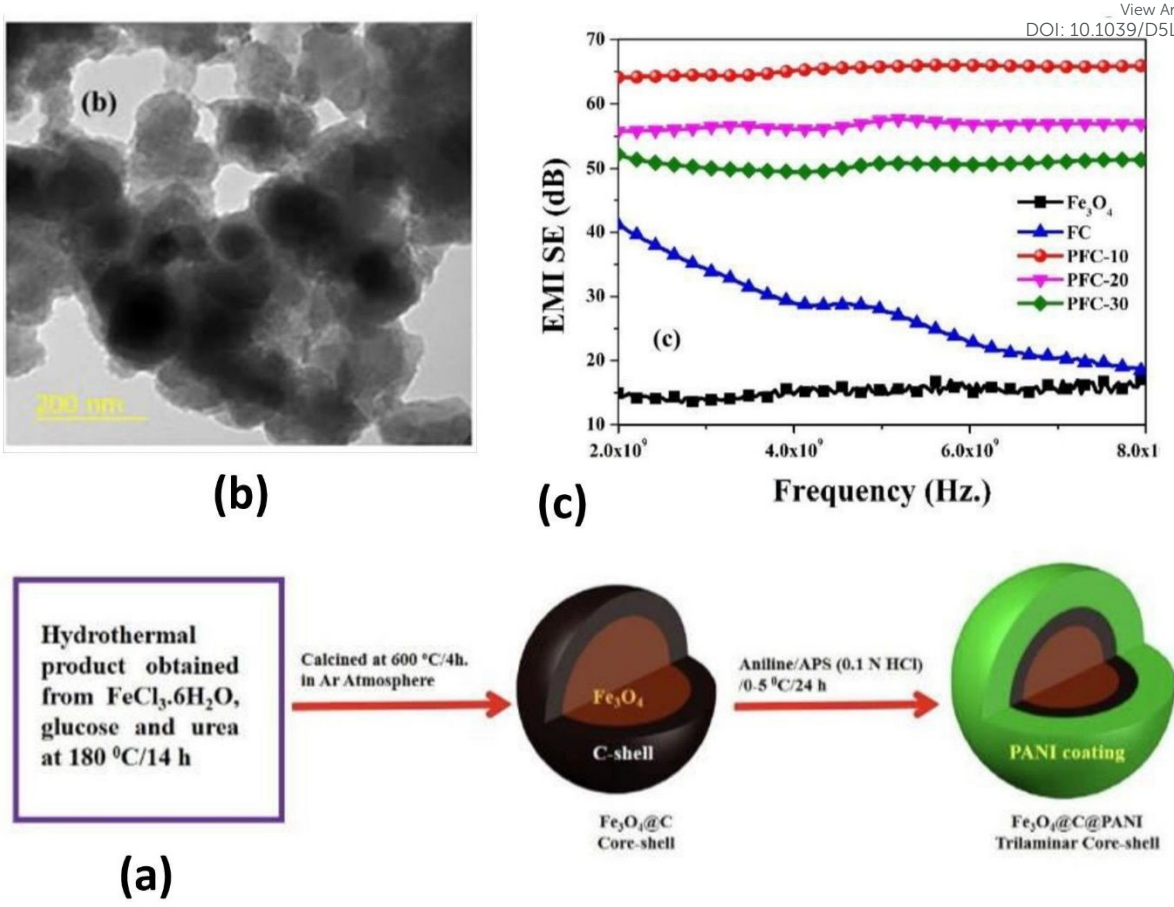

Figure 20 (a) Schematic presentation of the fabrication of Fe_3O_4@C@PANI ternary composite (aniline: Fe_3O_4@C (FC) = 9:1, 8:2, 7:3 with aniline monomer under identical reaction condition and procedure and designated as PFC-10, PFC-20 and PFC-30 respectively), (b) HRTEM images of PFC-10. and (c) Frequency vs. EMISE of PFC composites. [383] Reproduced with permission from ACS.

View Article Online
DOI: 10.1039/D5LP00230C

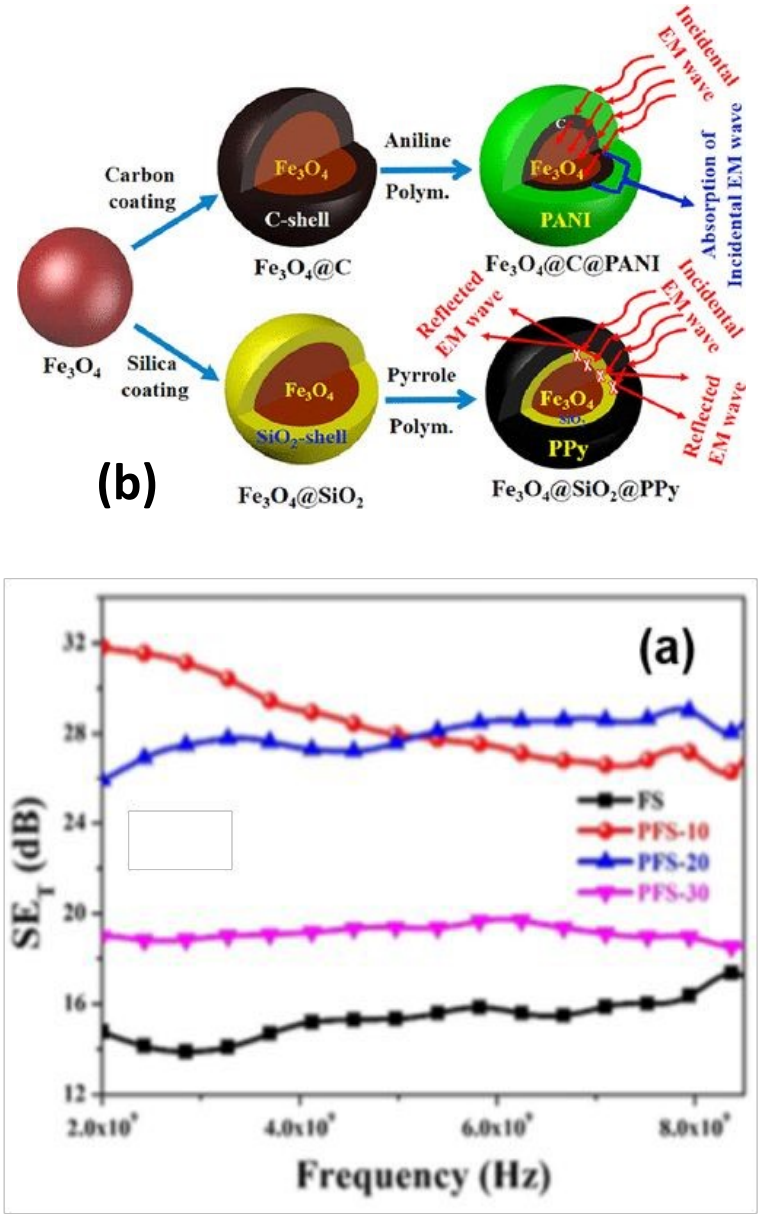

Figure 21 (a) Plot of frequency vs SE_T of Fe_3O_4@SiO_2@PPy (PFS) nanocomposites (Pyrrole/Fe_3O_4@SiO_2 (PS)= 9:1, 8:2, and 7:3) with the aniline monomer under identical reaction conditions and procedures, and the samples were designated as PFS-10, PFS-20, and PFS-30, respectively) and (b) Tuning of shells in trilaminar Fe_3O_4@SiO_2@PPy and Fe_3O_4@C@PANI core@shell nanocomposites in controlling electromagnetic interference through Switching of the shielding mechanism.[384] Reproduced with permission from ACS.

View Article Online
DOI: 10.1039/D5LP00230C

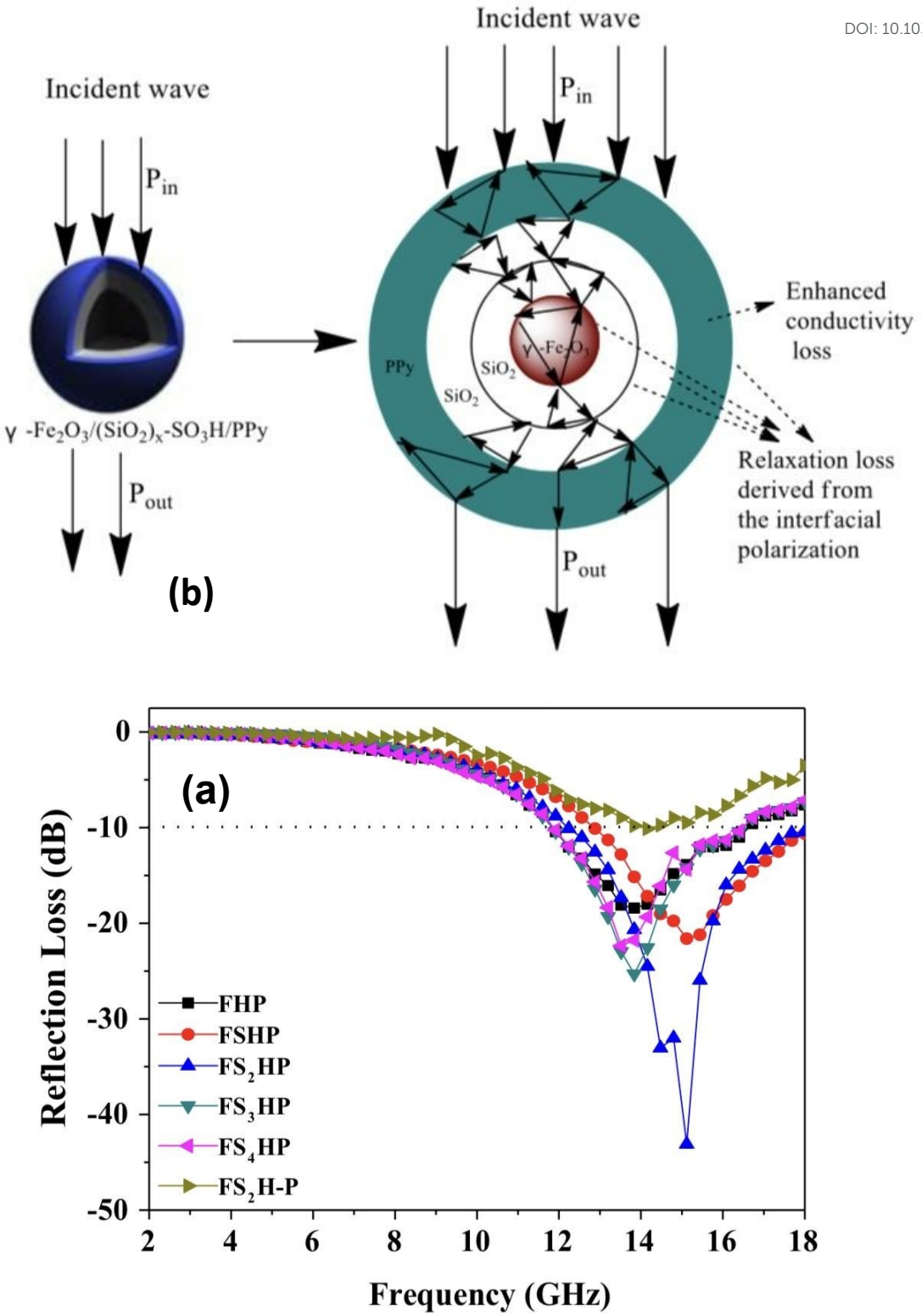

Figure 22 (a) Variation of R_L of γ-Fe_2O_3/$(SiO_2)_x$–SO_3H/polypyrrole (referred as FS_xHP, where x=0,1,2,3,4) core/shell/shell microspheres and FS_2H-P (physical blend of FS_2H and PPy) with the frequency (d = 2 mm), and (b) Physical model of the effects of core/shell/shell structures on the microwave absorption.[390] Reproduced with permission from Springer.

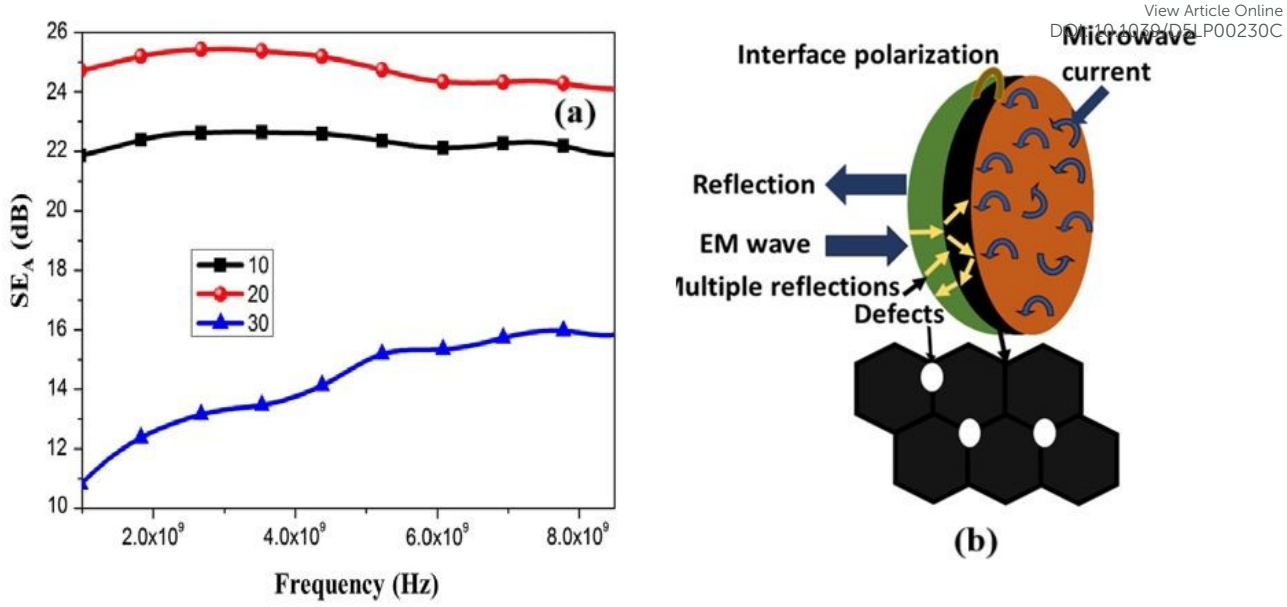

Figure 23 (a) Plots of frequency vs SE_T Fe_3O_4/C/PPy core/shell composites with pyrrole: Fe_3O_4/C = 9:1, 8:2,7:3) with pyrrole monomer under similar reaction situations referred as10, 20 and 30, respectively and (b) Schematic diagram of EMI attenuation mechanism.[405] Reproduced with permission from Springer.

View Article Online
DOI: 10.1039/D5LP00230C

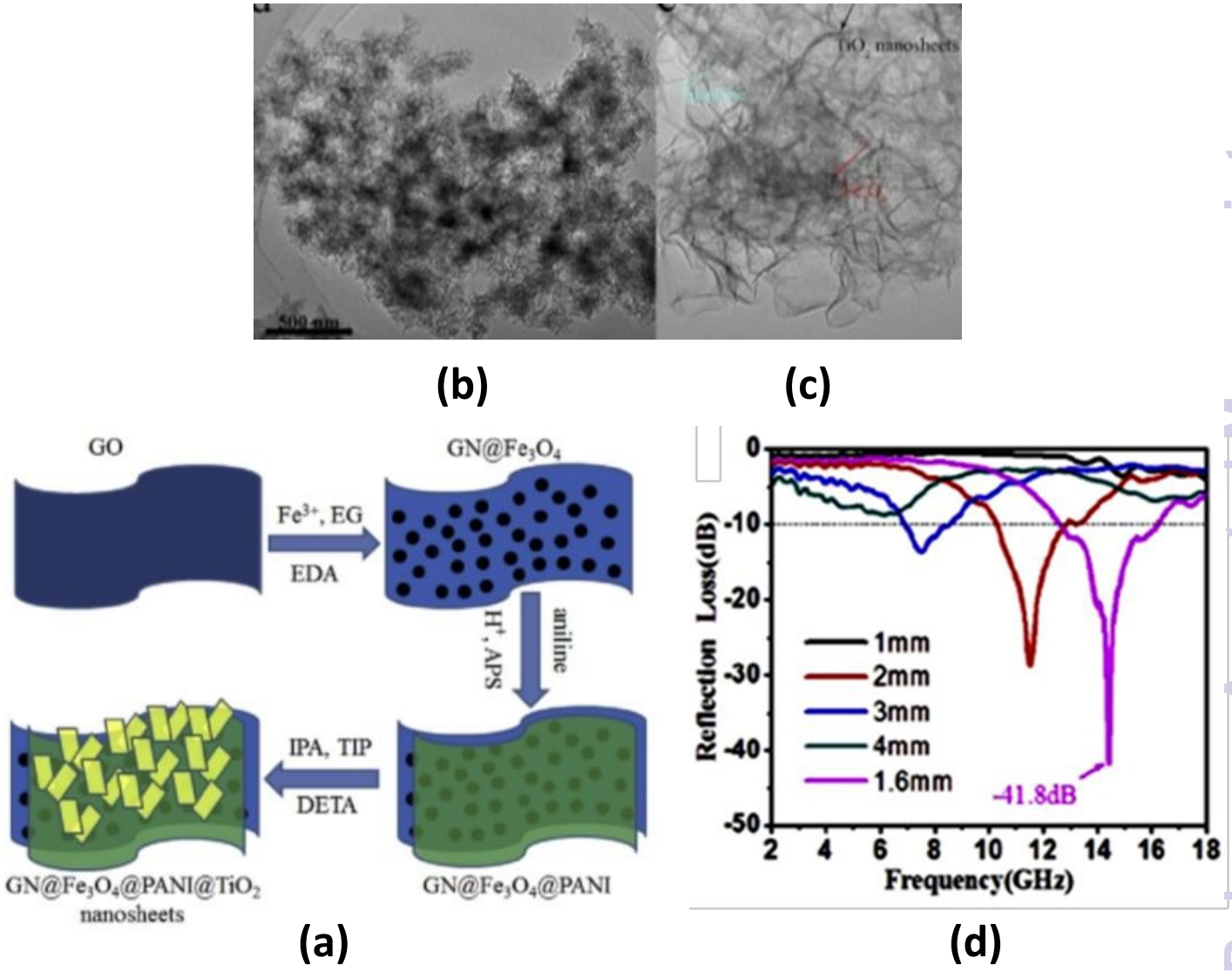

Figure 24. (a) Schematic illustration of the fabrication of the GN@Fe_3O_4@PANI@TiO_2 nanosheets, (b,c) TEM images of graphene GN@Fe_3O_4@PANI@TiO_2 nanosheets and (d) Reflection loss curves of GN@Fe_3O_4@PANI@TiO_2 nanosheets.[410] Reproduced with permission from Elsevier.

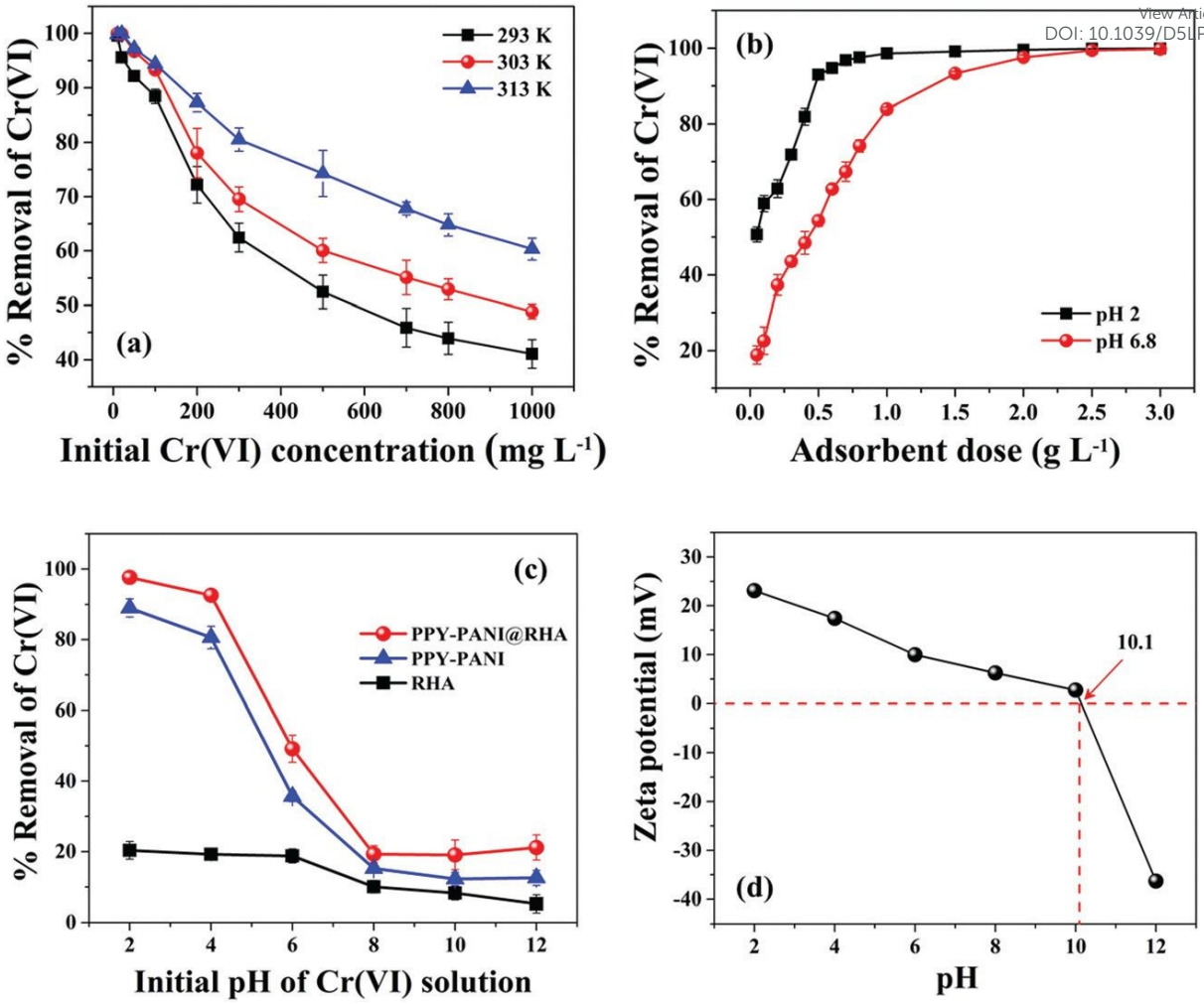

Figure 25 (a) Effect of initial concentration of Cr(VI) at a different temperature (PPY PANI@RHA dose: 0.8 g L^{-1}; contact time: 300 min; agitation speed: 200 rpm; pH~2), (b) Effect of adsorbent dose at pH 2 and without pH (~6.8) adjustment (initial Cr(VI) concentration: 50 mg L^{-1}; contact time: 300 min; agitation speed: 200 rpm; temperature: 303 K), (c) Effect of initial solution pH on % removal of Cr(VI) by PPY–PANI@RHA, PPY–PANI and RHA adsorbents (Initial Cr(VI) concentration: 50 mg L^{-1}; contact time: 300 min; agitation speed: 200 rpm; temperature: 303 K), and (d) Variation of zeta potential of PPY–PANI@RHA at different pH. [448] Reproduced with permission from RSC.

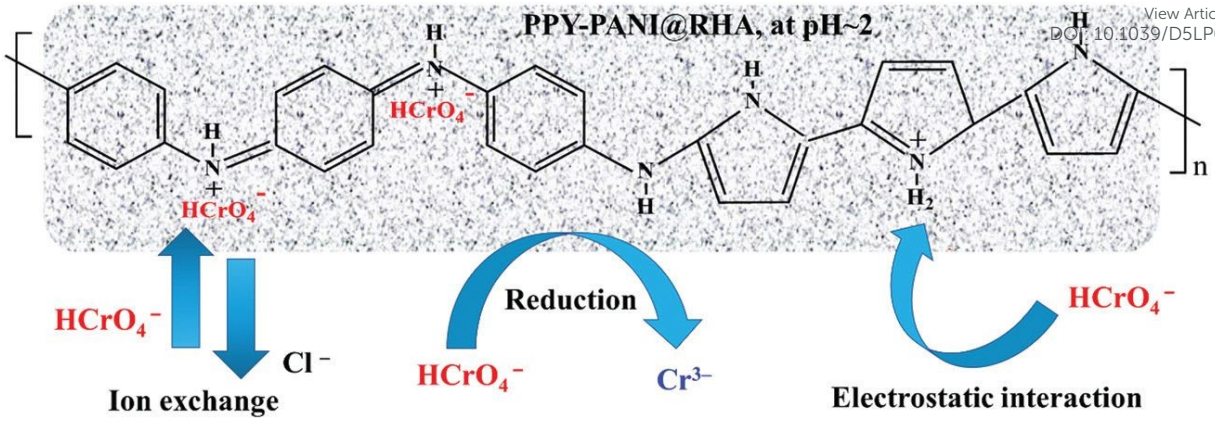

Figure 26 Representation of possible Cr(VI) adsorption by PPY–PANI@RHA.[448] Reproduced with permission from RSC.

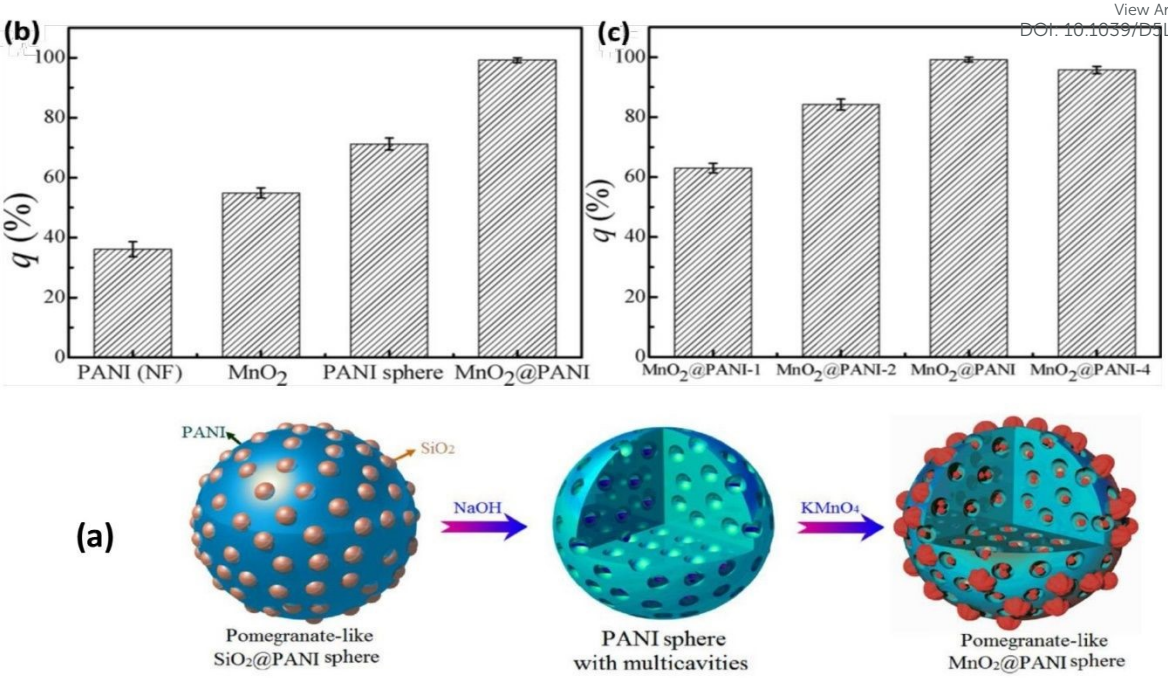

Figure 27 (a) Schematic representation of the preparation of pomegranate-like MnO_2@PANI sub-microspheres, (b) Removal ratios of Pb(II) ions with PANI(NF), MnO_2, PANI sphere and MnO_2@PANI as adsorbent. (c) Removal ratios of Pb(II) ions with MnO_2@PANI-1, to MnO_2@PANI-2, MnO_2@PANI and MnO_2@PANI-4 as adsorbent. Adsorption conditions: [Pb(II)] =60 mg L^{-1}, [adsorbent] =0.5 g L^{-1}, pH = 5.0 ± 0.1, T =25 ^{0}C, 12 h. [468] Reproduced with permission from Elsevier.

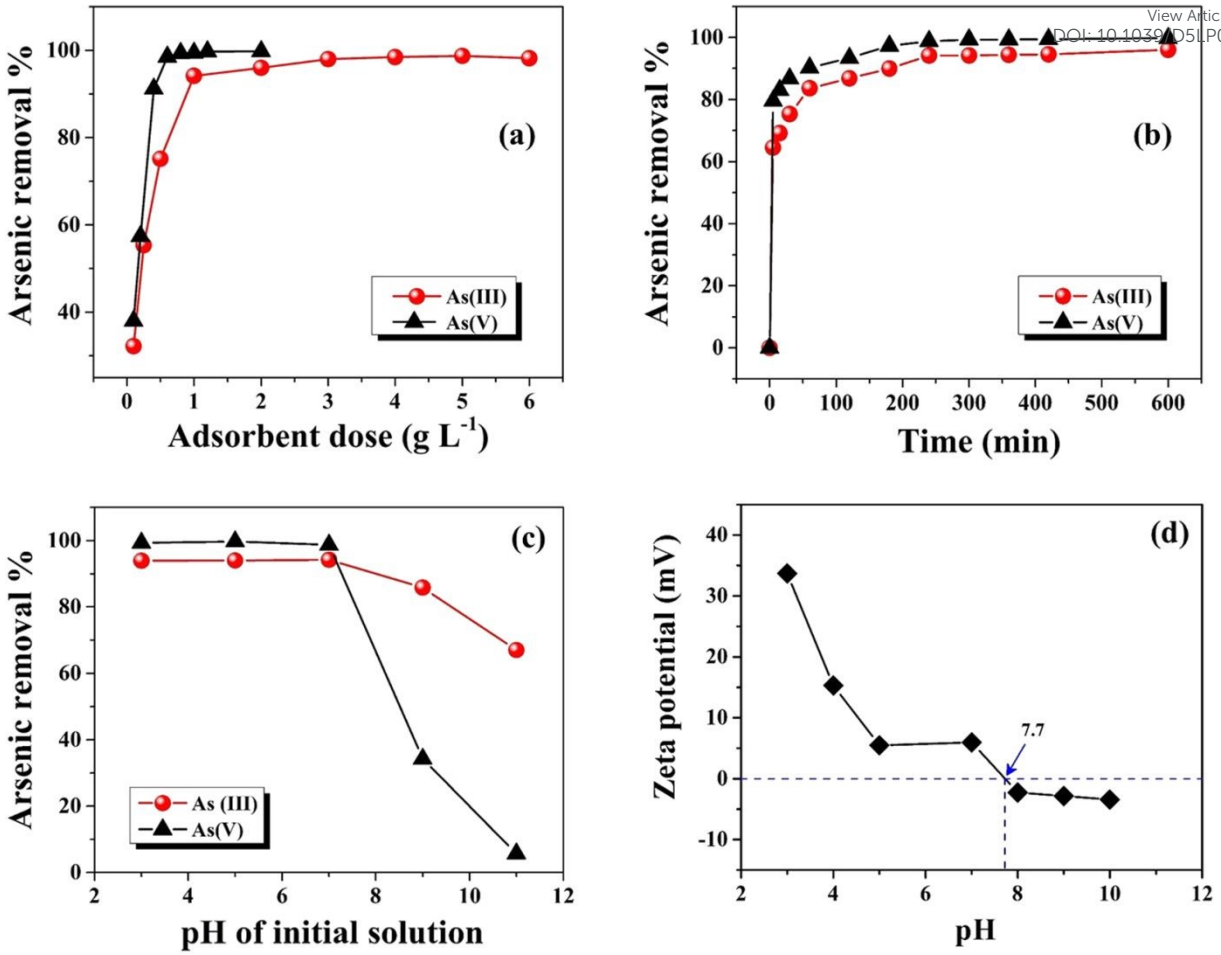

Figure 28 (**a**) Effect of adsorbent dose (Experimental conditions: C_0: 1000 µg L^{-1}; pH~7; contact time: 240 min; T: 300 ± 3 K), (**b**) Effect of contact time (Experimental conditions: adsorbent dose: 1 g L^{-1}; C_0: 1000 µg L^{-1}; pH~7; T: 300 ± 3 K), (**c**) Influence of initial solutions pH (Experimental conditions: adsorbent dose: 1 g L^{-1}; C_0:1000 µg L^{-1}; contact time: 240 min; T: 300 ± 3 K) on As(III) and As(V) removal efficiency using PNHM/Fe_3O_4-40. (**d**) ζ–potential of PNMH/Fe_3O_4-40 under various pH conditions.[476] Reproduced with permission from Nature Publication.

View Article Online
DOI: 10.1039/D5LP00230C

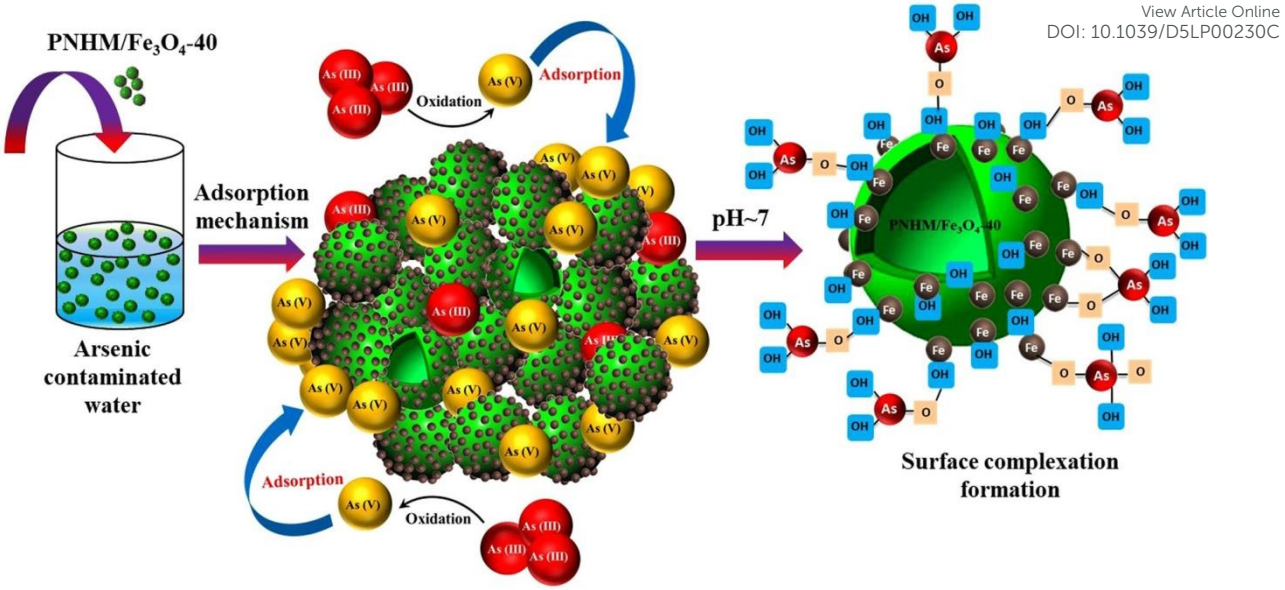

Figure 29 Schematic representation of arsenic adsorption mechanism in aqueous solution.[476] Reproduced with permission from Nature Publication.

View Article Online
DOI: 10.1039/D5LP00230C

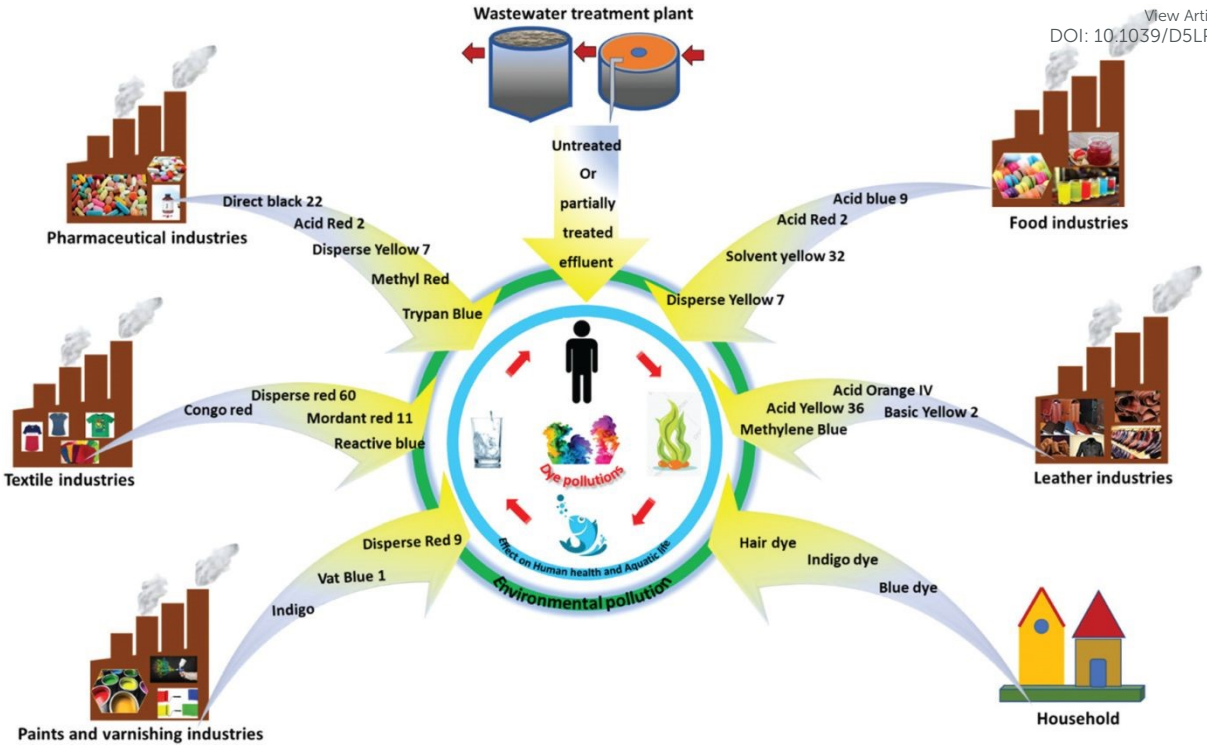

Figure 30 Sources and pathways of dyes in the environment.[88] Reproduced with permission from RSC

View Article Online
DOI: 10.1039/D5LP00230C

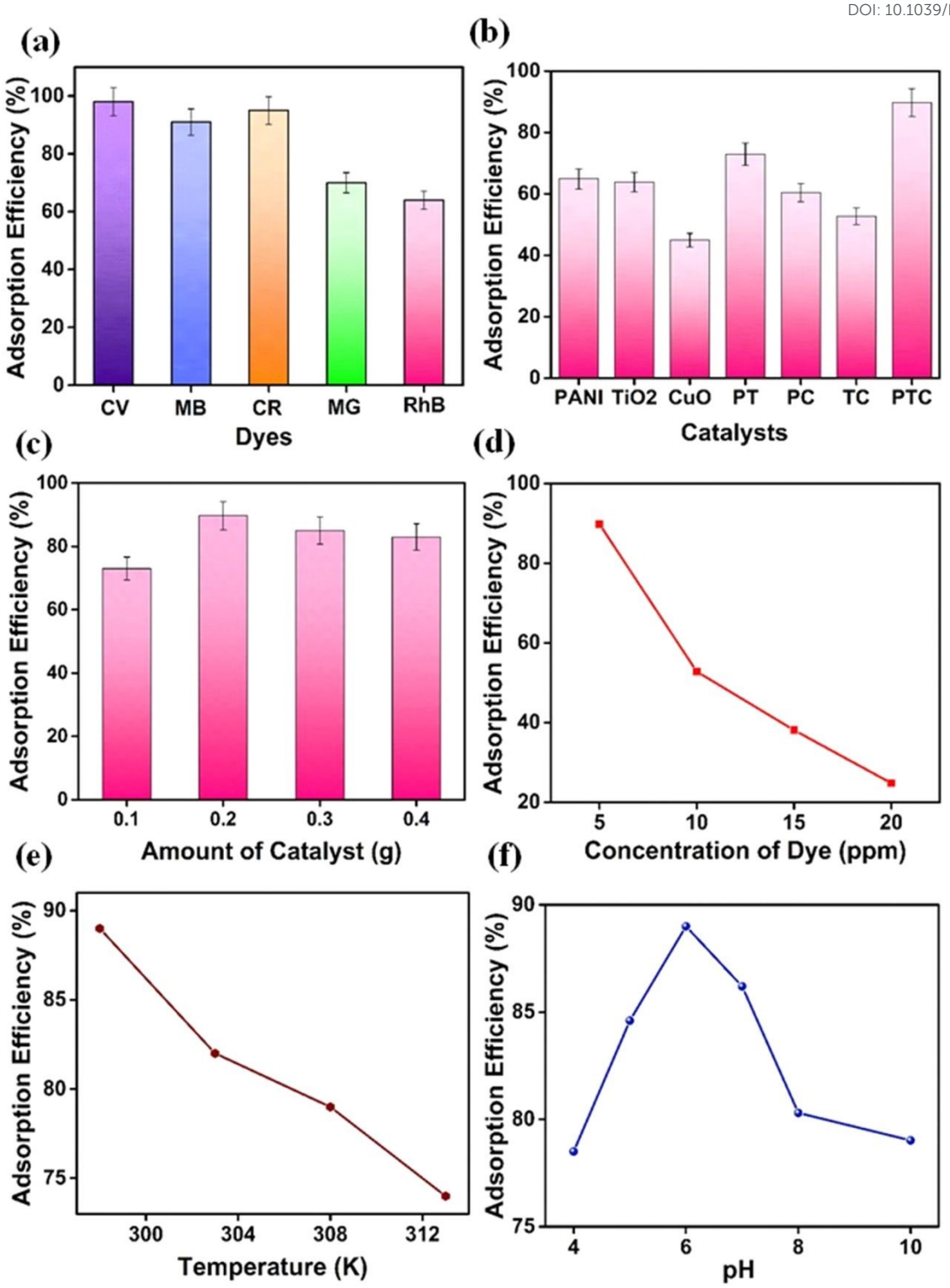

Figure 31 (a) Adsorption efficiency of various dyes using PANI/TiO_2/CuO at 120 min (b) A efficiency of RhB using different catalysts at 240 min (c) Effect of amount of adsorbent on RhB adsorption using PANI/TiO_2/CuO for 120 min (d) RhB adsorption at different dye concentrations using PANI/TiO_2/CuO for 240 min (e) Effect of RhB adsorption using PANI/TiO_2/CuO at different temperatures, and (f) Effect of Effect of pH on the adsorption of RhB using PANI/TiO_2/CuO.[504] Reproduced with permission from Elsevier.

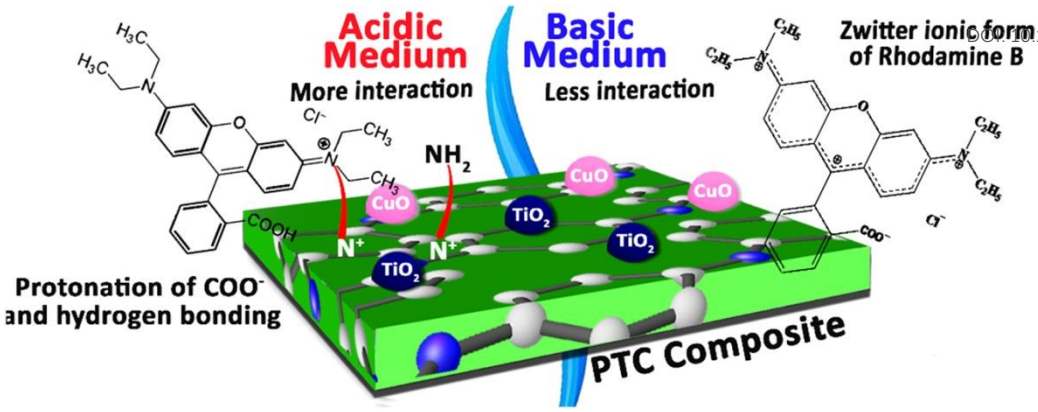

Figure 32 The effect of pH on the adsorption efficiency of PANI/TiO_2/CuO.[504] Reproduced with permission from ACS.

View Article Online
DOI: 10.1039/D5LP00230C

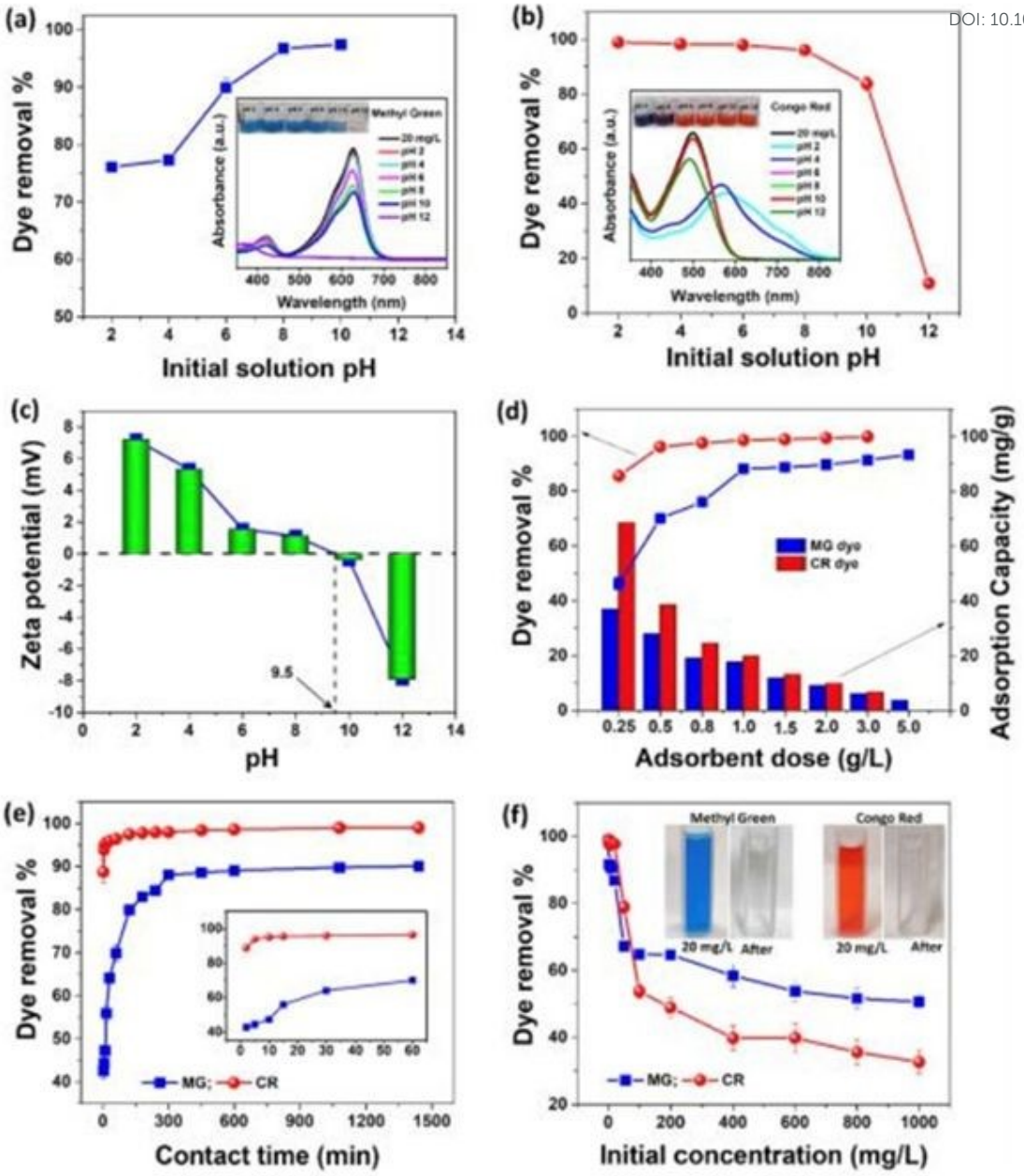

Figure 33 Effect of pH on (a) MG and (b) CR dye removal efficiency (inset: change of wavelength of the dye solutions at different solution pH); (c) zeta potential of PNHM/MnO_2/Fe_3O_4 with the variation of pH, effect of (d) adsorbent dose, (e) contact time and (f) initial dye concentration on MG and CR dye removal efficiency.[513] Reproduced with permission from ACS.

View Article Online
DOI: 10.1039/D5LP00230C

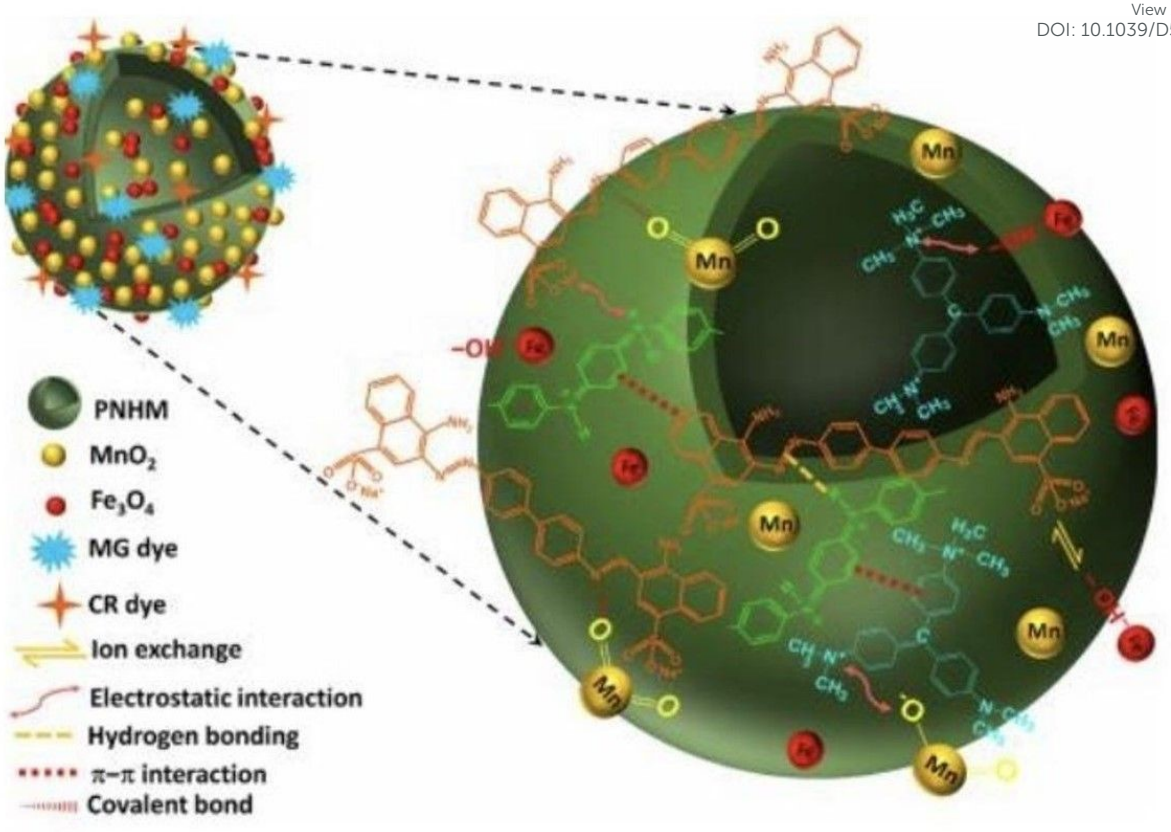

Figure 34 Schematic representation of plausible adsorption mechanism of MG and CR dye on the surface of PNHM/MnO_2/Fe_3O_4 at pH ~6.75.[513] Reproduced with permission from ACS.

View Article Online
DOI: 10.1039/D5LP00230C

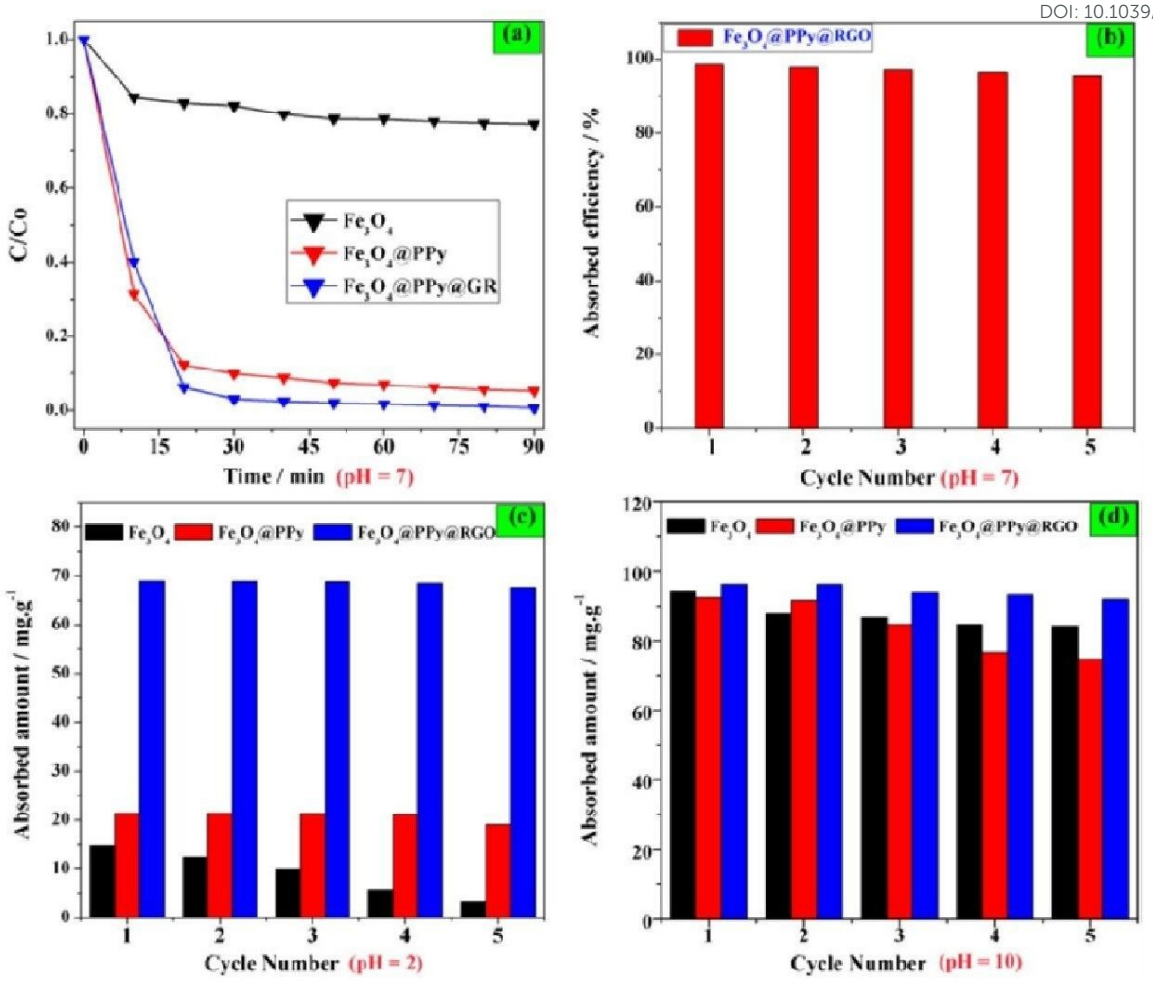

Figure 35(a) Removal efficiency of magnetic adsorbents in neutral solution (pH 7); (b) Removal efficiency of Fe_3O_4@PPy@RGO in five cycles, neutral solution (pH 7); (c) Removal efficiency of magnetic adsorbents in acidic solution (pH 2) and (d) alkaline solution (pH 10). [529] Reproduced with permission from Elsevier.

View Article Online
DOI: 10.1039/D5LP00230C

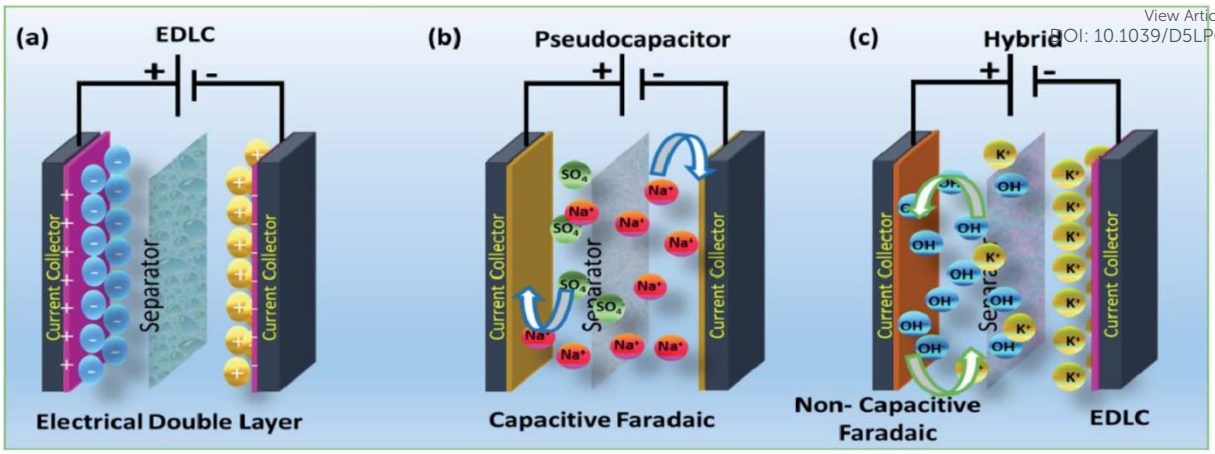

Figure 36 Charge storage mechanism of supercapacitors, (a) EDLCs, (b) pseudocapacitors and (c) hybrid supercapacitors,[551] Reproduced with permission from RSC.

View Article Online
DOI: 10.1039/D5LP00230C

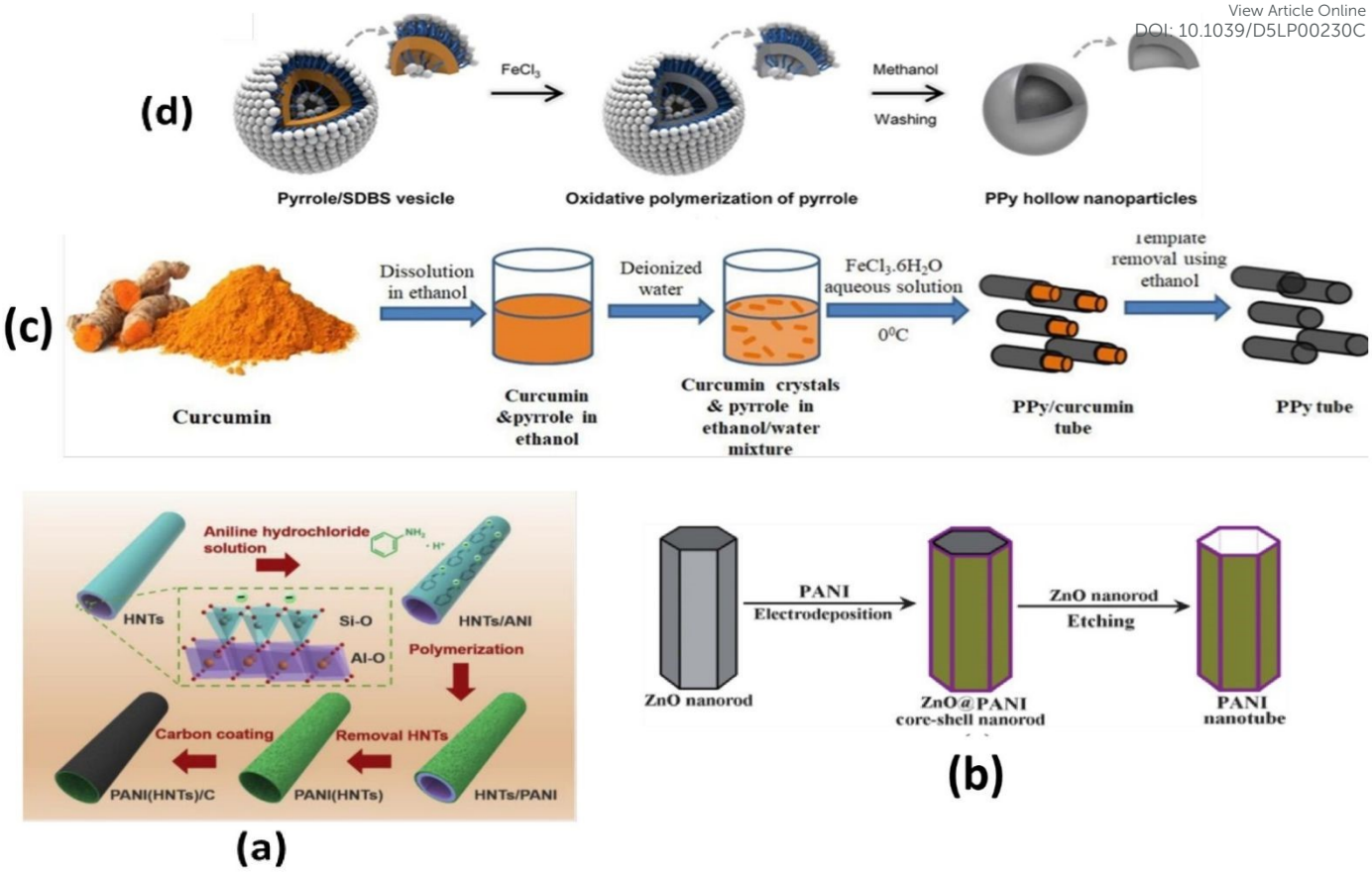

Figure 37 (a) Schematic presentation on the preparation procedure of PANI(HNTs) and PANI(HNT)s/C,[560] Reproduced with permission from Elsevier, (b) The illustration for the formation of PANI nanotubes via a sacrificial ZnO nanorods template route.[561] Reproduced with permission from RSC, (c) Schematic representation of the preparation of polypyrrole tubes using curcumin as template,[562] Reproduced with permission from RSC, and (d) Schematic diagram of the synthesis of PPy hollow nanospheres,[565] Reproduced with permission from RSC.

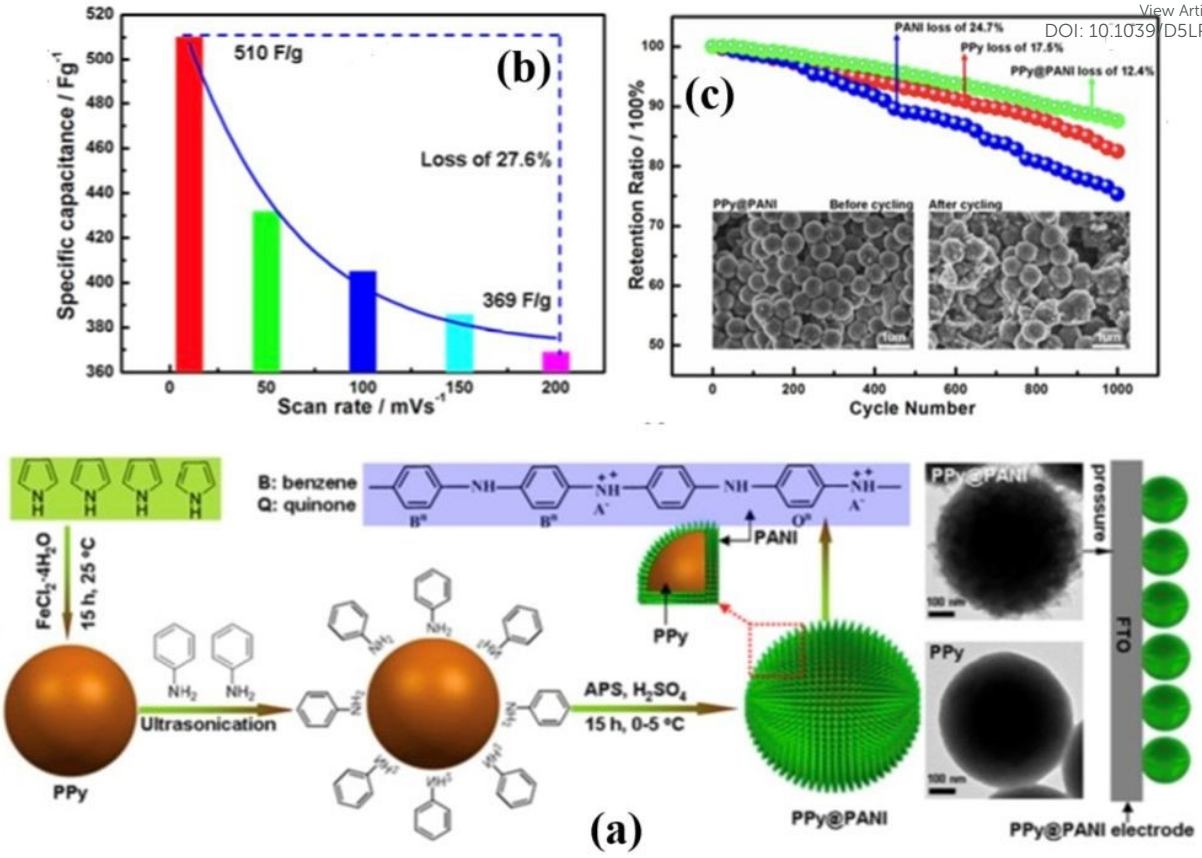

Figure 38 (a) Schematic diagram for the synthesis of core-shell PPy@PANI nanospheres. (b) SC values' plot of the scan rates and (c) Charge/discharge cycling of the core-shell PPy@PANI-0.008, individual PPy, and the PANI electrode are carried out at 5 A/g in H_2SO_4 aqueous electrolyte (1 M). The insert is the SEM images of the core-shell@PANI-0.008 before and after 1000 cycles. [585] Reproduced with permission from ACS.

View Article Online
DOI: 10.1039/D5LP00230C

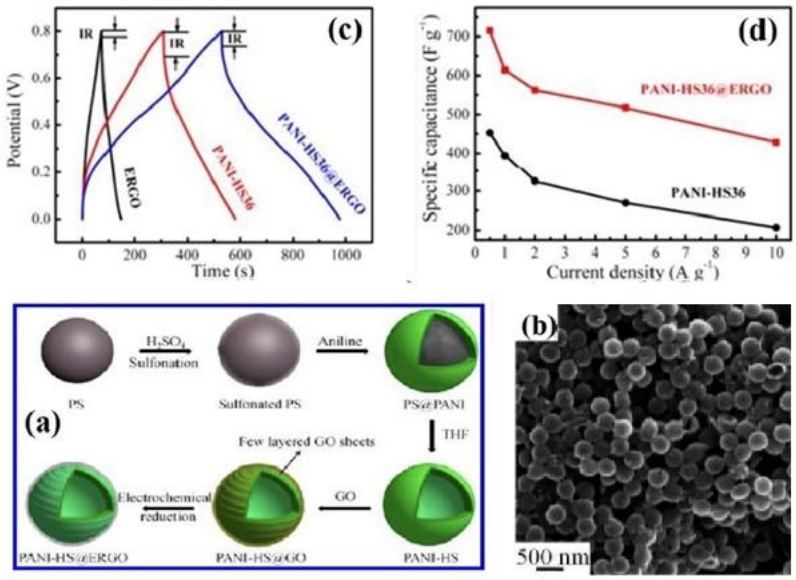

Figure 39 (a) Schematic Illustration on the Preparation of PANI-HS36@ERGO Hybrids (36 here refers to shell thickness in nm) hybrids, (b) SEM images of PANI-HS36@GO hybrids, (c) Galvanostatic charge−discharge curves of ERGO, PANIHS36,and PANI-HS36@ERGO hybrids within a potential window of 0−0.80 V at a current density of 1 A g^{-1} (modified), and (d) Plots of specific apacitance for PANI-HS36 and PANI-HS36@ERGO hybrids at various current densities (modified).[587] Figure Reproduced with permission from ACS.

View Article Online
DOI: 10.1039/D5LP00230C

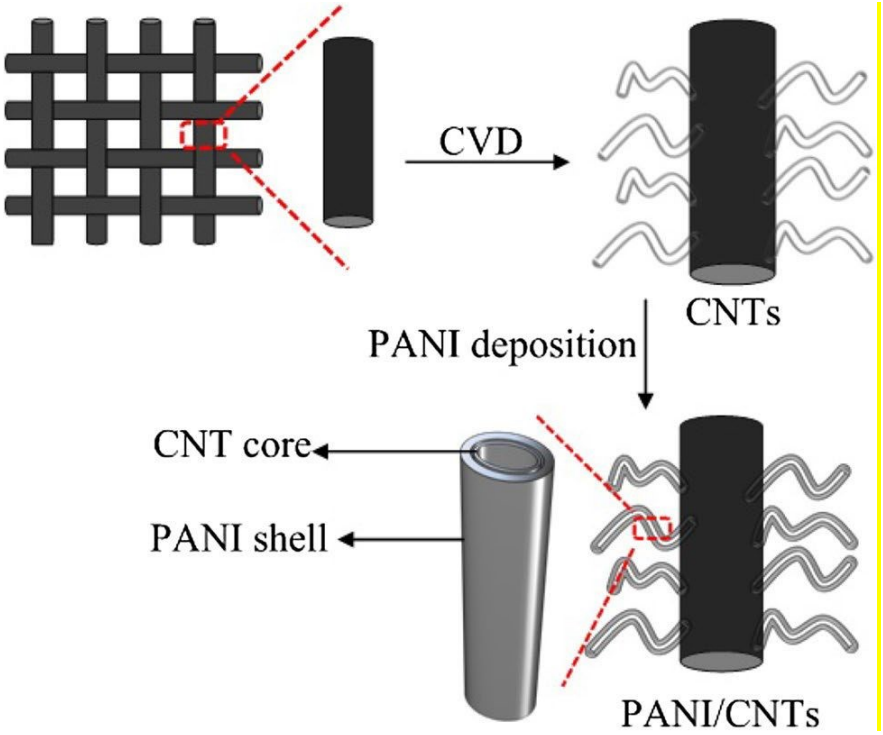

Figure 40 Illustrations of the fabrication process for PANI/CNTs on carbon cloth (CC).[606] Reproduced with permission form Springer.

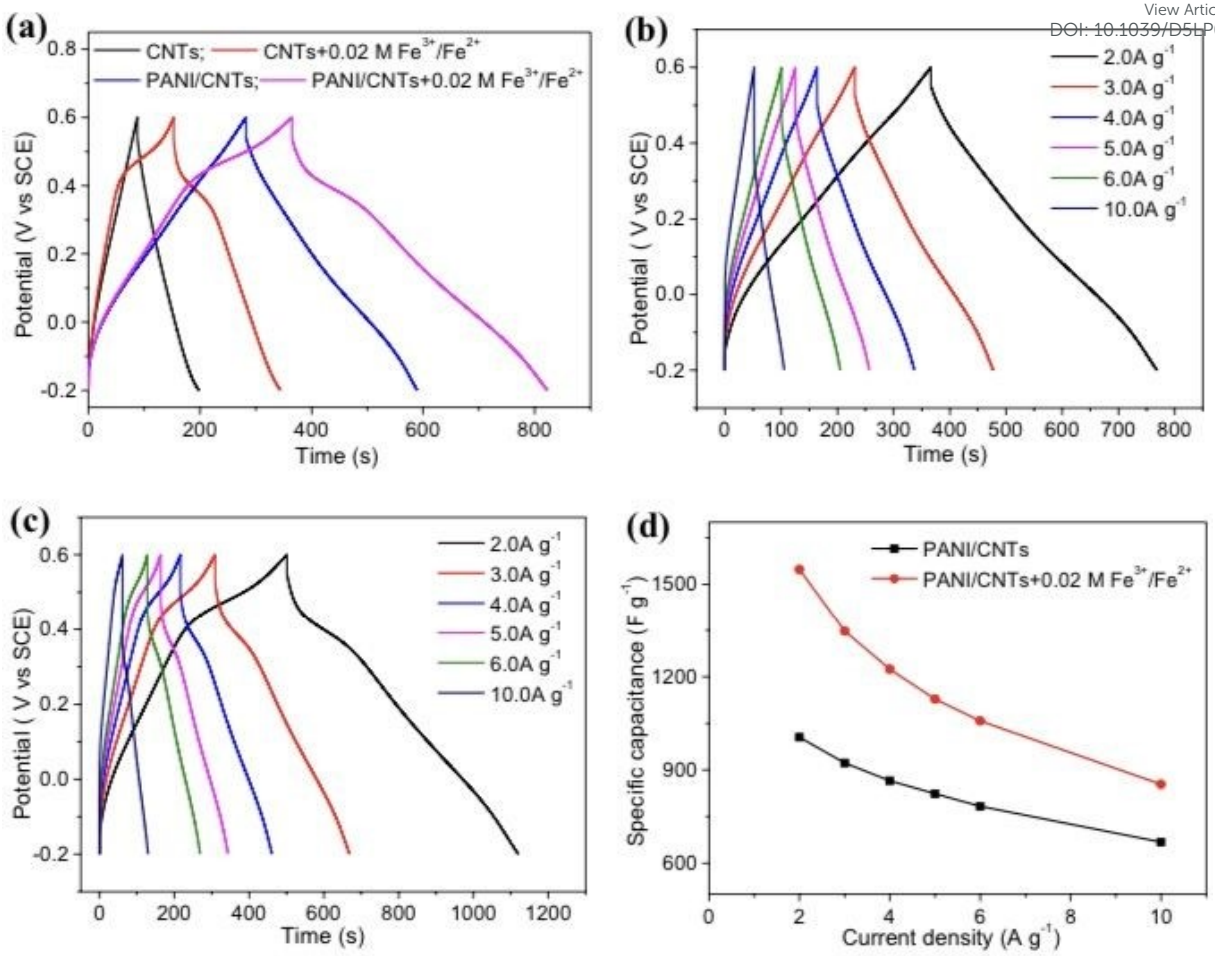

Figure 41 (a) GCD curves of CNTs and PANI/CNTs at 1.5 mA cm^{-2} in 1 M H_2SO_4 with and without the addition of 0.02 M Fe^{3+}/Fe^{2+}. (b) GCD curves of PANI/CNTs testing in 1 M H_2SO_4 electrolyte at different current densities. (c) GCD curves of PANI/CNTs testing in 1 M H_2SO_4/0.02 M Fe^{3+}/Fe^{2+} electrolyte at different current densities, and (d) Specific capacitance curves of PANI/CNTs at different current densities.[606] Reproduced with permission form Springer.

Statement: No data to share in this article,

View Article Online
DOI: 10.1039/D5LP00230C